

Foreword

Use the template *foreword.tex* together with the document class SVMono (monograph-type books) or SVMult (edited books) to style your foreword.

The foreword covers introductory remarks preceding the text of a book that are written by a *person other than the author or editor* of the book. If applicable, the foreword precedes the preface which is written by the author or editor of the book.

Place, month year

Firstname Surname

Preface

This volume includes the three main Echord++ instruments and ten selected contributions of the project achievements, which have been financed by the European Commission under the seventh Framework Program.

On October 3rd 2018, the Echord++ core partners presented the final results of this European Project in the International Conference on Intelligent Robots (IROS 2018). During the last five years, more than 100 Echord++ partners have developed robotic technology and giving tailor-made solutions to social, public and industrial challenges under the slogan "From Lab to Market".

Three instruments have been used – Experiments (EXP), Research Innovation Facilities (RIF) and Public end users Driven Technological Innovation (PDTI) – and 35 robotic prototypes have been financed and monitored bringing nowadays new innovative research solutions and in some cases pre-commercial products. The monitoring structure of the research and the technological activities has been the key to raise the technological level of the involved SMEs and to drive the robotic solutions to the market.

An intensive and coordinated structured dialogue between all the involved stakeholders and the core partners has been essential for the success of Echord++ project.

The Editors would like to introduce this scientific book through the headlines presented at the IROS 2018 Echord++ Forum:

CECILE HUET. It is actually the beginning of a new wave; because Echord++ has been pioneer in many tools, we are now using and mainstreaming in our program. From RIFs (Robotics Innovation Facilities) we have created the Digital Innovation Hubs (DIHs), from Experiments to Financial Support to Third Parties (FSTP) and Cascading Grants; and from PDTI (Public end users Driven Technological Innovation) to Pre-commercial procurements (PcP).

ALOIS KNOLL. Echord and Echord++: From 10 years to now. Bringing industry and academia together with no examples before in an open innovation ecosystem. The structured dialogue between more than 100 partners and more than 1000 individuals has been essential for the success of the project. We put a lot of effort

to convince researchers to not only develop good products and systems but also to make them known with a good high impact.

CHRIS MELHUIS. We want to create the environment for research institutes and robot manufactures to collaborate in innovation, entrepreneurship and industrial engagement to robotic technology. Focus on Small and Medium Enterprises (SMEs), the Research and Innovation Facilities (RIF) experience stimulate the economy and new supply chains helping the SMEs with expertise and reducing their economic risk. Echord++ has launched three RIFs in three European Regions: Bristol, Peccioli and Paris-Saclay. The lessons learned make possible the future Regional Strategies of Europe.

ALBERTO SANFELIU. Into the Innovative Public Procurement Instruments, Echord++ has developed the procedure "Public end-users Driven Technological Innovation (PDTI)". Two PDTI have been developed under Echord++: one in healthcare and one in urban scenarios. Two main objectives have been achieved: Public entities have been aligned with innovative – robotic – solutions to solve their needs improving public services or creating new ones; and new robotic solutions and products have been developed matching the functionalities required close to commercial products and boosting European SMEs.

PAOLO DARIO. The Experiments (EXP) is the main instrument used in Echord++, encouraging and supporting robot industry to bring technology foreword, working together with academia and building excellence. The results are measurable from basic research to real deployment of products and solutions. The EXP procedure, based in high quality, consistency and transparency of the calls preparation, evaluation and selection of the proposals, monitoring and coaching tasks, extraction of results, etc., has been followed in new European and National proposals with great success.

GEOFF PEGMAN. Echord++ has explored different ways in which European funding could be effectively set out to other organizations. Under the slogan "From Lab to Market Place" the three boosting instruments have engaged new key players in the innovation process: robotic manufacturers, end users and public entities have been essential part of the research and development of new products and solutions.

This scientific book represents a summary of the work done during these five years. Part I introduces the procedures of the three Echord++ instruments together with some use case studies, and Part II presents articles explaining some of the scientific and technological achievements.

We thank Professor Alois Knoll, coordinator of the Echord++ consortia and all the core partners as well as the EU project officer Cecile Huet and the reviewers, for their excellent guide through the development of the project. We also want to thank all the participants and the Springer tracts Editors to make possible this edition.

Barcelona, Spain
January 2019

The Editors

Acknowledgements

The Editors would like to acknowledge the researchers that have contributed with their scientific-technological articles to this book. Their participation in the robotic consortia for robotic Echord++ experiments, have brought us the opportunity to join efforts among researchers, companies, public bodies and end users.

This book collects the wide vision of the Echord++ core partners: "European Coordination Hub for Open Robotic Development". The instruments and the procedures developed under Echord++ project have created a robotic ecosystem, which includes the participation of all the stakeholders involved in innovative solutions and products life cycle.

Finally, the Editors thank the decision of Springer Tracts in Advanced Robotics to edit this scientific book and disseminate the Echord++ results over the scientific and technological community.

Contents

Part I Echord++ Instruments

- 1 The European Coordination Hub for Open Robotics Development++: An Overview** 5
Yannick Morel
- 2 The Experiment instrument in ECHORD++: cascade funding for small-scale research projects for facilitating the introduction of robotics technology into industry** 13
Francesca Cecchi and Paolo Dario
- 3 Robotics Innovation Facilities** 27
Farid Dailami, Chris Melhuish, Francesca Cecchi and Christophe Leroux
- 4 Public end-users Driven Technological Innovation (PDTI) in Urban Scenarios** 43
Ana Puig-Pey, Alberto Sanfeliu, Francesc Solé-Parellada, Yolanda Bolea, Josep Casanovas and Antoni Grau

Part II Echord++ Experiments and Contributions

- 5 Lessons Learned in Vineyard Monitoring and Protection from a Ground Autonomous Vehicle** 73
Ferran Roure, Luca Bascetta, Marcel Soler, Matteo Matteucci, Davide Faconti, Jesus-Pablo Gonzalez and Daniel Serrano
- 6 Automatized Switchgear Wiring: An Outline of the WIRES Experiment Results** 95
Gianluca Palli, Salvatore Pirozzi, Maurizio Indovini, Daniele De Gregorio, Riccardo Zanella and Claudio Melchiorri

7	Optimality criteria for the path planning of autonomous industrial vehicles	109
	Marina Raineri, Fabio Ronchini, Simone Perri and Corrado Guarino Lo Bianco	
8	FASTKIT: A Mobile Cable-Driven Parallel Robot for Logistics	123
	Nicolò Pedemonte, Tahir Rasheed, David Marquez-Gamez, Philip Long, Étienne Hocquard, Francois Babin, Charlotte Fouché, Guy Caverot, Alexis Girin and Stéphane Caro	
9	Heuristic Planning for Rough Terrain Locomotion in Presence of External Disturbances and Variable Perception Quality	143
	Michele Focchi, Romeo Orsolino, Marco Camurri, Victor Barasuol, Carlos Mastalli, Darwin G. Caldwell and Claudio Semini	
10	EXOtrainer Project Clinical Evaluation of Gait Training with Exoskeleton in Children with Spinal Muscular Atrophy	183
	Daniel Sanz-Merodio, Gonzalo Puyuelo, Amartya Ganguly, Elena Garces, Ane Goñi and Elena Garcia	
11	Technology for assisting during the Comprehensive Geriatric Assessment process: the ASSESSTRONIC project	199
	Giuseppe Palestra, Consuelo Granata, Isabelle Hupont and Mohamed Chetouani	
12	ARSI: An Aerial Robot for Sewer Inspection	215
	François Chataigner, Pedro Cavestany, Marcel Soler, Carlos Rizzo, Jesús Pablo Gonzalez, Carles Bosch, Jaume Gibert, Antonio Torrente, Raúl Gomez and Daniel Serrano	
13	SIAR: A ground robot solution for semi-autonomous inspection of visitable sewers	237
	David Alejo, Gonzalo Mier, Carlos Marques, Fernando Caballero, Luís Merino and Paulo Alvito	
14	Public Entity role in Robotic Innovation Barcelona participation in Echord++ PDTI Project for Urban Challenges	255
	Javier Varela, Ma José Chesa, Lina Martinez, Silvia Burdons and Josep Garriga	

Part I
Echord++ Instruments

Part I presents first an overview of the ECHORD++ project, with its mission and vision together with a detailed structure of its functionalities and instruments: Experiments, Robotic Innovation Facilities and Public end-user Driven Technology Innovation PDTI.

Chapter 1 explains how the project is born, the partners, the different instruments and the new concept of cascade funding projects. This novelty made ECHORD++ a special project along the huge number of research groups and consortia involved in the whole project. So far, it is the European funded project with more research team and partners involved in the robotic field.

In Chapter 2, one of the instruments in ECHORD++ is explained in detail: RIF. Robotic innovation facilities are a set of laboratories across Europe funded with the project with the goal of hosting consortia involved in any experiment that have special needs when testing their robotic research. In the chapter the three different and specific RIFs will be described and analyzed.

Chapter 3 explains an important instrument in ECHORD++: the Experiments. In this part, a big number of research groups have been involve in short time funded research projects. The chapter explains the management of such Experiments, from the call for participation, the candidate's selection, the monitoring, reviews and funding for each of the 36 experiments funded for Echord.

Chapter 4 is very special because it presents the innovation of funding public end-user driven technology, in particular, robotic technology. The robotic challenge is the key of such an instruments together with the management of the different consortia that participated competitively in the success of the robotic challenge proposed by a public entity, selected also with a very special and innovative process.

Chapter 1

The European Coordination Hub for Open Robotics Development++: An Overview

Yannick Morel

Abstract ECHORD++ is an FP7 project in robotics innovation, and a direct follow-up to the original ECHORD project. In this Chapter, we provide a rapid overview of the aims of the project and of the general context within which it is framed, in particular the manner in which it builds upon achievements of the original project, as well as the place it occupies in the current European research landscape in robotics. Further, we outline the structure of the project, which is organized around a number of distinct Instruments. The goal of the work performed is two-fold, as it is concerned with both achieving concrete, substantial impact in robotic innovation, but also with exploring different processes and support mechanisms to pursue and achieve said innovation. Hereafter, we provide a short overview of the format of the three technical Instruments implemented within the project: Experiments, Robotics Innovation Facilities, and Public end-user Driven Technological Innovation. We discuss the efficacy and relative merits of these different Instruments, and their impact on the European research community in robotics.

1.1 Introduction

The European Coordination Hub for Open Robotics Development++ (ECHORD++, Oct. 2013 to Jan. 2018, [1]) is a direct follow-up to the original ECHORD project (Jan. 2009 to Dec. 2013, [2, 3, 4]), both funded under the European Commission's (EC) 7th Framework Programme (FP7). The original ECHORD manifested itself as somewhat of an exotic animal in the European robotics research landscape of 2009. The fundamental ambition of the project consisted in bringing together robotics academia and industry or, in more general terms, technology providers and technology users, in the pursuit of innovation. At the times, within the European research community, Excellence remained the central focal point, innovation a foreign, if not outright base, notion ([5]). Placing innovation front and center was a bold initiative. This however was by design, the underlying intent being to promote a shift in the academic culture. Stranger and more radical yet, none of the core partners (composing the initial consortium) would perform Research and Technological Development (RTD) work. Instead, this work would be undertaken by (and the majority of the funding passed on to) additional, extended partners, integrated within the consortium over the project's runtime, using a cascade funding scheme.

Yannick Morel

Technische Universität München, Garching bei München, Germany, e-mail: yannick.morel@in.tum.de

The work conducted within ECHORD was structured around two complementary constructs, the Experiments Instrument, and the Structured Dialogue Instrument ([2]). The former is designed around a set of focused (in time and scope) RTD projects, the *Experiments* that gave its name to the Instrument. Core partners in ECHORD motivated proposals for Experiments from the robotics research community through the emission of Calls for Expression of Interest (CEoIs). These calls directly addressed the central focus of the project, Technology Transfer (TT), typically from an academic Experiment partner, to an industrial one. The scope of eligible RTD activities were framed by a number of defined application areas (referred to as Scenarii, e.g. human-robot collaboration), technological foci, and expected maturity level for the Experiment's outcome (from proof of concept to prototypes). Over fifty such Experiments were supported within ECHORD. The second Instrument, referred to as Structured Dialogue, had the ambition to engage conversation between the various (largely heterogeneous) stakeholders involved in robotics research in Europe (and beyond), following a systematic structure to frame exchanges. The concrete objectives being to develop common grounds between parties typically not engaging each others on a regular basis (such as academia and industrial robot manufacturers, for instance), in part to support the Experiments Instrument, but also with the goal of bringing together all actors composing the community, to chart a common way forward for robotics.

ECHORD proved to be a resounding success. Over fifty Experiments were supported over the project's runtime, a significant portion of which brought the developed innovation to market. Due to the breadth of community engagement involved in the project's Instruments, the novelty of the project's structure and of the specific Instruments developed, and owing to the magnitude of the RTD work performed, the project reached a high level of visibility in Europe and worldwide (see for illustration a discussion of the project's achievement by Commissioner Oettinger, [6]). This recognition also likely stemmed from more general, contextual factors, extending beyond robotics. Europe and the world were still in the process of recovering from the 2008 crisis. The political sphere was exploring different avenues to kick-start recovery. In 2014, the EC introduced the notion of a Digital Single Market (DSM), later defining its DSM Strategy (DSMS, [7]) in May of 2015. The intent of the DSMS was to extend the notion of Single Market to digital technologies, and in particular Information and Communication Technology (ICT). In support of its DSMS, the EC launched the Digitisation of European Industry (DEI) initiative in 2016. The premise of this initiative is that supporting and facilitating digital transformation of European industry, in particular gainfully exploiting ICT to transform processes and develop new products, will have a positive impact on industry competitiveness, and a necessary step to maximise the benefit to be withdrawn from the developing DSM (as discussed in [8]). The notion of industry digitisation itself finds its place within the current fourth industrial revolution, commonly referred to as Industry 4.0 (I4.0, [9, 10]).

ECHORD, the vision for which was shaped seven years prior to the DEI initiative, largely foreshadowed and anticipated this trend, the Instruments developed within the project finding themselves not only topical, but also very effective in support digitisation of industry. It is very naturally that the follow-up project ECHORD++, received support to build upon the achievements of the original. The success of ECHORD was predicated not only upon its achievements in terms of TT and innovation (although these were substantial), but also and probably more importantly upon the successful experimentation with a new way to pursue innovation: The Experiments Instrument. Following its success in ECHORD, format of this Instrument was broadly propagated through the European research scene, and has been used in a large number of EC projects. The mechanism has come to be referred to as Funding for Support of Third Party (FSTP, also called cascade funding), use of which is explicitly described within the Horizon 2020 Work Programme (see [11]). The follow-up project ECHORD++ built upon the original's achievements by introducing, in complement to Experiments, two additional technological Instruments, the Robotics Innovation Facilities (RIFs) and the Public end-user Driven Technological Innovation (PDTI) Instruments. The object of these was, at a conceptual level, to explore the efficacy of different setups and formats in pursuing robotics innovation.

Hereafter, we provide a rapid overview of the nature, intent, and first results of these Instruments following their implementation in ECHORD++. The respective Instruments are discussed in greater

detail in later Chapters of this book. Also offered is a short discussion of the impact of the work done in ECHORD++ on the European research landscape, and of its relevance within the frame of the continued digitisation of industry in Europe, in particular attempting to articulate relations between the new innovation mechanisms experimented with in the project, and recent development related to the DEI initiative, such as the upcoming Digital Innovation Hub networks in robotics.

1.2 Technical Instruments

As alluded to in the above, the ECHORD++ project is structured around a number of complementary Instruments. The Structured Dialogue Instrument, introduced in the original ECHORD, is still present, although it has taken somewhat of a secondary role to the three technical Instruments: Experiments, the RIFs, and the PDTI Instrument. All three address the same objective (giving substance to the project's motto *From Lab to Market*), extending support to technology providers and technology users, with the aim to provide conditions that facilitate the emergence of robotic innovation. Barriers to successful innovation are numerous and difficult to overcome (see for instance the discussion on the Valley of Death in [12]), and there exist no pre-made recipe guaranteeing success. Within that context, achievements of the Experiments Instrument developed in ECHORD stood out as very positive. That model was extended within ECHORD++ to include additional support towards productionisation. The RIF model, which can be thought of as a pilot Instrument for the Digital Innovation Hub model (DIH, [8]), explores a different setup and scope for innovation, directly providing technical expertise and access to robotics equipment to innovators. The last technical Instrument discussed, PDTI, explores a novel approach to a notoriously challenging innovation process, Pre-Commercial Procurement (PCP, [13, 14]).

Experiments

The format of the Experiments Instrument remains largely comparable to that developed in ECHORD. Core ECHORD++ project partners framed the scope of the RTD work to be pursued in the Instrument through the definition of targeted application areas (referred to as Scenarii, six of which were defined: Cognitive tools and workers for cognitive factories, general purpose robotic co-workers, cognitive logistics robots, medical robotics, agricultural and food robotics, and urban robotics), and four distinct technical areas (or Research Foci: Practical machine cognition, advanced perception and action capabilities, cooperative mobile manipulators, and system architectures, systems, software engineering, processes and tools). Two CEoIs were conducted, with a first set of fifteen Experiments joining the project and beginning RTD work in early 2015, and a second group of sixteen in mid-2016. The expected duration of each Experiment is eighteen months, with financial support of the order of €300,000.

The Experiments Instrument distinguishes itself in a number of key respects. In particular, the emphasis on innovation is pervasive throughout the process, from preferred Experiment consortium composition (including both technology provider and user, with the addition of a system integrator to facilitate TT when relevant, see the second CEoI's guide for applicants, [15]), to the development of an exploitation plan by each Experiment consortium (discussed during Experiments' kickoff events, followed-up through periodic monitoring over the Experiment's lifetime, and evaluated in final Experiments reviews), to the encouraged (and facilitated) participation to relevant professional fairs (raising visibility for the product developed), up to the implementation of measures for productionisation support, post-Experiment runtime (in the form of the Experiment Booster programme, further discussed in a later Chapter).

Another distinguishing feature is the nature of the support provided by the core ECHORD++ partners to Experiments partners, in terms of breadth, of frequency of exchanges, but also in terms of the procedural agility necessary to place Experiments in the best position to succeed.

In particular, the aforementioned emphasis on innovation implies the delivery of support services extending well beyond the sole provision of financial support. More specifically, services in terms of networking (brokerage days, Instrument-specific and project-wide community events), Public Relations (PR, support including coaching of Experiments partner, definition of PR plan, invitation to high-profile professional fairs, organisation of Instrument- or project-wide PR events), support for administrative aspects (in the form of a service desk, accessible to all Experiment partners), and support for productisation, business planning and development.

The structure of the Experiments Instrument, as detailed in the project's Description of Work, calls for frequent interactions between Experiment partners, performing RTD work, and core partners, providing support (as discussed above), but also monitoring progress of the Experiment. The monitoring process is organized around two-monthly calls, on the occasion of which Experimenters report recent progress, setbacks encountered and corresponding possible deviations. The content of these calls is not limited to technical aspects but also includes discussion of PR activities and refinement of the business plan for the developed product. Exchanges are supported by a dedicated online infrastructure, centralising relevant documents (in particular deliverables), and keeping track of deadlines, milestones, status of Key Performance Indicators (KPIs) and of the general progress of the Experiment. This frequency of monitoring calls is, relative to usual project progress-tracking procedures, high. In practice however, monitoring procedures, and more generally the specifics of the support provided, was adjusted for each Experiment, based on particular needs identified. In other words, we observed tremendous heterogeneity, in the different Experiments funded, in terms of the nature of the work being conducted, the maturity of the technologies involved, and the experience (and conversely, needs) of the Experiment consortium partners in different aspects (technical expertise, PR, business development). Adjusting the support provided in accordance has proved a key factor to success, although the implied agility in implementation of project procedures requires significant efforts from the core consortium partners overseeing the Instrument.

It is still very early to assess success of the Experiments Instrument in ECHORD++. The experience from ECHORD has shown that, in many instances, it takes time for the impact of the work performed to coalesce and take concrete substance. Specifically, although the ambition of the instrument clearly is to achieve the development of a product, in most cases the prototype developed requires additional efforts and investments to achieve the maturity necessary for market introduction. Aspects including system qualification, certification, and prototype industrialisation, for example, are all fairly effort- and time-intensive. Few Experiments are able to complete them within the relatively short project duration (eighteen months). In some cases, it is only years after the corresponding ECHORD Experiment came to an end that successful businesses were established. Nevertheless, early indicators are very positives; ECHORD++ Experiments already sold for over €1 million worth of robotic products in 2017, and a total of six different products, developed in the ECHORD++ Experiments Instrument, are expected to reach market (that is, Technology Readiness Level 9) by the end of 2018.

Robotic Innovation Facilities

The ECHORD++ Robotic Innovation Facilities (RIFs) form a network of Competence Centers (CCs) in robotics. They offer support in the form of access to equipment and expertise in robotics to interested beneficiaries. The network is composed of three different RIFs, located in Bristol (hosted by the Bristol Robotics Laboratory, BRL), in Paris-Saclay (at the Commissariat à l'Energie Atomique et aux Energies Alternatives, CEA), and in Peccioli (at the Scuola superiore Sant'Anna, SSSA). the particular form of the support extended to beneficiaries differed greatly depending on the specifics of the considered collaborations, however the prototypical RIF technical project was conducted over a duration of six weeks, in collaboration between the external beneficiary and RIF personnel. Relative to technical activities in Experiments, the scope here is narrower, and work is generally performed at lower Technology Readiness Levels (TRL). In particular, Experiments are expected to lead to the development of a system beyond laboratory prototype (that is, TRL5 and above).

Conversely, the target at the end of the six week RIF collaboration is a Proof of Concept (PoC, TRL3).

In contrast to the Experiments Instrument, which built upon the strong foundation laid in the original ECHORD, the RIFs were completely new to ECHORD++. The implementation of the Instrument and the response of the target audience differed from expectations in a number of key respects. In particular, procedures regimenting the work performed in the Instrument were designed to bring the barrier of entry as low as possible; potential beneficiaries need only identify which of the three RIFs has the resources (expertise and equipment) to support the desired collaboration, close to no paperwork is required (no more than a few pages describing the technical work foreseen and expected impact), the service is provided free of charge, and Intellectual Property of the foreground developed in the collaboration is left to the beneficiary. Accordingly, the expectation was that the RIFs would field large numbers of solicitations from prospective beneficiaries.

Reality proved somewhat different. In particular, if the RIFs did achieve a high volume of activities over the duration of the project (in excess of a hundred technical collaborations), the efforts required from the RIFs to motivate participation of beneficiaries proved significant. Value of the service provided did not appear to be self-evident, at least initially. Motivating active participation of the Instrument's core target audience (Small and Medium-sized Enterprises, SMEs) has demanded time, efforts, and pedagogy. In addition, the RIFs initially expected to develop collaborations with beneficiaries from across most of Europe. Instead, the overwhelming majority of successful RIF collaborations were developed with beneficiaries located in relative proximity to the RIFs' facilities.

These unexpected developments did not, however, prevent the RIF Instrument from achieving a significant impact. RIF collaborations have directly led to the creation of several startups, some of which have secured financial support from venture capital well in excess of €1 million. In addition, a significant number of the PoCs developed in collaboration with industry have led to the development of new products (or improvement to existing ones). Finally, the RIFs proved very successful in experimenting with different additional services in complement to the typical six-week technical collaboration, including: Educational workshops, Intellectual Property (IP) management support, networking support, connecting innovators with venture capital and system integrators, as well as due diligence services for investors in robotics, to name but a few. The insights gathered are of particular relevance to the networks of robotics Digital Innovation Hubs (DIHs) in the process of being established at time of writing, and which constitute spiritual successors to the ECHORD++ RIF network.

Public end-user Driven Technological Innovation

The Public end-user Driven Technological Innovation (PDTI) Instrument explores the active involvement of a public end-user in the robotics innovation process. In practice, the Instrument has strong similarities with Pre-Commercial Procurement (PCP, [16]), process widely acknowledged as challenging to enact (see the discussion of barriers to PCP in [17]). The PDTI process, as implemented in ECHORD++, involved the following steps. Initially, a set of relevant application areas, within which robotic technology could be expected to provide tools for innovation, were identified. Core ECHORD++ project members then motivated the definition of innovation challenges (corresponding to specific technological needs) in these application areas by European public bodies. A panel of experts ranked the proposed challenges, the top two being used as a basis for CEOs soliciting proposals for robotic solutions by RTD consortia.

The two selected challenges were in the areas of healthcare (specifically, Comprehensive Geriatric Assessment, CGA), and urban robotics (monitoring of sewer networks). For each challenge, three RTD consortia were initially selected. The subsequent steps in the process emulate those involved in a PCP, with three successive (and competitive) development phases, the first dedicated to solution design, the second to prototype development, the third to the implementation of a pre-commercial solution (see [16]). The significant differentiating factor of PDTI with respect to typical implementations of PCP consists in the development of involved intermediation processes,

between RTD consortia and public bodies, led by core ECHORD++ project partners. These processes have taken a form comparable to that of the monitoring procedures developed for the Experiments Instrument, and present a number of similarities to methods implemented for Public Procurement of Innovation ([18]).

The PDTI Instrument is still active at time of writing, it is accordingly difficult to assess the degree of success of the Instrument. However, early indicators are very positive. Involved RTD teams, two of which having proceeded to the third phase in each challenge, have managed to generate interest from a range of possible end-users for the technology developed. In many cases, this interest was for applications extending beyond those considered in their respective challenges, showing interesting potential for the technology to scale to different types of problems.

1.3 Conclusion

The ECHORD programme, comprising both the original project and its follow-up ECHORD++, has spanned a decade, starting in 2009 and concluding in January 2019. While its impact in terms of innovation (generating new products, new services, new processes) is sizeable, its main contribution to the community likely has been in its role as a laboratory, experimenting novel innovation procedures. ECHORD introduced cascade funding ten years ago; FSTP is now seemingly ubiquitous across the robotics research community (see, among many others, the H2020 projects RoboTT-Net, HORSE, RobotUnion), and beyond (it is for instance used in the Human Brain Project to promote community inclusiveness). ECHORD++ implemented the RIFs, a network of CCs providing technical support (and more) for robotics innovation. The RIFs' brainchilts, the DIH networks in robotics, will begin operation in 2019. Finally, the challenge-based innovation procedures implemented in ESMERA (another H2020 project) show shades of PDTI, mixed with the now usual FSTP model.

Another contribution of the ECHORD programme however, which has not heretofore been discussed, is its contribution to the emergence of a close-knit community for robotic research in Europe. The ECHORD network, composed of researchers, engineers, managers and more, having directly participated in the projects as core or extended partners, or taken part in proposal evaluations, Experiment or PDTI reviews, counts several thousands of the best experts in the field in Europe (the ECHORD contact list features over four thousand entries). Bringing these people together, lowering the entry barrier into European research for the growth and benefit of the community, providing the substrate over which new, successful, lasting collaborations emerge and grow, arguably constitutes the more significant contribution of ECHORD to robotics research in Europe.

References

1. echord.eu accessed: 2018-10-11
2. Röhrbein, F., Veiga, G., Natale, C.: Gearing up and accelerating cross-fertilization between academic and industrial robotics research in Europe: Technology transfer experiments from the ECHORD project **94**, Springer (2013)
3. Knoll, A., Siciliano, B., Pires, N., Lafrenz, R.: Echord- the new face of academia-industry collaboration in European robotics, *IEEE Robotics & Automation Magazine* **17(4)** 21-22 (2010)
4. <http://www.echord.info/> accessed: 2018-10-11
5. Boni, A.A., Weingart, L.R., Evenson, S.: Innovation in an academic setting: Designing and leading a business through market-focused, interdisciplinary teams. *Academy of Management Learning & Education* **8(3)**, 407-417 (2009)
6. Vom labor auf den markt, *Süddeutsche Zeitung* (2016)
7. A digital single market strategy for Europe. Communication from the European Commission (2015)

8. Digitising European industry reaping the full benefits of a digital single market. Communication from the European Commission (2016)
9. Lasi, H., Fettke, P., Kemper, H.G., Feld, T., Hoffmann, M.: Industry 4.0, Business & Information Systems Engineering **6(4)**, 239-242 (2014)
10. Semolic, B., Steyn, P.: Industry 4.0 collaborative Research, Innovation and Development (RID) projects. Project Management World Journal **7** (2018)
11. Actions involving financial support to third parties, Annex K, HORIZON-2020 Work Programme (2016)
12. Markham, S.K., Ward, S.J., Aiman-Smith, L., Kingon, A.I.: The valley of death as context for role theory in product innovation. Journal of Product Innovation Management **27(3)**, 402-417 (2010)
13. Edquist, C., Zabala-Iturriagoitia, J.M.: Public procurement for innovation as mission-oriented innovation policy. Research policy **41(10)**, 1757-1769 (2012)
14. Edquist, C., Zabala-Iturriagoitia, J.M.: Pre-commercial procurement: a demand or supply policy instrument in relation to innovation?. R&D Management **45(2)**, 147-160 (2015)
15. Guide for applicants: ECHORD++ Experiments Call 2. <http://echord.eu/portal/ProposalDocuments/download/6> accessed: 2018-10-11
16. Bos, L.: Pre-commercial procurement, European Commission: Strategy for ICT research and Innovation Unit (2008)
17. Turkama, P., Zálisová, I., Rolfstam, M., Ikävalko, S., de Oliveira, Á., Nina, M.: Policy recommendations for advancing PCP in Europe, FP7 CSA Enhancing Innovation in Pre-commercial Public Purchasing Processes, PreCo (2011)
18. Edler, J., Yeow, J.: Connecting demand and supply: The role of intermediation in public procurement of innovation. Research Policy **45(2)**, 414-426 (2016)

Chapter 2

The Experiment instrument in ECHORD++: cascade funding for small-scale research projects for facilitating the introduction of robotics technology into industry

Francesca Cecchi and Paolo Dario

Abstract ECHORD++ funds small-scale research projects called experiments with a maximum duration of 18 months. Cooperative research is done in academia-industry consortia, based on actual used cases. This article describes the procedure, the phases and the results reached under Echord++ Experiments instrument, encouraging and supporting robotic academia and industry in Europe, working together in tailor made solutions for their technological challenges. As the authors say, thanks to the effort spent in the first ECHORD and in the current ECHORD++, the Experiments instrument is now solid and ready to be seen as an example of good practice in cascade funding.

2.1 Introduction

As new branches of robot automation emerge, such as small, lot-size production of variants in SMEs, including such areas as (factory) logistics, recycling, human-care, security, home appliances, edutainment, personal robot companions, etc., radically new designs of robot systems are needed. With the competition in robotics ever increasing, (especially between Japan and Europe), cutting-edge technology will be the decisive factor which determines success. We believe Europe can achieve the "cutting-edge" advantage through a very close collaboration of robot manufacturers and research institutes. Thus, the E++ experiments overall objective is to encourage and support Europe's robot industry to bring technology forward and to build up excellence in well-defined areas. Within the experiments instrument, incentives are provided to encourage European robot manufacturers and research institutes to work together on an operational level, with tangible and measurable results to accelerate the development of technologies and their deployment into new application scenarios. It is worth saying that the experiments instrument is a well-proven backbone of the ECHORD project and it has been revised and improved in the ECHORD++ project. An experiment is a small to medium sized scientific research and/or technology development project carried out by a team of one or more research institutions and robot manufacturers, which typically lasts 18 months. They have clearly defined goals in terms of quantifiable technological advancement in the areas described in the research focus. Two or more partners collaborate within each experiment. These small projects are expected to result in both tangible and measurable outcomes in terms of the accelerated development of technologies, as well as the deployment of robotics technology into

F.Cecchi and P.Dario

Scuola Superiore Sant'Anna, Pisa, Italy, e-mail: frances-ca.cecchi@santannapisa.it; e-mail: paolo.dario@sssup.it

new scenarios for the direct application of the research results. Each experiment has a funding of 300.000€ given by the ECHORD++ Consortium as a cascade funding structure.

2.2 Materials and Methods

Different phases have been developed in order to successfully coach, evaluate, select and monitor the 31 funded experiments. The phases are six and are the following (see Fig.2.1):

- Phase I: Preparatory Activities
- Phase II: Consultation and coaching of experimenting partners
- Phase III: Call Issue
- Phase IV: Evaluation and Selection
- Phase V: Monitoring and Review
- Phase VI: Results Extraction and Exploitation

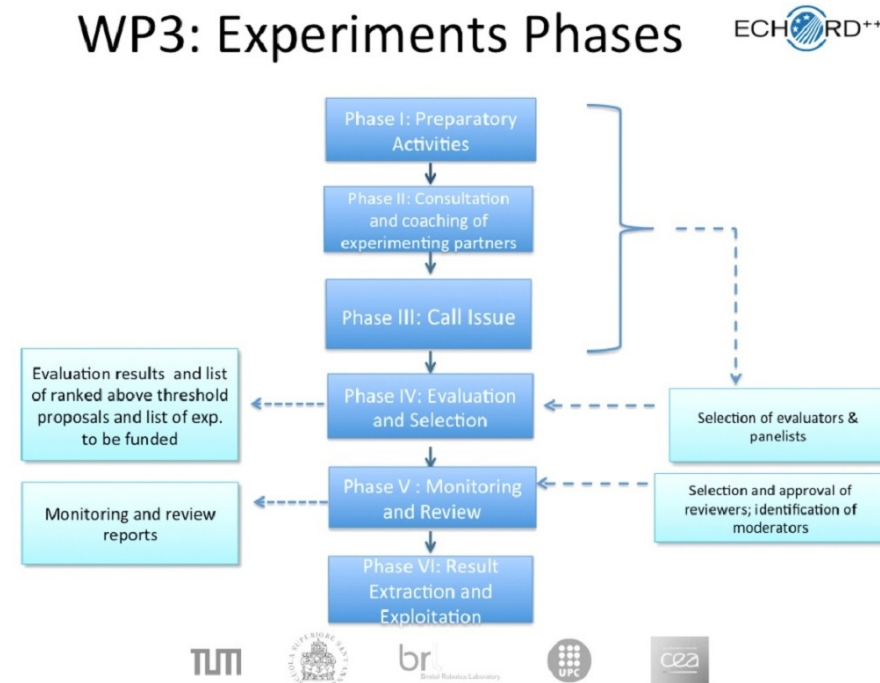


Fig. 2.1: Experiment Phases

In the following paragraph the deepened description of each phase. Two have been the Calls executed in order to fund 31 experiments. Such phases have been executed for each call.

2.2.1 Phase I: preparatory activities

The preparatory activities aim at improving and optimizing the application and the management processes of the experiments.

2.2.1.1 Templates and guidelines

Guidelines and the templates for pre-proposal, proposal, evaluation and correct delivery of the experiment were prepared and delivered (see Fig.2.2).

	Pre-proposal	Proposal	Experiments
Applicants	Pre-proposal template	<ul style="list-style-type: none"> Proposal template ECHORD++'s guide for applicants 	
Experts	Template for the evaluation of Pre-Proposal	<ul style="list-style-type: none"> Templates for the Evaluation of Proposal <ul style="list-style-type: none"> Individual Evaluation Report (IER) Draft Consensus Report Evaluation Summary Report (ESR) Guide for Independent Experts Evaluation Platform HOW TO 	
Experimenters			Guide for experimenters

Fig. 2.2: Templates and guidelines prepared

The proposal template is obtained through a more structured division and adding sub-paragraph such as "Concept, methodology and associated work plan", "Expected results" and "Exploitation plan of experiments results and management of knowledge and of intellectual property", with requirements as "Proofs-of-concept, prototypes, products" and "Dissemination plan of experiment results".

In addition, the instrument of RIF is defined as one indicator to assess the impact and the feasibility of the experiments.

Videos and any multimedia material are required as mandatory proof of "transfer output".

As a consequence, the templates are modified accordingly in order to include a plan for dissemination and outreach activities and description of impact and bring-to-market process.

2.2.1.1.1 Guide for applicants

The development of ECHORD++'s guide for applicants has seen different steps:

1. The introduction of a Glossary of Terms at the beginning of the document, to help applicants to go through the text and to fix the main concepts,

2. A general update of the information (new scenarios and research foci and evaluation criteria) and the addition of the new ECHORD++ instruments (i.e.: RIFs),
3. A shorter background description through the differentiation in different paragraphs on: General information, Types of Experiment, Scenarios and Research Foci,
4. The description of Scenarios, Research Foci and RIFs is just briefly reported in the main contents since wider information are provided in three different Annexes,
5. The addition of the description of the link between Experiments and RIFs to help the comprehension of the RIFs' scope in the experiment process.

The final aim was to provide a clear set of instructions in order to receive optimal proposals. Three documents were developed to support Phase IV (selection and evaluation):

1. the template for the evaluation of Pre-Proposal,
2. the templates for the Evaluation of Proposal,
3. the Guide for Independent Experts.

2.2.1.1.2 Pre-proposal evaluation template

In order to facilitate a correct and effective evaluation of pre-proposals, the template to be fulfilled by the evaluators is structured with specific questions that matched the ones asked to applicants in the pre-proposal form. In order to help evaluators to give a clear, strict and homogeneous feedback, suggested answers are provided too.

Once collected the answers, the evaluator is required to submit the feedback (within 5 business days) following a suggested template form.

2.2.1.1.3 Proposal evaluation template

The templates for the evaluation of proposals are divided in three: an Individual Evaluation Report (IER), who is developed by answering to five questions for each Section (Scientific and/or technological Excellence, Impact and Implementation); a Draft Consensus Report, which is a document filled by the rapporteur as summary of the result of the individual evaluations (IER) and it is structured as the summary of the arguments of each evaluator for each section and the Evaluation Summary Report (ESR), which is developed by the rapporteur, summarizing the views of the evaluators.

2.2.1.1.4 Guide for Independent Experts

The guide for independent experts was structured as follows:

1. an initial glossary of terms,
2. an introduction on the project and the final aim of the call,
3. description of the evaluation process:
 - a. evaluation steps,
 - b. evaluation criteria,
 - c. How to score,
 - d. directions for rapporteurs,
 - e. obtain the final scores,
 - f. conditions to involve a third evaluator,
 - g. rules for Conflicts of Interest,
 - h. evaluation timing

2.2.1.1.5 Evaluation platform: HOW TO (for experts)

The experts are provided also of a guide to correctly use the web-based evaluation platform. The guide describes the web platform functionality in order to implement the evaluation of proposals. It is structured as follows:

1. an initial summary of the evaluation process and deadlines,
2. instructions on how to access the proposals,
3. description of the independent evaluation:
 - a. evaluator role,
 - b. rapporteur role,
4. description on how obtain consensus,
5. description on how accept consensus.

2.2.1.1.6 Guide for Experimenters

The experimenters, once funded, receive a Guide for Experimenters to explain the experiment monitoring and reporting activities required by the project. The guide also contains the description of the experiments web platform and information on how to use it correctly.

The guide is structured as follows:

1. description of the scope of the guide,
2. description of the monitoring and reporting activities,
 - a. technical HOW TO use the web platform (how to log in, how to select the experiment section, description of the experiment dashboard, how to enter data for a monitoring period, how to fill in the report).

2.2.1.2 Database

Three databases were set up to disseminate the opportunity of E++ project: one for potential applicants (1386 contacts), one for manufacturers (136 contacts) and one for independent experts (366 contacts). A big effort was due to create a solid evaluators' list. Starting from ECHORD's one, in the first Call 43 industrial and 11 research experts have been contacted while in the second Call other 7 industrial and 3 research experts have been added.

2.2.1.3 Manufacturer list

As in ECHORD, manufacturers were asked to offer hardware at special prices for E++ activities. This list was published, but there has not been systematic handling of hardware purchase. The reasons are the huge amount of issues with depreciation and the relative high volume of non-list-equipment that ECHORD experienced. But in order to facilitate the purchase of standardized hardware, the product "catalogue" has been uploaded and updated in E++'s website just for registered users.

The total number of offers received was 76 in categories such as: robotic arms with different payload, mobile platforms, parallel kinematics, controller hardware (if not included in robot), sensor equipment and software.

2.2.1.4 Evaluators contract

For each evaluator, a web based expertise profile has been developed in order to facilitate the matching with the proposals and obtain an appropriate assignment. The expertise profile has been obtained from keywords provided by each of them when registering on the evaluator's portal.

Once the assignment is completed, an email is sent to all evaluators acting as a contract request with the following attachments:

- guide for Independent Experts: guidelines to be followed in order to develop a proper evaluation,
- conditions of Appointment: information about Conflict of Interest and Code of Conduct for Independent Experts,
- reply form of acceptance: form to be signed by each expert in order to be legally authorized to develop the assigned evaluations,
- appointment Letter: letter signed by the WP leader (Prof. Paolo Dario) at-testing the request to act as evaluator for the reported proposals assigned to each expert.

Only once received the signed reply form and downloaded both the "Guide for Experts" and the "How to" guidance to use the website, the expert had the access to the proposals assigned to him.

2.2.2 Phase II: Consultation and coaching of experimenting partners

In the second phase, contacts collected in the database were contacted through emails in order to first present ECHORD++ and then ask for their participation/contribution.

A team of customer service was developed with the aim to answer potential applicants' questions through phone and email.

In addition, in order to help potential applicants, common raised questions were collected and whose answers published on the web site in the "Frequently Asked Questions" section.

2.2.3 Phase III: Call issue

Phase III concerns the call issue. In E++ the call text provides information about the opening and the deadline of the call, the definition of experiment, the scope, the list of scenarios and the website link in which find more information. The Call 1 was opened on the 3.3.2014 and the deadline was on the 14.4.2014, 17:00 Brussels time and it was published in the following newspapers:

- Gazeta Wyborcza (Poland), 3rd March 2014
- EXPANSION (Spain), 3rd March 2014
- Les Echos (France), 4th March 2014.

It was also published in the magazine "the Engineer" (UK) on March 10th, 2014. The Call 2 was opened on the 4.5.2015 and the deadline was on the 23.6.2015, 17:00 Brussels time. The call was published in the following media

- Lietuvos Rytas (Lithuania) 12.05.2015
- Pravda (Slovakia) 12.05.2015
- Novi List (Croatia) 12.05.2015

It was also published in the magazine "EE times" (UK) in the May 15 issue as well as through the typical mailing lists such as eurobotics-dist, social networks, especially LinkedIn, and through the ECHORD++ web site. Call 1 re-sulted in 137 eligible proposals, while Call 2 in 114.

2.2.4 Phase IV: Evaluation and selection

The evaluation of Pre-Proposal is developed internally among the Core Consortium based on the competence of each member.

Each pre-proposal is evaluated by one member through the template developed in Phase I. A formal response has been provided within 5 business days.

The chance to submit the pre-proposal was given just in the first 3 weeks of the call and it was not mandatory but a service to support applicants and improve their proposals.

The workflow of the Evaluation of Pre-Proposal is shown in Fig.2.3.

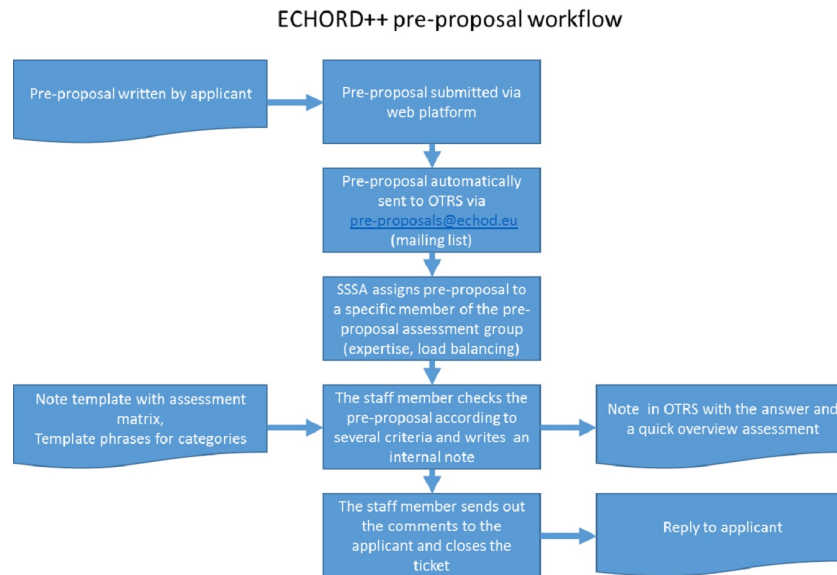


Fig. 2.3: Pre-Proposal Workflow

The evaluation of proposals is composed by different steps, see Fig.2.4. For each proposal, two evaluators and one moderator (called "rapporteur") are assigned, starting from the database of experts developed in Phase II. The assignment is based on the evaluators' expertise profile that had to match with the scenario and application of the proposal.

The evaluation process has been developed in 3 steps:

1. Step 1: a remote evaluation, in which the full proposal is evaluated by two anonymous independent experts who have to provide two individual evaluation reports (IER). The two IER's arguments have then to be converted into Individual Provisional Marks and compared. In contentious evaluations, with remarkable differences between experts' opinions, the rapporteur has to develop a third evaluation, compiling his own IER. In the end, the arguments of all three evaluators have to be combined.
2. Step 2: the provisional marks are computed by the rapporteur as a result of argument counts of the 2 (or 3) IERs, and reported in a Consensus Draft. Consequentially, there is a Consensus Blog discussion between the rapporteur and the evaluators in which the provisional marks are turned into a final score. The final marking is based too on the comments of the evaluators made on the appropriate Consensus Blog via web platform and not on the arithmetical mean of the argument

counts. The evaluators explicitly agree on the final mark for each criterion and consensus report. This report is then sent to the proposers after the evaluation phase. The rapporteur is in charge of writing a consensus report (Evaluation Summary Report, ESR), summarizing the views of the evaluators.

3. Step 3: once all the evaluations are completed and the ESRs ready, an on-site panel meeting has to take place, where a ranking of the proposals is established and the scores of the proposals calibrated. The panel meeting is held with a subset of experts who have acted as evaluators and/or rapporteurs. The final ranking has to be approved by the European Commission.

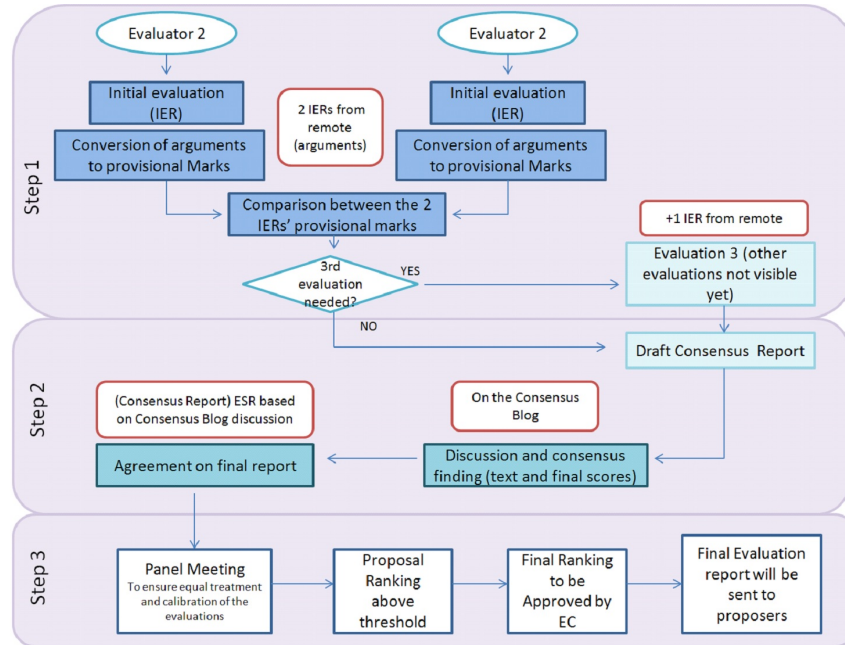


Fig. 2.4: ECHORD++ Evaluation Process Workflow

The proposals are evaluated by experts on the basis of three criteria:

1. Scientific and/or technological excellence relevant to the scenario and research focus.
2. Quality and efficiency of the implementation and the management.
3. Potential impact through the development, dissemination and use of project results.

For each criterion, a score from 0 (lowest) to 5 (highest) is assigned, half points are also allowed. The threshold for possible funding is 3 in each criterion, with the sum of all three marks not being less than 10.

The panel decides to use the following rules in the prioritizing procedure of the proposals:

- a Proposals are ranked by higher total score.
- b When there are an equal total score, groups of proposals with the same total scores are to be formed.

- c Within each group, the proposals are ranked by higher score for criterion 3, i.e. impact. As this issue is especially important in the ECHORD++ experiment scheme, the experts are asked to have a very close look at the expected exploitation, which includes the "transfer excellence" and a potential route to the market.
- d When, within a batch, there is an equal score for criterion 3 between the proposals, the proposals are ranked by higher score for criterion 1, i.e. scientific and/or technological excellence.
- e For proposals in the same group and with equal scores on all criteria, the panel decides in a comparative manner, based on the nature of the proposals' topics. The main aspects of the proposals are carefully analyzed to assess the match of the proposal's goals with the ECHORD overall goals and the panel agreed on their relative order in a consensual way.

These rules are applied in consecutive order until the final prioritization is achieved. This procedure is usually only applied to proposals that scored above thresholds. In the following, proposals with 10.0 or more points, but with one or more criterion failing the individual threshold of 3.0 are not listed.

A proposal will only be considered eligible if it meets all of the following conditions: (i) it is received before the deadline given in the call text, (ii) template and web forms (all sections!) are completed. The proposal must be submitted by legal entities which have been established in one of the member states of the EU or in an associated country.

2.2.5 Phase V: Monitoring and review

The monitoring of the experiments is developed by two moderators that belong to the Core Consortium: one technical and one managerial for each experiment. The technical moderator has to check the technical progress of the experiment, ensure the correct adherence to the agreed activity plan and support the experimenters when technical issues arise. The managerial moderator has to keep track of the deadline in providing deliverables, bi-monthly self-assessments and KPIs.

To foster the importance of impact creation, the monitoring procedure was re-vised and improved by adding technical and impact-related Performance indicators (KPIs), which were jointly defined within ECHORD++ core staff and the experiment partners for each single experiment. Additionally, ECHORD++ core staff has been supporting the experiments selecting the right communication channels and events with a special focus on the expected impact for each single experiment. Every two months, the experimenters are asked to report about the recent progress, through the monitoring platform. This is not intended to be in the form of lengthy reports, but rather in form of images, videos, drawings, etc. The experiments are also asked to provide:

1. Deliverables
2. Justifications to the completed milestones
3. Justifications to the completed technical, dissemination or impact related KPI

The experimenters are strongly encouraged to provide videos and any multimedia material. After each bimonthly self-assessment a telco is usually set for each experiment in order to discuss with the two assigned moderators the progresses, the criticality and clarify the use of the portal. The progress of each experiment is then mapped through bimonthly traffic lights that set their developments in the different areas. The "one page overview" sheet immediately delivers a top view of all experiments and "red", "yellow" and "green" areas of all the experiments are easily identified. For the underperforming experiments different actions were taken such increase the number of teleconference calls or set a Mid Term Review with external experts.

2.2.6 Phase VI: Results extraction and exploitation

Each experiment ends with a Final Review Onsite. For each Review two experts has to evaluate the project: one external and one internal of the Consortium of E++. Prior the onsite review, every experiment has to develop a Final Report and a questionnaire in order to provide information on the value chain developed, as requested by the reviewer, and having the following information: TRL, number of patents, number of jobs created, turn over from the experiment, applications in number of other areas. The evaluators, prior the onsite review, must have studied the project and all the material produced by the experimenters. During the review, they have to actively participate and provide two evaluation documents: one specific on the quality of deliverables, milestone, KPIs; one general recommendation of the project.

2.3 Results

2.3.1 Proposal

In Call 1 137 proposals have been received, while in Call 2 114. In Call 1 31% of organizations that have been funded were SMEs, whose number increased in Call 2 up to 38% (see Fig.2.5).

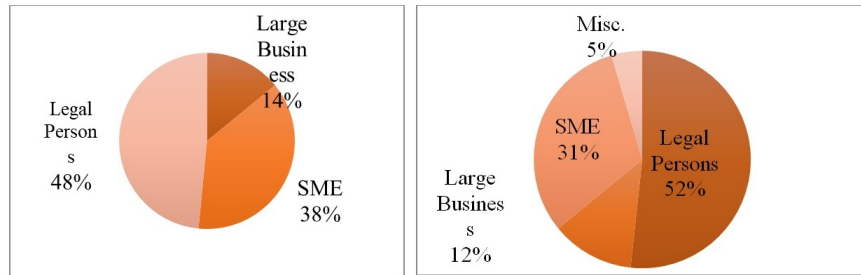


Fig. 2.5: Organizations distribution of proposal received: Call 1 (on the left) and Call 2 (on the right)

In Call 1 the countries that applied most were Italy, Germany and Spain while in Call 2 Italy, France, Spain and UK (see Fig.2.6).

2.3.2 Evaluators

Of the almost 400 experts contacted, in 54 acted as experts in Call 1, while in 37 in Call 2. The background distribution of the evaluators is reported in Fig.2.7, increasing the percentage of Industry background of 10% compared to the First Call. Note that some of the experts from academia had an industry-related background.

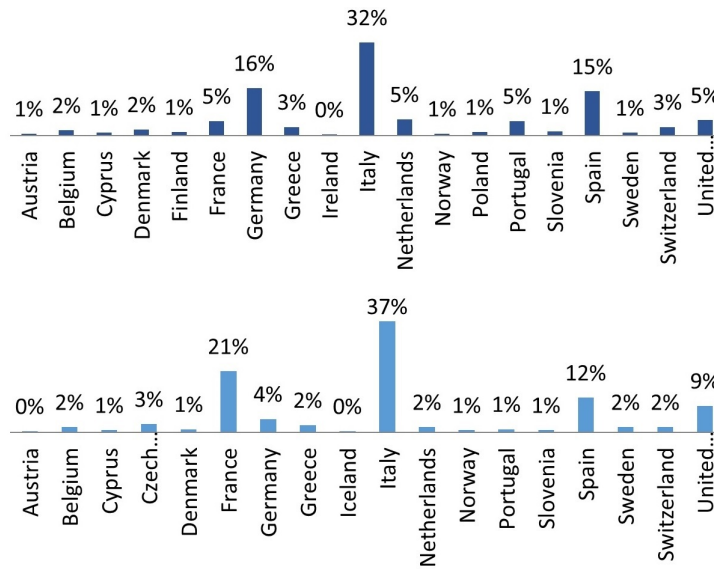


Fig. 2.6: Countries distribution of proposal received: Call 1 (on the top) and Call 2 (on the bottom)

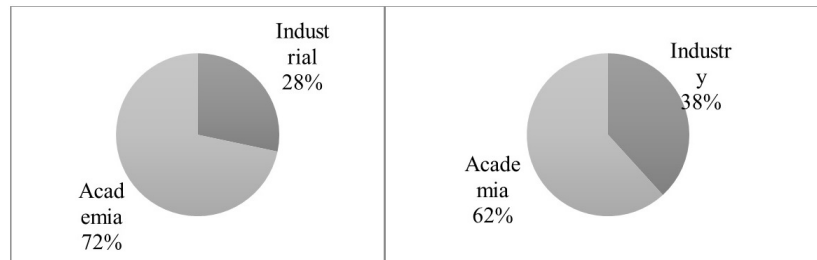


Fig. 2.7: Background distribution of evaluators: Call 1 (on the left) and Call 2 (on the right)

In call 1 the assignment of mixed experts (meaning at least one industrial and two academics) was of 66% and increased to 87% in Call 2. The other 13% was assigned to academic experts in which at least one of the three experts had industrial competences (see Fig.2.8).

2.3.3 Experiments selected/founded

In Call 1, 16 proposals were selected for funding. 8 out of the 16 selected proposals addressed the General Purpose Robotic co-workers, 3 proposals the Medical Robotics scenario, 3 proposals the Agricultural and Food robotics scenario, and 2 the Cognitive Tools and workers for Cognitive

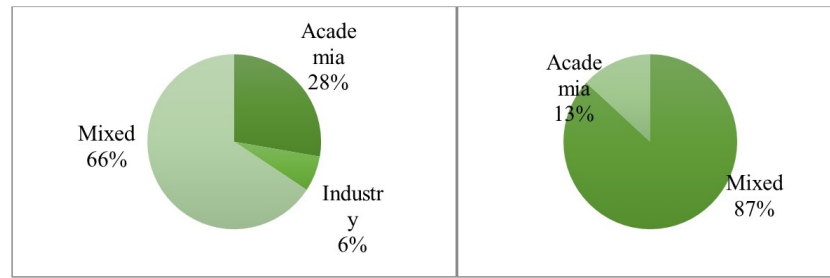


Fig. 2.8: Proposal assignment distribution of evaluators: Call 1 (on the left) and Call 2 (on the right)

Factories scenario (Fig.2.9, left). In Call 2, 16 proposals were selected for funding where 4 addressed the General Purpose Robotic co-workers, 4 proposals the Agricultural and Food robotics scenario, 5 the Cognitive Tools and workers for Cognitive Factories scenario and 3 Cognitive Logistics Robots, demonstrating a more balanced results compared to Call 1 (where General purpose had 50%, Agricultural and Food robotics had 19%, Cognitive Tools and workers 13% and nobody chose Cognitive Logistics Robots). No experiments address the Medical Scenario, either the Urban Scenario (Fig.2.9, right).

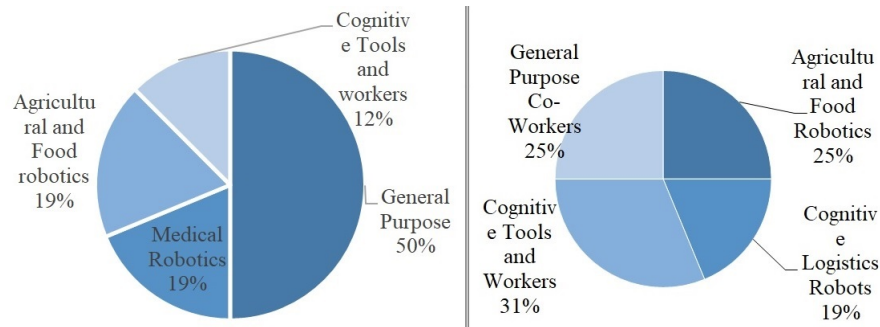


Fig. 2.9: Scenarios distribution of selected experiments: Call 1 (on the left) and Call 2 (on the right)

While in Call 1 SMEs represented the category most selected (43%) in Call 2 Legal person (meaning research institutes, foundations, etc...) resulted to be the most prominent presence (Fig.2.10).

In Call 2 the majority of the proposals showed a good scientific and/or technological quality (average 4,47/5, compared to 4,2/5 of Call 1), and even the average scores for the other criteria shows a high-quality level (4,25/5 for the Quality score, compared to 4,167/5 of Call and 4,44/5 for Impact score compared to 4,067/5 of Call 1). This proves that the chosen format of proposals allows for a lean and precise description of experiments, and the impact end exploitation descriptions have improved compared to the first call.

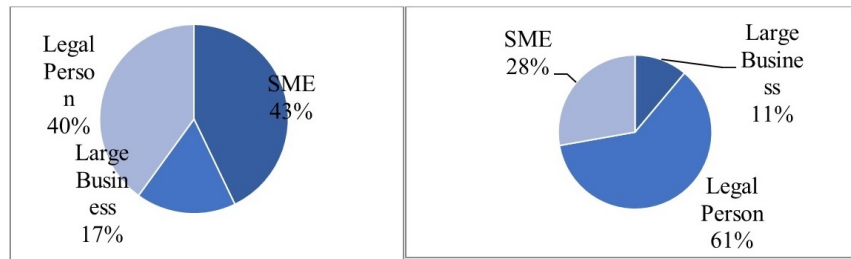


Fig. 2.10: Organizations distribution of selected experiments: Call 1 (on the left) and Call 2 (on the right)

2.3.4 Results extraction

The results are referred to Call I Experiments since Call II Experiments are still ongoing. The majority of the experiments (39%) claimed to have reached a TRL7, while the 25% reached TRL 5, and 19% TRL 6, see Fig.2.11.

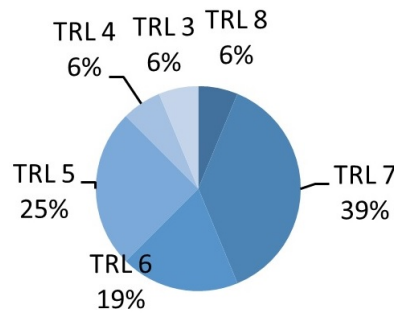


Fig. 2.11: Distribution of TRL at the end of Call 1 experiments

The 87% of the experiments will increase the TRL in two Years. Among them 31% will arrive at TRL 9 and the 31% at TRL 8.

Nine experiments out of fifteen actually created at least one new job position during the development of the experiments. Ten experiments will create new jobs in two years, as shown in Fig.2.12.

Two experiments created a Spin Off and the five produced at least one patent. Three experiments provided information of the turn over during the development of the project, but six more will have a significant turn over in the next 2 years.

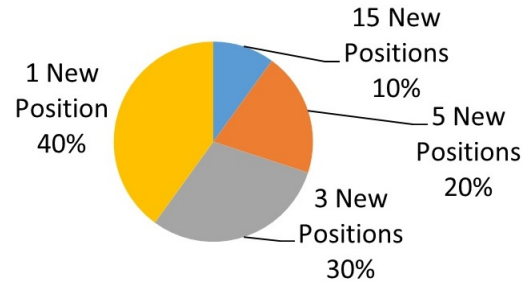


Fig. 2.12: Distribution number of positions that will be created in two years

2.4 Conclusions

E++ furtherly improved the methodology to implement the instrument of Experiments by optimizing the process, the supporting documents, the selection of successful experiments and the monitoring of correct activities in the development of them.

Results of Call 1 and preliminary outcomes of Call 2 show that the majority of selected experiments achieved the expected goals developing robotic platforms with a relevant TRL and foreseen impact significantly increased in the next two years. The collaboration between academia and industry proved to be beneficial from both sides having final products to be close to the market in just 18 months. The two calls of E++ allowed to 74 new organizations to be involved in the European funding scheme for the first time, 67 only in the first call. The involvement of SMEs and Large Enterprises has been unexpectedly successful.

Thanks to the effort spent in ECHORD and ECHORD++ the Experiments instrument is now solid and ready to be seen as an example of good practice in cascade funding and collaboration between academia and industry.

Acknowledgements This work has been funded with "ECHORD++ EU Project FP7-ICT-2012-601116".

Chapter 3

Robotics Innovation Facilities

Farid Dailami, Chris Melhuish, Francesca Cecchi and Christophe Leroux

Abstract Robotics Innovation Facilities (RIFs) are open to the public labs which provide state-of-the-art robotic hardware and software, as well as scientific and technical support. Anticipating market trends, the RIFs instrument cover a wide range of application areas. Users can come from all areas, regardless of if they already have robotics experience or not. This article exposes the procedure developed at the three Echord++ RIFs - Bristol, UK, Paris-Saclay, France and Peccioli, Italy- and some results and contributions in robotic technology.

3.1 Introduction

Over the past thirty-five years or so, the European Economic Community followed by the European Commission have helped fund a large number of robotics and automation research and development projects. By way of an example EUREKA-FAMOS program in the late 1980s funded a number of projects in the area of Flexible Assembly Systems. Historically, in Europe, therefore, robotics research has benefitted from long term funding. This has led Europe to become a world leader in this area of research.

Unfortunately, in a manner similar to many other areas of research, the out-come from many of these projects have not benefitted from commercial exploitation and the European taxpayer has not received the full benefits of their investment.

This, somewhat familiar outcome, is sometimes referred to as the 'Valley of Death' (See Figure 3.1). This is where monies are spent to carry out the necessary R& D for what are deemed commercially promising projects, however, on completion of the work, funds for commercial exploitation of the results are not available. Both ECHORD and its successor ECHORD++ were considered as partial solutions to this problem. The Experiment and RIF Instruments in ECHORD++

F. Dailami, C. Melhuish

Bristol Robotics Laboratory (BRL) University of the West of England and the University of Bristol.

e-mail: farid.dailami@uwe.ac.uk; e-mail: chris.melhuish@brl.ac.uk

F. Cecchi

Scuola Superiore Sant'Anna, Pisa, Italy, e-mail: francesca.cecchi@santannapisa.it

C. Leroux

French Alternative Energies and Atomic Energy Commission, Paris-Saclay, France e-mail: christophe.leroux@cea.fr

are mechanisms where assistance is provided to those projects that are near to market to help with bridging the gap between research and commercial exploitation.

This paper is concerned with the rationale, operation and results obtained from the Robotics Innovation Facilities (RIF) Instrument.

3.2 Background

The FP7 project ECHORD++ (European Coordination Hub for Open Robotics Development, Grant Agreement Number 601116, www.echord.eu) aims at strengthening the cooperation between scientific research, industry and the user community in robotics and automation. This is a follow-up to ECHORD (2009 – 2013).

In addition to call-based Experiments, small, focused research projects, ECHORD++ (2013-2018) introduced a new concept to allow for light-weight access to research infrastructure and expertise. In three European countries, so-called RIFs, Robotics Innovation Facilities have been set up. RIFs are physical infrastructures in these countries. A RIF is a "living lab" with close ties to the (academic) host institution and industry, and at the same time, it is a test bed for new robotic technologies. Robotics Innovation Facilities have allowed new robot customers and users to collaborate with roboticists with no entrance barrier, and at very low cost – so that new communities can form. Operationally, the RIFs are open "experimental facilities" physically located at a university or research organization. They provide equipment, services and personnel for anyone and everyone interested in robotics. In E++, this concept was piloted by establishing three RIFs to study how they can work in an optimal way to attract researchers from other fields, robot users and customers, to generate new start-ups and support SMEs. Moreover, RIFs have provided an excellent opportunity to test new markets for manufacturers and start-ups at different stages of development.

The efforts were especially to encourage SMEs and start-ups to participate in these robotics activities – RIFs are by their definition an ideal environment for developing and fostering new opportunities for commercialization of innovative ideas in robotics and automation.

RIF's access does not require the collaborator to formally become a new member of the ECHORD++ consortium (in contrast to the Experiment). This provided for a quick and regular decision procedure to evaluate light-weight application documents and to schedule stays in an interactive way. There were no fixed dead-lines; the assessment of the applications was generally within two months.

Facts in short:

- Three physical facilities providing robotics infrastructure and services
- Stay duration up to six weeks, re-application after a successful stay possible
- No application deadlines
- No need to become a member of the ECHORD++ consortium
- Evaluation panel every two months
- Acceptance and scheduling horizon: six months

3.3 RIF Rationale

Robotics Innovation Facilities offer a physical place to initiate collaboration with companies and individuals interested in the application of robots. The aim is to expand the use of robotics and automation across all manner of activities, for example traditional manufacturing and new products such as toy robots.

The results obtained thus far indicate that this aim has been achieved. Across the three RIFs a number of collaborations have resulted in projects that have generated significant income for

their owners. RIFs in themselves are an experiment as far as their intervention mechanism and the collaborative nature between three dispersed providers has not existed before.

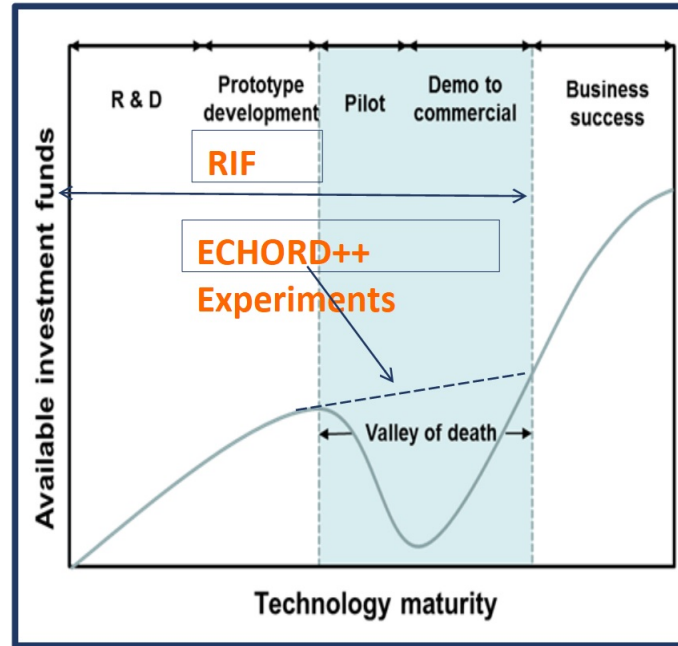


Fig. 3.1: Depiction of impact of RIFs in the development time line of robotics projects.

The outcome from this instrument may inform the Commission about the makeup of the future Digital Innovation Hubs for robotics and automation.

In this regard, the three RIFs are now registered as fully operational DIHs in the S3 Catalogue.

The intervention mechanism provided by the RIFs extends from very early stage exploration of concepts and ideas up to development of commercial demonstrators. The early stage engagement is the differentiator between RIFs and System Integrators. The basic RIF philosophy evolves around a long-term collaboration rather than a point solution. Moreover, RIFs can offer a 'one-stop shop' solution. As for example, the diagram below shows, a snapshot of the ecosystem around RIF@Bristol is extensive. This breadth and depth of service enables RIFs to provide a range of collaborations and assistance to their clients.

The RIFs have offered an easy engagement process. The interested party is sent a short application form that requires information about the collaborator, the area of work (The proposed project) and future exploitation strategy of the outcome of the project. This application is then assessed in accordance with RIF's scoring guidelines and projects that achieve a score of 60% and over are deemed suitable for assistance. Such applications are then progressed into a collaborative project with a nominal duration of six weeks. The proposed work is carried out at the RIF site and the results by way of reports, videos, demonstration etc. is transmitted to the collaborator. It is generally expected that the collaborators spend some time in the RIF. This is to assist with the development process and the ownership of the findings. However, in the case of start-ups and SMEs, due to lack of their resources, this opportunity is not always taken on board.



Fig. 3.2: Snapshot of RIF@Bristol's ecosystem

In some cases, further funded work was carried out by securing funds from the company concerned, government agencies and other funding mechanisms. This process has proved very effective in all three RIFs.

3.4 RIF Characteristics

A RIF is mainly a facility that provides equipment, infrastructure and personnel to assist individuals, companies, educational establishments and governmental agencies to explore application of robots and automation in their chosen area of interest. The main features are:

- The engagement may be in the form of an experiment or an investigation.
- RIF's investigations are highly focused, limited duration, minimally funded events that are by their nature of a feasibility format. The results from an ad-hoc investigation that may be an end in itself or form part of an application for a funded experiment.
- Provide a unified mode of operation and present the same interface to the outside world
- Provide mechanisms and interfaces for exploitation of innovative solutions
- Provide routes for raising funds via governments, venture capitalists, banks and other sources of finance
- Start-up companies and SMEs have been the main beneficiaries, and make up over 70% of the six-week collaborations since the program began.
- A degree of flexibility of each RIF helps to address specific local, procedural and other differences between the varying localities and in respect of each facility's strengths and weaknesses.
- The degree of autonomy afforded to each RIF has resulted in a combination of global policy adoption and local procedural deviations, reflecting and responding to the varying types of engagements and enquiries experienced at each RIF.

- RIFs have had to be marketed to attract clients, 'Build it and they will come' is not effective and this requires marketing effort, people and budget.
- RIFs must be located where local demands are sufficient to be 'Pump Prime' with collaborations
- RIFs benefit from co-location in established research institutions
- RIFs ought to be populated with or have access to personnel who have a wide range of experience and be able to interact with industry and commercial organizations as well as incubates, start-ups and SMEs
- Human resources are critical to ensure RIFs can provide a timely service for their clients and manage expectations
- A key feature of RIFs has been to Attract researchers from other fields, for instance in Bristol one of the collaborator's research was concerned with using robots to dress the infirm and elderly. Another discussion is with a group who are examining use of robots in producing ceramic artefacts
- Incubates and start-ups are one of key foci to create wealth and jobs
- RIF have operated with a no engagement fee policy; maintaining some version of this is a key concern in going forward.
- Experience with multinationals indicates that the RIF offering provide process or product champions in those firms to demonstrate the feasibility of their novel ideas to the upper management and thus secure internal funding for implementation of their ideas.

Integration challenges between the three RIFs:

- Longer time is needed to build relationships and a collaborative ethos
- In general there was a lack of time for regular dialogue between the three RIFs
- There were cultural and linguistic differences that sometimes led to differences in interpretation of key ideas
- The three RIF had different work practices and legal frameworks at different sites, this led to challenges to smooth operation
- Geographical distance between RIFs led to reduced chances for closer collaboration
- Failure of electronic communication systems was a key reason for reduced opportunity for conference calls.
- The creation of handbook for RIFs has already led the application of some key ideas to other projects

The SWOT analysis has highlighted some key aspects that need to be examined in detail for any future continuation of a RIF model to support expansion of robotics and automation across many stakeholders. These include:

- RIFs key Strength
 - The impartiality of RIFs enables them to give unbiased advice
 - RIFs are independent entities and are not representing particular suppliers.
 - Provision of varied range of equipment
 - RIFs have variety of equipment and on any training can expose the participants to many different types of robots and related equipment
 - Their access to the latest research output
 - By co-locating RIFs in research labs, RIFs can benefit from the latest research work.
- The perceived Weaknesses:
 - The lack of a speedy response and a change of view from an academic perspective to a commercial one
 - RIFs have originated in universities and research labs and can therefore have a tendency to operate on time scales that are somewhat longer than commercial research
 - Clarity of the RIF's Value Proposition and the differences from Systems Integrators
 - RIFs need to improve their mission and clarify their Value Proposition, given their recent creation, there is some lack of clarity in this respect

RIF SWOT Analysis



Fig. 3.3: . SWOT Analyses for RIFs

- The likely Opportunities:
 - Provision of low/zero risk engagement for applicants
 - RIFs provide access to their capabilities at zero or minimal costs while ensuring that any IP developed during the collaboration belongs to the client
 - Collaborate at high risk early TRLs
 - RIFs offer their services in the exploration of very early concept development, this is somewhat different from such suppliers as System Integrators
 - Offer broad scope of capabilities and training
 - RIFs' fairly extensive ecosystems and their co-location in universities enables them to offer wide range of services and off-ings
- The potential Threats:
 - RIFs will be replicated by others
 - RIFs are a model that is attractive and meets a specific need and as such could offer an alternative to current offerings from other suppliers
 - Unable to manage expectations
 - Given their research intensive backgrounds, RIFs may experience difficulties in meeting the commercial expectations of their clients
 - Unable to secure sustainable income
 - Post funded period (After completion of E++ Project) securing further fund to offer a free service will be somewhat challenging and this may limit the duration of free collaboration
 - Perceived Competition with System Integrators

- Throughout the duration of the RIF Project, there has been a concern regarding the similarity between RIFs and System Integrators. It is, however, clear that RIFs, as has been explained of-fer their services at a much earlier and riskier stage of development compared with SIs.

3.5 Impact of RIFs on Innovation

In examining the impact that RIFs have made in the innovation journey of our collaborators, the construct of Absorptive Capacity (Cohen and Levinthal, Zahra and George) provides a useful model for exploring the interaction between RIFs and RIFs' clients

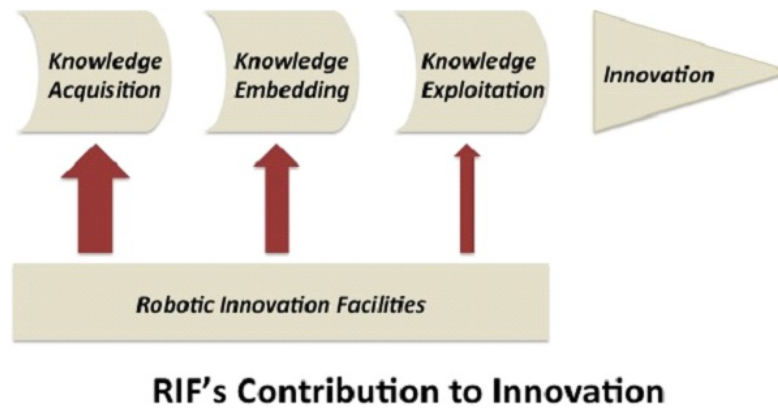


Fig. 3.4: Contributions of RIFs to the Innovation Pipeline

Absorptive Capacity (ACAP) may be used to identify the three-stage process that leads to innovation. Here the 'firm' has to identify the knowledge that it needs and the source of that knowledge to guide it in its pursuance of innovation. The firm will then needs to incorporate that newly acquired knowledge in its product or process. In the final stage the firm must exploit that new product or process commercially in the market place to generate its profit, thus completing the innovation cycle.

The role of RIFs has been primarily in the first two stages. In Knowledge trans-fer RIFs have collaborated with start-ups, SMEs and larger companies in both providing innovative solutions in robotics and automation and also in training and education. Generally, many of the collaborations have been at early the TRL levels. These collaborations have then led to embedding of the newly acquired knowledge and expertise into the firm's product and or processes. On many occasions these ideas have matured into marketable and profit earning outputs that the companies have exploited. As Figure 3.4 depicts RIFs influenced stage one of the innovation process significantly. In terms providing new knowledge and expertise to solve specific problems, and in introducing new concept and experiences via their training sessions RIFs were very effective. The influence and significance of contribution in the exploitation phase is less marked.

3.6 History of RIFs collaboration over the project period

In Figure 3.5 we illustrate the number of collaborations in a quarter in each of the three RIFs. The differences in performance can be partially explained by the earlier start of RIF@Bristol. As coordinators, it was decided to start in 2013-14 a 'Beta' phase by combining the set up and simultaneously pursue collaboration with suitable clients. This is reflected in the higher number of Bristol collaborations and engagements in the first year of operation. The overall target of the number of engagements was around ninety-six, the actual number of engagements is around one hundred and twenty.

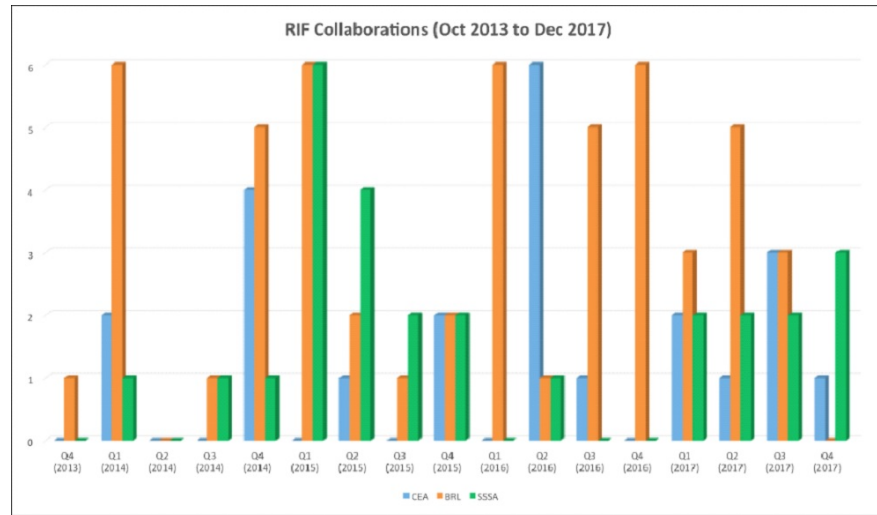


Fig. 3.5: Quarterly collaborations at each RIF during 2013-2017

3.7 Examples of RIF collaborations

3.7.1 RIF@Pisa-Pecciolli

Collaboration Title: Development of portable weather station of sports turf (Turf Europe)

Type of organisation: Large company.

Turf Europe srl was founded in 2009 by private partners and turf grass industry companies. All Turf Europe partners have over 10 years of experience in building and maintaining turfed areas of all types, and in carrying out scientific and applied turf grass research. In 2010 Turf Europe obtained the status of University of Pisa Spinoff Company, with the entry of the same University among the partners.

Client's Need: Development of innovative establishment techniques for field and greenhouse.

Provided Solution: Development of a robotic mobile platform able to check the soil conditions in football arenas.

Development of a portable box that connects iCloud the information of the soils in football fields (Agronomical and environmental data collection and analysis system)

The Turf Grow Lights shall be supported by a web based agronomical and environmental data collection and analysis system for assessment of the lighting hours required to support the daily use of the Turf Grow Light for maintenance of the natural sports turf pitch.)

The short engagement of six weeks led the parties to define the desired capabilities:

- Portable ("need to monitor different areas");
- Not plugged-into electric mains;
- Geolocalised ("what is the station monitoring right now?");
- Rugged and fool proof;
- Smartphone tablet PC remote access to data;

And develop a portable device connect with the real-time monitoring weather station.

The aim of this collaboration was to develop a portable weather station. The primary objective was to define the monitoring parameters to enable improved product to monitoring the varying microclimates and open a precision farming area.

Parameters	
Soil	MEASURED: Temperature, volumetric water content, EC CALCULATED: available water content
Air	Temperature, humidity, pressure, vapour pressure
Wind	Speed, direction.
Light	MEASURED: photosynthetically active radiation ($\mu\text{mol}/\text{m}^2/\text{s}$) CALCULATED: Daily Light Integral ($\text{mol}/\text{m}^2/\text{d}$)
Canopy	Evapotranspiration (mm/d)

Table 3.1: Parameters of Green Go platform

The main goal within 2018/2019 are summarized in Figure 3.6


Without the existence of RIF@Peccioli it would have been rather difficult to get such a project off the ground. The products are sold both in the Europa football clubs (Fig.3.7).

3.7.2 RIF@Paris-Saclay


Collaboration Title: creation of the European Company in collaborative robotics [iSybot](#)

Type of organisation: Start up and Large companies

The [RIF@Paris-Saclay](#) is proud to have contributed to the emergence of the new European robotic start up [iSybot](#) through the collaborations conducted as part of the project Echord++ project. Since March 2018, iSybot has been marketing an innovative collaborative robot called SYB3. This robot, safe for operators due to its design, considerably extends the possibilities of using barrier-free robotics in industrial applications.



The future (2018-19)



- Won Tuscany Region funding
- **"Green-GO" Project** – SME type
- 0,4 M€ over 2 years
- Robotization of the device
- Solar powering (no recharging)
- Rain meter
- Adaptation to field agriculture
- Further develop algorithms
- Automatic mapping
- Return to docking station
- Sales target: 50+ units/year




Fig. 3.6: Forecast 2018/2019



First customers (2017)














In talks with
Real Madrid FC

Fig. 3.7: Football clubs that adopted a Green Go platform in 2017

The [RIF@Paris-Saclay](#) has contributed, through several Echord++ [collaborations](#) conducted with different manufacturers (SMEs¹, integrators², large groups³), to validate the technical principles retained as well as to demonstrate the interest of this innovative collaborative robot in several fields of application. These validations led to the creation of the start-up, the creation of a new product, and the transfer of licenses on five patents held by the CEA. The start-up, which now employs six people, is growing rapidly and plans to hire six more people by the end of the year.

¹ Mécarectif (grinding), SEIV (moulding)

² GEBE2

³ Renault, Dassault Aviation, SNCF, AREVA



Fig. 3.8: RIF@Paris Saclay equipment

Several robots are already marketed for use in production at SNCF (rail) and Dassault Aviation (aeronautics).

The contribution of the RIF consisted in bringing its expertise for the electromechanical design and in particular on the use of an actuator allowing an estimation of the applied forces without requiring sensors. The [RIF@Paris-Saclay](#) also contributed its expertise on the control as well as on the programming by demonstration demonstration of the collaborative robot and the use of virtual guides to constrain the movements of the robot.

Collaborations conducted at the RIF@Paris-Saclay were decisive in several aspects:

- Identification and qualification of grinding and polishing use case at the stimulating the creation of the company
- Exhaustive specification of sanding mobile cobot
- Identification of collaborative robotics key performance indicators for return on investment calculation:
 - Ratio between programming time and automatic execution time of the tasks
 - Maximal effort to engage by an operator to support one size lot type of task, and flexible production
 - Adaptation to user profile, usability by operators non specialized in robotics (intuitive programming with two buttons only)
 - Mandatory aspect of the mobility of the robotic solution
- Adequacy between end user need and key technologies: programming by demonstration, force control, intrinsically safe force control actuation
- Opening of niche market on collaborative robotics market,
- Visibility of the Company from end users (large groups and SMEs) through demos, movies and fairs organized by Echord++,
- Identification of large set of clients in France, Germany with opening to new markets
- Perspective of expansion to other applications than sanding
- Identification of new needs from users, of needs for expansion of the capacities
- Commercialization of products

This success story example conducted to an increase notoriety of CEA and was crucial in helping how to organize the relations with end user: to prospect for innovative use cases, to understand and

capture user needs, to connect with the value chain, and to organize the dialog leading to successful results satisfying all parts



Fig. 3.9: SYB3 product from iSYBOT

3.7.3 RIF@Bristol

Collaboration Title: Feasibility of robotic assembly of Numatic International vacuum cleaners

Type of organisation: Large company

The aim of this collaboration was to explore the feasibility of a robot for fastening two parts of a vacuum cleaner using seven fasteners. The short engagement of ten weeks led the parties to believe that the operation could be automated and was technically feasible and commercially viable. Thus the short collaboration was followed by a two year long, funded project that resulted in the final system for the shop floor.

The aim was to explore and to embed design expertise in system automation and integration, using the Henry vacuum cleaner assembly as a pilot project. A particular emphasis of the collaboration was the use of Cobots.

The primary objective was to pilot and embed robotic automation assembly capability and knowledge into Numatic International, to enable improved products and processes to sustain global competitive advantage.

Numatic's operations strategy has been augmented by the funded project. It allowed the company to target its productivity and operator care agendas. The use of collaborative robot automation enabled it to both reduce the labour content of their products as well as enhancing their ability to utilise staff with a wide range of capabilities. This reduces product cost and allows the company to use its staff flexibly within the organisation.

The products are sold both in the UK and exported. Around 30%-40% of the turnover is exported. The export business is stronger in commercial markets and an opportunity exists for further penetration into the domestic segments of these markets. This is a very competitive sector and in order to profitably grow this market Numatic needs to increase capacity but also reduce production costs. UK productivity is considered to be less than similar economies and a factor often cited for this is the lower use of automation in the manufacturing business. The RIF collaboration followed by the two years long project was a key contributor to the growth strategy as the availability

of lower cost domestic vacuum cleaners will allow Numatic to target growth in the domestic sectors of the retail markets.

Without the existence of RIF@Bristol it would have been rather difficult to get such a project off the ground. The commercial return of the initial investment has already been realised in less than six month of the operation of the assembly system in the Numatic factory.

With the availability of around 99.5% the system has proven very robust and approval has been given for two additional systems to be installed.

Some lessons from this industrial application:

- Feedback from the operators was invaluable. Overall, operators are finding this automated assembly line to be easier than the manual lines, but the learning curve is somewhat steeper as the process now is less forgiving. On the positive side of implementing a tighter process, we have more consistency and better quality.
- The future systems shall be Scalable and Modular with staged introduction of automation.
- Improvements in quality of the injection molded parts would be very beneficial
- Robots with greater rigidity, may be Cartesian for example, would be more suitable for the screw fastening operation
- Simply having a safe robot does not mean we have a safe system, other elements of the assembly line e.g. the conveyor system, the electrical test location etc. also need to be safe
- The down side appears to be that humans can handle uncertainty with relative ease. Robots cannot, as expected!
- The situation gets more challenging when humans and robots are cooperating because the robot's performance effects the human's actions.

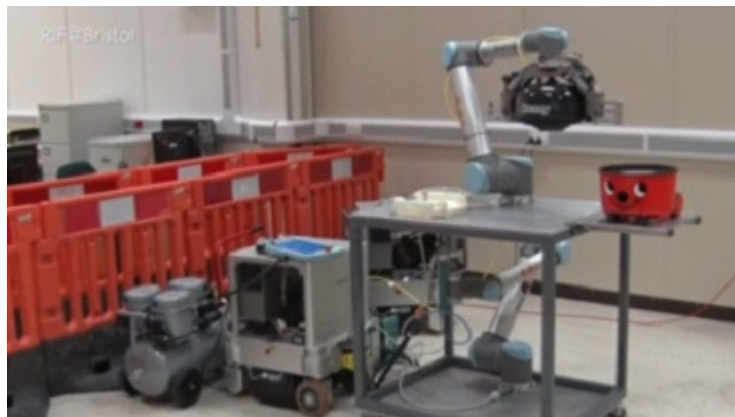


Fig. 3.10: Cobot Trials using twin assembly robots at RIF@Bristol

3.8 Assessment and perspectives

Innovation is more and more a collective process. No more researchers in their ivory towers (the R& D Department) who alone invent new products in order to sell them on the market. This requires technologically advanced products, but also products that meet real needs and products



Fig. 3.11: Robotic assembly system on Numatic shop floor

that are attractive to consumers. Technical feasibility, economic viability and desirability are the three pillars of successful innovations.

Echord++ was a forerunner in experimenting the concept of RIF (Robotics Innovation Facilities) to facilitate uptake of robotics and technology transfer of robotics and automation solutions. This concept of RIF can be related to the concepts of Open Innovation^{4,5}, of Innovation Labs. An early incarnation is the Media Lab founded in 1985 by [Nicholas Negroponte](#) and former MIT President [Jerome Wiesner](#)⁶.

RIFs have demonstrated their effectiveness through numerous collaborations with manufacturers. They have demonstrated their impact through several experiments that have led to the creation of new collaborative robotics products (COBOMANIP⁷, SYBOT) now on the market, the development of the activity of existing SMEs and the support for the creation of new European robotics companies (iSYBOT⁸).

The three RIFs of Echord++ have evolved since their creation. They learnt to work together and exchange good practices. They learnt how to establish links with industrialists and in particular with organizations, people with limited knowledge of robotics capabilities. The practice of RIFs has enabled RIF actors to make progress on the importance of awareness and support actions to demystify robotics. The Echord++ project provided an opportunity through the activity of the RIFs to focus on bilateral relations between scientists from research and industrial organizations. The work of the RIFs has also made it possible to make progress on the importance of connecting with the actors in the value chain: technology and service providers, integrators, certification and financing

⁴ *Open Innovation* refers in the fields of research and development to modes of innovation based on sharing, collaboration between stakeholders. Open Innovation is compatible with a market economy (via patents and licenses) and with Economic Intelligence, and allows alternative ethical or solidarity-based approaches (solidarity economy) to the free sharing of modern or traditional knowledge and know-how, including the use of free licenses. Depending on the case, the approach may therefore appear altruistic or, on the contrary, as a means of distributing (competition) or sharing (partnership) risk and investment outside an organization.

⁵ Penin, Julien, Caroline Hussler and Burger-Helmchen, Thierry, (2011): [New shapes and new stakes: a portrait of open innovation as a promising phenomenon \[archive\]](#) Journal of Innovation Economics, no 7, 11-29.

⁶ The Media Lab: *Inventing the Future at MIT*, 1987, ISBN 0-670-81442-3 (hardcover); 1988, ISBN 0-14-009701-5 (paperback)

⁷ <http://www.sarrazin-technologies.com/news/cobotic-zero-gravity-arm-2/>

⁸ <https://www.isybot.com/>

bodies, public authorities. These observations align perfectly with the initiative of the European Commission on Digitizing European Industry (DEI)⁹ and with the concepts of Competence Centres (CC) and Digital Innovation Hub (DIH)^{10,11}. During the Echord++, the RIFs started to imagine their future beyond the terms of the project. They three RIFs began the implementation of their financial sustainability, based on regional initiatives (DIGIHALL) and funding mechanisms, and in a collaborative way according to the achievements of their network activity based on cooperative projects (TERRINET, COVR, ESMERA, HORSE, . . .). The RIF's concept finds a happy extension in the initiatives led by the European Commission on the Digitisation of Industry (DEI) and the I4MS programme through the notions of Competence Centres (CC) and Digital Innovation Hub (DIH).

RIFs are the most original instruments of the Echord++ project. They are one of the most important instruments of Echord++ in terms of impact for the European economy. DIH and CC represent the new horizon for the RIFs. The three Echord++ RIFs are actively participating to effort undertaken to create networks of DIHs in robotics.

⁹ <https://ec.europa.eu/digital-single-market/en/policies/digitising-european-industry>

¹⁰ <https://ec.europa.eu/digital-single-market/en/digital-innovation-hubs>

¹¹ <http://s3platform.jrc.ec.europa.eu/digital-innovation-hubs-tool>

Chapter 4

Public end-users Driven Technological Innovation (PDTI) in Urban Scenarios

Ana Puig-Pey, Alberto Sanfeliu, Francesc Solé-Parellada, Yolanda Bolea, Josep Casanovas and Antoni Grau

Abstract The use of disruptive technologies - as the robotic one - to solve societal challenges is described in this article through the innovative PDTI (Public end users Driven Technological Innovation) instrument, where the public entity drives the research and development of innovative solutions assisted by a technological expert team. The PDTI and the use case developed in urban scenarios through the ECHORD++ European Project offered us the opportunity to check the procedure of the innovative public procurement PCP (Pre Commercial Procurement) instrument and propose changes and improvements in order to improve public services or create new ones boosting robotic SMEs, products and services to the market. This novel procedure, the PDTI is based in the participation of all the stakeholders involved along the process. The ECHORD++ Urban PDTI results bring two pre commercial robotic solutions waiting for a large order to be commercialized and 14 innovative robotic challenges proposed by European cities that could be the starting point for new innovative public procurement PCPs or PDTIs. The specific results obtained in this robotic use case could be generalized to other technological domains and to other scenarios.

A. Puig-Pey and A. Sanfeliu
Institute of Robotics IRII, Technical Univ of Catalonia UPC, Llorens i Artigues 4-6, Barcelona 08028, Spain, e-mail: {apuigpey, sanfeliu}@iri.upc.edu

F. Solé-Parellada
Universitat Politècnica de Catalunya. Jordi Girona 31. Barcelona 08034, Spain, e-mail: francesc.sole@upc.edu

Y. Bolea
Automatic Control Dept, Technical Univ of Catalonia UPC, Pau Gargallo 5, Barcelona 08028, Spain, e-mail: yolanda.bolea@upc.edu

J. Casanovas
Statistics and Operations Research Dept, Technical Univ of Catalonia UPC, Jordi Girona 1-3, Barcelona 08034, Spain, e-mail: josepk@fib.upc.edu

A. Grau
Automatic Control Dept, Technical Univ of Catalonia UPC, Pau Gargallo 5, Barcelona 08028, Spain, e-mail: antoni.grau@upc.edu

4.1 Objectives and scope

Focused on application-oriented research and development, ECHORD++ (E++) is being funded by the European Commission in the 7PM to improve and increase the innovation in robotic technology. Three instruments and processes are being developed under the ECHORD++ project: experiments (EXP), Research Innovation Facilities (RIF) and Public End-user Driven Technological Innovation (PDTI), all of them aimed at improving and increasing the innovation in robotic technology within SMEs companies and addressing answers to societal and industrial needs.

Two PDTIs have been developed under the E++ project: one in Healthcare and one in Urban scenarios. This article focuses on the PDTI procedure and the use case developed in urban scenario to contribute and join efforts to improve current public services or create new ones through robotic technology. The PDTI is included in the Innovative Public Procurement Instruments and its process is described with emphasis in the relationships with one of its instruments, the Pre-Commercial Public Procurement (PCP) (Figure 4.1).

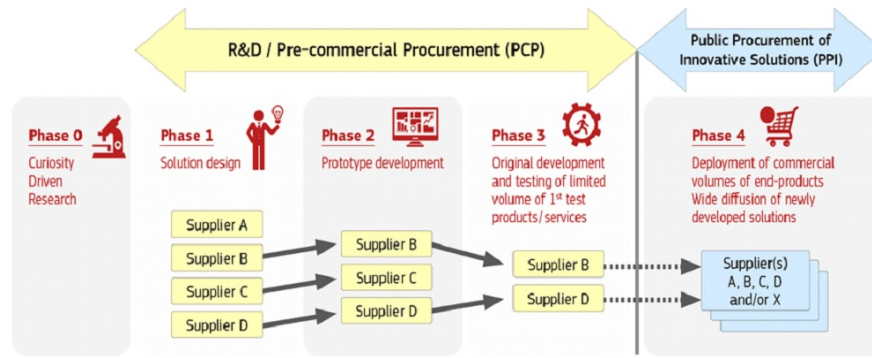


Fig. 4.1: The Innovative Public Procurement Instruments

The Europe 2020 strategy includes innovative public procurement as one of the key market-based policy instruments for smart, sustainable and inclusive growth. Public Procurement has an immense potential to fully exploit research and technology for innovation while also delivering more cost effective and better quality of public services. In some cases, the technologies needed to make these breakthroughs exist or are close to the market (PPI); in other situations, investment in R&D is needed to assure the progress of technological solutions that meet the defined societal needs. In this last case, the instrument used by public entities is the Pre-Commercial Public Procurement (PCP) [1]. During the last years very few PCP have been initiated in Europe and in some cases the calls have been declared void.

The PDTI uses cases developed under the E++ project offered us the opportunity to study and analyze the deficiencies that exist in the PCP process and propose improvements. Two main objectives lead the PDTI procedure: 1. To increase the number of urban robotic challenges proposed by Public Entities and 2. To boost new robotic products or services to the market. An intensive dialogue between all the stakeholders [5] involved and the coordination of their different roles has been essential for the PDTI success: the public entities as procurers; the technological consortiums as suppliers; the users and citizens as surveyors and an expert re-search team as coordinator of all the process.

4.2 The PDTI process

Routed in the product innovation life cycle, and based on Pre-Commercial Procurements, the PDTI proposes a process that comprises two main phases (Figure 4.2):

- + Activities for understanding public demand
- + Activities for research and technological development of pre-commercial products

PRODUCT INNOVATION LIFE CYCLE			
	PCP PHASE 0	PCP PHASE I-II-III	PPI PHASE IV
	ACTIVITIES FOR UNDERSTANDING PUBLIC DEMAND	ACTIVITIES FOR RESEARCH AND TECHNICAL DEVELOPMENT OF PRE-COMMERCIAL PRODUCTS	PUBLIC PROCUREMENT FOR COMMERCIAL ROLL-OUT
	PDTI		

Fig. 4.2: Relationship between PCP and PDTI processes

The "Activities for understanding public demand" increase and structure the tasks developed in the phase 0 of a common PCP; the "Activities for research and technical development of pre-commercial products", match and improve the phases I, II and III of the PCP, ending in a pre-commercial product. Looking to bring future needs and future supply together at an early stage, the first part of the PDTI process, the Activities for understanding public demand, develops four qualitative phases inspired by the Delphi methodology (2-3): Brainstorming, Narrowing Down, Ranking and Challenge Description.

Coordinated rounds between the stakeholders involved is essential for the success of these activities in order to bring and explore innovative challenges. This group of activities ends in a Call for Proposals /Tenders, initiating the Activities for research and technical development of pre-commercial products structured in three phases: Solution Design, Prototype Development and Small Scale Test Series (Figure 4.3). A continuous and expert monitoring during these technological phases makes possible to offer pre-commercial products close to the market at the end.

PUBLIC END USERS DRIVEN TECHNOLOGICAL INNOVATION PDTI							
ACTIVITIES FOR UNDERSTANDING PUBLIC DEMAND				CALL FOR RTD PROPOSALS	ACTIVITIES FOR RESEARCH AND TECHNICAL DEVELOPMENT OF PRE-COMMERCIAL PRODUCTS		
BRAIN STORMING	NARROWING DOWN	RANKING	CHALLENGE BRIEF		SOLUTION DESIGN	PROTOTYPING	SMALL SCALE TEST SERIES

Fig. 4.3: PDTI process and activities

4.2.1 The PDTI process: Activities for Understanding Public Demand

This part of the PDTI process, Activities for Understanding Public Demand, is a qualitative procedure inspired by Delphi methodology and allows a group of stakeholders to systematically approach a particular task or problem [4]. In our case, the objective is the reliable and creative exploration of social needs related to public services that could be solved through robotic technology. The stakeholders and their roles are: the public entities as procurers; the technological consortia as suppliers; the end users as surveyors and finally an expert team as coordinator. The coordinator will give the technological support to the public sector for developing and implementing the innovation-oriented procurement [5]. The role of the coordinator is needed to drive and lead the complete process based on innovation. At the same time the knowledge of what the new technology can offer to solve social needs is introduced into the public entities, departments and managers. Due to the complexity of this process, it is valuable that the coordinator has a team of people coming mainly from technological areas but also from other areas such as economics, psychology or political science fields [6]. The participation of users and citizens will take place all along the development of the PDTI to survey the process and participate in it, through several activities.

The methodology employs iterations of questionnaires and feedback through series of rounds to develop a consensus of opinion from the participants. There is not a limit of time, but it is necessary to consider a minimum and a maximum number of rounds. After each step, specific documentation will be generated as the conclusion of the developed activities as well as the starting point of the next phase.

Brainstorming: The process starts with an identification of the real needs as perceived by the users and budget holders. A draft Questionnaire of Public Needs and its associated Innovative Technology will be prepared based on an improvement of existing public services. The success arises through interactions between the stakeholders in several rounds. The information elaborated in each round will be collected, edited and returned by the coordinator to prepare the next round. Finally, an agreed upon PDTI Questionnaire is elaborated.

Narrowing down: This phase has the objective of focusing the needs proposed in the PDTI Questionnaire using specific criteria. A group of impact indicators already used by the public entities or created during the process will be used in the evaluation and selection of the PDTI Challenge List. Users, Industry and Academia Consortiums are invited to participate in order to gain their opinion through workshops and Open consultations.

Ranking: The third phase is undertaken by an expert panel composed by designated people from the Public Entity and the Expert Team that will evaluate and select a number of Innovative Challenges to be developed under an Innovative Public Procurement. The number of innovative challenges will depend on the budget of the Public Entity and of the potential market offered by the procurer weighted according to the size relative to the costs involved in the development of the Innovation.

Challenge Brief: Finally, a document with a clear explanation of the public product or service should be described with enough information about the functions to be developed by the new technology. It is important to ensure that this Challenge Brief is not a common procurement document, but an innovative one, and has to be written taking into account the required innovative functionalities benefitting the public service instead of the standard requirements that could narrow the innovation field [4]. The translation of needs/problems/challenges into functionalities requires highly developed competences, or at least understanding, at the technological level on the part of the procuring organization [6] and the role of the expert coordinators is essential. The Challenge Brief will be the main document for the Call for Proposals/Tenders and the starting point of the second part of the PDTI process, the "Activities for research and technical development of pre-commercial products".

4.2.2 The PDTI process: Activities for Research and Technical development of Pre-commercial products

As we have explained before, this part of activities starts with a Call for Re-search and Technological Development (RTD) proposals and will be structured in three competitive phases (Figure 4.4) that match those described in a common Innovative Pre-Commercial Procurement with some improvements along the process in order to reach the second PDTI objective: to boost new robotic products or services to the market.

PDTI ACTIVITIES FOR UNDERSTANDING PUBLIC DEMAND				
<u>PHASE I</u> SOLUTION DESIGN FIRST RESULTS (TLR 4)	EVALUATION AND SELECTION	<u>PHASE II</u> PROTOTYPING (TLR 6)	EVALUATION AND SELECTION	<u>PHASE III</u> SMALL SCALE TEST SERIES (TLR 7-8)

Fig. 4.4: Activities for research and technical development of Pre-Commercial Products

The call for RTD proposals has the Challenge Brief as main document. This call should be launched in local, national and international media in order to receive high level proposals. The RTD consortia should be composed by Companies, SMEs and Academies looking to measure innovation risk in front of social and economic benefit. An external expert panel and the public entity will evaluate and select the RTD proposals that will start the competitive activities for research and development of pre-commercial products. The evaluation criteria should include marks given according to: Scientific and/or technological excellence; Quality and efficiency of the implementation and the management of the project; Potential Impact through the development, dissemination and use of the project. The economic viability of the proposal is required from the different companies involved: the robotic manufacturer, the public services company and the public entity. The benefits should be analyzed for the full life cycle of the new product or service.

The Phase I of the RTD Activities establishes the design of the technological solution and has to show how it will perform the different tasks assigned in the Challenge Brief specifications. At the beginning of this phase a monitoring procedure and an evaluation criteria document will be prepared. The monitoring procedure will include periodic deliverables and milestones, technical and impact key performance indicators and tests. A detailed explanation of the solution design is required but it is recommended to start with a first prototype in order to test the viability of the robotic solution as soon as possible. Also if we are developing a technology to give tailor-made solutions to improve or create a public service, the new operational procedure has to be aligned with the new technology all along the process. Instead of a "product", what the Public Entity needs is a "service". The marketability and the economic viability of the proposal will be discussed and checked after this phase. Phase I has a duration around 6 months including some rounds between all the stakeholders. At the end of Phase I an expert panel will evaluate and select the prototypes that continue the PDTI process to phase II.

The PDTI's Phase II goal is that the design concept developed during Phase I achieve the TRL6 level in which the prototype system is tested in a relevant environment. This level represents a major step up in the technology's readiness as the prototype should be near to the desired configuration in terms of performance, weight, and volume. The robotic solution has to perform the different functionalities described in the Challenge Brief specifications, incorporating the comments that

received in the previous evaluation (phase I). A monitoring procedure and an evaluation criteria document will be prepared for phase II jointly to the results and recommendations of the expert panel evaluation of phase I.

The Phase II had a duration around 12 months and it is structured in monitoring periods. At the end of each one of these monitoring periods, different documentation and tests were required to the consortia, including a report about changes and improvements in the robotic requirements and technological functionalities after phase I. A round or telco between all the stakeholders involved will be made after each monitoring period. It is necessary to test the prototypes during this phase. One test in lab environment in the middle of phase II and one test in real environment at the end will offer a real perspective about how the technology matches the functions required. Again the operational procedure with the new technology should be tested and the marketability and economic viability of the new products should be discussed and evaluated. At the end of Phase II an expert panel will evaluate and select the prototypes that continue the PDTI process to phase III.

In spite of these two first PDTI phases are not specific testing ones, open tests should be available to the RTD consortia. The public entity has to be aligned to offer demos and test fields to get scientific results during the process. In Phase III, the prototypes developed in Phase II should be further developed and installed at the sites of the public body in a small-scale test series to accelerate their route to commercialization [7]. The PDTI's Phase III goal is that the developed prototypes in Phase II achieve the TRL7-8 level, improving the characteristics of the prototypes evaluated in Phase I and II, and incorporating to the prototype the technological improvements needed to perform the functions required in the challenge brief. At the same time this phase should offer a major step up in the marketability of the developed robotic solutions. Several robotic platforms are required in this phase in order to demonstrate the replicability of the solution and the full operational procedure to be done.

A monitoring procedure and an evaluation criteria document will be prepared for phase III jointly to the results and recommendations of the expert panel evaluation of phase II. During the monitoring periods, several documents and tests will be done. A marketing workshop programmed in the middle of the period could help to improve the marketability of the technology. The PDTI process will be concluded by a final assessment that will establish the readiness reached by the new prototypes and the next steps to be done by the public entity. This is a new opportunity to include new public entities aligned with the same technological challenge in order to launch a public procurement for commercial roll out of the new technology.

Dissemination activities should be done along the process in order to get visibility and to receive feedback of all the stakeholders involved: Workshops, citizens' consultation, open markets, etc., will offer a valuable feedback aligned with the European slogan of "Science with and for society".

4.3 The case study of E++ PDTI in urban scenarios

Urban areas have been identified as one of the application scenarios for the E++ PDTI. Cities cover 2% of the earth surface, and they represent more than 50% of the world's population. And increase day to day. Smart cities have become an important area where technology has an important impact. In this section we will explain, how the PDTI procedure described in the previous section has been applied to 1. To involve European cities in robotic technology proposing innovative urban challenges and 2. To find robotic solutions to the urban challenge proposed by Barcelona City Council and BCASA based in the "Inspection and clearance of sewer network at cities".

In October 2013 we started the Activities for understanding public demand by a structured dialogue between all the stakeholders involved, coordinated by the UPC expert team and following the four steps described in Section 4.2. We started with the Brainstorming step, asking to the European City Councils about their innovative urban challenges and answering them how the robotic technology could provide solutions to them. We used a variety of different means: questionnaires, personal interviews with different departments, emails and telephone calls, meetings, etc. We

undertook several rounds of discussion and the outcome was the first E++ Urban PDTI Questionnaire (Figure 4.5).

To prepare the Narrowing Down step we reviewed the existing documentation regarding impact and evaluation criteria and we elaborated a list of impact criteria [8], which included the following elements:

ECHORD++ PCP URBAN ROBOTICS: URBAN CHALLENGE EVALUATION		
Public authorities are faced with societal challenges in present cities. Technology is setting a new landscape of possible improvements in public services. ECHORD++ PCP Pilot in Urban Robotics looks for reliable robot systems in urban tasks.		
Please, let us know your opinion about these city challenges and its associated robot technology		
First column: ECHORD++ Urban Challenges list and its associated robot technology Second column: Write your comments and opinions through impact indicators. (1) Third column: Evaluate: Are you interested in this challenge? (5-Very interested, 4-Somewhat interested, 3- Neutral, 2-Not very interested, 1-Not at all)		
Name and position	City	Contact
Cities and citizens challenge		Comments Interest (1-2-3-4-5)
E++ Challenge Collaborative society Improve the quality of life ensuring citizens feel safe and secure		Include your comments here
<i>Robotic assistants in emergency situations</i>		Include your comments here
<i>Robotic surveillance system</i>		Include your comments here
E++ Challenge Mobility and ICT Technology Goods distribution technology to improve local retail		Include your comments here
<i>Robotic System for goods distribution in pedestrian areas</i>		Include your comments here
E++ Challenge Energy and mobility Approach the uptake and storage of energy in the place of consumption		Include your comments here
<i>Robotic infrastructure for cleaning and maintenance of solar panels</i>		Include your comments here
<i>Robotic infrastructure for distribution of electric rechargeable batteries</i>		Include your comments here
E++ Challenge ICT Technology and Collaborative society Technological solutions to manage big agglomerations		Include your comments here
<i>Mobile robotic repeaters to enlarge the connectivity in large agglomerations</i>		Include your comments here
<i>Mobile infrastructure to manage information and security in large events</i>		Include your comments here
E++ Challenge Mobility and Environment Technology for traffic infrastructure maintenance. Detection and alerts of damage roads surface. City infrastructure surveillance		Include your comments here
<i>Robotic system for automatic detection of damaged roads surface</i>		Include your comments here
<i>Robotic system for roads maintenance and streets dust cleaning</i>		Include your comments here
<i>Robotic infrastructure for sewage networks</i>		Include your comments here

ECHORD++ PCP URBAN ROBOTICS: URBAN CHALLENGE EVALUATION		
Cities and citizens challenge	Comments	Interest (1-2-3-4-5)
E++ Challenge Environment and ICT Technology Environmental monitoring and control (e.g. pollution, soil pH, beaches, water)	Include your comments here	
<i>Robotic system to control de soil pH and reduce water waste</i>	Include your comments here	
<i>Mapping and controlling the quality of the beaches</i>	Include your comments here	
E++ Challenge Environment and Mobility Improving waste management and streets cleaning	Include your comments here	
<i>Robotic street cleaning infrastructure</i>	Include your comments here	
E++ Challenge Mobility and Collaborative Society New technology to help citizen mobility in pedestrian areas	Include your comments here	
<i>Robotic wheelchair for elderly</i>	Include your comments here	
E++ Challenge Collaborative Society and Mobility Improve mobility at the city. Helping tourist services.	Include your comments here	
<i>Land robotic system in the planning of accessible routes</i>	Include your comments here	
<i>Information Robotic system at the city</i>	Include your comments here	
E++ Challenge Collaborative Society and Mobility Improving the attendance of people with dependence	Include your comments here	
<i>Robots for dependable people in pedestrian areas</i>	Include your comments here	
E++ Challenge Mobility and Environment Management, planning and urban city knowledge	Include your comments here	
<i>Aero robotic system to map the old part of the city</i>	Include your comments here	
Your Challenge / Robotic technology	Include your comments here	
(1) Impact Indicators		
Social & Cultural Impact: Does this challenge improve citizens' independence, accessibility and mobility? Does it improve quality of life and better public services?		
Environmental Impact: Does this challenge address resource efficiency? Does it show potential for sustainable growth? Does it improve sustainable mobility?		
Economic Impact: Does this challenge increase the support SME enterprises? Does it increase or improve employment opportunities? Does it give a positive relation cost/benefit?		
Innovation Impact: Does the proposal give a better relation risk/benefit? Does it give a positive evaluation of the product life cycle? Does it present capacity to integrate systems and synergies?		

Fig. 4.5: E++ Urban PDTI Questionnaire

- i) Social and Cultural Impact, to improve citizen's participation, independence, accessibility and mobility, and to improve the quality of life, better public services and replicability of the proposal in other districts and cities;
- ii) Environmental Impact, to improve resource efficiency, to improve sustainable mobility and potential for sustainable growth;
- iii) Economic Impact, to increase the support to small and medium companies and leverage private funding, increase or improve employment opportunities and the evaluation of the cost/benefit of the new technology;

- iv) Innovation Impact based on the ability to execute, the evaluation of the risk/benefit of the proposal, the innovation in robotics and the capacity to integrate systems and synergies. Finally, we also evaluated the City Presentation and its implication with the objective to increase and improve technological robotic innovation through public demand in urban environments.

The E++ Urban PDTI Questionnaire, completed with the impact criteria for evaluation was sent to European City Councils, City Council Departments, Cities Associations, Smart City World Congress'13 Speakers, Robot Manufacturers and Research Institutions and Organizations. Two local living labs and the European Network of Living Labs (ENOLL) were also contacted. These living labs offer us a real-life test and experimentation environment where users and producers co-create innovation in a trusted and open ecosystem. We also programmed a work-shop in a propitious scenario, the Smart City World Congress, inviting all the involved stakeholders to participate. This Narrowing Down phase brought us four-teen Urban Robotic Challenges' proposals from European Cities addressing specific challenges with a detailed description of the public service to improve or create by robotic technology (Table 4.3).

Table 4.1: E++ Urban Robotic Challenges

HELSINKI Finland	Traffic infrastructure inspection and maintenance. Decreasing the cost of maintenance and increasing the area liveability through robotisation of the city's maintenance traffic at the Smart Kalasatama designated smart city area, including both vehicles and installed infrastructure in the area.
BARCELONA Spain	Automatic detection and road surface damage warnings. To find a solution that can gather data and analyse the 11Mm2 of asphalt paving surfaces, road, cycle and pedestrian across the whole city
CORNELLA Spain	Improving waste management and street cleaning. Perform tasks with less cost for the maintenance of parks and gardens.
BARCELONA Spain	Utilities infrastructures condition monitoring. To mechanize sewer inspections in order to reduce the labour risks, objectify sewer inspections and optimize sewer cleaning expenses of the city.
MALAGA Spain	Environmental monitoring and control. This challenge aims at the deployment of a robotic collaborative network for monitoring and mitigating the presence of air pollutants (including pollen), as well as odours that may be unpleasant to citizens.
GREENWICH United Kingdom	Improving tourist services at the city. To provide a cost effective way of interacting with visitors to provide accurate information based on real time management data as well as information on attractions and related services.
SEVILLA Spain	Improving the management, planning and urban city observations. The use of aerial robots in the management, planning and urban city knowledge.
SEVILLA Spain	Planning and information of urban accessible routes. The realization of a LAND ROBOT, as the basis for a group of them deployed around the city taking mobility accessibility data that are inherent in the development of the Planner.
PADOVA Italy	Providing safe and secure environments for citizens. The new technology should improve the limits of traditional surveillance cameras and should have more features compared with the actual passive video surveillance/acquisition.
VALENCIA Spain	Improving the management, planning and urban city observations. An innovative monitoring system applied to urban bus lines to monitor Origin and Destination and sustainable mobility modes.

BARCELONA Spain	Personalized mobility support for pedestrian areas. To create a system or service that will guide the transport or mobility impaired through the neighbourhood. The system must be integrated into the pedestrian area of the new city model raised.
SITGES Spain	Providing safe and secure environments for citizens. New robotic infrastructure where now there is a human intensive service. Objectives: noise reduction, surveillance and management of public spaces, especially in crowded events and support to disabled people in pedestrian areas.
BARCELONA Spain	Goods distribution technology to improve local retail. To create a sustainable system to make the distribution from the neighbourhood Warehouse to each commerce. This robotic system must to be integrated in the pedestrian areas of new neighbourhoods.
COIMBRA Portugal	Personalized mobility support. To contribute to the downtown urban life revitalization, improving the existing personalized transport as a key issue to connect activities and people. To select and apply the best mobility solution that can assure an effective transportation role in the downtown.

The third step, the Ranking one, consisted in the evaluation and selection of the most promising Urban Robotic Challenges to be funded through the E++ project. The evaluation was done by a panel of experts that selected the ECHORD++ PDTI Urban Robotic Challenge. The final document included a prioritized challenges' list and the selected proposal: "To mechanize sewer inspections in order to reduce the labor risks, objectify sewer inspections and optimize sewer cleaning expenses of the city" presented by Barcelona City Council - BCASA.

Finally, we prepared the Challenge Brief, the main document for the Call for RTD Proposals. As we have said before, the translation of the needs into functional requirements requires a team of people with highly developed competences. The team was formed by four UPC robotics researchers and four people of the city council directly involved in the performance of the public service. The functions were described looking to facilitate the innovation on one hand and answering the real needs of the public service on the other hand.

The figure 4.6 summarizes the functions required in the sewer inspection performance and its weight. The new device has to be able to answer to these requirements that are fully explained along the challenge brief document.

With the elaboration of the challenge brief, the first group of activities was finished and the first main objective of the PDTI instrument - to increase the number of urban robotic challenges proposed by Cities - was reached: 14 urban robotic challenges were proposed by European cities with specific description of each one that could be the starting point of a new Innovative Public Pre-Commercial Procurement and at the same time, the European cities were introduced into the robotic technology knowledge.

The second part of the E++ PDTI develops the Activities for research and technical development of the pre-commercial products. This part started with a Call for proposals and was structured in three phases: solution design, prototype development and small scale test series (Figure 4.5).

The call for proposals was open 6 weeks at the E++ website and was announced in international media. The call documentation included the Challenge brief, and a guide for applicants with the PDTI procedure and the evaluation criteria. The evaluation and selection of the RTD proposals included an expert panel with BCASA, UPC, TUM and two external experts and was based on marks given according to three basic criteria:

Scientific and/or technological excellence

- *How well the proposed technology addresses the challenge as detailed in the respective challenge description?*

FUNCTIONS				WEIGHT	
Sewer serviceability inspection	Sewer performance (at least 1000 lineal meter/labour day)			10%	80%
	Images (Video)			40%	
	Geometric analysis (scanning)			20%	
	Monitoring	Air		9%	
		Water		1%	
Structural defect inspection				15%	
Sampling				5%	

Fig. 4.6: Functions required to the new technology and weight into the full operation procedure

- *How well does the proposed technology integrate the required functionalities? How intuitive is the technology for the end users? How easy can the technology be integrated in the environment? How robust is the technology? Does it solve specific technological challenges (Mobility, Communication, etc.)?*
- *To what extent shows the proposal a clear plan for the development of a working solution.*

Quality and efficiency of the implementation and the management

- *How effectively will the project be managed?*
- *To what extent appears the consortium to have dedicated the resources (e.g. Human capital, equipment, man hours, etc.) necessary to perform the scope of the proposal*
- *To what extent the crucial risks (technical, commercial and other) to project success appear to have been identified and how effectively will these be managed*

Potential Impact through the development, dissemination and use of project

- *Does the project clearly identify a partner (as part of the consortium) who will bring the technology to the market?*
- *Does the project include a commitment to the commercialization of the technology?*
- *To what extent has the proposal the potential to address future / wider challenges in the area*
- *Return on Investment: Time span required to have the break even with the purchase of the device*
- *Time to commercialization*
- *Marketability*
- *The price of the solution (including installation, training, maintenance) for total cost - independent of the business model (sale or leasing).*

Three RTD proposals have been selected to be financed by ECHORD++ project:

Robodillos: *Networked Mobile Robotic Platform for Shared Autonomy Sewer Inspection Operations* presenting an advanced robotic platform for sewer inspection operations that synergistically integrates state-of-the-art wireless communication technologies with autonomous multi-robot systems technologies in a unique, robust, agile, scalable and reliable solution.

Partners: Cyprus University of Technology (Cyprus) and HELIKAS ROBOTICS LTD (Cyprus)

ARSI: *Aerial Robots for Sewer Inspection.* The ARSI consortium planned to tackle the pipelines and galleries inspection using a micro aerial vehicle (MAV), multi-rotor type, endowed with sensors

for its autonomous navigation along the network, collecting data for its inspection. The aerial option avoids the mobility constraints that suffer the vehicles that should advance along paths having steps, steep drops and even objects like the own domestic waste or elements dragged by pluvial waters.

Partners: Fundació Privada EURECAT (Spain), Fomento de Construcciones y Contratas (Spain), Simtech Design S.L. (Spain), IBAK Helmut Hunger GmbH & Co. KG (Germany) and Fundació Barcelona Media (Spain)

SIAR: Sewer Inspection Autonomous Robot. The SIAR project would develop a fully autonomous ground robot able to autonomously navigate and inspect the sewage system with a minimal human intervention, and with the possibility of manually controlling the vehicle or the sensor payload when required. Key platform features like 5 hours' autonomy, more than 3 Km per battery charge, adjustable body width and a flexible pay-load system will definitely ease the system setup in sewers, adapting the robot to a wide spectrum of galleries and tasks.

Partners: The Consortium is composed of a SME called IDMind (IDM) and two Universities, Universidad de Seville (USE) and Universidad Pablo de Olavide (UPO). The project is coordinated by IDM, which also leads the commercial exploitation of the SIAR system.

The Phase I, Solution design and first results (TLR4), had a duration of six months. At the kick off meeting a document elaborated by UPC and BCASA about monitoring and evaluation criteria was discussed with the consortia. The main issues to evaluate were: Positive evaluation of the tasks and documentation required during the period; Deliverables and Milestones; Dissemination Milestones; Detailed explanation of the solution design; Logistics required and operational issues by using the solution and Test Series Phase I.

The test series would check the viability of the robotic solution mobility in the sewer network conditions (4.7).

<i>Mobility: Description and conditions</i>	<i>Evaluation</i>
<i>Robot motion:</i> <i>100 meters (autonomous)</i>	<i>The speed will be evaluated. 60 minutes is the maximum time in 100 meters</i>
<i>Conditions:</i> <ul style="list-style-type: none"> <i>The robot has to include the equivalent weight of the sensors</i> <i>One trial in straight line and another one with a curve</i> <i>The trial will be done in Barcelona or in their place in a sewer</i> <i>The trial will be done at different illumination conditions</i> 	

Fig. 4.7: Mobility: Description and conditions

Then the communications suitability in underground sewage system network. The communication in the sewer conditions, as an underground infrastructure, is also one of the aspects to be solved in this project. It is proposed to perform a test to check the suitability of the communication technology planned by each robotic solution, using the following description and conditions (4.8).

<i>Communications: Description and conditions</i>	<i>Evaluation</i>
<i>To send information from one to another point at different distances (100m, 200m, 300m, 400m).</i>	<i>Communication suitability.</i>
<i>Conditions:</i> <ul style="list-style-type: none"> <i>• The robot has to include the equivalent weight of the sensors</i> <i>• One trial in straight line and another one with a curve</i> <i>• The trial will be done in Barcelona or in their place in a sewer</i> <i>• The trial will be done at different illumination conditions</i> 	

Fig. 4.8: Communications: Description and conditions

And the autonomy versus mobility of the robotic solution have been tested (4.9). The mobility and the autonomy must be assessed jointly, since these properties depend on the performance of the functions to be done by the robotic solution.

<i>Autonomy: Description and conditions</i>	<i>Evaluation</i>
<i>Proof that in 8h the robotic solution can arrive to 1 km. The batteries can be charged or changed several times in the trial.</i>	<i>Mobility versus autonomy.</i>
<i>Conditions:</i> <ul style="list-style-type: none"> <i>• The result of the above tests will be extrapolated considering the energy consumption in each case, and the performance in 8 h will be simulated.</i> <i>• The robot has to include the equivalent weight of the sensors</i> <i>• The trial will be done at different illumination conditions</i> 	

Fig. 4.9: Autonomy: Description and conditions

Finally, the Economic Viability of the proposal with a detailed business plan was required with the cost structure and cash flow for the three companies involved in the marketability of the solution: the robotic manufacturer, the public services company and the public entity that improve the public service required and reduce the costs of it.

The Phase I final test (Figure 4.10) and expert panel was fulfilled in July 2016, evaluating the three robotic solutions.

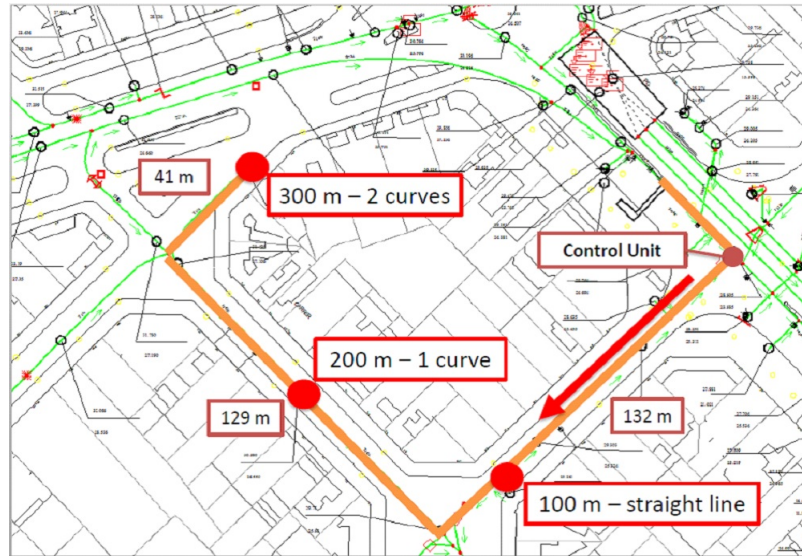


Fig. 4.10: PDTI Sewer. Phase I. Final Test. Facility location and trial characteristics

The ARSI Consortium has delivered very detailed and thorough reporting on Operation requirements and system design. The consortium has made good use of the expertise available at different consortium partners and has reached a commendable level of integration given the limitations of budget and time in phase 1 of the project. In particular, the proposed integration with the DRACMA system for operational planning and execution is impressive and shows that the consortium is in close communication with the potential end user of the solution. The choice of an aerial solution has clear advantages in a sewer environment which contains many different obstacles and geometries. The tests have demonstrated that semi-autonomous flight is a must for a viable operational solution. Robust tele-operated flight will not be possible without it so it is critical for the success of the solution. Regarding to the autonomy, the analysis and flight tests carried out in Phase 1 of this project suggest that an autonomy between 15 and 20 minutes. Given an estimated battery life of 10 minutes and an inspection speed of 0.5 m/s, we obtain an inspection range of 300 meters. This would give an estimated inspection rate of 300 meters per hour, or 2.4 km per 8h day what exceeding the challenge brief minimum requirement of 1000m/day for robots, or even 1500m/day currently achieved by current inspection protocols. (Figure 4.11)

The design solution for the ROBODILLOS system was based on the Atum Rover, an existing solution. The tests in the sewer have demonstrated that this design with a fixed axle and fixed width will not be able to cope robustly with the various geometries and obstacles encountered in the sewer system. The recovery tests performed during the trials have shown that there are a number of situations from which the platform cannot recover. A strong point for the ROBODILLOS solution,



Fig. 4.11: PDTI Sewer. Phase I. Final Test. ARSI

at least in principle, was the communication system and the method of deployment with multiple robot platforms to relay the signal. However, the Silvus system selected did not perform significantly better than conventional Wifi systems during the trial. The conceptual solutions proposed for the sensing, sampling and inspection is satisfactory. The range of Robodillos platform demonstrated during the autonomy trials is satisfactory. In conclusion the current mechanical design of the platform and concept design presented offers little hope of a robust working remotely operated or semi-autonomous solution. The consortium would have benefitted from more direct interaction with an end user, early trials in the actual sewer and/or having an end user in the consortium (Figure 4.12).



Fig. 4.12: PDTI Sewer. Phase I. Final Test. ROBODILLOS

The SIAR consortium has made radical design changes compared to their initially proposed solution in order to accommodate the real world environment in the sewer. Their proposed tracked solution has been replaced by a 6-wheel crawler and further changes to the 6 wheeled design are

proposed to accommodate the various widths of the gutters in the sewer system. Based on the trial results and the design specification offered it is still likely that the design will have operational limitations. It is unlikely that the current design would have been able to perform the test in remote control or semi-autonomous mode. The autonomy test was satisfactory and it is likely that the final design will have sufficient range (in terms of power) to operate under practical conditions. Communications rely on line of sight. As long as this line of sight is maintained the range and performance is satisfactory. The consortium intends to use repeaters to maintain communication beyond line of sight. The implementation of the sensors for 3D mapping, navigation, air sampling and inspection is commendable and worked well during the demonstration. Further attention may be needed to implement the right lighting conditions for visual inspection. The consortium assessment of the sewer inspection cost reduction to 0,51 Euro per meter seems realistic. Very significant technical challenges remain and the SIAR consortium should be able to resolve them to a sufficient extent to produce a commercially viable solution (Figure 4.13).



Fig. 4.13: PDTI Sewer. Phase I. Final Test. SIAR

Two solutions, ARSI and SIAR were selected to start the phase II of the activities of research and technical development of pre commercial products.

Phase II of Activities for Research and Technical development of Pre-commercial products started with a kick off meeting linked to the Smart City World Congress 2016 where the first robotic prototypes were showed. The Evaluation results of Phase I and recommendations were sent to the consortia to be incorporated to the next prototypes. A document including the monitoring procedure and the evaluation criteria for phase II was exposed to the selected consortia. Phase II was structured in four monitoring periods, deliverables and tests. During all the period the prototypes were tested several times and the sewer network was open and attended by BCASA to do demos and tests.

The Phase II final test and expert panel was celebrated in October 2017 by an expert panel composed by BCASA, UPC, TUM and two external experts. Both consortia were evaluated and selected to continue to phase III of the RTD Activities:

In phase II the ARSI consortium had achieved an important milestone, which is demonstrating stable semi-autonomous flight in the sewer. This was of crucial importance for the viability of the solution, as manually controlled flight is almost impossible in the narrow sewers. The MAV platform had a flight time of 7-9 minutes. During the trials it was observed that pilots were hesitant to fly beyond 25% battery remaining battery, effectively limiting the flight time to 5-7 minutes. In addition, the payload restriction was very critical and the consortium has made considerable compromises with respect to carrying on-board sensors and electronics which are

negatively affecting the overall performance of the solution. The localization of the MAV in the YZ plane was satisfactory and allowed for relatively stable flight, the X localization along the length of the sewer, based on odometry needed improvement as it diverged by up to 20%, also it was desirable to have a graphic representation on a GIS map of the drone actual position. The flight Control was satisfactory. Communication bandwidth was a critical issue. The band-width seemed very limited and was compromising the ability to send real-time data and control information. The inspection performed during the trials needed most improvement. Visual data was marginally acceptable by end users however; the 3D reconstruction was inadequate. It didn't show most of the defects and gross distortions in geometry reconstruction. The control interface was simple and adequate for the purpose. Improvement was needed on the 3D Data presentation. Finally, the working procedures needed to be further optimized to improve the efficiency. The requirement to open many hatches for access and retrieval of the MAV and communication was an operational complication and undesirable as many hatches in the city are located in the middle of roads with traffic. The performance demonstrate that the efficiency can be improved by careful analysis of the working procedures (Figure 4.14).



Fig. 4.14: PDTI Sewer. Phase II. Final Test. ARSI

The SIAR consortium has made commendable progress since the last evaluation at the end of phase I. The design of the robot has been significantly improved, the addition of the spring-loaded suspension with variable width has increased the reliability of operation and the versatility of the system. Nevertheless, further improvement to the systems and design are needed to further reduce the likelihood of the robot getting stuck in unrecoverable situations, in particular when taking turns or negotiating obstacles. It is recommended that operator information about position of the wheels and immediate surrounding of the robot should be improved, eg. by adding a wide angle camera. Key operational parameters for negotiating bends and obstacles should be studied and used for automating navigation as much as possible. The communication with the robot was satisfactory, as was the repeater system. The payload of the vehicle is satisfactory. The consortium has made commendable progress in inspection procedure, but this area still needs improvement. The consortium should take due note of the reporting requirements as outlined in the challenge brief and should interact as much as possible with end users to understand the inspection and reporting requirements. The lighting was adequate. The SIAR solution presented a robotic arm that was recommended to be removed as it added complexity and costs and adds too little benefit. Water protection needed to be further improved specifically for the motors. Also material choice was not optimal for the sewer conditions e.g. use of carbon steel bolts instead of stainless steel. A significant design overhaul should be required to arrive at a robust commercial solution. A strong point was that the robot could be reversed in order to save a lot of time. The control interface was simple and adequate for the purpose. Finally, the mission execution and working procedures were efficient and adequate (Figure 4.15).

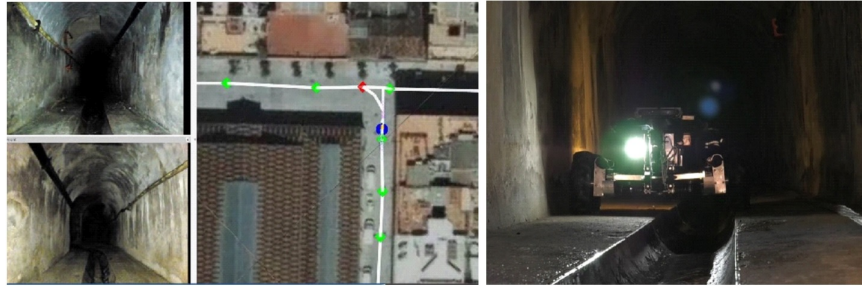


Fig. 4.15: PDTI Sewer. Phase II. Final Test. SIAR

The Evaluation results of Phase II and recommendations had been sent to the consortia to be incorporated to the next prototypes to be developed in Phase III. A document including the monitoring procedure and the evaluation criteria for phase III was exposed and discussed. In Phase III, the prototypes developed in Phase II were fully developed and installed at the sites of the public body in a small-scale test series incorporating to the prototype the technological improvements needed to perform the inspection and clearance of the sewer network, mentioned in the Challenge Brief, looking to achieve TRL7-8 and accelerating their route to commercialization. The monitoring procedure of this phase included three specific tests to be performed at the sewer network: the first one about serviceability inspection, the second one about structural defects inspection and the final one about the performance of the new technology. A marketing workshop with specific experts was celebrated in the middle of the period to analyze the robotic market and to push both solutions to commercial roll out.

The phase III and the PDTI process will be concluded by a final assessment. The expert panel composed by BCASA, UPC and two external experts assessed the readiness level of the advanced prototypes in a final test at the sewer network and evaluated the marketability of the proposals and the future actions to perform. The information is not available at the time this article is written but we are convinced that the second objective of the PDTI instrument was reached: Two pre commercial robotic solutions would be available for cities to improve the sewer network inspection and clearance waiting for a large volume of end products to be developed as commercial ones.

4.4 Comparison and Conclusions

Municipalities could boost procurement for innovation in the initiation phase of the technology life cycle, co-creating new solutions with the private sector to sustainability challenges and opportunities in the cities [9]. The development of technology is the key to mastering these challenges and transformations in the European Cities and the Innovative Public Procurement Instruments as the PDTIs are the right tools to accelerate them.

Cities and citizens have specific needs, not solved by existing market products, which require innovative solutions. These innovative solutions are based in new technologies that are unknown for public managers [10]. Few examples of Public Procurement for Innovation have been developed in Europe over the last few years. In spite of this, the European cities are prepared. Their competitiveness makes them strong and at the same time, the innovative public procurement makes them more competitive. The lead-user role played by several cities working together can have spectacular results in innovative public procurement and the case study of ECHORD++ PDTI bring us a structured and proactive process to achieve them.

The PDTI instrument has matched the two main objectives proposed: fourteen urban robotic challenges posed and defended by European City Councils, all of them with robotic technology associated one step below an innovative RTD public call and two robotic pre commercial solutions to inspect and maintain the sewer network at cities which development has been driven by public entities, services companies, SMEs, and academia.

The results achieved in the ECHORD++ PDTI procedure in a continuous learning by doing, brought information about what robotic technology works on and can do to solve social challenges; an intensive and coordinated dialogue between all the stakeholders involved has been essential for the PDTI success; the monitoring structure of the RTD activities was the key to push the technological level of the robotic solutions and drive them to the market and finally the role of the academia was essential, not only in technological topics but also in the coordination and management of the whole process.

Acknowledgements This work has been funded with "ECHORD++ EU Project FP7-ICT-2012-601116".

References

1. Edler, J., Georghiou, L.: Public procurement and Innovation-Resurrecting the demand side. *Research Policy* **36**, 949-963 (2007)
2. Dalkey, N.C., Helmer, O.: An Experimental application of the Delphi method to the use of experts. *Management Science* **9**, 458-467 (1963)
3. Paré, G., et al.: A systematic assessment of rigor in information systems ranking-type Delphi studies. *Information and Management* **50**, 207-217 (2013)
4. Georghiou, L., Edler, J., Uyarra, E., Yeow, J.: Policy instruments for public procurement of innovation: Choice, design and assessment. *Technological Forecasting & Social Change* **86**, 1-12 (2014)
5. Dalpé, R.: Effects of Government Procurement on Industrial Innovation. *Technology in Society* **16**, no.1, 65-83 (1994)
6. Edquist, C., Zabala-Iturriagoitia, J.M.: Public Procurement for Innovation as mission-oriented innovation policy. *Research Policy* **41**, 1757-1769 (2012)
7. Cohen, B., Amorós, J.E., 2014. Municipal demand-side policy tolos and the strategic management of technology life cycles. *Technovation* **34**, 797-806 (2014)
8. Delbecq, A., Van de Ven, A., Gustafson, D.: *Group Techniques for Program Planning*, Scott Foresman and Company, Glenview IL (1975)
9. Lember, V; Kalvet, T; Kattel, R: Urban Competitiveness and Public Procurement for Innovation. *Urban Studies* (2011)
10. Uyarra, E., Edler, J., García Estevez, J., Georghiou, L., Yeow, J.: Barriers to innovation through public procurement: A supplier perspective. *Technovation* **34**, 631-645 (2014)

Part II
Echord++ Experiments and Contributions

An overview of all the Experiments and PDTIs selected by ECHORD++ project is presented introducing this Part II. Then 10 scientific-technological articles of the Experiments and PDTIs expose the results reached and their contributions to the scientific community.

Chapter 5 describes the “Lessons Learned in Vineyard Monitoring and Protection from a Ground Autonomous Vehicle”. This project is focused on the improvement of plague control tasks, specifically on the distribution and placement of pheromone dispensers for matting disruption, currently a labor intensive and time consuming task.

Chapter 6 expose an overview of the experience and the results achieved during the development of the robotized system for switchgear wiring carried out in the WIRES experiment. The preliminary experimental results show that the developed system can achieve a success rate of about 95% in the wire insertion and connection task.

Chapter 7 describes the “Optimality criteria for the path planning of autonomous industrial vehicles”. The proposed investigation aims to establish the most appropriate offline path planning criterion to be used for the design of autonomous warehouses, in order to improve the plant performances.

Chapter 8 presents the results of “FASTKIT: A Mobile Cable-Driven Parallel Robot for Logistics”. The subject of this paper is about the design, modeling, control and performance evaluation of a low cost and versatile robotic solution for logistics from a combination of mobile robots and a Cable-Driven Parallel Robot (CDPR).

Chapter 9 explains a heuristic planning for rough terrain locomotion in presence of external disturbances of a quadruped robot platform. This approach enables the quadruped robot to successfully traverse a significantly rough terrain in absence of visual feedback. The experiments demonstrate the effectiveness of the approach in rough terrains and the capability of the platform to estimate and compensate in case of disturbances.

Chapter 10, describes EXOtrainer platform. This chapter presents the challenges and main features of the ATLAS 2020, an active pediatric exoskeleton developed in the frame of the EXOtrainer project. The result of the evaluation of ATLAS 2020 exoskeleton in the clinical trials performed in the hospital Sant Joan de Deu in Barcelona (Spain) during three months are summarized.

Chapter 11, describes the ASSESSTRONIC platform, one of the winning consortia for the PDTI challenge “Comprehensive Geriatric Assessment CGA)” for healthcare. In this chapter a wheeled ground robotic platform architecture is explained. Additionally, the interaction for cognitive tests and the mobility of the platform for the physical tests are described with the preliminary results of usability evaluation and reliability of cognitive and physical tests.

Chapter 12, describes the ARSI platform, one of the winning consortia for the PDTI challenge “Robots for the inspection and clearance of the sewer network in cities”. In this chapter an autonomous Micro Air Vehicle (MAV) is explained, describing the the robotic platform with the sensors and communications systems. It also includes the robot functionalities navigation, perception, mapping and localization), the serviceability and defects inspection and the experiments performed.

Chapter 13, describes the SIAR platform, one of the two winning consortia for the PDTI challenge “Robots for the inspection and clearance of the sewer network in cities”. In this chapter a six-wheeled ground robot is explained, describing the robotic platform with the sensors and communications systems. It also explained the robot functionalities (navigation, perception, mapping and localization), the serviceability and defects inspection and the experiments performed.

The last paper in this part, the Public Body BCASA explains the selected challenge in the urban robotic scenario, “Robots for the inspection and clearance of the sewer network in cities”, describing the PDTI procedure for this challenge, the challenge brief technical documentation, the current situation of the service, the functions and conditions for the new technology, the evaluation criteria and end-user guidance along the whole project.

In the following, the abstracts of the 31 experiments funded by ECHORD++ are reported in alphabetical order.

2F (*The Flooring Fellow*) experiment aims at introducing robotics in construction yards by developing a co-working robot for a specific function related to floor building: grout removing and floor cleaning with acid. The 2F experiment will be introduced to the market in the next years as a new product for the building sector. The use of 2F will impact directly on the entire working cycle related to the flooring realization and the developed co-working robot, together with related accessory range, will increase safety, ergonomics, and eco-sustainability during the specific working phases. More specifically the expected impact is the reduction of construction workers labour time and cost and the reduction of construction worker hazards and risks (noise, vibration and electric shock). The concrete outcome of the Experiment is the conception of a TRL 7 prototype of the robotic platform, and submission of a patent on the technology developed.

The goal of the 3DSSC (*3D Smart Sense and Control*) experiment was to develop a robot operated cheese peeling solution. With the help of smart 3D sensing, thinner coating of a block cheese is removed resulting in reduced losses. As another objective, the project also targets to increase the speed of cheese peeling. In the current state, the speed of operation is 30% slower than the manual one with comparable losses. However, the system will be optimized to improve upon the current prototype. The demonstrated results have attracted significant commercial interest, in particular with the objective to further develop the demonstrator into industrial implementation. The project also resulted in filing one patent (pending) and a planned journal publication.

AAWSBE1 (*Adaptive Automated WEEE Sorting 1: Battery Extraction*). In order to address legislation regarding increased reuse of batteries and rare metals in WEEE, the AAWSBE1 experiment aims to sort batteries inside Waste Electrical and Electronic Equipment (WEEE) by using deep learning techniques. It will detect potential battery-containing items from residuals in a WEEE small electronics stream, as well as presort battery streams for more efficient recycling of the batteries. The AAWSBE1 system will be adaptive in order to address changing market values, and changes in legislation. Furthermore, it will employ design strategies from industry 4.0 by learning from process data new prioritizations regarding gripper types and gripping points by measuring success rates and employing a secondary camera to measure changes in the scene in between picks. It will be designed to work as an individual sorting station in a line, with either manual or robot sorting stations, capable of either working alone or of integration into a cognitive factory

CATCH (*Cucumber Gathering – Green Field Experiments*). Harvesting represents one of the costliest and most critical phases in horticultural value chain production. The advantageous and opportunities of automation of harvesting tasks by means of innovative robotic technologies (agricultural robots, terms also used agrobots, hortibots etc.) has been recently widely identified as one of the most advantageous green-techniques approaches capable of ensuring improved crops yield and environmental sustainability impacts. CATCH experiments deal with the shortage of flexible, cost-efficient and reconfigurable/scalable hortibotic out-door solutions for automated harvesting in difficult natural conditions by addressing critical problems: fruit perception and fast picking actions. The use case of outdoor cucumber harvesting has been selected taking into account the need from relevant end-users, the technological challenges, as well as the economic impact in various European regions.

CoCoMaps (*Collaborative Cognitive Maps*) experiment uses an expanded version of the existing Cognitive Map Architecture implemented on Honda's ASIMO robot in an environment with more complex tasks than already attempted. This will allow the robot to interact in more complex ways, in particular, to simultaneously interact with another robot and more than one person at a time. Thus, the project aims for a group of 2 robots and 2 humans. These systems will enable social interactions that can coexist with the robots' attention to – and completion of – practical tasks in the workplace. A particular focus is on human detection and tracking algorithms and on an improved dialogue system.

CoHRoS (*Cooperative Programming for Highly Redundant Robot Systems*). Highly redundant robots with up to ten or more degrees of freedom are commonplace for welding, grinding, or varnishing

of large in sectors like earthmoving equipment, agricultural machines or automotive engineering. Programming these systems is tedious, costly and needs highly specialized expertise, which is an important factor to achieve a reasonable return-of investment for automation. The project CoHRoS aimed at redefining and advancing the state-of-the-art in programming for such highly redundant robot systems through developing a practical and robust method for assistive teaching using machine learning techniques. The project has allowed the development and testing of a software solution for such programming tasks. This solution was integrated into an industrial setup, to allow demonstration in an operational environment. Results achieved have led to discussions with a number of interested potential industrial partners.

DEBUR (*Automatd robotic system for laser deburring of complex 3D shape parts*). The overall objective of the experiment was to design and set up an automated robotic station for laser deburring of metal casting 3D parts. The experiment has developed a flexible, low-maintenance and environmentally friendly prototype, able to replace the current hydraulic deburring and manual sanding operations of casting industries, for components with different geometry and burrs thickness (< 2.0 mm). Therefore, it was intended to obtain quality, uniform and low roughness cutting edges, with protrusions lower than 0.2 mm, and without thermal affection, all of them done in competitive cycle times (60 - 90 s for the selected parts). An adaptive cognitive robotic system has been developed, to carry out the process of deburring and manipulating the parts autonomously, and to provide overall process inspection using 2D and 3D machine vision techniques. This system corrects the predefined trajectory, implementing a burr tracking system based on machine vision techniques, and finally determines the optimum cutting path. Building upon the strength of the prototype developed, collaborations with a number of industrial partners is being pursued.

DexBuddy (*Dexterous Robotic Co-Worker*) was mainly a software capability demonstrator experiment. It showed the potential of the combination of 3D-vision, finger-based force sensing and wrist-based force sensing used with online grasp and motion planning as well as force-controlled motions. Furthermore, it showed how concepts of intuitive programming can be used to parameterize arm and finger motions for dexterous manipulation. The overall setup was demonstrated in the context of a dexterous industrial assembly use-case with cables. The work performed in the Experiment has led to a partnership with a large industrial group.

DUALARMWORKER (*Dual-arm robot closed kinematics chain motion planning for flexible industrial components assembly*) will solve one of the key issues to the real use of dual-arm robots in industrial applications: the planning and execution of highly-constrained closed-chain dual-arm motions. No industrial software or open source library available today allows these capabilities. The objective of the experiment is to: 1) Transfer the knowledge and algorithms for closed-chain dual-arm motion planning from academic research labs (in particular LAAS-CNRS) to the industry through Tecnaia; 2) Implement them into a cognitive dual-arm robot for flexible assembly operations; 3) Deploy them into an Aeronautics pilot station in AIRBUS Spain to evaluate their performance. The technology will be demonstrated by applying it to deburring process of HTP (Horizontal Tale Plane) and VTP (Vertical Tale Plane) ribs of the A380 airplane. Depending on their size and shaped, ribs have to be manipulated using two arms. This experiment targets to give the means to manipulate the bigger sized ribs with two hands. The experiment will conclude with a robust closed-chain dual-arm planner that will be tested in a pilot station manipulating a selection of bigger sized ribs. A successful result of the experiment will open the doors to many other exploitation opportunities for the automation of aero and non-aero applications where dual-arm coordinated manipulation is required. After the conclusion of the experiment, the dual-arm trajectory planner will be released as a MoveIt! open source plugging by LAAS-CNRS, which will make the results available to be exploited by many other companies and institutions.

EXOTrainer (*Clinical Evaluation of Gait Training with Exoskeleton for Children with Spinal Muscular Atrophy*) addresses the introduction of wearable gait exoskeletons for the therapy of children affected by Spinal Muscular Atrophy (SMA). Although a rare disease, SMA is the first cause of child mortality, affecting all countries, races and gender. There is still no known cure for SMA,

and treatments mainly focus on maintaining the physical state of the patient, and delay the onset of side effect like scoliosis and loss of range of motion which lead to more serious illnesses. Walking is key to retard these side effects, and EXOTrainer will provide a solution through wearable gait exoskeletons. EXOTrainer builds over available technology and thus addresses a new target group and new diseases, as current commercial devices are targeted to adult paraplegics. The prototype exoskeleton developed in the project has achieved the level of maturity necessary to provide a walking ability to patients. In the final stages of the Experiment, the technology developed is undergoing clinical trials, paving the way towards CE marking and future series production.

The goal of the FASTKIT (*Collaborative and mobile cable driven parallel robot for logistics*) project is to provide a low cost and versatile robotic solution for logistics using a combination of mobile robots and Cable-Driven Parallel Robot (CDPR). The FASTKIT prototype addresses an industrial need for fast picking and kitting operations in existing storage facilities while being easy to install, keeping existing infrastructures and covering large areas. The FASTKIT prototype consists of two mobile bases that carry the exit points of the CDPR. The system can navigate autonomously to the area of interest and deploy the CDPR at high velocity by controlling the cable tension.

The FlexSight (*Flexible and Accurate Recognition and Localisation System of Deformable Objects for Pick-Place Robots*) experiment aims to provide a robotic solution for the "pick& place" class of applications with rigid and deformable objects. The project focuses in building a prototype smart camera - the FlexSight Sensor (FSS) - which can be integrated in the chassis of an existing robot to empower it with detection and localization capabilities. The main objectives of the FlexSight experiment are: (1) Enable a robot to perceive a large and widespread class of rigid and deformable objects in an accurate and reliable way, with a particular emphasis on the computational speed of the whole system. (2) Implement a prototype of a compact industrial sensor (the FSS), that integrates inside a robust and small chassis all the required sensors and a processing unit suitable to run the detection and localization algorithms. (3) Integrate the FSS inside a working system that will be tested in several industrial and logistic use cases. The FSS will integrate latest generation components, such as high speed, low noise CMOS cameras, laser random pattern projectors, and a compact but powerful computer board with integrated GPU. The experiment will exploit state-of-the-art deep learning techniques for the object detection step. At the end of the project, we plan to produce and commercialize the FSS.

The main goal of GARotics (*Green asparagus harvesting robotic system*) was to improve/redevelop a 3D detection system for green asparagus and the development of a robotic tool for selective harvesting. Both had to reach a reliable success rate of more than 95% under real conditions in order to bring a commercially viable product to market. The project led to the development of a detection and harvesting device prototype, which was successfully tested in an operational environment. Using a 3D camera and a corresponding image processing program, detection rate of 100% was reached. Using an active cutting and gripping device, 95% of detected asparagus stalks were harvested successfully, in tests on an asparagus field in UK.

GRAPE (*Ground Robot for vineyard Monitoring and Protection*). Precision agriculture practices aim to significantly reduce the negative environmental impact of farming due to over-application of chemicals, while still producing enough food to satisfy a growing demand. The introduction of advanced sensing capabilities allows monitoring at plant level, spotting problems before they spread. Furthermore, introducing farming robots, chemicals can be applied with honeybee precision, pesticides and fungicides can be used only when needed and in the smallest necessary amount, or even be substituted by less impacting techniques (e.g., mechanical instead of chemical thinning, biological control instead of chemical pesticides). GRAPE project aims at creating the enabling technologies to develop vineyard robots that can increase the cost effectiveness of their products. The project addresses the market of instruments for biological control by developing the tools to execute (semi) autonomous vineyard monitoring and farming tasks with Unmanned Ground

Vehicles and, therefore, reducing the environmental impact with respect to traditional chemical control.

HOMEREHAB (*Development of Robotic Technology for Post-Stroke Home Tele-Rehabilitation*). Rehabilitation can help hemiparetic patients learn new ways of using their weak arms and legs. However, reductions in healthcare reimbursement pressures rehabilitation specialists to reduce the cost of care and improve productivity. Service providers have responded by shortening the length of patient hospitalization. Additionally, early home supported discharge of subacute stroke patients has been proved to have a significant impact on motor recovery after stroke, but equires some level of innovation of methods and tools for service delivery to really become a sustainable solution for the healthcare system. The HOMEREHAB project will develop a new tele-rehabilitation robotic system for delivering therapy to stroke patients at home. It will research on the complex trade-off between robotic design requirements for in home systems and the performance required for optimal rehabilitation therapies, which current commercial systems designed for laboratories and hospitals do not take into account.

HyQ-REAL (*From the research lab to the real world*). Disaster response and other tasks in dangerous and dirty environments can put human operators at risk. Today's remote-controlled vehicles with wheels and tracks have limited use in such missions due to their reduced mobility on rough terrain. In the wake of recent disasters (e.g. Fukushima power plants) we have witnessed how tracked robots can struggle and eventually get stuck in unstructured environments, such as stairs with rubble. A new generation of all-terrain vehicles, with legs instead of wheels and tracks, is finally reaching performance levels that show superior mobility on rough terrain. The HyQ-REAL experiment will bring IIT's new quadruped robot HyQ2Max from the laboratory to the real world applications. Under the experiment, ruggedization of the HyQ2Max robot and providing it with power autonomy are the main goals.

INJEROBOTS (*Universal Robotic System for Grafting of Seedling*). Grafting in horticultural seedling industry is a common hand-made practice, with the objective to achieve a stronger and more productive plant. Currently, grafting of seedlings is a very important part of the horticultural production industry in Europe, accounting for solanaceae (tomato, pepper and eggplant) market up 38% of world production, with more than 200 million of grafted plans annually, and for cucurbitaceae (watermelon, melon and cucumber) market up to 47% of world production, with more than 120 million of grafted plants annually. INJER-ROBOT'S goal is to perform a universal and flexible robotic system to make grafting of horticultural seedlings, based on the cooperative work of two commercial robotic arms supported by artificial vision, and external devices.

KERAAL (*Kinesiotherapy and Rehabilitation for Assisted Ambient Living*). Low back pain is a leading cause disabling people. It particularly affects the elderly, whose proportion in European societies keeps rising, incurring growing concern about healthcare. Assistive technology in general and assistive robotics in particular may help to address the increasing need for healthcare. In particular, it can help people with musculoskeletal conditions that need keeping mobility of joints and increase of muscle force and coordination. In this context, the experiment proposes to develop a robot coach for rehabilitation exercises. The goal is to increase the time patients spend exercising, by alleviating the lack of time a physiotherapist can spend monitoring a patient. With this perspective, the experiment will develop a robot coach capable of demonstrating rehabilitation exercises to patients, watch a patient carry out the exercise and give him feedback so as to improve his performance and encourage him.

The LA-ROSES (*Laser Assisted Robotic Surgery of the anterior Eye Segment*) project aimed to develop a robotic platform dedicated to Laser-assisted Keratoplasty (cornea transplantation), with the objective to substitute the laser tip currently handled by the ophthalmic surgeon. The solution proposed offers a tool capable to safely assure the welding (suturing, without needle and stitches) of the cornea in a way not possible with other techniques. The surgeon has an on-line control of the trajectory of the laser and of the temperature of welding, critical to the safe success of the

surgical procedure. A robotic arm is used to position the end-effector over patient's eye, then three motors move the laser along the desired trajectory. Work performed in the project has led to the development of a proof-of-concept prototype. Additional work is considered to reach higher TRLs. Possible alternate uses of the developed technology are being pursued, both in the medical field (laser welding of tissues), and for industrial applications

LINarm++ (Affordable and Advanced LINear device for ARM rehabilitation). The goal of the project was to realize a technological solution enabling a multisensory, multimodal and patient-oriented neuromuscular rehabilitation of the upper limb, currently unavailable among off-the-shelf devices. The developed solution integrates a variable-stiffness end-effector rehabilitation device, a wearable neuromuscular electrical stimulation system, a virtual rehabilitation scenario, a low-cost unobtrusive sensory system, and a patient model for adapting training task parameters according to the patient. Work performed in LINarm++ led to advances in several areas, including that of unobtrusive measurements of physiological parameters, sensor fusion and interpretation of human data, bio-mimetic and bio-feedback FES for upper-limb rehabilitation, and design of variable stiffness actuators and related control techniques. Building upon the strength of the prototype developed in the project, clinical trials are expected in the coming months.

MARS (Mobile Agricultural Robot Swarms). The goal of the experiment is the development of swarm-robotic solutions for precision agriculture, targeting automated seeding tasks in particular. The technology developed is intended to 1) reduce usage of seeds, fertilizers, and pesticides, 2) reduce soil compaction, and 3) provide an easily scalable and automated solution. The product developed will address expanding needs in terms of food production in the near future, and significantly reduce the associated environmental impact. In the project, two cloud-connected, small-size ground robots, equipped with precision localization technology and integrated seeding units, were developed to successfully demonstrate the approach. The work performed has led to the development of a strong partnership with the industrial end-user, active work on further development of the technology is being pursued.

MaxES (An Embedded Software for Autonomous Industrial Vehicles). The proposed experiment aims to develop, to implement and to test navigation software for delivery robots in an industrial environment. The experiment is part of the smelter of the future framework, aiming to integrate fully autonomous unmanned vehicles in an industrial process. The integration of unmanned vehicles in a factory raises some very challenging problems such as the robustness of the navigation for indoor and outdoor operations and the safety of goods and people. The proposed experiment is the first of its kind in the world involving a robot for handling and delivering heavy loads in a realistic situation alongside other vehicles and pedestrians. In addition, the experiment will demonstrate the feasibility of implementing an autonomous form of logistic in an existing plant, without guiding infrastructures and while keeping the existing road network.

MODUL (Modular Drive Units for Legged Locomotion). In the project MODUL a highly integrated series elastic actuator module was developed. To this end, a motor, harmonic drive gear, custom titanium spring, sensors, and specifically developed motor control electronics were compactly integrated in a single joint unit. This drive combines perfect impact robustness with precise torque regulation and is made for operation in harsh environments (IP67). It is well suited for applications involving interaction tasks such as manipulation, rehabilitation robotics, prosthetic devices, or walking robots. Over the last year, the drive was successfully tested in ANYmal, an autonomous quadrupedal robot that is capable of walking and running. Projects achievements have led to the development of a very well defined, conceived, and received new product (attracting significant attention from interested customers), and the creation of a spin-off.

MOTORE++ (A new Rehabilitation Robot for the upper limb: refinement and experimental trials). Stroke is one of the leading causes of adult disability in the world, and is the second cause of death for individuals over 60 years of age. Most of the patients who survive such an accident are left with a severe partial paralysis and need professional help for rehabilitation. It is predicted that expenses

for medical care and rehabilitation in this case will grow steadily. The goal of MOTORE++ is to continue the development of a planar rehabilitation robot named MOTORE (MOBILE roboT for upper limb neurOrtho Rehabilitation) aimed to restore upper limb functionality and to assess performance in patients with neurological diseases. MOTORE is the first robot small enough to be easily carried, it is the first robot really suitable for home based rehabilitation. Proprietary software has been developed with several exercises/games. The core business of humanware is the production of medical devices and MOTORE++ will be the flagship product of the company. CE marking was obtained during the run-time of the project, and the first product sales were recorded.

PICKIT (*Multi-modal bin-picking for new industrial tasks*). The objective of the experiment was to incorporate tactile sensors into the grippers of an off-the-shelf bin-picking system. A gripper thus equipped introduces an essential modality to a bin-picking system, especially if the object's surfaces are challenging to detect optically and do not allow for a precise position estimation. In this case, the haptic modality, which offers tactile feedback from slight physical contact between the gripper and the content of the bin can be used to support the gripping process. The experiment identified various potentials in bin-picking through use of tactile sensors in the gripper. This applies in particular to the Grip Monitoring after picking a part, more precisely detecting collisions, verifying a successful grip operation and an accurate part placement. The presented method reduces the cycle time by up to 36%. Supplementing inadequate optical data by tactile data offers new opportunities for e.g. the detection of transparent parts. We successfully demonstrated our approach for picking glasses and blackened washers, which so far could not be detected by the camera. Commercialization of the technology is to be discussed in the short term, and additional technological developments are being pursued within a new European project.

RadioRoSo (*Radioactive Waste Robotic Sorter*). The scope of RadioRoSo is decommissioning operations performed in nuclear waste storage facilities. A significant amount of old and undocumented nuclear waste is buried underground in unused mines in several countries. Many of these facilities, created as far as 50 years ago, pose a safety and environmental risk, and thus several countries have started or considering the decommissioning of these waste in safer facilities. Decommissioning is a complex and expensive process. Large industrial cells are manufactured around the storage silos. Sorting is done manually by using mechanical master-slave manipulators. The process is very slow and tiring for the workers, thus requiring short shifts, a high number of workers and a long time of training. The overall cost is huge. RadioRoSo intends to reduce the costs of the operation by means of intelligent automation of pick-n-place tasks. Specifically, the experiment will demonstrate autonomous sorting of Magnox swarf (debris from the deconstruction of nuclear fuel cells) intending to isolate medium radioactivity parts from low radioactivity waste.

The SAFERUN (*Secure and fast real-time planner for autonomous vehicles*) experiment aims at developing and implementing a new planning methodology for Laser Guided Vehicles (LGV). Such vehicles, which are largely used in industrial environments for the autonomous transportation of huge loads, share their workspace with several independent agents, like other LGVs or humans. For efficiency, but also for safety reason, LGVs move along pre-specified path segments. This implies that they cannot skip unexpected obstacles placed along their route: collisions are normally avoided through the execution of emergency stops. The drawback of this approach is that, in the absence of a thorough study, collisions can only be avoided by greatly reducing the average vehicle speeds: evidently, the plant productivity is negatively affected by such commonly used strategy. The new planning method proposed for the SAFERUN project aims at improving the safety standards in LGV plants – such to preserve the physical integrity of human coworkers – by simultaneously increasing the plant productivity.

SAGA (*Swarm Robotics for Agricultural Applications*) goal is to prove the applicability of swarm robotics to precision farming. The application of swarm intelligence principles to agricultural robotics can lead to disruptive innovation, thanks to the parallel operation of multiple robots and their cooperation. The experiment aims at demonstrating such advantages and compare with the current state of the art within the context of a monitoring/mapping scenario. By exploiting swarm

robotics principles, a group of small UAVs will be deployed to collectively monitor a field and cooperatively map the presence of weed. An existing multi-rotor UAV will be enhanced with on-board camera and vision processing, radio communication systems and suitable protocols to support safe swarm operations. The experiment will develop robust on-board vision routines capable of supporting local navigation and discerning weeds from cultivated plants. Collectively, the robots will build a map of the field with semantic tags associated with different areas, so as to convey precise information about the presence and amount of weed in the different parts of the field. This will facilitate optimal spatiotemporal planning of weeding operations, and autonomous precision weed removal in the future.

SAPARO (Safe Human-Robot Cooperation with high payload robots in industrial applications). Current industrial applications with human-robot collaboration focus on the use of small robots such as the KUKA iiwa, Universal Robots UR5 etc. due to safety considerations. However, many industrial applications where human-robot cooperation would be very beneficial require higher payload capacity and robots with large workspaces. In the SAPARO experiment we propose an innovative and trendsetting solution for safeguarding collaborative human-robot workplaces with high payload robots through a combination of safeguarding technologies. This consists of a tactile floor with spatial resolution together with a projection system to warn the human. The safety zone is dynamically created, according to the relevant guidelines in ISO/TS 15066, based on the velocity and joint angle positions of the robot instead of statically. Safe human-robot interaction is a key strategic area intrinsically related to Industry 4.0 and Factories of the Future. The industrial partner has committed to bringing the product to market, and the sale of an early prototype has already been recorded.

TIREBOT (A TIRE workshop robotic assistant). The goal of the experiment was to build TIREBOT, a cooperative robotic assistant for helping the tire workshop in the heavy part of the tire changing process. By delegating to TIREBOT the low level tasks we aimed at making the work of the operator less tiring and more efficient. TIREBOT employs advanced control, localization, perception and cooperation strategies in order to cooperate with the operator. The operators have experienced a 63% reduction of the efforts compared to the manual exchange of tires. The experiment has led to the development of a TRL 7 prototype. Strength of this prototype has attracted expressions of interest from a number of possible end-users of the developed technology.

WIRES (Wiring Robotic System for Switchgears). The experiment aims to improve production quality of switchgears by automatizing the wiring process which is currently handled manually due to high complexity of the involved manipulation tasks. The experiment will contribute in software as well as hardware (grippers) to come up with a robotic solution for wiring. The main challenge is to develop a novel gripper with tactile sensors which can handle deformable objects such as wires and simultaneously operate on screw/clip type connection points. During the WIRES experiment, manipulation strategies exploiting tactile feedback for tolerant wire grasping and handling during connection on electromechanical components in a laboratory setup will be evaluated. For limited simple cases, the applicability of the results to the switchgear production in a realistic scenario will be tested. All the technologies developed within the WIRES experiment aim at reducing the time for switchgear wiring and at improving the product quality. The foreseen reduction of the wiring time is about 40% with respect to the overall wiring time, due to the fact that at least part of the overall wiring process can be executed by the automatic system also overnight. It is clear that the achievement of these objectives will have a very strong impact on product cost and company income. IEMA estimated on its 2016 data that the time saved in the wiring process can generate an additional sales volume of about 4M€, with an increase with respect to the "conventional" manufacturing of about 53%. This estimation can be extended proportionally to all companies, even of different market fields, whose products currently require a long wiring time.

Chapter 5

Lessons Learned in Vineyard Monitoring and Protection from a Ground Autonomous Vehicle

Ferran Roure, Luca Bascetta, Marcel Soler, Matteo Matteucci, Davide Faconti, Jesus-Pablo Gonzalez and Daniel Serrano

Abstract Vineyard protection is a key task for winegrowers to maximize crop yield. Control of plagues, fungi and other threats are recurrent tasks in winery. This project is focused on the improvement of plague control tasks, specifically on the distribution and placement of pheromone dispensers for matting disruption, currently a labour-intensive and time consuming task. The operators walk through the vineyard hanging the dispensers in a regular distribution pattern. Grape project aims to automate the dispenser distribution in the vineyard using an outdoor autonomous ground platform with a robotic arm. Furthermore our platform is used to monitor the vineyard status and retrieve this information to the producer in order to provide timely and precise information from the field.

5.1 Introduction

The application of robotics in agricultural tasks, either as automated systems or as a support tool for farmers, can offer the necessary step change in farming production in order to meet the future needs of an increasing world population (34% by 2050 according to FAO¹). GRAPE aims at contributing to this technological breakthrough by developing a mobile robotic system endowed with a robotic arm able to perform precise agricultural tasks at plant level for vineyards. GRAPE project is based on four main technological components designed and integrated to monitor plants health in vineyards and to apply a biocontrol mechanism consisting of pheromone dispensers for plague control. These results have been validated in real scenarios covering a predefined range of scenarios in Italy and Spain, two of the EU countries with the largest wine production. The four technological components are:

- Vineyard navigation module based on advanced localization and mapping capabilities and path planning techniques considering terrain characteristics and kino-dynamic constraints to enhance safety and robustness.

L. Bascetta, M. Matteucci
Dipartimento di Elettronica, Informazione e Bioingegneria, Politecnico di Milano, Milano, Italy,
e-mail: name.surname@polimi.it

F. Roure, M. Soler, D. Faconti, J-P. Gonzalez, D. Serrano
EURECAT Technology Center, Barcelona, Spain e-mail: name.surname@eurecat.org

¹ Food and Agriculture Organization of the United Nations. <http://www.fao.org/>

- Plant health monitoring module implementing advanced perception capabilities for plant detection in highly unstructured and geometrically variable scenario and plant health assessment for early detection of problems.
- Precise manipulation and deployment for a targeted pheromone dispenser distribution.
- User friendly operational interface enabling robot teleoperation, data visualization and reporting.

As a main target of the project the automatic deployment of pheromone dispensers is seen by the producers as a first step for the work-in-field automation. However, the real-time monitoring of the field status is also an important and valuable aspect for the stakeholders. Due to the huge extension of the fields, accurate monitoring is sometimes difficult. Having a robot continuously acquiring data and providing reports to the farmers will enhance the productivity and the quality of the product. The successful development of these tasks will be reflected in the seasonal costs and will represent a step forward in precision farming.

In this project we focused on two different species: Eudémis (*Lobesia botrana*) and Cochylys (*Eupoecilia ambiguella*). The former has presence in southern vineyards. The larva, a yellow, dirty green at the final stage, is very strong. Butterflies are 5 to 8 mm; they have an activity threshold at 14° C and are crepuscular. The latest, rather northern, may also occur in some southern vineyards. The larva slow movements; color "lees of wine" and his glossy black head are very characteristic. Butterflies are 6 to 7 mm and are slightly larger than those of Eudémis. They are of yellow ocher color, with a dark brown band, blocking the wing.



Fig. 5.1: Eudémis (left) and Cochylys (right) specimens.

Depending on the specific dispenser, the distribution ratio varies between 200 and 700 dispensers per hectare, with a border reinforcement. Starting from one corner of the field, the robot travels through the vineyard rows putting the dispensers in a regular pattern, following the vendor's indications. During the mission, the robot collects relevant data about the vineyard growth and health status allowing agronomists to assess in an objective quantitative way the plant status without walking along the vineyard to collect information. Real-time monitoring and control is also needed in order to react to any failure occurring in the field. Remote control and real-time view using a portable device, like a smartphone or a tablet, has been appreciated by the producers.

5.2 GRAPE robot

In order to speed up developments and ensure appropriate progress towards a final success on each of the objectives, GRAPE consortium proposed to rely on hardware COTS (Commercially off-the-shelf) components as much as possible. The added value of GRAPE project resides on the on-board autonomy. Therefore, the project will not design or manufacture new robots configuration or sensors. This section describes the COTS components selected for the hardware integration, namely, the mobile robot platform, the robotic arm and the navigation and agricultural sensors.

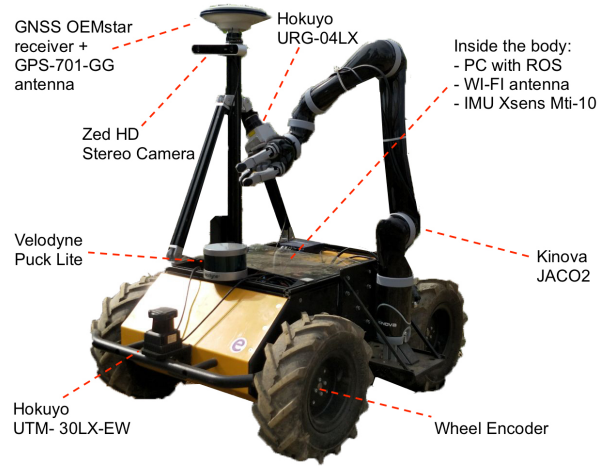


Fig. 5.2: GRAPE robot prototype

5.2.1 The mobile platform

The GRAPE consortium has selected for this project an outdoor mobile platform called Husky, which is a medium sized robotic development platform manufactured by Clearpath. Its large payload capacity and power system accommodate for an extensive variety of payloads, customized to meet research needs. Stereo cameras, LIDAR, GPS, IMUs, manipulators and more can be added to the UGV by our integration experts. The Husky's rugged construction and high-torque drive train can take research where no other robot can go. Husky is fully supported in ROS (Robot Operating System) with community driven Open Source code and examples.

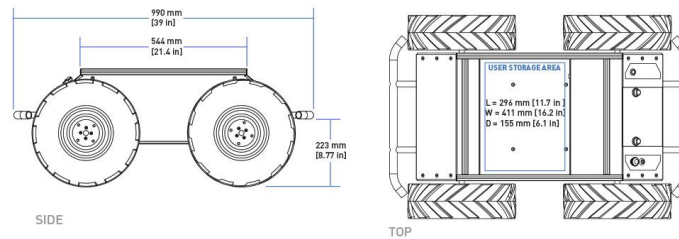


Fig. 5.3: Autonomous mobile platform Husky from Clearpath.

5.2.2 The manipulator

For the automatic dispenser deployment we selected the Jaco2 from Kinova, which is a 6DOF lightweight robotic arm, made of carbon fiber and aluminum, with a weight of 4.4kg and a reach of 90cm. The arm can mount a 2-finger or a 3-finger gripper. The design of the robot that includes the power electronics in the base, the possibility to power the arm with low voltage and the low power consumption makes this robot the best solution for mobile robotics. The control system can be reparametrized and Jaco2 is fully supported in ROS with community driven Open Source code and examples.



Fig. 5.4: Robotic manipulator Jaco2 by Kinova

5.2.3 The sensors

In order to acquire as much information as possible, we equipped the robot with a lot of sensors. Mainly, in the first stages of the project the number of sensors was probably over-sized. Then, during the implementation, we reduced the hardware to decrease both the power consumption and the final cost of the product. The final sensor configuration is as follows (Figure 5.2):

- Wheel odometry;
- IMU;
- GNSS receiver;
- 2D laser for navigation;
- 3D laser for environment 3D reconstruction;
- 2D laser for plant reconstruction;
- visual cameras for mission control and crop monitoring;
- depth camera for dispenser deployment control.

5.3 Autonomous navigation in vineyards

Being in the contest of field robotics, the aim of GRAPE navigation system is to be innovative, if needed, but most of all it has to be reliable, since it must guarantee to work in a difficult scenario

like the vineyard. The system has been designed based on a simple but very stable solution, and then one component at the time has been added until the final architecture presented in this paper has been reached. This approach has been possible thanks to the use of ROS, which allows to create very modular solutions in which the different components can be easily added or deleted.

The basic structure which compose the skeleton of the proposed solution is the standard ROS navigation stack, where the most relevant parts are:

- the odometry estimator and the sensor sources;
- the SLAM method in case of a mapping task;
- the AMCL localization algorithm;
- the move_base components to control trajectory planning and execution.

Figure 5.5 reports a simplified schema of the architecture. From this figure it is important to observe how the odometry estimation is the most critical component for both the SLAM and the localization methods. Indeed, if the estimated odometry is erroneous the navigation and mapping modules have a more complex scenario to face and they could not fulfill their goals.

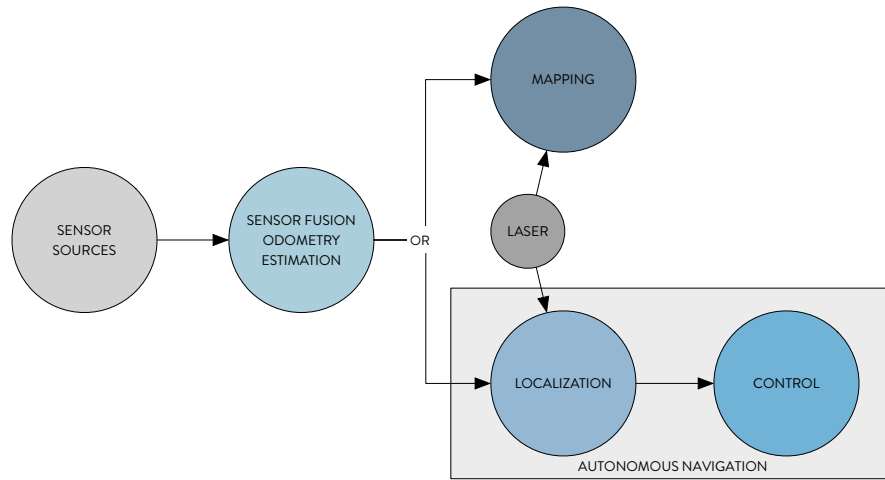


Fig. 5.5: Navigation system skeleton

5.3.1 Sensor fusion odometry estimation

Odometry estimation depends on the quality of the measurements coming from the motion sensors. In our case the variability of the environment introduces a significant amount of noise in these measurements. For this reason, we adopted a sensor fusion approach in which we exploit the wheels encoder, the IMU, and the GPS sensor all together. We implemented and compared two different sensor fusion tools testing different sets of sensors.

The first implementation of the sensor fusion odometry estimation module was based on the robot_localization package which merges the wheels encoders readings and the IMU, but this was not reliable since it accumulated error constantly during time. To solve this problem, we

introduced the GPS readings in the sensor fusion, obtaining an important reduction of the error due to the periodic correction made by the GPS. We implemented this second solution by creating two ROS nodes: `navsat_transform` node and `EKF_localization` node, where `navsat_transform` is responsible for the LLA to ENU conversion of the GPS coordinates, while `EKF_localization` estimates the odometry, i.e., it publishes the odometry frame transformation with respect to the robot frame, taking as input the converted GPS, the IMU, and the wheels encoder readings. This solution, being EKF-based, is computationally very efficient and it proves the importance of the GPS in obtaining accuracy and a good reliability. Unfortunately, it has also shown some important limits; it has an excessive confidence on the GPS measurements and does not leverage on previous poses estimates, indeed Kalman filters consider only the latest pose in the estimation of the current one. We implemented a third and final solution where we exploited the ROAMFREE framework.

The ROAMFREE framework allows to create a factor graph filter where readings coming from different sources are merged for an arbitrary interval of time. The amplitude of such time interval determines how many old poses are considered for the estimation of the current one. The factor graph employed by ROAMFREE represents the full joint probability of sensor readings (nodes) given the current estimate of the state variables, representing its factorization in terms of single measurement likelihoods. The factors represent measurement constraints: each factor is an hyper-edge and connects multiple pose and calibration parameters nodes. The filter estimates the odometry by means of max-likelihood estimation over the joint distribution, which can be efficiently done using non-linear optimization algorithms.

In our solution we designed a main node, `raroam`, which is a ROS implementation of ROAMFREE adapted to our specific case. The `raroam` node is in charge of building a factor graph filter combining wheel encoders, accelerometer, magnetometer, gyroscope, and GPS sensor (with measurements converted in ENU coordinates). For each sensors a covariance matrix is provided; the higher the values for the covariance components, the lower is the filter confidence (importance) on the corresponding sensor. ROAMFREE contains also an outliers rejection mechanism, called robust kernel, which allows to handle measurements for which the noise is too high. These measurements are indeed considered less in the optimization process, but not completely ignored. We exploited the robust kernel especially for the GPS and the wheel encoders; the former for its high noise (i.e., up to few meters) the latter for the presence of wheel slippage.

`raroam` needs an initial guess for the position of the robot in order to initialize correctly the factor graph. We implemented an auxiliary node, `initial_pose` node, which records the GPS and the magnetometer measurements for a fixed time and then computes the mean (x, y, θ) pose for factor graph filter initialization. The `raroam` node optimizes the estimation error by exploiting a Gauss-Newton optimization algorithm. Then, `raroam` publishes the transformation between the odometry frame and the robot frame.

5.3.2 Mapping

In the GRAPE experiment we expect to map the vineyard once and then let the robot navigate autonomously with its support. During the mapping the robot is manually driven along the vineyard rows. Then a SLAM software is used for map reconstruction.

As mentioned in the previous sections, we spent a lot of energy in building an accurate and reliable odometry estimation module for field operations. This allowed us to reuse methods of indoor autonomous navigation also on the field, including a laser SLAM system. We compared three different SLAM tools: Gmapping, Google's Cartographer, and KartoSLAM. All these methods require the same input information, i.e., an odometry estimate and some LIDAR readings, to produce an occupancy grid map. These three methods implement different approaches for laser SLAM: Gmapping is based on a particle filter, Cartographer and KartoSLAM use a graph based filter with an advanced scan matching. The final solution we propose to use in our experiments,

after evaluating the three methods, uses Gmapping as SLAM module, since it has proved to have a good trade-off between reliability and accuracy.

5.3.3 Localization and control

Robot localization is the problem of estimating a robot's pose with respect to a known map. This problem has been recognized as one of the most fundamental problems in mobile robotics [1]. The mobile robot localization problem comes in different flavors being position tracking the simplest one. Position tracking assumes the initial robot pose to be known, and localization seeks to correct small, incremental, errors in robot odometry. This can be seen as a problem of coordinate transformation where a map is described as a global coordinate system, independent from the robot pose, and localization is the process of establishing a proper correspondence between the map coordinate system and the robot local coordinate system.

In the ROS community the most adopted localization technique is Adaptive Monte Carlo Localization (AMCL), thus we tested it in our scenario. AMCL is a concrete implementation of a particle filter with some improvements, i.e., the count of used particles is not fixed. The decision of how many particles should be used is based on KLD-Sampling (Kulback-Leibler-Divergence) as described by [2]. AMCL requires the set of particles of the last known state \mathcal{X}_{t-1} , the control data u_t to perform a prediction step, and the measurement data z_t plus the map m to correct the pose.

We inserted the `amcl` package in our architecture aside the `move_base` control module. We tuned the AMCL parameters, especially the number and the range of particles because the repeatability of the vine rows can induce to some confusion during particles resampling, thus possibly producing localization jumps.

The `move_base` node, used for navigation, contains the planners and the costmaps. It is very important to correctly configure the local and global costmaps parameters since they are the base for the planning and control. One parameter that is very influent is the obstacles inflation radius and in our case it is very difficult to correctly set it. Indeed, a large inflation is useful to avoid the planning of paths the vine stocks, while a too large one could induce obstacles like weeds or high grass to affect the vine line traversability. We have realized this, because during an initial simulation phase we adopted a large value, but later during the real tests phase the robot often got stuck due to the presence of high grass.

We adopted a standard configuration of the global and local planners, since we were also interested to build a solution which is general and easily reproducible.

5.3.4 Navigation results in a real vineyard scenario

We have run several experiments to validate our architecture and the choice of its modules; some experiments have been done in simulation, some others have been real field tests.

A ROS architecture can be tested using real data collected on the field thanks to the possibility of logging data via the `rosvbag` tool. In the log file used during the tests, the GRAPE robot runs back and forth along two consecutive rows, then at the end of the second line it bypasses one line and goes in the next one, from here it runs again a back and forth path between two consecutive rows.

This log has been acquired during the winter, in a Spanish vineyard (Figure 5.6), when the vegetation is bare, that is also the period in which the robot is expected to work according to the GRAPE project requirements. Since in real scenarios it is almost impossible to have a ground truth of the robot position, we did not repeated the evaluation procedure adopted in simulation. Instead

we decided to compare the two sensor fusion odometry estimators using the mapping tests, i.e., by comparing the accuracy of the maps generated with the same SLAM method.

In the mapping tests we verified the SLAM methods with the two sensor fusion odometry estimators. The first thing we noted using real data was the huge difference in terms of perceived noise between the simulation environment and the real environment. In addition, in simulation we forced the presence of noise by generating it with Gaussian distributions, while the real data does not follow any known distribution, turning out to be more unpredictable. The presence of such noise led, as expected, to a decrement of the performance of our system. We partially solved this performance drop by deeply tuning and optimizing the configuration of our estimators.



(a) Satellite view



(b) Vine rows

Fig. 5.6: The vineyard used for testing

In EKFlocalization estimator the presence of noise in the sensors readings does not affects much its configuration since it has a small number of parameters that really influences the result of the estimation. For this reason, the configuration we adopted for EKFlocalization on real data is very similar to the one we used for simulation tests. This feature can be seen as a prove of the generality of the estimator and thus an advantage. In practice this does not hold true; this is an important limit for the estimator which is not adaptable to the increasing complexity of the environment.

Conversely, noise strongly affected the ROAMFREE implementation and configuration. Indeed, we spent much effort in setting the covariance of each of the sensors we adopted. Analyzing the noise of each sensor, we found, a good configuration of ROAMFREE. As it is possible to see in Figure 5.7, once properly tuned, the superiority of ROAMFREE with respect to robotlocalization is evident; all the maps built using it are clearly better than the ones obtained using the EKF filter.

The main differences on the maps generated with ROAMFREE in Figure 5.7 come from the different vegetative state of the vineyard. In fact, in the logged data there are no lives on the vines and only small weeds on the terrain, while when the robot was on the field, in summer, the vines are full of leaves and the grass on the terrain is more developed. In addition the soil cohesion changes, causing robot wheels skid in a different way. Nevertheless we have been able to generate maps in both conditions as it was aimed by the project.

5.4 Vineyard monitoring and plant inspection

One of the requirements of the project is the control of the vineyard. During all year and especially when the harvesting season is approaching, the farmer inspects the vineyard meticulously. The weeks before harvesting, this operation may occur practically every day. The introduction of an

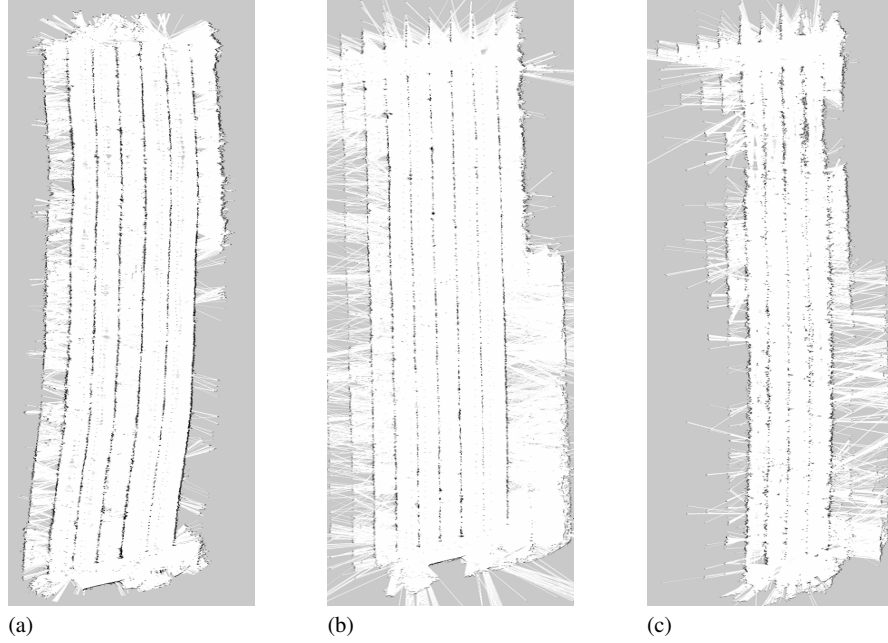


Fig. 5.7: Maps of the vineyard built using: (a) robotlocalization on logged data, (b) ROAMFREE on logged data, (c) ROAMFREE on field data

autonomous robot will reduce the dedication of the farmer to this task. Our proposal in this task is give useful tools to the farmer to speed up the inspection of the vineyard.

5.4.1 3D reconstruction of the vineyard

A 3D reconstruction of the vineyard is a useful tool to have a general overview of the field. Due to the extension of the vineyard, this reconstruction must be lightweight and manageable. Our aim is to use this global reconstruction as a base layer where all other information can be located. Thus, we generated a rough 3D map of the entire vineyard and we will add other information layers, like 2D map from navigation tasks or a precise 3D reconstruction of single plants using our scanning system. As we have a precise geolocalization system, with precision less than 10cm, each vine can be precisely located in the map. Our aim is make a comprehensive user interface where the producer can explore the entire 3D map and consult all information available. In order to generate a 3D reconstruction of the field we equipped the robot with a 3D laser (Velodyne Puck Lite). This laser is mounted in the front of the robot and is able to produce 300,000 points per second, covering 360° with 100 meters of range. However, we reduced the field of view of the laser in order to not be interfered by the robot itself. As all data from the other sensors, each scan must be corrected according to the robot movement. Figure 5.8 shows the 3D reconstruction of the vineyard and the surrounding facilities, obtained in one of the test missions from the 3D laser.

For a more precise information of the plants, we obtained a fine 3D reconstruction of each plant using a 2D laser attached to the robotic arm in a push-broom configuration. During the navigation,

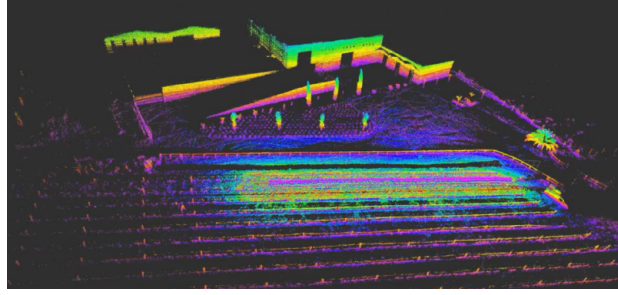


Fig. 5.8: 3D reconstruction of the entire vineyard using a 3D laser.

the robotic arm is safely folded over the robot, but with the end-tool and, thus, the 2D laser, pointing to the left side, towards the vineyard line. Taking into account the robot pose estimation, we concatenated all 2D beams from the laser over the time, and we obtained a 3D reconstruction of all plants. Figure 5.9 illustrates this result for a single row.

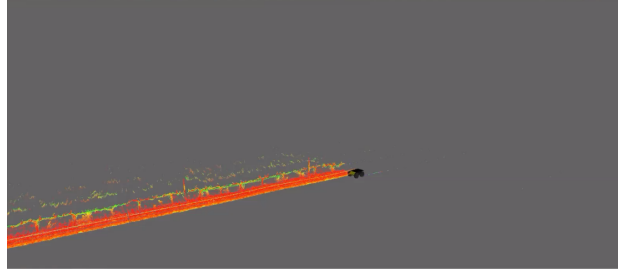


Fig. 5.9: 3D reconstruction of the entire vineyard using a 2D laser in pushbroom configuration.

5.4.2 Frondiness information

With the precise plant reconstruction we can extract useful information for the farmers, which can be used for real-time growth control. We segmented the plant reconstruction taking only the regions where the leafs are located. Then, we projected the points to the ground plane counting the points lying in the same vertical axis. In other words, for each vertical laser beam, we count the number of detected leafs. The result is a map of frondiness where the farmer can identify the plants without leaves, which used to mean that there some growing problem (see Figure . Obviously this tool can only be used during the flowering seasons.

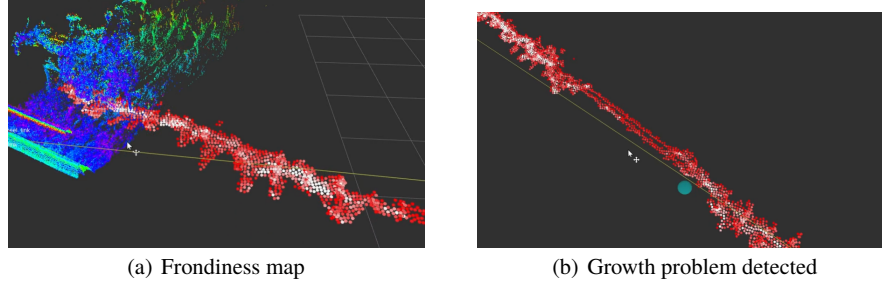


Fig. 5.10: a) 3D reconstruction of a single plant, and the frondiness map generated by our algorithm. b) Detection of growing problems; no leaves are detected, only the metal cables of the vine row. We used false-coloring to show the leaf density: from red (min) to white (max).

5.4.3 Real-time video monitoring and control

The real-time monitoring is mandatory for quick intervention. Despite the robot must work autonomously, the farmer will be able to control the current status of the mission at any time. During the mission, the farmer can remotely connect to the robot and see a live video streaming. For this purpose, we mounted a stereo camera (Zed) pointing toward the robot direction. We decided to use this kind of camera in order to have stereo imagery to build a 3D reconstruction with color information, because although the Velodyne is more precise, it doesn't have color available. Furthermore, the real-time streaming can be visualized with a stereo viewing device, having an immersive experience. Furthermore, the farmer can remotely control the robot at any moment with the user interface provided in case that a quick intervention is needed.

5.4.4 Plant reconstruction and deployment point selection

In order to accomplish the objectives in the dispenser deployment task, the system must know the morphology of the plant. The dispenser distribution is done during the first months of the year, when the plants are naked, without leaves, immediately after the pruning. This particular situation of the field determines the pipeline of the task. In this section our 3D reconstruction method is explained, as well as our strategy for the automatic deployment point selection.

3D vine reconstruction

We tested different 3D reconstruction methods in order to enhance the possibilities and achieve the best approach. Our first proposal was using a depth camera to obtain a 3D reconstruction of the plant. We tested different options: Microsoft Kinect and Orbbec Astra. Both cameras are RGBD. The depth field is acquired projecting an infrared pattern to the scene. The problem of this technology is that it not works properly outdoors. Used in a shadowed scenario, the camera retrieves some depth information, but if the under the sunlight, the camera is not able to detect anything.

Our second approach was based on structure-from-motion technology, which consist on extract 3D information from a set of consecutive images. The algorithm finds representative pixels in each image (key-points) and analyses the movement of these key-points across the images to compute the camera movement and, thus, extract a 3D reconstruction. Outdoors scenarios are better for RGB cameras because the lighting conditions are suitable. Our second prototype was conceived focused on acquire enough images to cover the entire plant. For this reason, we used three RGB cameras at different heights and pointing towards the plant. The main lack of this approach is the computation time because structure-from-motion algorithms requires high computing capabilities.

For this reason, we proposed a different solution, based on a 2D laser scanning system. Our approach consists of build a 3D reconstruction of a plant using a 2D laser attached to the end-tool of the robotic arm, given that the base platform does not move and the reconstruction is local to the robot current pose. Thus, our approach consists of moving the 2D laser along a known path, storing all 2D lines across the time, and projecting the scan from the current position estimate of the end-effector. This operation produces a 3D reconstruction of the scene. We attached the 2D laser in the end-tool of the arm and we designed a scanning path which covers the entire plant. Our system is able to fuse all 2D lines given by the laser and move them according to the movement of the laser. With this strategy we achieve a usable 3D reconstruction in real-time.



Fig. 5.11: 2D laser attached to the end tool of the arm.

Automatic deployment-point selection

Once the scanning process is finished, we obtained a 3D reconstruction of the plant. Then, this point-cloud is analyzed in order to find the a reachable point to hang the pheromone dispenser. Taking into account the plant morphology we noticed that the all pruned plants used to have the same shape: For the correct growth of the vine, the agriculturist cut the all the branches of the plant at 2 or 3 cm of the main trunk. Furthermore, all these branches used to point up. Thus, our target is to recognize these small branches and hang the dispensers there. The first step of our algorithm consist on remove the outliers of our raw scan. Then, we apply an Intrinsic Shape Signature descriptor [3] in order to select the key-points of the cloud. We used this descriptor because we wanted to extract the points lying in the boundary of the cloud. Although other detectors/descriptors exist focused on edge detection [4], we used ISS for its performance with noisy datasets. We developed a selection

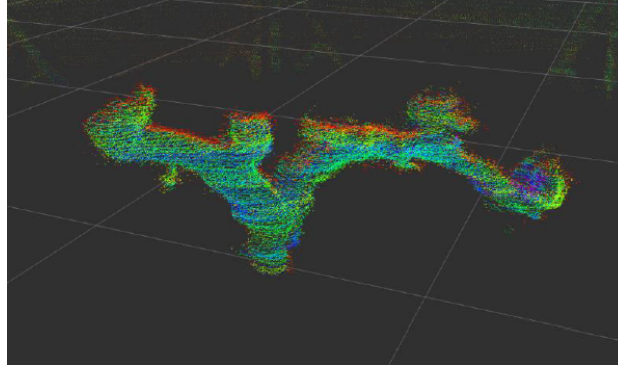


Fig. 5.12: Real-time results of our scanning procedure.

algorithm that finds the best point candidates in the key-point cloud according to its position and the normal vector associated. As we saw in our previous experiments, the best candidates used to be the isolated branches located at the end of the main trunk, or the highest ones. We decided to follow this strategy in order to prevent collisions between the arm and the plant, and to avoid complex arm movements. Thus, our system automatically selects a list of possible candidates and propose the best one. This algorithm can be executed in a fully automatic way, selecting the best point and starting the deployment, or in a semi-automatic way, which shows the selected point in a 3D reconstruction using the user interface of the system (See Figure 5.13). Thus, the user can accept this recommendation or select other deployment point.

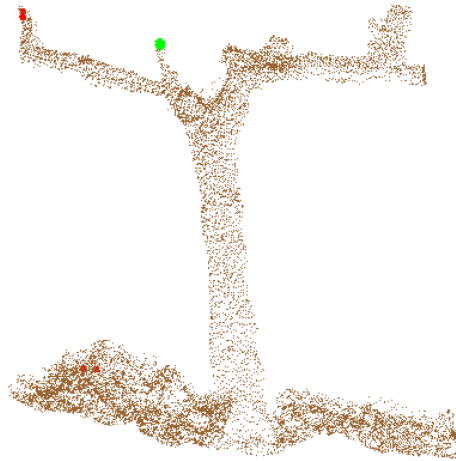


Fig. 5.13: 3D reconstruction of the plant done by the 2D laser. The green point shows the deployment location automatically selected and the red points are other possible candidates.

5.5 Dispenser manipulation and deployment

The manipulation task is completely decoupled from the navigation of the mobile base in the vineyard, indeed during the navigation phase the arm is kept in a safe position. Once the robot reaches a plant, the arm moves along a precomputed path to scan the vine using a laser scanner, and a 3D model of the plant is reconstructed. Analyzing this geometric model the best point where a dispenser can be deployed is automatically determined and the deployment procedure is executed.

The manipulation procedure is composed of the grasping and the deploying phase, in both cases a visual servoing control strategy is used to cope with the low accuracy and repeatability of the arm, and the variability of the external environment. Pheromone dispensers are small and flexible objects (see Figure 5.14). For this reason robot fingers have been equipped with nails able to robustly grasp and hold them during the operations. A feeder (see Figure 5.15), placed on the platform, keeps dispensers open so that they can be easily taken one by one by the robot.

The grasping and deploying tasks are executed following a simple procedure. First of all, the arm is moved above the feeder where a RGB-D camera is used to determine the height of the first available dispenser, then a visual servoing controller moves the end effector into the desired grasping position. For the deploying procedure, the dispenser can be released using three different strategies:

1. a simple position control to reach the target pose;
2. a partitioned visual servoing controller based on information about the branch provided by the RGB-D camera;
3. a visual servoing controller to deploy on a hook placed on a vineyard pole.

Images provided by the camera are also used to check that dispensers have been properly picked up and released on the plant.

The entire control system has been implemented using Robot Operating System (ROS) framework ², and exploiting MoveIt! library ³ trajectory planning an execution.

5.5.1 Dispenser manipulation tools

This section describes the devices that have been developed in order to manipulate the dispensers with the Jaco 2 hand. An example of these dispensers, the ISONET L E manufactured by Biogard, is shown in Figure 5.14. A dispenser is composed by two flexible plastic capillaries, welded at the end, full of pheromones, with a length of approximately 15 cm. Pushing the two ends the dispenser can be deformed, enlarging the two capillaries, so that it takes the shape of a ring and it can be hang to a branch of the vineyard.

Different versions of dispenser feeder, i.e., the device that allows to store dispensers keeping them open so that they can be taken one by one using Jaco 2 hand, and nails, i.e., the devices that are mounted on the fingers in order to make dispenser grasping operation easier and more robust, have been designed and realized to ease the manipulation, make it more robust, and increase the number of dispensers that can be manipulated.

One of the most important reason that makes this solution still far from a market-ready device is that Jaco 2, and in particular its hand, are general purpose devices not optimized for the specific application. Therefore, the length of the fingers is too large and the third finger interferes with, instead of aiding, the manipulation task. For all these reasons, the design of feeder and nails has been targeted to the creation of tools that allow to increase the manipulation robustness being able to support a reasonable demonstration of the GRAPE robot functionalities.

² <https://www.ros.org>

³ <https://moveit.ros.org/>



Fig. 5.14: The ISONET L E manufactured by Biogard.

Feeder and nail prototypes have been then realized using 3D printing and choosing, as printing material, ABS (Acrylonitrile-Butadiene Styrene). The last designed feeder and nails are shown in Figure 5.15.

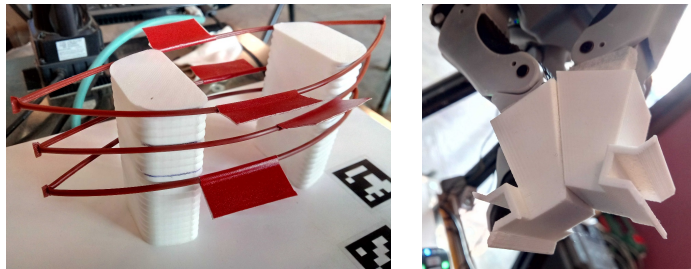


Fig. 5.15: Feeder and nails designed to manipulate dispensers.

The feeder is characterized by a continuous vertical surface with a zigzag pattern, i.e., a saw-tooth profile. The zigzag pattern aims at introducing enough friction to hold dispensers in the desired positions while its small indents should not allow them to get stuck in the feeder during the detaching operation.

Nails, on the other side, are characterized by a rectangular guide and two inclined edges. In the case of a small positioning error, this design eases dispenser entering inside the rectangular guide.

5.5.2 Grasping and deploying tasks

The dispenser deployment is the most critical task for the arm because of the uncertainties in the position of the feeder and the deployment location, and to the elasticity/deformability of

the dispenser that makes it an object difficult to be grasped and manipulated. These issues are particularly critical, as the size and characteristics of Jaco 2 hand do not fit for the purpose of dispenser manipulation, as already explained in Section 5.5.1, and because the positioning accuracy of Jaco 2 is too rough to allow for a solution, based on calibration and proprioceptive sensors only, to grasp the dispenser from the feeder. To overcome these issues, the task has been decomposed into the following parts:

- approaching feeder: the arm starts from the navigation position and a trajectory is planned and executed to move the end-effector to a pose close to the grasping zone;
- grasping dispenser: to increase the robustness with respect to positioning errors, the last part of the approaching trajectory and the grasping operation are executed using an eye-in-hand-camera and a visual servoing control law (for further details see Section 5.5.3);
- approaching deploying location: once the dispenser has been grasped and detached from the feeder the robot plans and executes a trajectory that connects the grasping zone to the deploying zone, i.e., a neighborhood of the selected deploying location;
- deploying dispenser: being this another critical task, dispenser deploying is performed using either position control only or visual servoing;
- homing to navigation position: once the deploying operation ends, the robot plans and executes a trajectory to the navigation position.

These macro-tasks are now decomposed, describing the specific activities that are included in each of them.

5.5.2.1 Dispenser grasping

The dispenser grasping task, that has been already decomposed into the two activities of approaching feeder and grasping dispenser, is now described in more details. The task can be decomposed into the following activities:

1. approaching feeder zone: a trajectory is planned and executed from the actual robot position to a position located approximately 45 cm above the feeders. This position has been selected in accordance with Realsense camera specifications in order to shot a RGB image and a depth image of the feeder zone.
2. measuring graspable dispenser: from the position reached at step 1 a RGB and a depth image are acquired. Processing these images, the height associated to the plane at which the graspable dispenser (the highest one on the feeder) belongs and the dispenser center with respect to the world frame are determined using two red tape strips placed at the two sides of each dispenser.
3. measuring marker position: a set of ArUco markers is located at the base of the feeder and is used to guide the grasping operation during the visual servoing control phase. The RGB-D image considered in step 2 is here used to determine the 3D marker positions with respect to the world frame.
4. computing visual servoing reference image: using the world position of the dispenser center, the end-effector pose given by the robot, the camera pose with respect to the end-effector frame, and the position of the nails in the grasping configuration with respect to the camera frame, the desired end-effector and/or camera position (with respect to the world frame) required to grasp the dispenser are computed. Using camera intrinsic parameters and 3D marker positions computed in step 3, a desired positions of marker corners on the image plane can be determined, as the image of the markers seen by a virtual camera located at the desired grasping position.
5. approaching grasping zone: a trajectory is planned and executed from the actual robot position to a position located approximately 25 cm above the feeders.
6. moving to grasping position: from the robot position reached at the end of step 5, the visual servoing control law described in Section 5.5.3, aiming at taking the robot to the grasping position, is applied and the robot is moved to the grasping position.

5.5.2.2 Dispenser deploying

Three different deploying techniques are considered for dispenser deploying. One is based on the deploying point computed on the 3D model of the plant and uses only position control. The second one reconstructs the plant region around the deploying point using RGB-D data and drives the robot with a visual control approach. The last one, being the most “industrial oriented”, deploys the dispenser on a hook placed on a vineyard pole using a visual servoing controller based on an ArUco marker.

Once the dispenser is grasped from the feeder, the approaching movement locates the arm in front of the plant, approximately 45 cm from the selected deploying location. This movement is common for all the deploying techniques.

Position control: In case deploying task is performed using only position control, it can be decomposed into the following sub-tasks:

1. moving to deploying position: from the approaching position a linear trajectory along the end-effector z -axis, connecting the actual position of the robot to the deploying position (i.e., the position selected by the user or computed using the 3D plant reconstruction and then tuned according to the nail position with respect to the end-effector frame), is planned and executed, using only joint position control. The end-effector pose at the deploying position has been selected, in order to ease the procedure and increase its success rate, in this way: x -axis parallel to the vineyard cables, z -axis pointing down and forming an angle of approximately 45 deg with the normal to the vineyard plane.
2. dispenser deploying: once the deploying position is reached, fingers are closed in order to deploy the dispenser.

RGB-D camera: The deploying task performed reconstructing the plant region around the deploying point using the RGB-D camera, can be decomposed into the following sub-tasks:

1. approaching deploying zone: the deploying position is transformed, using camera intrinsic and extrinsic parameters, into a position on the image plane and the region of the image around that point is analyzed, applying a suitable image processing algorithm, in order to determine the minimum area around the given position including the contour of the plant that approximates the shape of the deploying point. This portion of the contour is then fitted with a circle or an ellipse, whose center represents the feature tracked by a partitioned visual servoing controller in order to take the end-effector to the deploying location. A detailed description of this control algorithm is reported in Section 5.5.3.
2. dispenser deploying: from the robot position reached at the end of step 1 a precomputed motion, constituted by a linear motion along the end-effector z -axis and a rotation around the end-effector x -axis to make the z -axis pointing down and forming an angle of approximately 45 deg with the normal to the vineyard plane, is executed, and fingers are closed in order to deploy the dispenser.

Industrial-oriented solution: Finally, in case the dispenser is deployed on a hook, the task can be decomposed into the following sub-tasks:

1. moving to deploying position: from the approaching position, assuming that the ArUco marker placed on the vineyard pole is in the camera field of view, a visual servoing control is applied having as features the marker corners and as desired features a precomputed value of those points corresponding to the end-effector in the deploying pose. A detailed description of this control algorithm is reported in Section 5.5.3.
2. dispenser deploying: once the deploying position is reached, fingers are closed in order to deploy the dispenser.

5.5.3 Image based controllers

As mentioned in the previous section, the deploying procedure is based on two different image based controllers. The former is an image based visual servoing control law [5], whose features are three out of the four corners of an ArUco marker. The camera velocity determined by this controller is given by the following expression

$$v_{cam} = -k_1 (L^T L)^{-1} L^T e(t)$$

where

- v_{cam} , is the camera velocity vector, including linear and angular camera velocity, in the camera frame;
- $e(t)$, is the feature error computed on the image plane;
- k_1 , is the visual controller gain;
- L , is the interaction matrix obtained stacking the interaction matrices of the three considered feature points, each one computed for a fixed depth corresponding to its desired value.

The latter is a partitioned image based visual servoing control law [6], where the motion along the z -axis of the camera frame is decoupled from the motion on the xy -plane. In particular, the camera velocities v_{cam_x} and v_{cam_y} are computed using the following image based control law

$$\begin{pmatrix} v_{cam_x} \\ v_{cam_y} \end{pmatrix} = -L_{v_{xy}}^{-1} (k_2 e(t) + L_{v_z} v_{cam_z})$$

whose feature is the center of the deploying zone, as described in Section 5.5.2.2, and where

- $e(t)$, is the feature error computed on the image plane;
- k_2 , is the visual controller gain;
- $L_{v_{xy}}, L_{v_z}$, are the partitions of the interaction matrix of a feature point corresponding to the linear velocities in the xy -plane and the linear velocity along the z -axis, computed for a fixed depth corresponding to its desired value;
- v_{cam_z} , is the camera linear velocity along the z -axis.

The camera velocity v_{cam_z} , instead, is computed using a proportional controller based on the z -position error $e_z(t)$, i.e.,

$$v_{cam_z} = k_z e_z(t)$$

where k_z is the gain.

In order to increase the performance of the visual controller, without affecting its stability, an adaptive gain has been selected, computing k_1 and k_2 as an exponential function of the norm of the feature error vector, so that the gains increase as the error norm decreases.

5.6 Results

In this section we evaluate the results obtained during the last integration week of the project, where the final prototype was tested in the real scenario.

The dispenser deployment task consists of different strategies working together. As is explained in Section 5.4.4, we used the movement of the arm to scan the target plant. In order to measure the accuracy of this reconstruction, we have to take into account, not only the laser resolution but also the accuracy of the arm encoders, which produces the final movement of the arm. The laser resolution (Sick TIM 571) at 40mm of the plant is 3mm and its accuracy is 10mm. The arm has a tested accuracy of 10mm with 5mm of repeatability. Taking into account all these characteristics,

the maximum error would be 20mm for the final reconstruction. In practice, according to the results obtained in our preliminary tests, where the arm was requested to touch a set of control points obtained from a scan, we achieve a mean accuracy of 9.6mm. Table 5.1 shows the results of these tests.

Table 5.1: Results of accuracy tests of our scanning system in a controlled scenario.

Point	error (mm)	Point	error (mm)	Point	error (mm)
A	9	B	9	C	8
A	8	B	15	C	8
A	9	B	12	C	10
A	10	B	9	C	9

The target branches where the dispenser must be placed has between 10 and 15mm of diameter. Thinner branches are not desirable because the dispensers should remain there during a complete season. Thus, the resolution of the obtained 3D reconstruction is precise enough for correct branch detection. However, some eventual problems may arise in a real scenario, like branch occlusions or weed disturbances during the detection. For this reason our systems monitorize the deployment and detects if the dispenser is deployed correctly using visual supervision with the camera integrated in the arm. We tested the system in the real scenario with a set of controlled experiments. We deployed the dispensers in 10 different plants. In 7 plants the procedure was executed correctly, and the selected branch was the best option for the deployment. In 2 plants, although the selected branch was able to sustain the dispenser, the path which must be executed for the arm was too difficult for a correct placement. Finally, in 1 case, due to the weed which was interfering the reconstruction, the algorithm was not able to select a branch for the deployment.

Another critical part of the dispenser deployment is the dispenser grasping phase, either for possible robustness issues of the image processing algorithm and for the efficiency of the grasping device, whose optimization was out of the scope of the project. For this reason, the robustness of the image processing algorithm used to localize the height of the dispensers has been tested in a controlled environment, repeating seven times for each of the three different grasping heights the measurements. Table 5.2 reports the seven measurements and Table 5.3 the mean and variance.

Table 5.2: Height estimation of the dispenser.

Test	High	Intermediate	Low
1	0.04610	0.02681	0.01375
2	0.04593	0.02766	0.01394
3	0.04632	0.02738	0.01332
4	0.04630	0.02695	0.01353
5	0.04589	0.02688	0.01322
6	0.04656	0.02734	0.01391
7	0.04596	0.02801	0.01411

The detection of the markers used to localize the dispenser feeder is also a complicated task. As this detection is particularly affected by changes in the environment light, the image processing algorithm has been tested, artificially simulating different lighting condition. The algorithm was always able to determine the markers, except when the camera is dazzled by light reflection on the marker. This effect could be avoided if the markers are not covered by a protective plastic film, that

Table 5.3: Mean and variance of height estimation.

	High	Intermediate	Low
Mean	0.04615	0.02729	0.01368
Variance	5.344 E-08	1.686 E-07	9.628 E-08

is however necessary due to the outdoor dusty environment. A possible solution would be to print directly the marker on the feeder base.



Fig. 5.16: GRAPE prototype being tested in the field.

5.7 Conclusions

GRAPE project concluded being able to successfully complete the proposed task, deployment of pheromone dispensers. We are able to autonomously navigate through complicated terrains, avoiding obstacles and collisions. Our system automatically finds the best path taking into account the location where the pheromone dispensers must be deployed. We are able to obtain coarse and fine 3D reconstructions of the vineyard and we are able to extract useful information for the farmers like the frondiness indexes of the crop. Furthermore we used a robotic arm for automatic pheromone dispenser deployment, being able to hang the pheromone dispenser in any plant without human intervention, proposing three different solutions which can be used depending on the vineyard configuration. For a complete overview of the project results, review the project video at <https://youtu.be/Qaz3B5Wvolg>.

References

1. Cox, I.J., Wilfong, G.T.: Autonomous Robot Vehicles. Springer-Verlag, New York, USA (1990)
2. N Johnson, S.K., Balakrishnan, N.: Continuous univariate distributions (1995)
3. Zhong, Y.: Intrinsic shape signatures: A shape descriptor for 3d object recognition. In: IEEE Int. Conf. on Computer Vision Workshops, 689-696 (2009)
4. Díez, Y., Roure, F., Lladó, X., Salvi, J.: A qualitative review on 3d coarse registration methods. ACM Computing Surveys (CSUR) **47(3)**, 45 (2015)
5. Chaumette, F., Hutchinson, S.: Visual servo control. Basic approaches. Rob Autom Mag **13(4)**, 82-90 (2006)
6. Chaumette, F., Hutchinson, S.: Visual servo control. Advanced approaches. Rob Autom Mag **14(1)**, 109-118 (2007)

Chapter 6

Automatized Switchgear Wiring: An Outline of the WIRES Experiment Results

Gianluca Palli, Salvatore Pirozzi, Maurizio Indovini, Daniele De Gregorio, Riccardo Zanella and Claudio Melchiorri

Abstract This chapter reports an overview of the experience and the results achieved during the development of the robotized system for switchgear wiring carried out in the WIRES experiment. This specific application is particularly challenging for a robotic system due to the complexity of the manipulation task. As a matter of fact, in this task deformable linear objects, such as electric wires, are involved. Moreover, the precision requested during the assembly task and the typical crowded space inside the switchgear imply, on one side, the development of specific hardware and software tools and, on the other side, high adaptability and flexibility of the robotic system. In the WIRES experiment, a software package to extract the wiring information and to generate the robot task sequence directly from the switchgear CAD files has been developed. Additionally, a computer vision system able to recognize the location of the wires and of the electromechanical components inside the switchgear has been developed. To deal with the wire deformability and occlusion problems during the wire insertion, machine learning and sensor fusion techniques have been adopted to enable the wire manipulation by means of tactile sensors and 2D cameras feedback. From the hardware point of view, a specific end effector has been developed to manipulate and connect the wire to the components. This end effector is equipped with an electric screwdriver and a customized tactile sensor used to evaluate the wire shape, the wire end pose and its interaction with the environment during the manipulation. The entire task pipeline, going from the switchgear information extraction, to the wire grasp and manipulation, its connection and the routing along the desired wire path is presented in this chapter. The preliminary experimental results show that the developed system can achieve a success rate of about 95% in the wire insertion and connection task.

Gianluca Palli, Daniele De Gregorio, Riccardo Zanella and Claudio Melchiorri
Università degli Studi di Bologna, Viale Risorgimento 2, 40136 Bologna, Italy,
e-mail: gianluca.palli@unibo.it, d.degregorio@unibo.it, claudio.melchiorri@unibo.it
Salvatore Pirozzi
Università degli Studi della Campania, Dip. di Ingegneria, Via Roma 29, 81031 Aversa (CE), Italy
e-mail: salvatore.pirozzi@unicampania.it
Maurizio Indovini
I.E.M.A. Srl, Via XXV Aprile 1945, 16, 40016 San Giorgio di Piano, Italy
e-mail: indovinim@iemasrl.com

6.1 Introduction

The main objective of the WIRES experiment [1] is the robotized cabling of switchgears. The cabling process is a very challenging task, which can be divided into the following subtasks:

1. localization in the switchgear of the components to be connected;
2. first wire end connection;
3. wire routing inside the wire collector;
4. second wire end connection.

Moreover, the wire end connection subtasks (i.e., (b) and (d)) can be further decomposed in the following phases:

1. wire localization;
2. wire grasping;
3. wire pose detection and correction;
4. insertion into the terminal;
5. tightening of the terminal screw;
6. wire connection check.

To achieve the project objective, the robotic system will make use of a suitably designed end effector equipped with a vision system and a tactile sensor for the wire precise manipulation. Preliminary results obtained within the WIRES experiment are presented in [2, 3].

Switchgears and control panels are basic components in a wide range of applications. Currently, the switchgear wiring is executed by human operators due to the the complex manipulation tasks, related to the large variability of the design, characterized by highly-customized solutions, small lot and single item production. Nowadays, robotic systems integrate more and more often advanced grippers or robotic hands for the successful execution of complex manipulation tasks. This is due to the fact that the knowledge of object features is of paramount importance during the interaction with unknown and unstructured environments, as well as to operate with deformable objects and to execute complex manipulation tasks. Conventional approaches to this class of problems are almost always based on collecting vision and/or tactile data. In many research papers, vision is used alone due to its efficiency in data collection [4, 5]. However, this solution may fail in practical application due to several reasons, such as in presence of obstacles, occlusions and varying lighting conditions. A way to improve the success rate and overcome environment limitations is based on the acquisition of additional object features by exploiting tactile sensors. Many researchers have been working on integrating vision and tactile data since many years [6]. Among the most recent applications of this approach there are: the object pose estimation [7], the object shape estimation [8], the estimation of surface features [9], the mapping of object surfaces [10], the combination of visual and tactile exploration procedures [11] and object recognition by using a cross-modal approach [12].

In this chapter, an overview of the different components developed for the WIRES experiment will be provided. To summarize, the system is composed by:

- A software package to extract the data needed by the robotic system from the switchgear design files;
- A vision system used both to correct the location of the electromechanical components in the switchgear and to estimate the wire terminal pose during grasping;
- A tactile sensor used to detect the presence and preliminary orientation of the wire after grasping, as well as to the detect collision of the wire tip during the insertion into the component terminal;
- A 4-DOF end effector equipped with video camera, tactile sensor, Force/Torque (F/T) sensor and computer-controlled screwdriver;
- A task planner and manager that manages the whole task execution.

In the following, these components will be briefly described. Additionally, preliminary experimental results are presented. Moreover, for a larger dissemination of the experiment results, the way how these components have been integrated into a portable demonstrator will be outlined.

6.2 Data Extraction From the CAD Design

The main aim of the WIRES experiments is to automatize as much as possible the wiring process executed by the robot. For this reason, the switchgear design data needed by the robot are automatically extracted by the spread sheets generated during the design process. These files report all the components and related information, see Tab. 6.1. Moreover, the 3D model of the switchgear is exported by the designers in X3D format. The 3D switchgear model is of crucial importance to this experiment since it allows to estimate the location of the components and their terminals, the distance between them and the path and length of the cables. The X3D file format is very easy to process for the extraction of the switchgear information since it is a text file describing all the elements in the scene. Moreover, together with the X3D file, a text file (called WRI table) is also exported, see Tab. 6.2, which reports the links between the component table reported in Tab. 6.1 and the component names used in the X3D model in a hierarchical way. These data can be automatically extracted and exploited for the generation of the manipulator trajectories. Moreover, dedicated opensource software, such as the CyberX3D C libraries, are exploited in this experiment to manipulate the X3D switchgear design file.

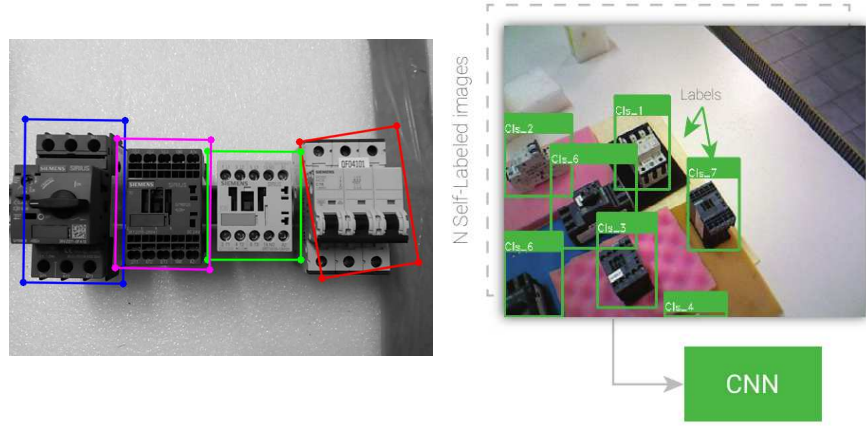
Component Code	Article Num.	Description	Commercial Code	Destination
=F0030.1	6502086	INT.AUT.1P 10A (C)	SIEMENS 5SY4110-7	Q
=F0030.1	6502088	AUX 1NO+1NC	SIEMENS 5ST3010	Q
=F0030.2	6502084	INT.AUT.1P 4A (C)	SIEMENS 5SY4104-7	Q
=F0030.2	6502088	AUX 1NO+1NC	SIEMENS 5ST3010	Q
=F1500.1	6503798	INT.AUT.3P 4,5..A	SIEMENS 3RV2011-1GA20	Q
=F1500.1	6503808	AUX 1NO+1NC	SIEMENS 3RV2901-2E	Q

Table 6.1: Some items extracted from the switchgear design component list.

...	...
ID000070 =-X1600 6012928	DEF ID000074 Transform {
ID000071 =-Q1500.3 6503377	translation 112.500000 -0.500021 9.999981
ID000072 =-Q1500.3 6503809	rotation -1.000000 0.000000 0.000000 1.570797
ID000073 =-U7 WEI.TS35/15	...
ID000074 =-F1500.1 6503798	geometry IndexedFaceSet {
ID000075 =-F1500.1 6503808	point [
ID000076 =-F1500.2 6503798	5.150000 -51.828000 -51.700000,
ID000077 =-F1500.2 6503808	...
ID000078 =-F1500.3 6503798	DEF ID000083 Transform {
ID000079 =-F1500.3 6503808	translation 785.200000 0.000000 15.000000
ID000080 =-F0030.1 6502086	rotation 0.707107 0.707107 0.000000 3.141593
ID000081 =-F0030.1 6502088	...
ID000082 =-T0030 6032224	geometry IndexedFaceSet {
ID000083 =-F0030.2 6502084	point [
ID000084 =-F0030.2 6502088	2.000000 26.210000 -35.857071,
...	...

Table 6.2: Connection between the WRI table (left) and the 3D model information from the X3D file (right).

6.3 The Vision System

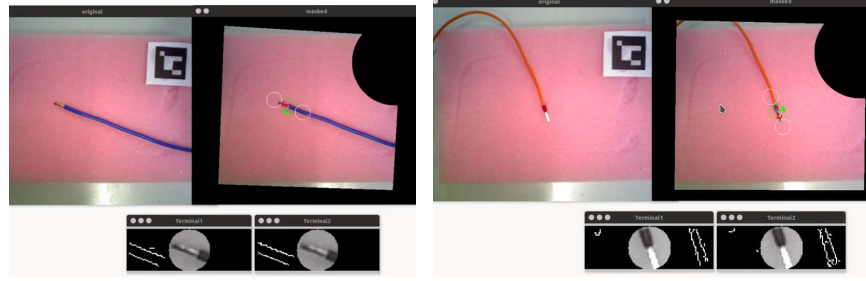


(a) Electromechanical component detection using feature recognition. (b) Electromechanical component detection using left-label CNN recognition.

Fig. 6.1: Electromechanical component detection using feature recognition (left) and left-label CNN recognition (right).

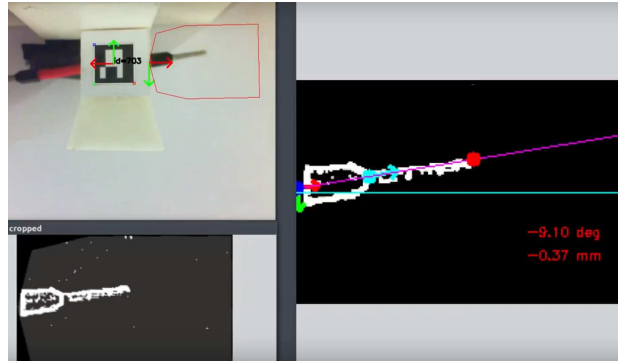
The end effector developed for the WIRES experiment is equipped with a video camera, whose main purpose is to provide the location of the components mounted in the switchgear before executing the wire connections. Due to the large variety of components available on the market and the continuous introduction of new ones, it is convenient to develop a vision system able to exploit the data provided by the component manufactures, and in particular the CAD design of the component itself. Moreover, since the component will be already mounted into the switchgear during the detection phase, only the frontal view can be considered for detection. Therefore, the vision system will directly use this information to detect the components on the switchgear, exploiting the BOLD algorithm [13] developed and patented by CVLAB (University of Bologna). This algorithm detects and describes 2D lines in the images as geometric primitives to perform matches between different scenes. Secondly, other geometric primitives like circles have been provided in BOLD to increase its matching performance. From the performance comparison among different component localization algorithms, it results that the approach based on the BOLD algorithm using the CAD models of the component as feature models seems really promising since it allows to exploit directly the CAD models, therefore avoiding the inclusion in the component database of images taken from the real component. In Fig. 1(a), it is possible to see that the vision system is able to correctly detect the components.

A potential problem of the previously described approach may emerge when components are partially occluded or arranged very close one to the others. To overcome this issue, a novel approach based on the combination of self-labeled images and Convolutional Neural Networks (CNN) has been adopted. This procedure has been patented, and the details are subject of a devoted publication, see [14]. To show the performance of this algorithm, Fig. 1(b) reports the detection of several electromechanical components arranged on a multicolor background. This procedure allows to detect multiple occurrences of the same component also in case they are partially occluded.



(a) Detection of an ultrasound-soldered wire terminal.

(b) Detection of a metallic wire terminal.



(c) Detection of the wire terminal after the grasp and measurement of the terminal length and angle.

Fig. 6.2: Detection of the wire tip by means of the vision system exploiting the camera mounted on the end effector (a)-(b) and by the fixed camera (c).

The vision system developed in the WIRES experiment is also adopted to estimate the position and orientation of the wire in order to perform the grasp. Figures 6.2(a) and (b) show how the vision system is able to detect the wire terminal both in case of ultrasound-soldered wire terminal or in case of metallic wire terminal. Moreover, an additional fixed camera is adopted to evaluate the length of the wire terminal out of the gripper jaws as well as the terminal orientation. The result of this procedure is shown in Fig. 6.2(c). This component is exploited to correct the alignment of the wire tip before executing the wire insertion in order to improve the task success rate.

6.4 The Tactile Sensor

6.4.1 The design

Starting from the previous version of the tactile sensor presented in [15], a new version suitably optimized for wire manipulation has been developed for the WIRES project. The main differences

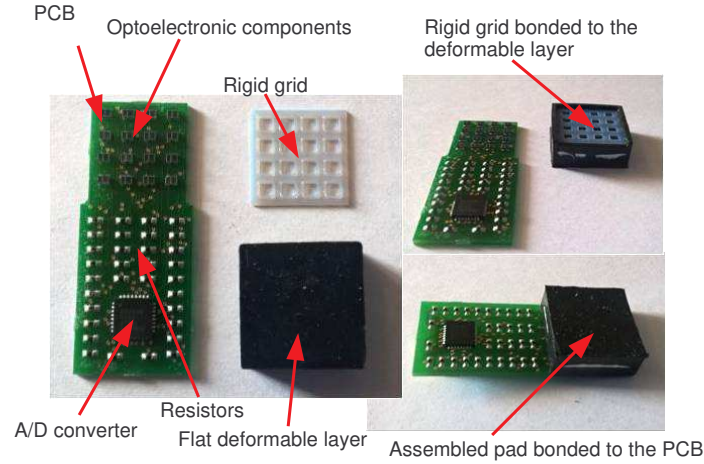


Fig. 6.3: Some pictures of the tactile sensor during the assembly.

regard the overall size and the shape of the deformable layer. In particular, according to the requirements of the WIRES experiment, the maximum allowed thickness for the tactile sensor is 7 mm, and the maximum width is 20 mm. Then, by considering that the wires to grasp have a diameter of few millimeters, a deformable layer with a flat shape has been selected in order to obtain a lower thickness and a tactile image directly related to the grasped wire shape. The working principle is the same of [15]. The deformable layer covers a Printed Circuit Board (PCB), which integrates a matrix of photo-reflectors. On the bottom side of the deformable layer there are empty cells, with white silicone ceilings on top of the photo-reflectors to enhance light reflection, while the walls among the cells are black to reduce cross-talk effects. When an external force acts on the silicone layer, it produces vertical displacements of the white ceilings for all taxels. The distances between the photo-reflectors and the white surfaces change, producing variations of the reflected light and, accordingly, of the photocurrents measured by the phototransistors. In [3], an in-depth Finite Element (FE) analysis has been implemented and the results have been used for the tactile sensor optimization. On the basis of a suitable metric, defined to quantify the alignment error during the insertion phase, the final tactile sensor, reported in Fig. 6.3, has been realized. The electronic PCB constitutes of 16 infrared photo-reflector (manufacturer code NJL5908AR). The NJL5908AR has a surface encumbrance of 1.06×1.46 mm. The components have been positioned on the PCB in order to obtain a matrix of photo-reflectors, spaced of 3 mm. As a consequence, the PCB reaches a total width of 13 mm. The silicone pad is flat on the top, with sixteen empty cells. Each cell is square with a side of 2 mm. The intermediate black walls have a thickness of 1 mm, while the walls on the edges have a thickness of 2 mm. The total dimensions of the deformable pad is 15×15 mm. A rigid grid, made of plastic ABS has been designed to force the optical devices to work in a monotonic range of their electrical characteristics.

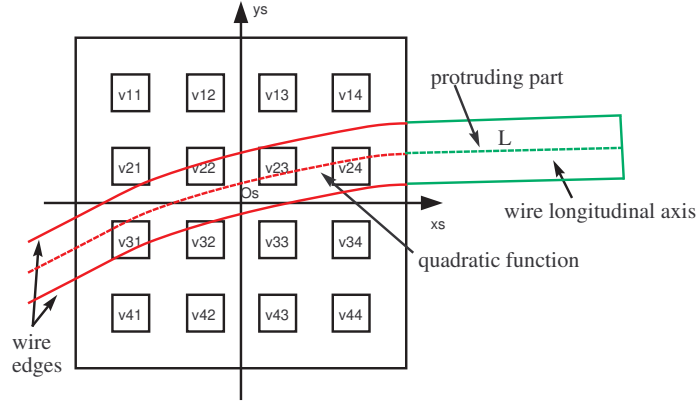


Fig. 6.4: Sketch of a generic grasp.

6.4.2 Estimation of Grasped Wire Shape and Evaluation of insertion Task

The estimation of the wire shape play a crucial role for the insertion subtask. In particular, the estimation of position and orientation of the grasped wire can be used by a standard control algorithm for the alignment between the hole and the wire axes. If these axes are perfectly known the insertion operation becomes simple. A first solution evaluated for the estimation of the wire shape is based on the use of tactile sensor map as described in the following. Figure 6.4 reports a sketch of a generic grasped case, where the wire is gripped at one end, leaving it to stick out of an amount L , which has to be inserted into the hole. The proposed solution uses the tactile data to estimate the parameters of a quadratic function, which represents a model for the wire shape along the grasping area, and to approximate the protruding part as a segment, of length L , lying on the tangent of the quadratic function on the sensor edge. To implement this solution, let $\Sigma_s(O_s, x_s, y_s)$ be the sensor reference frame, fixed at the center of the tactile sensor pad, while the 16 cells are organized as a matrix (see Fig. 6.4). Each (i, j) -th cell is uniquely identified by its (x_i, y_j) coordinates of the mechanical center. Let Δv_{ij} be the voltage variation measured by the photo-reflector of the (i, j) -th cell. Each voltage variation is represented by a circle with radius proportional to the measured Δv centered on the cell coordinates. The tactile map in Fig. 6.5, corresponds to a grasped wire configuration similar to the one reported in Fig. 6.4. The cells positioned beneath the grasped wire present higher voltage variations compared to the others.

The objective is to estimate the quadratic shape of the wire grasped with the sensor pad and consequently to estimate the protruding part of the wire end, which has to be connected to the switchgear component. Since the size of the cross section of the grasped wire is *a priori* known from the switchgear design, the estimation of the grasped wire shape corresponds to estimate its longitudinal axis shape. In the Σ_s frame, depending on the grasped wire longitudinal direction, the following equations can be written to model the proposed solution

$$y_s = a_x x_s^2 + b_x x_s + c_x \quad (6.1)$$

$$x_s = a_y y_s^2 + b_y y_s + c_y \quad (6.2)$$

Let us assume to know if the wire longitudinal axis can be expressed as (6.1) or (6.2), since the wire is grasped by the robot in a known position. These two possible cases are very similar and

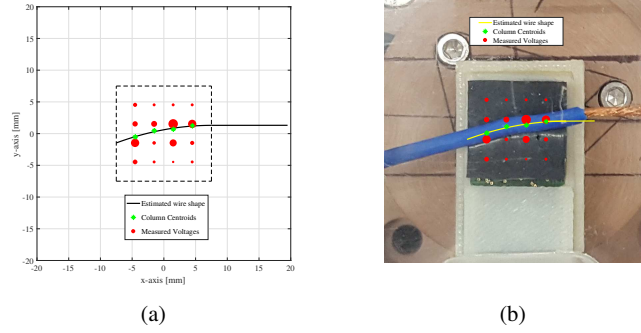


Fig. 6.5: Wire shape estimation from experimental data (a) and comparison of estimated wire shape and the actual one (b).

the observations made for one case are equally valid for the other case. As a consequence, only the case with the wire longitudinal direction lying along the x_s axis will be handled. In this case, the wire shape is modeled by the quadratic function (6.1), whose parameters (a_x, b_x, c_x) have to be estimated. The proposed algorithm is:

- For each j -th column, the y -coordinate y_{m_j} of the column centroid is calculated as

$$y_{m_j} = \frac{\sum_{i=1}^n y_i \Delta v_{ij}}{\sum_{i=1}^n \Delta v_{ij}} \quad j = 1, \dots, n \quad (6.3)$$

where y_i is the y -coordinate of the i -th row, while $n = 4$ for the designed sensor.

- For each column, the centroid coordinates (x_j, y_{m_j}) $j = 1, \dots, n$ are defined, where x_j is the x -coordinate of the j -th column.
- The function parameters (a_x, b_x, c_x) are estimated by using a least square method applied to the (x_j, y_{m_j}) $j = 1, \dots, n$ data set.

After the estimation of the grasped wire shape, the protruding part of the wire can be easily computed as a segment, of length L , lying on the line tangent to the estimated quadratic function. Figure 6.5(a) reports the experimental results of the proposed solution and the Fig. 6.5(b) reports the comparison of the estimated shape and the actual one.

The estimated wire end can be used to directly perform the insertion task or as input data for the vision system. In the latter case, the vision system can refine the estimated wire end position and orientation by elaborating the images over a limited area, so that to drastically reduce elaboration time.

During the execution of the insertion task, the tactile data can be used in order to automatically evaluate if the insertion task has been correctly completed or not. The proposed tactile sensor is able to estimate all force components by exploiting the whole tactile maps. In particular, as detailed in [15, 16], the normal force component is related to the absolute values of measured voltage variations, while the tangential components are related to the asymmetric variations of the tactile map. On the basis of these sensor characteristics, it is possible to define a simple index (related to external tangential forces applied on the wire) to evaluate asymmetric variations of the measured voltages after the end of the wire grasping. Also in this case, let consider the grasped wire mainly aligned with x_s axis. A similar index can be easily defined when the alignment is mainly with the y_s axis. The proposed index is

$$J(t) = \sum_{i \in T_p} (v_i(t)) - \sum_{j \in T_n} (v_j(t)) \quad (6.4)$$

where T_p is the set of the four taxels on the right edge of the sensor pad and T_n is the set of the four taxels on the left edge, while $v_i(t)$ and $v_j(t)$ represent the measured voltages. This index will assume a more or less constant value if the insertion task is correctly completed, i.e., the wire end is inserted without collision. If the task is not correctly completed (i.e., the wire strikes outside the hole) the index J will present high variations. By comparing J with a suitably selected threshold the success of the task can be automatically evaluated. Example of this index can be found in Sec. 6.6.

6.5 The WIRES End Effector

The end effector developed in the WIRES experiment for the implementation of the whole cabling process can be seen in Fig. 6.6. The end effector integrates a 2D camera providing top view of the scene, a computer-controlled screwdriver (to tight the terminal screws) and a 4-DOFs gripper (gripper opening and finger x-y-z position w.r.t. to the screwdriver tip) equipped with the tactile sensor described in Sec. 6.4.

The end effector is also equipped with an integrated torque/controlled screwdriver with remote PLC control and process data recording capabilities (Kolver PLUTO3CA electric screwdriver + EDU2AE/TOP/E control unit).

In the final process implementation, the robot arm will be used to position the screwdriver tip on the terminal screw, and the FT sensor will be used to control the contact with the screw during the tightening. Therefore, the end effector will be held in an almost fixed position, just the screw motion during the tightening will be compensated. Consequently, the wire insertion will be performed by using the gripper DOFs only. It results that the FT sensor can be used to estimate the interaction between the screwdriver and the terminal screw, but it cannot be used during the insertion and for the wire tightening check, because the magnitude of the force generated by the wire contact is much lower than the one generated by the contact between the screwdriver and the screw, making the former indistinguishable. For this reason, the use of the tactile sensor installed into the gripper fingertips during the insertion and for the wire tightening check is fundamental for the correct execution of this operations, in order to reach a suitable success rate.

Stepper motors with integrated encoder and lead screws have been adopted for the actuation of the end effector. This solution significantly simplifies the control, reduce the weight, the mechanical complexity and the cost of the end effector. Limit switches have been used for absolute position detection on both sides of all the end-effector movement axes.

Each motor is driven by a Hydra servo drive control board, used as HW low-level motor controllers. These control boards are arranged on the end effector itself. The communication between the motor control boards and the high level WIRES controller is implemented through CAN bus. A ROS node has been developed to allow the control of the end effector and to ease the integration with other component of the WIRES system. At low level, the motors are controlled by means of the PLCOpen standard, allowing an easy implementation of the end effector controller.

The tactile sensor has been integrated into the jaw tips (fingertips). Several versions of 3D printed fingers have been produced in order to evaluated different configurations during experiments. In facts, the fingertips can be easily substituted with passive ones (without tactile sensor) on one or both sides to save space or for preliminary tests.

6.6 Experimental Results

A sequence showing the wire pose correction and insertion into the component simulacrum hole in case the wire alignment is adjusted exploiting or not the wire pose estimation is shown in Fig. 6.7. The two sequences start from a common configuration (1). To show the effect of collisions, the

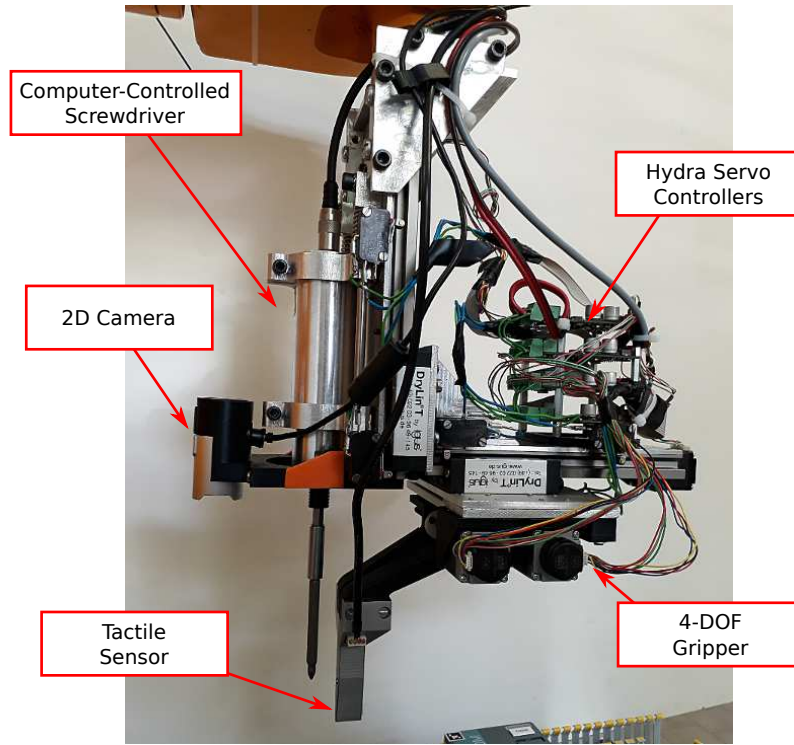


Fig. 6.6: The end effector developed for the WIRES experiment. It is equipped with computer-controlled screwdriver, tactile sensor, 2D camera, Hydra servo controller boards, and a 4-DOF gripper.

sequence shown in the top row reports a wrong alignment provided to the system at step (2). As a consequence, the wire terminal is not aligned with the reference line, resulting in hole misalignment at stage (3). This configuration causes a collision with the object at stage (4). The effect of the wrong wire terminal orientation adopted to test this procedure is reported in Fig. 6.8(a). This figure reports the robot x -axis position and the J index computed by using the tactile sensor data during the wire pose correction and insertion task. The effect of the collision measured by the tactile sensor can be clearly seen in the final part of the insertion phase looking at the J index.

On the other hand, the bottom sequence in Fig. 6.7 shows how the vision system allows to correctly align the wire terminal with the reference line at step (2) and, consequently, with the insertion hole at step (3). It results that the wire is correctly inserted into the hole at step (4). The wire terminal orientation, position and the J index during the wire pose correction and insertion task computed in the good sequence of Fig. 6.7 are reported in Figure 6.8(b). First, the initial estimation of the wire terminal pose is performed, then the end-effector orientation is corrected and the insertion task is executed. During the wire insertion, the J index allows to detect a contact between the wire terminal and the internal part of the hole causing friction. In order to avoid false positive, the J index is not considered during the other phases.

A set of 30 different task configurations are used to evaluate the performance of the overall insertion pipeline over a wide range of working conditions. Two subsets of 15 runs executed with two wires which external diameter is 2 mm and 3.5 mm, respectively, are reported in Tab. 6.3. In

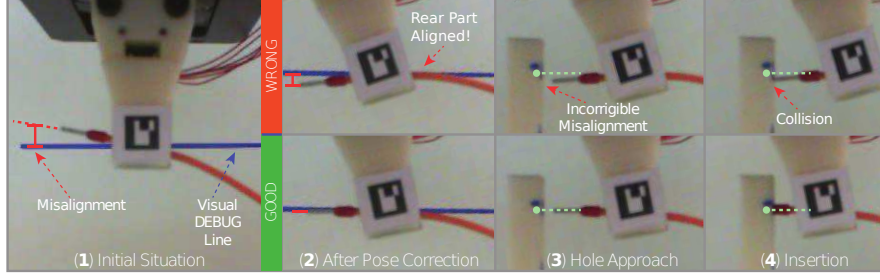
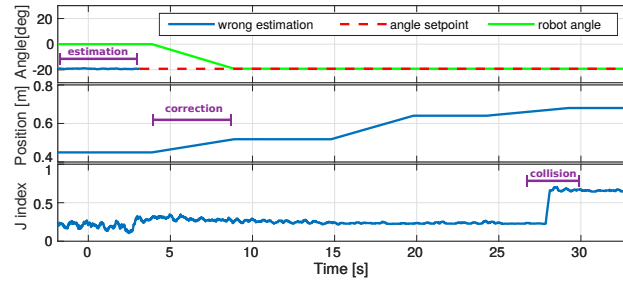
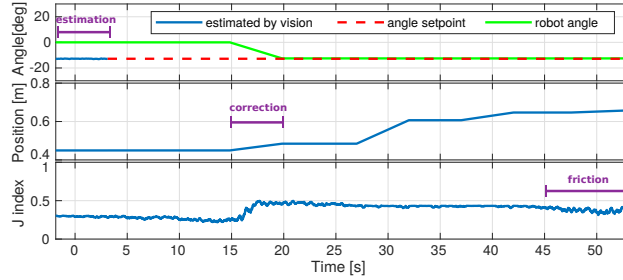


Fig. 6.7: Evaluation of the whole insertion task. Collision detection exploiting tactile feedback in case of wrong alignment (top sequence) and wire terminal pose correction and insertion using the vision feedback (bottom sequence).



(a) Collision detection using the tactile sensor.



(b) Wire pose correction and insertion using the vision system.

Fig. 6.8: Execution of the wire pose correction and insertion tasks.

these tables, m is the estimated wire terminal orientation, d denotes the distance of the wire tip from the finger center and c is 1 in case of successful insertion or 0 in case of failure. With reference to Fig. 6.8, the parameter is computed as:

$$c = \begin{cases} 0, & \text{Position} > 0.65 \wedge J \text{ index} > 0.5 \\ 1, & \text{Position} > 0.65 \wedge J \text{ index} < 0.5 \end{cases}$$

where the position threshold is selected to ensure that the wire terminal is inserted. The data reported in Tab. 6.3 include also experiments performed in conditions that are out of the foreseen production scenario. However, these configurations are selected to test the system robustness. Looking at the

Table 6.3: Wire insertion results for a cable with external diameter of 2.0 mm on the left and 3.5 mm on the right. Parameters m and d refer to initial condition of the wire w.r.t. the gripper, while c refers to the result of insertion where $c = 1$ is a positive outcome.

#	m [deg]	d [mm]	c
1	-5.7	48.0	1
2	-1.0	32.5	1
3	4.0	38.9	1
4	-2.9	27.6	1
5	27.5	46.5	1
6	-32.6	40.6	0
7	-15.6	38.5	1
8	12.4	39.4	1
9	14.0	29.5	1
10	10.8	24.4	0
11	46.4	56.0	0
12	42.9	60.9	1
13	-28.4	45.3	0
14	41.3	65.9	0
15	33.0	39.0	1
#	m [deg]	d [mm]	c
1	13.5	27.0	1
2	-20.3	30.0	1
3	4.6	29.4	1
4	4.0	30.0	1
5	-12.4	29.0	1
6	23.3	43.0	0
7	-19.8	41.0	1
8	0.6	40.0	1
9	24.2	48.0	0
10	21.8	52.0	1
11	52.9	56.0	0
12	7.4	35.6	1
13	47.5	52.0	1
14	58.6	95.0	0
15	44.7	69.2	0

whole experiment set, an overall success rate of about 66% is obtained. Figure 6.9 reports the experiment results in the $\{m, d\}$ -plane, from which it is possible to define an admissible working region of $m = \pm 20\text{deg}$ and $d \leq 50\text{mm}$ containing almost only successful wire insertions, 15 over 16, resulting in a success rate of about 95%. This working region can be easily addressed in the partially structured application scenario. Further details about the implementation of the insertion task execution pipeline are reported in [17].

For dissemination purposes and to demonstrate the whole task sequence, a portable demonstrator of the WIRES experiment has been developed, see Fig. 6.10. In this setup, the WIRES end effector is mounted on a small portable industrial manipulator. Despite the reduced workspace and motion capabilities, this system allows to fully demonstrate how the switchgear wiring process can be automatically executed thanks to the technology developed during the WIRES experiment. To this end, a devoted testing switchgear characterized by reduced dimensions has been produced.

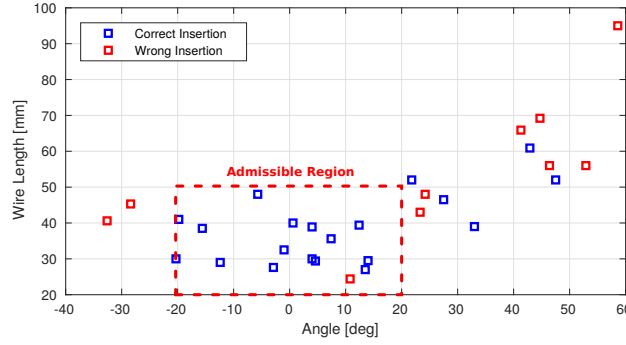


Fig. 6.9: Evaluation of the admissible operating range of the developed wire manipulation and insertion system.

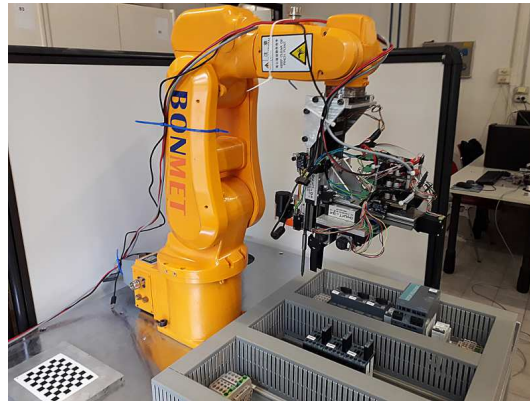


Fig. 6.10: The WIRES experiment portable demonstrator.

6.7 Conclusions

In this chapter, the components of the WIRES experiment are outlined. This experiment tries to solve a complex manipulation problem of large industrial interest. To deal with the complexity of the scenario, the crowded workspace and the deformability of objects such as electric wires, vision and tactile data have been combined. Moreover, a 4-DOF end effector equipped with computer controlled screwdriver has been developed to accomplish the wire insertion and connection task. Considering the partially structured environment in which the task is executed in the industrial scenario, this approach demonstrated to be effective within a suitable range of working conditions, since a success rate of 95% has been obtained during early experimental evaluation. The failure in the insertion task can be mainly ascribed to the limited resolution of the low-cost camera adopted to estimate the wire terminal position. Therefore, we expect the success rate of the system can be further improved by adopting a high-resolution camera for the wire terminal position correction.

Aiming at a large dissemination of the experiment results, a portable demonstrator has been developed. This system was shown at the Automatica 2018 fair.

References

1. Website of the wires experiment. URL <http://www-lar.deis.unibo.it/people/gpalli/WIRES/>
2. Busi, M., Cirillo, A., De Gregorio, D., Indovini, M., De Maria, G., Melchiorri, C., Natale, C., Palli, G., Pirozzi, S.: The wires experiment: Tools and strategies for robotized switchgear cabling. *Procedia Manufacturing* **11**, 355–363 (2017)
3. Cirillo, A., De Maria, G., Natale, C., Pirozzi, S.: Design and evaluation of tactile sensors for the estimation of grasped wire shape. In: *Proc. IEEE Int. Conf. on Advanced Intelligent Mechatronics*, pp. 490–496. Munich, Germany (2017)
4. Saxena, A., Driemeyer, J., Ng, A.Y.: Robotic grasping of novel objects using vision. *The International Journal of Robotics Research* **27**(2), 157–173 (2008)
5. A strategy for grasping unknown objects based on co-planarity and colour information. *Robotics and Autonomous Systems* **58**(5), 551–565 (2010)
6. Allen, P.K.: Integrating vision and touch for object recognition tasks. *The International Journal of Robotics Research* **7**(6), 15–33 (1988)
7. Bimbo, J., Seneviratne, L.D., Althoefer, K., Liu, H.: Combining touch and vision for the estimation of an object's pose during manipulation. In: *Proc. Int. Conf. on Intelligent Robots and Systems*, pp. 4021–4026 (2013)
8. Björkman, M., Bekiroglu, Y., Högman, V., Kragic, D.: Enhancing visual perception of shape through tactile glances. In: *Proc. Int. Conf. on Intelligent Robots and Systems*, pp. 3180–3186 (2013)
9. Bhattacharjee, T., Sheno, A.A., Park, D., Rehg, J.M., Kemp, C.C.: Combining tactile sensing and vision for rapid haptic mapping. In: *Proc. Int. Conf. on Intelligent Robots and Systems*, pp. 1200–1207 (2015)
10. Jamali, N., Ciliberto, C., Rosasco, L., Natale, L.: Active perception: Building objects' models using tactile exploration. In: *Proc. Int. Conf. on Humanoid Robots (Humanoids)*, pp. 179–185 (2016)
11. Lepora, N.F., Aquilina, K., Cramphorn, L.: Exploratory tactile servoing with active touch. *IEEE Robotics and Automation Letters* **2**(2), 1156–1163 (2017)
12. Falco, P., Lu, S., Cirillo, A., Natale, C., Pirozzi, S., Lee, D.: Cross-modal visuo-tactile object recognition using robotic active exploration. In: *Proc. of the IEEE Int. Conf. on Robotics and Automation*, pp. 5273–5280 (2017)
13. Tombari, F., Franchi, A., Di, L.: Bold features to detect texture-less objects. In: *2013 IEEE International Conference on Computer Vision*, pp. 1265–1272 (2013)
14. De Gregorio, D., Tonioni, A., Palli, G., Di Stefano, L.: Semi-automatic labeling for deep learning in robotics. In: *Submitted to Int. Conf. on Intelligent Robots and Systems* (2018)
15. DeMaria, G., Natale, C., Pirozzi, S.: Force/tactile sensor for robotic applications. *Sensors and Actuators A: Physical* **175**, 60–72 (2012)
16. DeMaria, G., Natale, C., Pirozzi, S.: Tactile data modeling and interpretation for stable grasping and manipulation. *Robotics and Autonomous Systems* **61**(9), 1008–1020 (2013)
17. De Gregorio, D., Zanella, R., Palli, G., Pirozzi, S., Melchiorri, C.: Integration of robotic vision and tactile sensing for wire-terminal insertion tasks. *IEEE Trans. on Automation Science and Engineering* p. in press (2018)

Chapter 7

Optimality criteria for the path planning of autonomous industrial vehicles

Marina Raineri, Fabio Ronchini, Simone Perri and Corrado Guarino Lo Bianco

Abstract – The trajectories planning problem for autonomous industrial vehicles requires facing significant issues concerning the efficiency and the safety of the plant. The solution of such issues is complicated by the necessity of generating paths and time-laws in different moments: plant layouts must be designed a priori, while velocity profiles must be generated in real time in order to manage variable operating conditions and safety concerns. One possible solution to the real-time velocity planning problem has been recently proposed in the framework of the European project ECHORD++. The study in this work will conversely focus on the path planning problem. More precisely, the proposed investigation aims to establish the most appropriate offline path planning criterion to be used for the design of autonomous warehouses, in order to improve the plant performances. The goal is to obtain curves which allow swift direction changes which minimally impact on the system efficiency.

7.1 Introduction

Laser Guided Vehicles (LGV) are largely used in industrial plants in order to maximize the overall efficiency, which is the typical issue of all productive systems. LGVs are adopted in such contexts since they can carry precisely and efficiently huge loads between different locations of the plant. On the other hand, LGVs are complex systems which need to be smartly managed since several factors may potentially impact negatively on their performances. For example, LGVs are subject to many physical constraints like the ones imposed by the vehicle kinematics and dynamics: if such constraints are not accounted for, performances degenerate. Autonomous vehicles must also take care of the structured environment in which they move: rigid rules exist so as to guarantee the safety

Marina Raineri and Fabio Ronchini
University of Parma, Dip. di Ingegneria e Arch., Parco Area delle Scienze, 181/A, Parma, Italy
e-mail: marina.raineri@unipr.it; e-mail: fabio.ronchini@studenti.unipr.it

Simone Perri
Elettric80, Via Guglielmo Marconi, 23, Viano, Italy
e-mail: Perri.S@elettric80.it

Corrado Guarino Lo Bianco
University of Parma, Dip. di Ingegneria e Arch., Parco Area delle Scienze, 181/A, Parma, Italy
e-mail: corrado.guarinolobianco@unipr.it

of the other LGVs and, more important, of the human co-workers who share their workspace with them. The best performances can only be achieved by means of a proper trajectories synthesis.

The motion planning problem has been widely discussed in the literature. In case of applications concerning unstructured environments trajectories are planned as a whole, i.e., the path and the velocity references are planned simultaneously so as to obtain the best possible performances. Planning criteria depend on the presence of fixed or moving obstacles, traffic conditions, surface characteristics. Several optimality criteria have been proposed in the literature. The most common of them are certainly represented by traveling time and energy efficiency. For example, in [1] optimal paths and speed references are computed by taking into account different constraints such as the vehicle dynamics and the terrain topography, while in [2] a near time-optimal strategy is proposed for a wheeled mobile robot by also considering constraints on the feeding voltages and currents of the motors. A different optimal function is used in [3]: path and velocity are both optimized in order to reduce the energy consumption, which represents an important aspect for battery powered autonomous vehicles.

As shown in the survey paper [4], the planning problem is typically handled by means of nonlinear optimization techniques, but other methods are also available. For example, a state-time space approach was introduced in [5] so as to generate a space which contains both positional coordinates and time references. Recent papers draw the attention toward algorithms to be used in real time. For example, [6] proposes a Mixed-Integer Quadratic Programming (MIQP) method for the generation of smart maneuvers for autonomous vehicles. When the trajectory is planned by assuming the path-velocity decomposition scheme, an alternative procedure can be adopted (see, e.g., [7]) which iteratively changes path and velocity shapes looking for the best performance index.

The methodology used for the synthesis of optimal trajectories must necessarily change in LGV based plants, since the path and the speed planning phases are temporally separated, according to the scheme initially proposed by [8] and [9]. Indeed, for safety and for traffic reasons, in autonomous warehouses the vehicles must move along predefined paths chosen during the plant design. Conversely, velocity references are directly evaluated at run time depending on the operating conditions of the vehicle. Paths are generated so as to account for the presence of fixed obstacles like shelves or columns, however further degrees of freedom often remain which can be used to improve the system performances. Several alternative optimality criteria can be assumed depending on the desired target. Different works in the literature impose constraints on the maximum path curvature in order to limit tangential accelerations. For example, [10] and [11] consider superiorly bounded curvatures for problems in which energy or traveling times are minimized. Moreover, [12] underlines the importance of generating paths with continuous curvature, while an algorithm is devised in [13] for the generation of paths with superiorly limited curvature derivative.

An appropriate velocity reference must be generated once the path has been selected. Differently from the path, it must be planned in real time so as to account for the operative conditions of the LGV. More in detail, LGVs seldom execute a constant route but, conversely, they follow paths obtained from the combination of short segments which are assembled in real time by the plant supervisor: the sequence of segments changes at each mission. Furthermore, vehicles need often to be stopped for traffic reasons or for the presence of unexpected obstacles. The natural conclusion of these reasonings is that the speed profile can not be evaluated in advance. In the past years the optimal velocity planning problem has been widely studied for mobile robots. For example, [14] proposed a speed planning algorithm which limits the maximum velocities and accelerations. More recent works (see, e.g., [7] and [15]) propose planners that are able to generate speed references in real time, but many of them do not account for jerk limits. A real-time velocity planner able to limit velocities, accelerations and jerks was first proposed in [16]. It was also conceived to manage variable velocity bounds. A further planner, specifically conceived for automated warehouses, has been later proposed in [17]. Differently from the previous one, it is also able to guarantee safe operating conditions. In particular, safeness is achieved by generating an analytical velocity bounding function based on the path shape and on the characteristics of the vehicle detection system: when a potential collision is detected, the vehicle is stopped by guaranteeing a safety margin independently from its position along the path. The real-time velocity profile is obtained through a heuristic method which returns almost time optimal solutions, so as to increase the plant productivity. The resulting motion is

very smooth since velocities, accelerations and jerks are explicitly limited. The real-time planner is an outcome of the SAFERUN experiment (Secure And Fast rEal-time planner for aUtoNamous vehicles), financed in the framework of the ECHORD++ project.

The previous discussion pointed out that paths for LGV plants can not be modified at run time. The study proposed in this paper intends to establish the most appropriate performance index to be adopted for the offline synthesis of the paths, bearing in mind that a minimum-time velocity planner will be later used at run time. In particular, the one designed in [17] is adopted in this work, although alternative choices are possible. The analysis will consider several objective functions. The requirements to be fulfilled are essentially two: the combination between path and velocity profile should lead to minimum time transients and, secondly, the areas swept by the curves should be kept as small as possible. The two targets are somehow concurrent since small areas are swept by tight curves which, in turn, usually require longer transient time. The paper will show that the path selection obtained through an appropriate performance index can even allow the efficient execution of tight curves.

The paper is organized as follows. Section 7.2 analyzes some possible performance indexes to be used for the optimal path planning. In particular, the results will be compared in terms of the traveling times returned by the velocity planner designed in [17]. Section 7.3 proposes an alternative performance index conceived to reduce the surface swept by the LGVs, while simultaneously limiting their traveling times. Final conclusions are drawn in Section 7.4.

7.2 The path planning optimization problem

Any planar curve can be defined through a parametric function $\mathbf{p}(u) \in \mathbb{R}^2$. For the curves considered in this paper u will span in the interval $[0, 1]$, hence $u = 0$ indicates the beginning of a segment, while $u = 1$ is used for its end. All curves are considered “regular”, i.e., $\mathbf{p}'(u) = \frac{d\mathbf{p}}{du} \neq 0$. Any position along a curve is uniquely identified by u or, alternatively, by means of the curvilinear coordinate s defined as follows

$$s(u) := \int_0^u \|\mathbf{p}'(\tilde{u})\| d\tilde{u} . \quad (7.1)$$

For regular curves, the function between s and u is bijective and their length can be evaluated as follows

$$s_f := \int_0^1 \|\mathbf{p}'(\tilde{u})\| d\tilde{u} . \quad (7.2)$$

A tangent unit-vector $\boldsymbol{\tau}(u) = \frac{\mathbf{p}'(u)}{\|\mathbf{p}'(u)\|}$ is associated to each point of the curve together with an osculating circle whose center is identified as follows (see also Fig. 7.1)

$$\frac{d\boldsymbol{\tau}}{ds}(u) = \frac{d\boldsymbol{\tau}}{du} \frac{du}{ds} = \frac{d\boldsymbol{\tau}}{du} \frac{1}{\frac{ds}{du}} = \frac{d\boldsymbol{\tau}}{du} \frac{1}{\|\mathbf{p}'(u)\|} = \kappa(u) \mathbf{v}(u) .$$

$\kappa(u)$ is the path curvature in u and it is the reciprocal of the radius of the osculating circle, i.e., the circle which best approximates the curve in $\mathbf{p}(u)$.

Curves for LGV plants must possess some peculiar characteristics. The most important is certainly the smoothness, since gentle curves allow a better tracking, less stress on the vehicle, higher speeds and, therefore, a greater efficiency. The path smoothness is directly correlated to its curvature – a low curvature causes smaller vehicle solicitations – as well as to the curvature derivative w.r.t. the curvilinear coordinate, i.e., to the following term

$$\frac{d\kappa}{ds}(u) = \frac{d\kappa}{du} \frac{du}{ds} = \frac{d\kappa}{du} \frac{1}{\frac{ds}{du}} = \frac{d\kappa}{du} \frac{1}{\|\mathbf{p}'(u)\|} .$$

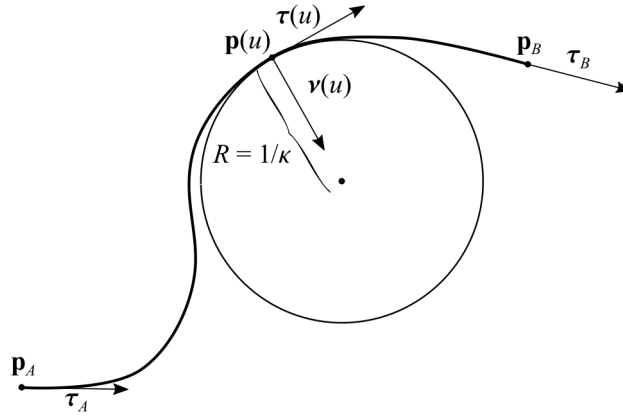


Fig. 7.1: A curve with its interpolating conditions, \mathbf{p}_A , $\boldsymbol{\tau}_A$, \mathbf{p}_B and $\boldsymbol{\tau}_B$. For a generic point $\mathbf{p}(u)$ of the curve the following elements are shown: the radius of the osculating circle R , the curve tangent unit vector $\boldsymbol{\tau}(u)$ and the curve orthogonal unit vector $\boldsymbol{\nu}(u)$.

Previous considerations motivated the study in this paper, whose target is the individuation of the most proper optimization criterion to be adopted for the generation of smooth curves which allow the best performances. In this section the focus is entirely posed on efficiency concerns, while in the next one the discussion will be extended to the space occupied by the curves.

The path planning performance index can be selected on the basis of alternative criteria. For example, if the vehicle transversal acceleration must be kept smaller than an assigned threshold \tilde{a} , the vehicle longitudinal speed must never exceed the following value

$$\tilde{v}(s) = \sqrt{\frac{\tilde{a}}{|\kappa(s)|}}. \quad (7.3)$$

Consequently, low curvature paths potentially allow higher speeds. Similarly, safety considerations (see also [17]), which are very important in LGV plants, suggest limiting path curvatures in order to increase average speeds.

At the same time, the variation of the vehicle steering angle, i.e., $\dot{\theta}$, is superiorly limited by the actuators capabilities, so that a curve is feasible only if condition $|\dot{\theta}| \leq \dot{\tilde{\theta}}$ holds, where $\dot{\tilde{\theta}}$ represents the maximum steering speed. For car-like vehicles – which represent the typical LGV model – this constraint can be easily converted into an equivalent longitudinal maximum speed through the following expression

$$\tilde{v}(s) = \frac{1 + L^2 \kappa^2(s)}{L \left| \frac{d\kappa}{ds}(s) \right|} \dot{\tilde{\theta}}, \quad (7.4)$$

where L indicates the wheelbase length. Equation (7.4) suggests that, depending on the interpolating conditions, better performances can be achieved by minimizing the curvature derivative.

The procedure adopted for the investigation is described in the following. First of all, a set of interpolating conditions were assigned for the generation of the curves commonly used in LGV plants. The curves generated by means of the interpolating conditions reported in Table 7.1 can be classified as follows

1. symmetric U-turn curves (ID 10–12);
2. asymmetric U-turn curves (ID 1–3);
3. 90° curves (ID 4–6);

Table 7.1: Interpolating conditions of the seventeen test curves.

ID	\mathbf{p}_A (m)	\mathbf{p}_B (m)	$\boldsymbol{\tau}_A$	$\boldsymbol{\tau}_B$
1	[9.7, 13.5]	[5.9, 7.5]	[-1, 0]	[1, 0]
2	[9.7, 13.5]	[5.9, 8.5]	[-1, 0]	[1, 0]
3	[9.7, 13.5]	[5.9, 10.1]	[-1, 0]	[1, 0]
4	[9.7, 8.6]	[5.9, 7.2]	[-1, 0]	[0, 1]
5	[9.7, 7.6]	[5.9, 8]	[-1, 0]	[0, 1]
6	[9.7, 6.1]	[5.9, 8.9]	[-1, 0]	[0, 1]
7	[13.3, 15.2]	[10.1, 8.5]	[1, 0]	[1, 0]
8	[10.2, 13.5]	[10.1, 8.5]	[1, 0]	[1, 0]
9	[7.5, 13.5]	[10.1, 7.5]	[1, 0]	[1, 0]
10	[15.2, 15.2]	[7.5, 5.9]	[1, 0]	[-1, 0]
11	[15.2, 15.2]	[8.5, 5.9]	[1, 0]	[-1, 0]
12	[15.2, 15.2]	[10.1, 5.9]	[1, 0]	[-1, 0]
13	[8.6, 10.4]	[7.2, 8.5]	[0, 1]	[1, 0]
14	[7.6, 10.2]	[8, 10.1]	[0, 1]	[1, 0]
15	[6.1, 7.5]	[8.9, 10.1]	[0, 1]	[1, 0]
16	[15.2, 10.2]	[8.5, 10.4]	[1, 0]	[-1, 0]
17	[10.2, 13.5]	[10.4, 7.5]	[-1, 0]	[1, 0]

4. lane changes (ID 7–9);
5. junction curves (ID 13–17).

The interpolating conditions were chosen so as to generate a complete and realistic plant layout. For each one of the first four classes, three sets of interpolating conditions were proposed, so as to generate paths with high, medium, and low curvatures. Some of the interpolating conditions were specifically conceived to produce very sharp and tight bends, which would normally be traveled at low speeds. The fifth category of curves was introduced so as to close the plant layout. Some further straight segments were finally added in part with the same purpose – i.e., the closure of the plant layout – and in part to be used for the initial acceleration of the vehicle, since speed tests require to enter the curves at full speed.

For each of the seventeen interpolating conditions, several optimal paths were generated through a nonlinear programming algorithm which assumed alternative performance indexes. Eventually, the velocity reference signal for each curve was obtained by means of the algorithm proposed in [17], looking for the best possible combination between path and velocity planner.

Three integral cost functions were assumed for the tests. They are respectively associated to κ , to $(d\kappa)/(ds)$, and to $(d^2\kappa)/(ds^2)$. An integral performance index was used in order to attempt limiting the curvature and its derivatives along the whole curve. More in detail, the following three indexes were adopted:

$$J := \int_0^1 \kappa^2(\tilde{u}) d\tilde{u}, \quad (7.5)$$

$$J := \int_0^1 \left[\frac{d\kappa}{ds}(\tilde{u}) \right]^2 d\tilde{u}, \quad (7.6)$$

$$J := \int_0^1 \left[\frac{d^2\kappa}{ds^2}(\tilde{u}) \right]^2 d\tilde{u}. \quad (7.7)$$

The optimization problem solved for the optimal path planning can be formulated as follows

$$\min J \quad (7.8)$$

subject to

$$\mathbf{p}(0) = \mathbf{p}_A, \quad \mathbf{p}(1) = \mathbf{p}_B, \quad (7.9)$$

$$\boldsymbol{\tau}(0) = \boldsymbol{\tau}_A, \quad \boldsymbol{\tau}(1) = \boldsymbol{\tau}_B, \quad (7.10)$$

$$\kappa(0) = \kappa(1) = 0, \quad (7.11)$$

$$\frac{d\kappa}{ds}(0) = \frac{d\kappa}{ds}(1) = 0, \quad (7.12)$$

$$s_f < \bar{s}, \quad (7.13)$$

where J is one of the cost functions (7.5)–(7.7), \mathbf{p}_A and \mathbf{p}_B are the initial and the final points of the curve, $\boldsymbol{\tau}_A$ and $\boldsymbol{\tau}_B$ are the initial and the final unit vectors which are tangent to the curve. The interpolating conditions used in this work are listed in Table 7.1. Constraint (7.13) is required since problem (7.8)–(7.12) may admit optimal solutions with very long, and consequently unusable, paths. As a consequence, s_f is limited by means of threshold \bar{s} .

Bézier curves are widely known for their versatility and represent a robust planning tool. For this reason, they have been adopted in this paper for the generation of swift curves. To this purpose, some definitions concerning Bézier curves are now recalled. Given $n \in \mathbb{N}$, a Bernstein polynomial of degree n is defined as follows:

$$B_{i,n}(u) := \binom{n}{i} u^i (1-u)^{n-i} \quad i = 0, \dots, n. \quad (7.14)$$

Bernstein polynomials of degree n represent a base for all polynomials up to degree n . Given a set of control points $\mathbf{p}_0, \dots, \mathbf{p}_n$, a Bézier curve is defined by the following linear combination of functions $B_{i,n}(u)$

$$\mathbf{p}(u) := \sum_{i=0}^n \mathbf{p}_i B_{i,n}(u). \quad (7.15)$$

In the remainder of this paper, the polynomial degree of all curves $\mathbf{p}(u)$, $u \in [0, 1]$, is fixed to $n = 7$, so as to satisfy boundary conditions (7.9)–(7.12) while using the least number of control points. Consequently, only eight control points are needed, defined as follows

$$\mathbf{p}_0 = \mathbf{p}_A, \quad \mathbf{p}_7 = \mathbf{p}_B, \quad (7.16)$$

$$\mathbf{p}_1 - \mathbf{p}_0 = d_0 \boldsymbol{\tau}_A, \quad \mathbf{p}_6 - \mathbf{p}_7 = d_3 \boldsymbol{\tau}_B, \quad (7.17)$$

$$\mathbf{p}_2 - \mathbf{p}_1 = d_1 \boldsymbol{\tau}_A, \quad \mathbf{p}_5 - \mathbf{p}_6 = d_4 \boldsymbol{\tau}_B, \quad (7.18)$$

$$\mathbf{p}_3 - \mathbf{p}_2 = d_2 \boldsymbol{\tau}_A, \quad \mathbf{p}_4 - \mathbf{p}_5 = d_5 \boldsymbol{\tau}_B, \quad (7.19)$$

where $d_0, d_1, d_2, d_3, d_4, d_5 \in \mathbb{R}^+$. Practically, points $\mathbf{p}_0, \mathbf{p}_1, \mathbf{p}_2, \mathbf{p}_3$ must be aligned along the direction specified by $\boldsymbol{\tau}_A$, while $\mathbf{p}_4, \mathbf{p}_5, \mathbf{p}_6, \mathbf{p}_7$ must be aligned along the direction specified by $\boldsymbol{\tau}_B$. Thus, by defining $\mathbf{d} := [d_0, d_1, d_2, d_3, d_4, d_5] \in \mathcal{D} \subset (\mathbb{R}^+)^6$, where \mathcal{D} is a chosen compact, the optimization problem can be written as follows

$$\min_{\mathbf{d} \in \mathcal{D}} J(\mathbf{d}), \quad (7.20)$$

where $J(\mathbf{d})$ denotes one objective function chosen among (7.5), (7.6) or (7.7).

The paths obtained through the solution of the optimization problem are shown in Fig. 7.2. In order to discuss the results, it is necessary to explicit the two typical desiderata which are satisfied by plant designers. First of all, they try limiting the surface covered by the curve since in automated warehouses LGVs move in confined spaces and a few centimeters are sufficient to make a path unfeasible. As a consequence, shorter curves should be preferred, so as to reduce the surface swept by vehicles. This requirement normally conflicts with another important target: the traveling time, which must be kept small for efficiency reasons. Traveling times clearly depend on the velocity planner adopted. This work uses the one proposed in [17], but it is important to stress that similar results could have been achieved with alternative minimum time velocity planners. The distinguishing characteristic of the planner devised in [17] is that it was conceived for the real-time generation of velocity profiles for LGVs subject to kinematic and safety constraints.

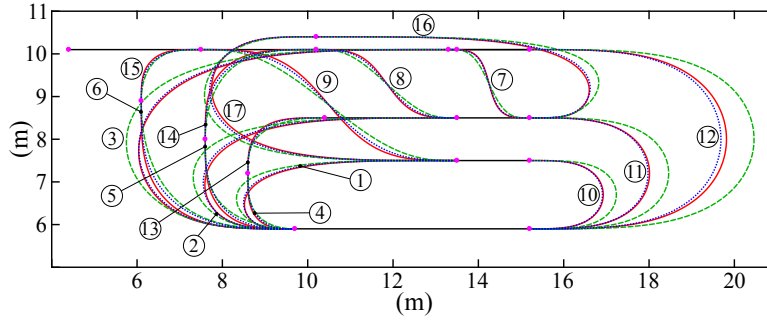


Fig. 7.2: Plant layouts obtained through the three proposed cost indexes: dashed green lines refer to index (7.5); dotted blue lines refer to index (7.6); solid red lines refer to index (7.7). Circled numbers specify the curve ID.

Table 7.2: A comparison between the path lengths and the traveling times obtained with the proposed Performance Indexes (PI). Boldface text highlights the best performances, i.e., the shortest paths and the shortest traveling times.

	Path length (m)			Traveling time (s)		
	PI (7.5)	PI (7.6)	PI (7.7)	PI (7.5)	PI (7.6)	PI (7.7)
1	7.2071	6.8929	6.8507	9.7989	9.3890	9.2909
2	9.7273	9.2900	9.2114	10.0784	9.5896	9.4132
3	13.6601	13.1390	13.1337	11.9294	11.4107	11.3788
4	1.9893	2.0186	2.0521	7.6360	4.7580	4.7856
5	3.4740	3.5122	3.5738	6.2571	4.4881	4.4751
6	5.4711	5.5527	5.6472	6.8647	5.0460	5.1623
7	2.7081	2.8149	2.8328	8.8855	8.8966	9.0946
8	3.7952	3.8656	3.9094	6.5400	6.5043	6.7886
9	6.7187	6.8206	6.8961	6.4113	5.8529	6.1524
10	4.8443	4.2293	4.2662	6.9731	6.6341	6.5682
11	7.7809	6.8698	7.0638	8.3587	7.7682	7.8968
12	12.5590	11.0995	11.3390	10.9922	10.0474	10.2093
13	2.5883	2.6361	2.6685	6.9131	4.7328	4.6630
14	3.9037	3.9650	4.0248	6.5629	4.5884	4.6169
15	2.1548	2.1851	2.2219	7.2981	4.7377	4.8151
16	9.0246	8.6455	8.5963	10.8582	10.4908	10.3918
17	9.8657	9.6605	9.5674	9.8566	9.4906	9.3926

Traveling times are obtained according to the procedure proposed in the following. Each one of the test curves is always preceded and followed by two segments: the first one is used to enter the curve at full speed (compatibly with the constraints), while the second one is used to decelerate and stop the vehicle. Statistics on traveling times only concern the execution of the test curves, i.e., times referring to the acceleration and deceleration sections are not considered.

Given these premises, the results obtained through the solution of (7.20) can be discussed with the aid of Table 7.2, which reports the path length of each curve and the corresponding traveling time. Boldface text highlights the best performances. The table shows that the best results can not be unambiguously attributed to a single performance index but, conversely, they depend on the curve typology. For what concerns the path length, for 90° curves and lane changes the shortest paths are

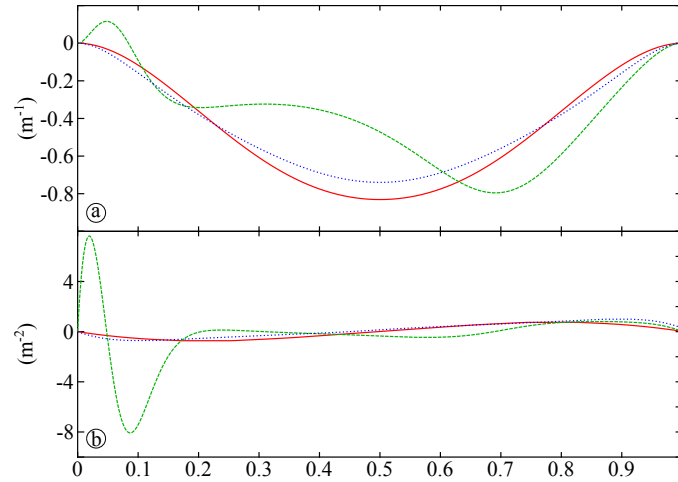


Fig. 7.3: Curvatures (a) and curvature derivatives (b) for the three performance indexes: the dashed green lines refer to (7.5); dotted blue lines refer to (7.6); solid red lines refer to (7.7). The abscissa has been normalized w.r.t. the three path lengths.

obtained by minimizing (7.5), while for the other interpolating conditions the best solutions are obtained through (7.6) or (7.7). The situation totally changes if the trajectory is studied from an efficiency point of view. In most cases the shortest traveling times are obtained by adopting (7.6) or (7.7) and are, generally, very similar for the two indexes. In the same way, also the path lengths for (7.6) and (7.7) are similar, so that the two performance indexes can be considered equivalent from several point of view. Conversely, performance index (7.5), despite it often leads to shorter paths, gives rise to traveling times which are, sometimes, very long.

In order to understand the reasons of this behavior, the results obtained for the 5th curve are deeper analyzed in the following. Fig. 7.3 compares curvatures and curvature derivatives of the paths obtained with the three performance indexes: curvatures have the same order of magnitude, but curvature derivatives differ a lot. In particular, index (7.5) generates a path whose initial curvature derivative is very high. The consequences of such behavior are immediately visible in Fig. 7.4 which shows, for the same curve, the constraints on the longitudinal speed, obtained from (7.3), (7.4), and the fulfillment of the safety conditions: at the beginning of the curve, constraint (7.4) imposes very low admissible speeds.

Still considering the 5th set of interpolating conditions, Fig. 7.5 compares the velocity profiles obtained for the three curves returned by (7.20). For completeness, it also shows the velocity references for the launch and the stop segments despite they are not used for the statistics. The solid black lines in Fig. 7.5 indicate the velocity bounds: the constraint of Fig. 7.5a is clearly given by the worst case envelope of the limits shown in Fig. 7.4. The visual comparison between the three solutions immediately points out the problems deriving from cost index (7.5): the high curvature derivatives at the beginning of the curve force very low speeds. Conversely, much better performances are obtained through (7.6) or (7.7).

The cumulative results evidently prove that cost index (7.5) leads to paths which penalize the plant performances. As a consequence, such index will be no longer considered in the remainder of the paper.

Further conclusions can be drawn from the analysis of Table 7.2. Indexes (7.6) and (7.7) give rise to paths with very similar lengths and traveling times. In most cases, shorter curves are traveled in shorter times. This behavior is in general not straightforward, since vehicles traveling along short

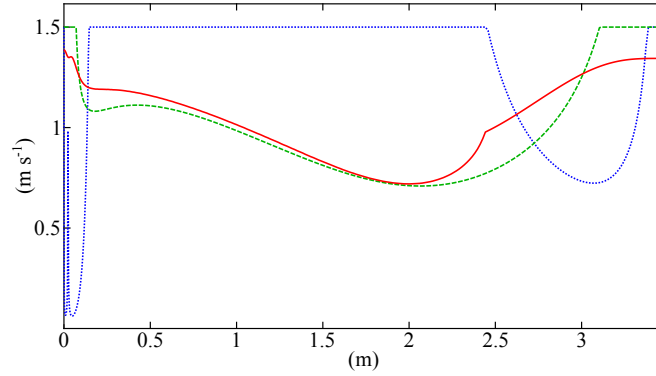


Fig. 7.4: Velocity constraints for the 5th curve expressed in function of the curvilinear coordinate s for the solution obtained by minimizing (7.5). The dashed green line is obtained from (7.3); the dotted blue line is obtained from (7.4); the solid red line is obtained from the safety conditions.

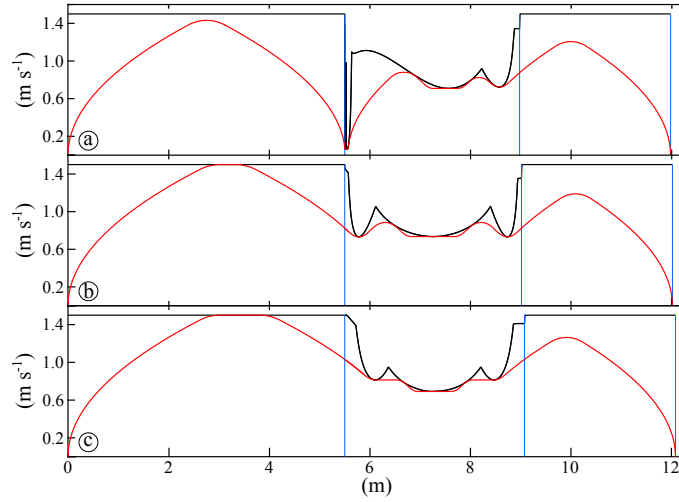


Fig. 7.5: Velocity profiles (solid red lines) for the 5th curve, as obtained through the planner proposed in [17]: (a) performance index (7.5); (b) performance index (7.6); (c) performance index (7.7). Solid black lines indicate the velocity constraints, vertical blue lines separate the path segments.

curves must execute tighter bends which force lower speeds: short paths do not necessarily imply short traveling times. Consequently, the following question arises naturally: how does the curve length affect traveling times? An alternative optimization problem is proposed in Section 7.3 in order to answer to such question.

7.3 The hybrid path planning optimization problem

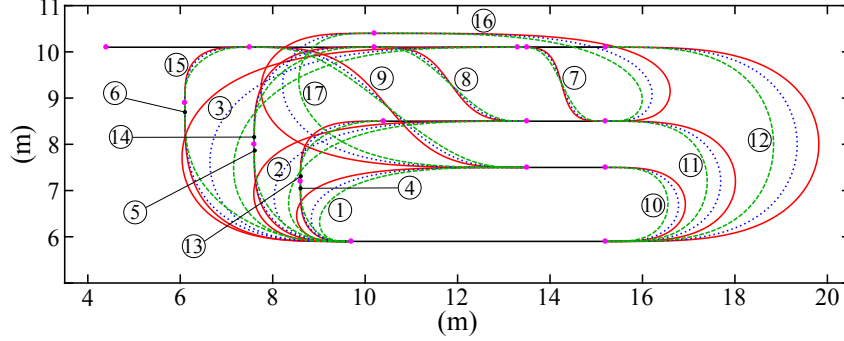


Fig. 7.6: Plant layouts obtained by solving (7.22) with J given by (7.7). Red solid curves refer to $\lambda = 0$; blue dotted curves refer to $\lambda = 0.4$; green dashed curves refer to $\lambda = 0.8$.

The ideal solution to the path planning problem for LGVs would be represented by short paths traveled in short times. Clearly, manual modifications of the optimal curves obtained by solving (7.20) do not lead to satisfactory results, so that the original optimization problem was reformulated by introducing an alternative optimality criterion. In particular, Section 7.2 has already shown that traveling times can be reduced by considering one of the two objective functions (7.6) and (7.7). Conversely, if the curve length needs to be limited, the following alternative cost index can be taken into account

$$J_s(\mathbf{d}) := s_f(\mathbf{d}) - d, \quad (7.21)$$

where $s_f(\mathbf{d})$ is the path length, $d = \|\mathbf{p}_B - \mathbf{p}_A\|$ is the Euclidean distance between the beginning and the end points of the curve. Obviously, $s_f(\mathbf{d}) \geq d$ so that $J_s(\mathbf{d}) \geq 0$. Evidently, the minimization of $J_s(\mathbf{d})$ leads to shorter curves. In order to accomplish both the efficiency and the space occupation requirement, the following new performance index was conceived from the convex combination of the two concurrent targets

$$\min_{\mathbf{d} \in \mathcal{D}} (1 - \lambda) J(\mathbf{d}) + \lambda \alpha J_s(\mathbf{d}). \quad (7.22)$$

$J(\mathbf{d})$ is one of the two cost indexes (7.6) or (7.7), while $\lambda \in [0, 1]$ is a fixed weighting coefficient. Evidently, the new problem coincides with (7.20) if $\lambda = 0$. A scalar value α has been introduced in order to balance $J(\mathbf{d})$ and $J_s(\mathbf{d})$. It is worth to point out that the two cost functions are dimensionally different, have different amplitudes and, moreover, show a different sensitivity with respect to \mathbf{d} . In order to obtain consistent results, seventeen constant values of α were required, one for each set of interpolating conditions. They were chosen so as to account for the variability of $J(\mathbf{d})$ and of $J_s(\mathbf{d})$. In particular, by defining \mathbf{d}_0 the initial guess used for (7.20) and \mathbf{d}^* the resulting final minimizer, if α is evaluated as follows

$$\alpha := \left| \frac{J(\mathbf{d}_0) - J(\mathbf{d}^*)}{s_f(\mathbf{d}_0) - s_f(\mathbf{d}^*)} \right|, \quad (7.23)$$

the two cost functions in (7.22) are properly balanced.

The plant layouts returned by (7.22), for $J(\mathbf{d})$ given by (7.7) with $\lambda = 0$, $\lambda = 0.4$, and $\lambda = 0.8$, are shown in Fig. 7.6. Evidently, shorter curves are obtained as λ increases. A similar behavior is pointed out by the curves obtained through (7.6).

Table 7.3: A comparison between the path lengths and the traveling times obtained with (7.22) where J is given by (7.6).

	Path length (m)					Traveling time (s)				
	$\lambda = 0$	$\lambda = 0.2$	$\lambda = 0.4$	$\lambda = 0.6$	$\lambda = 0.8$	$\lambda = 0$	$\lambda = 0.2$	$\lambda = 0.4$	$\lambda = 0.6$	$\lambda = 0.8$
1	6.8929	6.4717	6.2435	6.0101	5.7274	9.3890	9.1520	9.1063	9.1498	9.1571
2	9.2899	8.5577	8.1605	7.7363	7.3112	9.5896	9.1951	9.0297	8.9458	9.1176
3	13.1390	11.9180	11.2604	10.6566	9.9706	11.4107	10.6288	10.2524	10.0968	10.4027
4	2.0186	2.0065	1.9889	1.9646	1.9283	4.7580	4.7739	4.9257	5.2046	5.7151
5	3.5122	3.4990	3.4799	3.4492	3.3922	4.4881	4.5625	4.6932	4.9289	5.3322
6	5.5527	5.5242	5.4777	5.4120	5.3124	5.0460	5.0539	5.1229	5.3267	5.5348
7	2.8149	2.7865	2.7543	2.7178	2.6726	8.8966	8.9806	8.9554	8.8933	8.8669
8	3.8656	3.8484	3.8285	3.8062	3.7794	6.5043	6.2950	6.2692	6.3929	6.6678
9	6.8206	6.8037	6.7818	6.7535	6.7153	5.8529	5.8196	5.8498	5.9634	6.4684
10	4.2293	3.8166	3.6565	3.4551	3.1748	6.6341	6.8622	6.9197	6.7633	7.0002
11	6.8698	6.2872	6.0225	5.6864	5.2150	7.7682	7.4329	7.1875	7.0780	7.2624
12	11.0995	10.1729	9.7502	9.2096	8.4466	10.0474	9.4796	9.1721	8.8529	8.5038
13	2.6361	2.5244	2.4762	2.4389	2.3994	4.7328	5.5335	6.1435	6.8051	8.5316
14	3.9650	3.9411	3.9047	3.8536	3.7807	4.5884	4.6492	4.8058	5.1008	5.6974
15	2.1851	2.1673	2.1436	2.1143	2.0739	4.7377	4.8232	5.0066	5.3349	5.9253
16	8.6455	8.0865	7.8264	7.5509	7.2187	10.4908	10.2081	10.2830	10.4637	10.6057
17	9.6605	8.7510	8.3313	7.8642	7.4013	9.4906	9.0408	8.9105	8.8672	9.0689

Table 7.4: A comparison between the path lengths and the traveling times obtained with (7.22) where J is given by (7.7).

	Path length (m)					Traveling time (s)				
	$\lambda = 0$	$\lambda = 0.2$	$\lambda = 0.4$	$\lambda = 0.6$	$\lambda = 0.8$	$\lambda = 0$	$\lambda = 0.2$	$\lambda = 0.4$	$\lambda = 0.6$	$\lambda = 0.8$
1	6.8507	6.4367	6.2196	6.0301	5.8442	9.2909	9.1104	9.1564	9.1102	9.1949
2	9.2114	8.6943	8.3479	8.0422	7.7272	9.4132	9.1586	9.1215	8.9876	9.0603
3	13.1337	12.5585	11.9577	11.5224	10.9837	11.3788	11.0109	10.6514	10.4276	10.3157
4	2.0521	2.0466	2.0352	2.0133	1.9853	4.7856	4.7824	4.7735	4.8474	5.0869
5	3.5738	3.5600	3.5395	3.5084	3.4551	4.4751	4.4867	4.5169	4.6695	4.8942
6	5.6472	5.6199	5.5760	5.5056	5.4168	5.1623	5.1333	5.0975	5.1593	5.1584
7	2.8328	2.8077	2.7848	2.7487	2.7059	9.0946	9.2482	9.2408	8.9955	8.8777
8	3.9094	3.8731	3.8514	3.8284	3.8041	6.7886	6.4856	6.3177	6.3178	6.5637
9	6.8961	6.8413	6.8005	6.7659	6.7311	6.1524	5.9139	5.9541	6.0335	6.3137
10	4.2662	4.1719	3.9717	3.8793	3.5823	6.5682	6.5809	6.7399	6.5979	6.7351
11	7.0638	6.7883	6.3298	6.0580	5.8330	7.8968	7.7109	7.4303	7.2183	7.1155
12	11.3390	10.9236	10.4754	10.0915	9.5666	10.2093	9.9382	9.6043	9.3848	9.0769
13	2.6685	2.6517	2.6034	2.5725	2.5328	4.6630	4.6838	4.9637	5.1566	5.5069
14	4.0248	4.0094	3.9733	3.9249	3.8601	4.6169	4.6108	4.6156	4.8097	5.0618
15	2.2219	2.2073	2.1866	2.1600	2.1262	4.8151	4.7685	4.7803	5.0174	5.2920
16	8.5963	8.0693	7.8213	7.5878	7.3636	10.3918	10.1557	10.1612	10.1646	10.2793
17	9.5674	9.0552	8.6535	8.3471	7.9814	9.3926	9.1482	8.9850	8.9598	8.8931

The trend is also confirmed by Tables 7.3 and 7.4: the first one refers to the curves obtained through (7.6), while the second one refers to the paths given by (7.7). From the two tables it is possible to evince that for small values of λ traveling times and path lengths generally reduce as λ increases: this is clearly a desired behavior. For high values of λ the situation changes depending on the curve typology: paths are always shorter, but traveling times can be higher or smaller depending

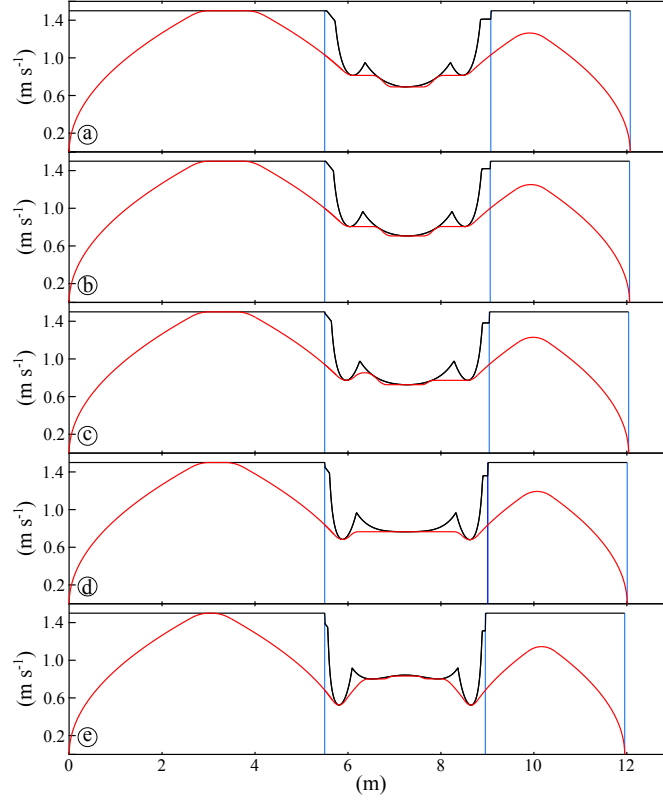


Fig. 7.7: Visual comparison between the velocity functions obtained by solving (7.22) with $J(\mathbf{d})$ given by (7.7) for the 5th curve and by assuming: (a) $\lambda = 0$; (b) $\lambda = 0.2$; (c) $\lambda = 0.4$; (d) $\lambda = 0.6$; (e) $\lambda = 0.8$.

on the curve. In any case, and this is really important, traveling times obtained for $\lambda = 0$ are very close to the ones obtained for $\lambda = 0.8$: tight curves can be adopted to handle space problems, since they minimally impact on the plant efficiency. Evidently, this is true only if a smart velocity planner, like the one proposed in [17], is used.

Tables 7.3 and 7.4 can also be used for a comparison between cost indexes (7.6) and (7.7). For each one of the seventeen curves of the test set, two solutions have been selected – one in Table 7.3 and another in Table 7.4 – admitting similar path lengths: they have been highlighted by means of boldface numbers. The comparative analysis points out that the two solutions are always characterized by similar traveling times, further proving that the two performance indexes return very similar solutions.

The reasons why traveling times are only partially affected by the choice of λ can be easily explained by means of the following considerations. Fig. 7.7, which compares the velocity profiles associated to the 5th set of interpolating conditions for $\lambda \in \{0, 0.2, 0.4, 0.6, 0.8\}$, highlights that the adoption of shorter curves has a negative impact on the shape of the velocity constraint. In fact, the imposed minimum speed decreases from 0.6916 ms^{-1} at $\lambda = 0$ to 0.5235 ms^{-1} at $\lambda = 0.8$: high values of λ limit the speed near the beginning and the end of the segment because of the sharpest curvatures they impose. However, such negative effect is partially compensated by the smart velocity

planner proposed in [17] and by the shorter curve lengths, so that traveling time marginally worsens from the smoothest curve ($\lambda = 0$) to the sharpest one ($\lambda = 0.8$). Such characteristic is particularly relevant for curves to be adopted in warehouses: in presence of obstacles such as columns or shelves, or in case of paths which are very close to walls, curves obtained by adopting $\lambda = 0.8$ allow a consistent space saving w.r.t. the ones obtained for $\lambda = 0$, especially for segments with a small curvature (see curves ID 3 or 12 in Fig. 7.6).

7.4 Conclusions

A study concerning the optimal path planning for the LGVs used in automated warehouses has been proposed in the paper. In such working environment, optimal trajectories are always generated by considering two separate phases: the path planning, carried out offline, and the speed planning, typically performed online in order to react to variable operating conditions or to unexpected events. The problem analyzed was related to the prior selection of paths that would allow the best performances during the online generation of the optimal speed profiles. The analysis proposed has shown that, in order to obtain high performances in terms of efficiency, it is necessary to generate curves characterized by low curvature derivatives. Further studies pointed out that the choice of an optimization criterion based also on the curve length leads to even better results, both by shortening the execution times of the trajectories and by allowing reduced space occupations. It is worth highlighting that this result is achieved through the use of a smart speed planner, like the one developed for the ECHORD++ project, which considerably mitigates the negative effects deriving from the use of tight curves.

Acknowledgment

This work was supported in part by the European Project ECHORD++ (The European Coordination Hub for Open Robotics Development) financed in the framework of the FP7 EU program.

The Authors would like to thank the Elettric80 staff for its profitable support during the whole SAFERUN project. A particular thank goes to Eng. Francesco De Mola and Eng. Domenico Di Terlizzi for the advices provided during the preparation of this work.

References

1. Shiller, Z., Gwo, Y.R.: Dynamic motion planning of autonomous vehicles. *IEEE Trans Robot and Autom* **7**(2), 241–249 (1991)
2. Choi, J.S., Kim, B.K.: Near-time-optimal trajectory planning for wheeled mobile robots with translational and rotational sections. *IEEE Trans. Robot Autom.* **17**(1), 85–90 (2001)
3. Tokekar, P., Karnad, N., Isler, V.: Energy-optimal trajectory planning for car-like robots. *Autonomous Robots* **37**(3), 279–300 (2014)
4. Paden, B., Čáp, M., Yong, S.Z., Yershov, D., Frazzoli, E.: A survey of motion planning and control techniques for self-driving urban vehicles. *IEEE Trans Intell Veh* **1**(1), 33–55 (2016)
5. Fraichard, T.: Trajectory planning in a dynamic workspace: a ‘state-time space’ approach. *Advanced Robotics* **13**(1), 75–94 (1998)

6. Qian, X., Althché, F., Bender, P., Stiller, C., De La Fortelle, A.: Optimal trajectory planning for autonomous driving integrating logical constraints: An miqp perspective. In: IEEE Int. Conf. Intell. Transp. Syst. (ITSC16), pp 205–210 (2016)
7. Solea, R., Nunes, U.: Trajectory Planning with Velocity Planner for Fully-Automated Passenger Vehicles. In: IEEE Conf. Int. Transp. Syst., ITSC06, pp 474–480 (2006)
8. Kant, K., Zucker, S.: Toward efficient trajectory planning: The path-velocity decomposition. *Int. J. Robot Res.* **5**(3), 72–89 (1986)
9. Fraichard, T., Laugier, C.: Path-velocity decomposition revisited and applied to dynamic trajectory planning. In: IEEE Int. Conf. Robot. and Autom. ICRA93, **2**, pp 40–45. Los Alamitos, CA (1993)
10. Delingette, H., Hébert, M., Ikeuchi, K.: Trajectory generation with curvature constraint based on energy minimization. In: IEEE/RSJ Int. Conf. Intell. Robots and Syst., pp 206–211. Osaka, Japan (1991)
11. Kim, K.B., Kim, B.K.: Minimum-time trajectory for three-wheeled omnidirectional mobile robots following a bounded-curvature path with a referenced heading profile. *IEEE Trans Robot* **27**(4), 800–808 (2011)
12. Nelson, W.: Continuous-curvature paths for autonomous vehicles. In: IEEE Int. Conf. Robot. and Autom., ICRA89, **3**, pp 1260–1264. Scottsdale, AZ (1989)
13. Fraichard, T., Scheuer, A.: From Reeds and Shepp’s to continuous-curvature paths. *IEEE Trans Robot* **20**(6), 1025–1035 (2004)
14. Muñoz, V., Ollero, A., Prado, M., Simón, A.: Mobile robot trajectory planning with dynamic and kinematic constraints. In: IEEE Int. Conf. Robot. and Autom., ICRA94, **4**, pp 2802–2807. San Diego, CA (1994)
15. Consolini, L., Locatelli, M., Minari, A., Piazzzi, A.: An optimal complexity algorithm for minimum-time velocity planning. *Systems & Control Letters* **103**, 50–57 (2017)
16. Perri, S., Guarino Lo Bianco, C., Locatelli, M.: Jerk bounded velocity planner for the online management of autonomous vehicles. In: IEEE Int. Conf. Autom. Sci. and Eng., CASE 2015, pp 618–625 (2015)
17. Raineri, M., Perri, S., Guarino Lo Bianco, C.: Online velocity planner for Laser Guided Vehicles subject to safety constraints. In: IEEE/RSJ Int. Conf. Intell. Robots and Syst., (IROS17), pp 6178–6184 (2017)

Chapter 8

FASTKIT: A Mobile Cable-Driven Parallel Robot for Logistics

Nicolò Pedemonte, Tahir Rasheed, David Marquez-Gamez, Philip Long, Étienne Hocquard, Francois Babin, Charlotte Fouché, Guy Caverot, Alexis Girin and Stéphane Caro

Abstract The subject of this paper is about the design, modeling, control and performance evaluation of a low cost and versatile robotic solution for logistics. The robot under study, named FASTKIT, is obtained from a combination of mobile robots and a Cable-Driven Parallel Robot (CDPR). FASTKIT addresses an industrial need for fast picking and kitting operations in existing storage facilities while being easy to install, keeping existing infrastructures and covering large areas. The FASTKIT prototype consists of two mobile bases that carry the exit points of the CDPR. The system can navigate autonomously to the area of interest. Once the desired position is attained, the system deploys the CDPR in such a way that its workspace corresponds to the current task specification. The system calculates the required mobile base position from the desired workspace and ensures the controllability of the platform during the deployment. Once the system is successfully deployed, the set of stabilizers are used to ensure the prototype structural stability. Then the prototype gripper is moved accurately by the CDPR at high velocity over a large area by controlling the cable tension.

N. Pedemonte, D. Marquez-Gamez, E. Hocquard, F. Babin, C. Fouché and A. Girin
IRT Jules Verne, Chemin du Chaffault, 44340, Bouguenais, France, e-mail:
[nicolo.pedemonte](mailto:nicolo.pedemonte@irt-jules-verne.fr), [david.marquez-gamez](mailto:david.marquez-gamez@irt-jules-verne.fr), [etienne.hocquard](mailto:etienne.hocquard@irt-jules-verne.fr), [francois.babin](mailto:francois.babin@irt-jules-verne.fr),
[charlotte.fouche](mailto:charlotte.fouche@irt-jules-verne.fr), [alexis.girin](mailto:alexis.girin@irt-jules-verne.fr)

T. Rasheed
Centrale Nantes, Laboratoire des Sciences du Numérique de Nantes, UMR CNRS 6004, 1, rue de la Noë, 44321 Nantes, France, e-mail: tahir.rasheed@ls2n.fr

P. Long
RIVeR Lab, Department of electrical and computing engineering, Northeastern University, USA,
e-mail: p.long@northeastern.edu

G. Caverot
B2A Technology, Mordelles, France, e-mail: guy.caverot@basystemes.fr

S. Caro
CNRS, Laboratoire des Sciences du Numérique de Nantes, UMR CNRS 6004, 1, rue de la Noë, 44321 Nantes, France, e-mail: stephane.caro@ls2n.fr

8.1 Introduction

Cable-Driven Parallel Robots (CDPRs) form a particular class of parallel robots whose moving platform is connected to a fixed base frame by cables. The cables may be coiled/uncoiled by motorized winches allowing a control system to adjust the cable lengths between the winch exit points and the cable attachment points on the platform. Appropriate length adjustment of cables allows one to control the degrees of freedom of the moving platform. CDPRs have several advantages such as mechanical simplicity and a potentially very large workspace. They have been used in several applications, e.g. heavy payload handling and airplane painting [1], cargo handling [2], warehouse applications [3], large-scale assembly and handling operations [4], and fast pick-and-place operations [5]. Other possible applications include the broadcasting of sporting events, haptic devices Fortin2014, simulators [7], and search and rescue deployable platforms [8]. The performance improvement of CDPRs is still a challenge because the cable unilaterality (cables can pull but cannot push) makes their analysis much more complex than parallel robots with rigid legs. Indeed, it is necessary to introduce cable models in the analysis, that are usually complex, non-linear, non-algebraic and computer demanding.

As we have seen CDPRs may perform various kinds of applications but they impose a strong requirement regarding the free circulation of the cables without interference with the environment. It is therefore reasonable to adjust their geometry (which has a large influence on the performances) according to the task requirements and the robot's environment. FASTKIT has aimed therefore at developing an mobile, deployable and autonomous CDPRs, called Mobile Cable-Driven Parallel Robots (MCDPRs), that can be adapted to the logistic task. From a mechanical point of view changing the geometry of CDPR is relatively easy either by moving the winches, by using pulleys to modify the location of the winches exit points or by changing the location of the cable attachment points on the load. Preliminary studies on reconfigurable CDPRs were performed in the context of the NIST RoboCrane project [9]. Izard *et al.* [10] also studied a family of RCDPRs for industrial applications. Beside the mechanical modularity, a challenge is to develop a strategy that will allow one to determine the best CDPR geometry for a given task to be fulfilled. Discrete reconfigurations where the locations of the cable exit points are selected from a finite set of possible values have been recently studied in [11].

This paper deals with the design, modeling and performance analysis of a Mobile Cable-Driven Parallel Robot (MCDPR), named FASTKIT, developed in the framework of ECHORD++ FASTKIT project. FASTKIT project addresses an industrial need for fast picking and kitting operations in existing storage facilities while being easy to install, keeping existing infrastructures and covering large areas. Nowadays there exist several robotic solutions for logistic applications. One of the most popular automatic storage systems is the multi-shuttle system described in [11], which guarantees high performance in terms of working rate. The main drawbacks of such systems are the high investment cost, the long installation time and the lack of flexibility.

Such systems are usually installed over large warehouses presenting a high entry and exit flow of storage boxes. In such conditions, an acceptable Return On Investment (ROI) is usually guaranteed. On the other hand, this solution is no longer possible or profitable for small warehouses, where there is no room for the installation of a large multi-shuttle system, or for warehouses characterized by a very low entry and exit flow of storage units, for which the high investment cost of a multi-shuttle solution is not justified.

The FASTKIT concept shown in Fig. 8.1 and developed in the scope of FASTKIT project is made up of CDPR mounted on two mobile platforms. As a result, it combines the autonomy of mobile robots with the advantages of CDPR, namely, large workspace, high payload-to-weight ratio, low end-effector inertia, deployability and reconfigurability. Moreover, CDPRs lead generally to low cost and easy maintenance solutions. Thanks to their characteristics, CDPRs can be used for different tasks such as the manipulation of heavy payloads or fast pick-and-place operations. Indeed, logistics is a very interesting field of application for CDPRs. Accordingly, FASTKIT aims at providing the user with a flexible and low cost logistic solution to equip small warehouses.



Fig. 8.1: FASTKIT concept: A cable-driven parallel robot mounted on two mobile platforms

Therefore, the novelty of FASTKIT lies in the combination of autonomous mobile platforms and a CDPR. The main challenge in FASTKIT dealt with the design, modeling and assembly of the CDPR and the two mobile bases as well as the synchronization of their control laws.

This paper is organized as follows. Section 2 describes the main components, the control strategy and the architecture of the navigation stack of FASTKIT. Section 3 deals with the kinematic modeling and kinematic performance evaluation of FASTKIT. The wrench capability of FASTKIT is assessed in Sec. 4. Some discussions and conclusions are given in Sec. 5.

8.2 FASTKIT Prototype

Figure 8.2 shows the FASTKIT prototype developed in the framework of ECHORD++ FASTKIT project. It is composed of a Moving-Platform (MP) equipped with a gripper, an active Mobile Base (MB) and a passive MB connected to each other through eight cables.

FASTKIT is capable of autonomously navigating in its environment to reach the task location referred to as a navigation mode. During this mode, the two Mobile Bases (MBs) are coupled together and act as a single working unit while the MP is fixed on the two MBs (see Fig. 3(a)). The twist of the MP and the passive mobile base is equal to the twist generated by the active

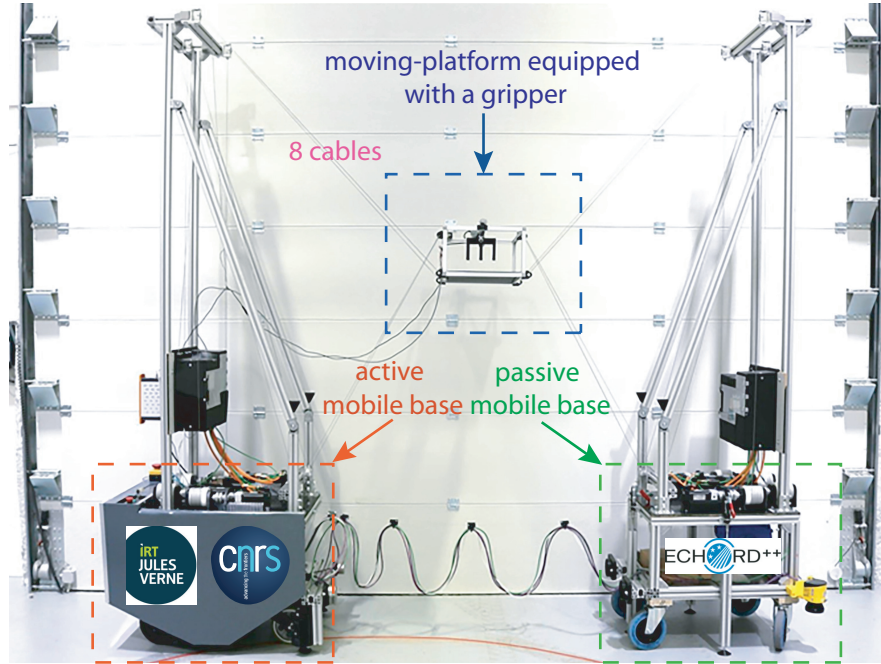


Fig. 8.2: FASTKIT prototype

mobile base. No cable motion is generated during the navigation mode. The second working mode, referred to as the task mode, deploys the system at the desired location such that the desired pick or/and place operation is achievable within the defined workspace. During this mode, the passive mobile base is static while the motion of the cables and the active mobile base is used to deploy the complete system (see Figs. 3(b) and 3(c))¹. It should be noted that during the task mode, FASTKIT is kinematically redundant due to the additional mobility of the active mobile base as explained in [12].

8.2.1 Main Components

The main components of FASTKIT are: (i) the main structure, (ii) the actuation system, (iii) its twelve pulleys, (iv) its MP equipped with a gripper, (v) Two s300 sick laser scanners, and (vi) two electrical cabinets. Here are the FASTKIT specifications:

- a desired workspace of 5 meters long by 2 meters high,
- a linear velocity of the moving-platform equal to 1 m/s,
- a 7 kg payload.

The 2.4 m high main structure is made up of aluminum profile bars. The eight feet of the two structures are directly fixed on the top of the two mobile bases.

¹ Videos on FASTKIT YouTube channel: <https://www.youtube.com/channel/UCJ8QRs818MBc8YSbn-bZVja>

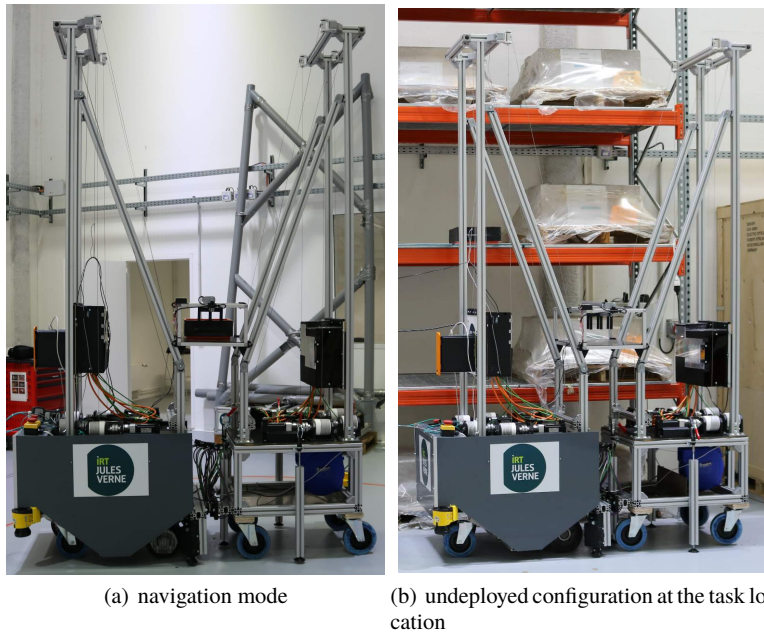


Fig. 8.3: FASTKIT working modes

8.2.1.1 Actuation and Transmission System

The actuation system consists of eight identical modules, each module being composed a motor, a gearbox, an elastic coupling, a transmission shaft, two bearings and a winch, as shown in Fig. fig:FASTKITactsystem.

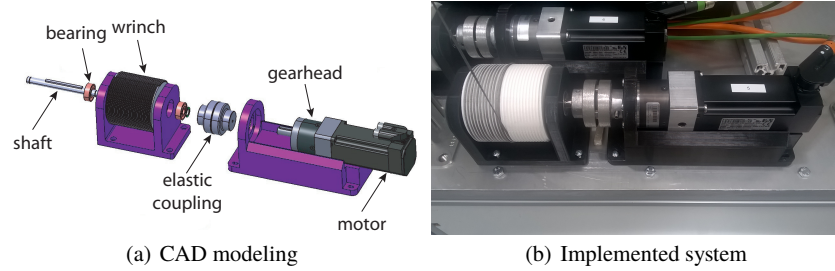


Fig. 8.4: FASTKIT actuation and transmission system

Based on the foregoing specifications, the required maximum cable tension and maximum cable velocity are equal to 45 N and 2 m/s, respectively. As a result, 8LVA23 B&R motors coupled with 8GP30 B&R gearboxes were selected. Table 8.1 gives the characteristics of the selected motors.

Requirements	
Maximum cable tension	45 N
Maximum cable velocity	2 m/s
Actuators	
Actuation system efficiency	70%
Gearhead ratio	5:1
Wrines	
Drum diameter	0.08 m
Motors (working point)	
Torque	0.6 Nm
Angular velocity	1600 rpm

Table 8.1: Characteristics of the selected motors

8.2.1.2 Pulleys

The pulleys have been realized in such a way that the friction is a minimum and the pulley to be sustainable. Hence, the pulley must be designed such that the cable can easily roll around the sheave and that the sheave itself can rotate freely around its vertical axis. Accordingly, the sheave is equipped with a ball bearing whereas two angular contact ball bearings are used to free the sheave rotation around the vertical axis.

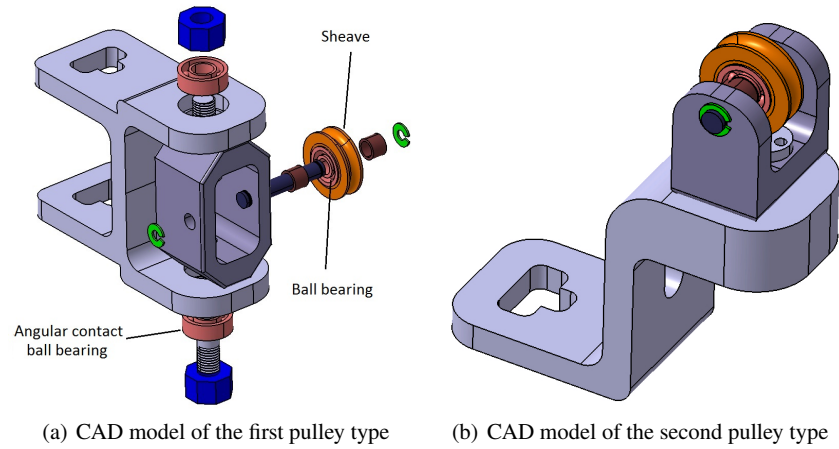


Fig. 8.5: FASTKIT pulleys

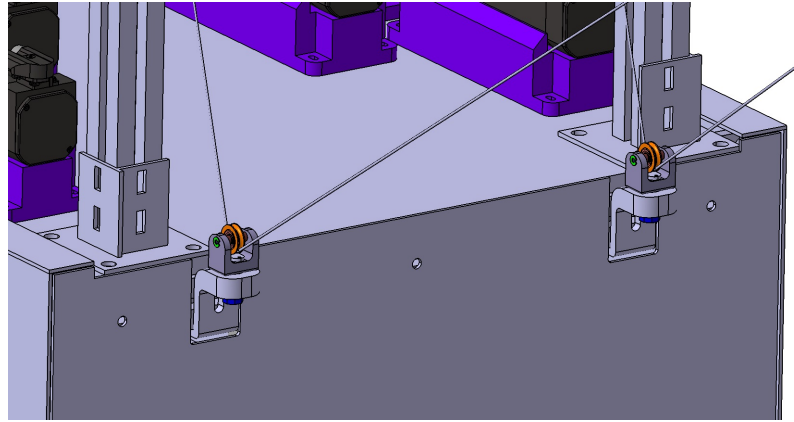


Fig. 8.6: Location of the additional pulleys for the CDPR to be in a fully constrained configuration

Figure 5(a) shows the CAD model of the eight pulleys used for the assembly of the CDPR in a suspended configuration. Figure 5(b) shows the CAD model of the additional four pulleys that have been realized to assemble the CDPR in a fully constrained configuration represented in Fig. 8.6.

8.2.1.3 Moving-Platform and Gripper

The moving-platform has been designed to be capable of grasping, carrying and dropping a box of size $0.4 \text{ m} \times 0.3 \text{ m} \times 0.15 \text{ m}$, which is a typical size of the storage units used in logistics. Inner dimensions of the platform are $0.6 \text{ m} \times 0.36 \text{ m} \times 0.2 \text{ m}$. Figure 7(a) depicts the CAD model of the MP equipped with its gripper. Here, the mass of the moving-platform should be a minimum.

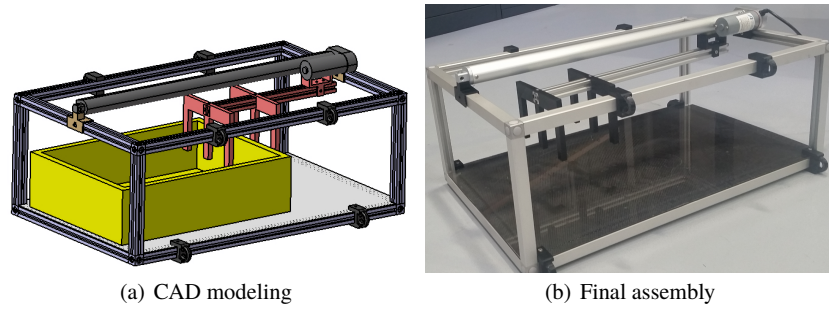


Fig. 8.7: Moving-platform with its gripper grabbing a storage unit box

The actual moving-platform, shown in Fig. 8.7, weighs 5 Kg. A Firgelli linear motor ² was used to realized the MP gripper. It should be noted that the MP tilt, required to grab and release boxes, is controlled through the cable lengths. Indeed, no exteroceptive sensor is used to manage the pick-and-place task and the MP tilt. Note that the good FASTKIT's repeatability allows us to execute this task in open-loop. On the other hand, ongoing work is dedicated to increase FASTKIT's accuracy in the initial MP positioning by means of cameras.

8.2.1.4 Sick Laser Scanners

Each mobile base is equipped with a s300 sick laser scanner shown in Fig. 8.4. It has 3 m field range and 270° scanning angle. This kind of scanner is usually used for obstacle avoidance and the navigation of the overall system described in Sec. 8.2.3.

8.2.1.5 Electrical Cabinets

The actuation system of the CDPR is controlled and powered by means of two electrical cabinets, one installed onto each mobile base. Those two cabinets are slightly different. Both electrical cabinets are composed of: (i) two variable speed drives; (ii) two 80V power supplies for the synchronous motors; (iii) one 24V power supply for the drives and (iv) one safety relay. In addition, the electrical cabinet embedded in the active mobile base is equipped with an industrial PC that controls the whole robot. Figure 8.8 shows the main electrical cabinet with the industrial PC. For the sake of compatibility, the speed drives, the power supplies and the industrial PC have been provided by the motor supplier, namely, B&R AutomationTM.

8.2.2 Control Strategy

The first control law that has been tested on the FASTKIT CDPR is a velocity control law. In order to implement it, the geometric and kinematic models of the CDPR are required. The velocity

² <https://www.firgelliauto.com/products/mini-track-actuator#ptab-specifications>

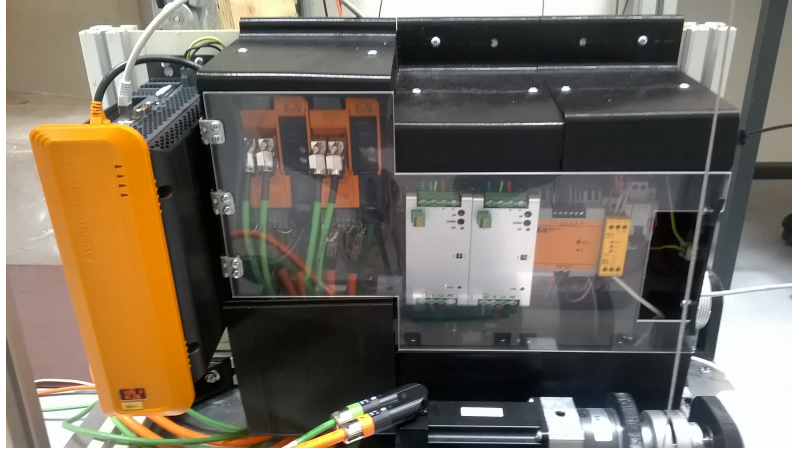


Fig. 8.8: The FASTKIT electrical cabinet mounted onto the active mobile base

control is quite easy to implement and apply, but one major inconvenient arises: the cable tensions are not necessarily well distributed. Hence, during the task execution and because of ineluctable model errors, cables might get slack or too stretched. In order to cope with this undesired behavior, a torque control can be applied. First, one needs to estimate the intrinsic frictions (static, Coulomb and viscous frictions) for each motor. Once these values are established, they can be compensated in the final control law. Secondly, the optimal cable tension distribution should be computed to properly move the robot in its workspace. Several approaches to this problem are described in the literature [13, 14, 15].

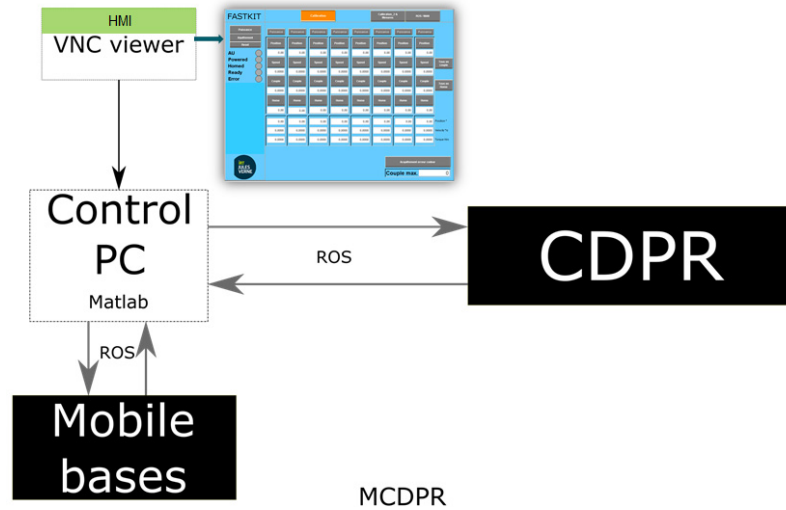


Fig. 8.9: The FASTKIT control architecture

The last strategy adopted in the scope of FASTKIT is described in Fig. 8.9. It aims to write the control algorithms in Matlab and then to communicate with the industrial PC through R.O.S. (Robot Operating System)³. A ROS package for communicating with the B&RTM motors had already been implemented in [11]. There is no need of code generator for Automation Studio. However, it should be noted that R.O.S. cannot run as fast as the B&RTM industrial PC. Hence, some data might get lost during the communication and the system does no longer conform to an industrial standards in terms of robustness and response time.

8.2.3 Navigation

This section deals with the implementation of a navigation stack by means a set of interconnected algorithms. As shown in Fig. 8.10, those algorithms create altogether a complex decision making process:

- Base driver:* low-level software to control the velocity of the mobile platform ;
- Sensor driver:* low-level software to get sensor information, here a scanner distance readings from the two lasers;
- Localization:* software to localize the robot in the environment;
- Collision avoidance:* software, with high priority, to compute free-path for the robot w.r.t. environment dynamics ;
- Path planning:* global planner to compute shortest path to goal ;
- User Interface:* visualization tool to control robot behaviour.

Therefore, the robot is able to model its environment, plan and move to a specific goal while avoiding obstacles.

The system uses ROS navigation algorithms. The core of the framework is to provide a set of standards, namely, sensors information, actuators control and transmission protocols, to allow users to share work and generic algorithms for multiple and various robotic systems. The reader is referred to as [16] for further details about the ROS framework⁴.

The key challenge for an autonomous mobile robot relies on the *perception* of its environment and the *decision* it makes accordingly. By means, from the robot point of view answer to the main questions: Where am I? Where am I going? How should I get there? Navigation can therefore be separated in three problematics: (i) mapping, (ii) localization and (iii) planning motion. For more details about autonomous navigation, the reader is referred to as [17, 18, 19, 20, 21].

Figure 8.11 shows a result of planned trajectory in dynamic environment. The computed polygons can be seen in red. Note that if no polygon can be found, a single point still considers the obstacle. In this scenario, people were around the mobile base, hence the planned trajectory to go toward the red arrow (i.e. objective) required a step backward and a move toward the goal while avoiding obstacles. The obtained results are very promising. However, the computation cost remains high and requires fine tuning of parameters.

8.3 Kinematics

The kinematic performance of any robotic system can be analyzed from its first order kinematic model [22] and the Available Twist Set (ATS). The ATS of CDPRs was defined in [23]. Thus,

³ <http://www.ros.org/>

⁴ Ros navigation stack [online]. <http://wiki.ros.org/navigation>. Accessed: 2015-06-11.

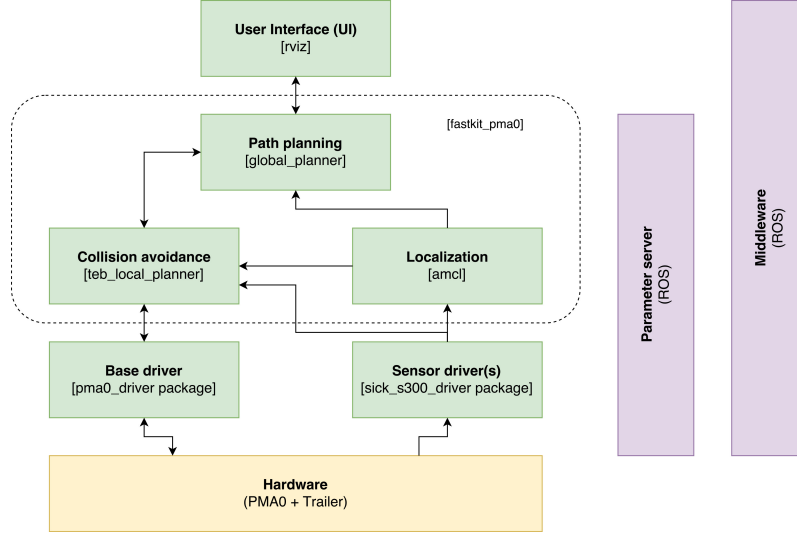


Fig. 8.10: Architecture of the Fastkit navigation stack. Green boxes represents software packages, names of packages are in brackets

this section aims at presenting the kinematic model and ATS of FASTKIT. The mobile bases of FASTKIT are four-wheeled planar robots with two-DoF translational motions and one-DoF rotational motion, thus, they can be modeled as a virtual RPP kinematic chain between the base frame \mathcal{F}_0 and the frame \mathcal{F}_{b1} (\mathcal{F}_{b2} , resp.) attached to active (passive, resp.) mobile base.

The cables attached to the active mobile base are named in ascending order as \mathcal{C}_{11} , \mathcal{C}_{21} , \mathcal{C}_{31} and \mathcal{C}_{41} respectively. Similarly, the cables connected to the passive mobile base are named in ascending order as \mathcal{C}_{12} , \mathcal{C}_{22} , \mathcal{C}_{32} and \mathcal{C}_{42} respectively. The twist ${}^0\mathbf{t}_p^{cables}$ of the moving-platform as a function of cable velocities is expressed as follows:

$$\mathbf{A} {}^0\mathbf{t}_p^{cables} = \dot{\mathbf{l}}, \quad (8.1)$$

where \mathbf{A} is the (8×6) parallel Jacobian matrix, containing the actuation wrenches applied by the cables onto the moving-platform. The twist ${}^0\mathbf{t}_p = [\boldsymbol{\omega}, \dot{\mathbf{p}}]^T$ is composed of the platform angular velocity vector $\boldsymbol{\omega} = [\omega_x, \omega_y, \omega_z]^T$ and linear velocity vector $\dot{\mathbf{p}} = [\dot{p}_x, \dot{p}_y, \dot{p}_z]^T$, expressed in \mathcal{F}_0 . ${}^0\mathbf{t}_p^{cables}$ denotes the platform twist only due to the cable motions. $\dot{\mathbf{l}}$ is a eight-dimensional cable velocity vector. Here, Eq. (8.1) can be expressed as:

$$\begin{bmatrix} \mathbf{A}_1 \\ \mathbf{A}_2 \end{bmatrix} {}^0\mathbf{t}_p^{cables} = \begin{bmatrix} \dot{\mathbf{l}}_1 \\ \dot{\mathbf{l}}_2 \end{bmatrix}, \quad (8.2)$$

where $\dot{\mathbf{l}}_1 = [\dot{l}_{11}, \dot{l}_{21}, \dot{l}_{31}, \dot{l}_{41}]^T$ and $\dot{\mathbf{l}}_2 = [\dot{l}_{12}, \dot{l}_{22}, \dot{l}_{32}, \dot{l}_{42}]^T$. \mathbf{A}_1 and \mathbf{A}_2 are expressed as:

$$\mathbf{A}_1 = \begin{bmatrix} [({}^0\mathbf{b}_{11} - {}^0\mathbf{p}) \times \mathbf{u}_{11}]^T \mathbf{u}_{11}^T \\ [({}^0\mathbf{b}_{21} - {}^0\mathbf{p}) \times \mathbf{u}_{21}]^T \mathbf{u}_{21}^T \\ [({}^0\mathbf{b}_{31} - {}^0\mathbf{p}) \times \mathbf{u}_{31}]^T \mathbf{u}_{31}^T \\ [({}^0\mathbf{b}_{41} - {}^0\mathbf{p}) \times \mathbf{u}_{41}]^T \mathbf{u}_{41}^T \end{bmatrix}, \quad \mathbf{A}_2 = \begin{bmatrix} [({}^0\mathbf{b}_{12} - {}^0\mathbf{p}) \times \mathbf{u}_{12}]^T \mathbf{u}_{12}^T \\ [({}^0\mathbf{b}_{22} - {}^0\mathbf{p}) \times \mathbf{u}_{22}]^T \mathbf{u}_{22}^T \\ [({}^0\mathbf{b}_{32} - {}^0\mathbf{p}) \times \mathbf{u}_{32}]^T \mathbf{u}_{32}^T \\ [({}^0\mathbf{b}_{42} - {}^0\mathbf{p}) \times \mathbf{u}_{42}]^T \mathbf{u}_{42}^T \end{bmatrix} \quad (8.3)$$

where \mathbf{A}_1 and \mathbf{A}_2 contain the actuation wrenches associated with cables connected to the active and passive mobile bases, respectively. \dot{l}_{11} to \dot{l}_{42} denote the velocity of cables \mathcal{C}_{11} to \mathcal{C}_{42} . ${}^0\mathbf{b}_{11}$ to ${}^0\mathbf{b}_{42}$

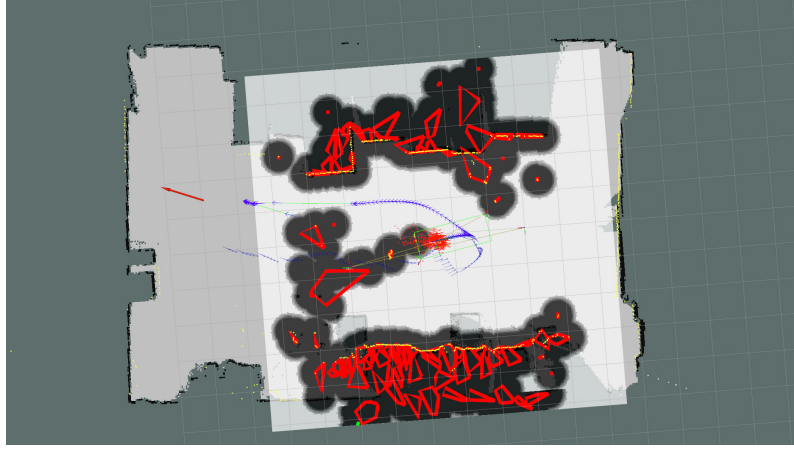


Fig. 8.11: Visualization of the planned trajectory towards a goal. The robot is represented by the green box. The planned trajectory is represented by the blue arrow, red polygons represent obstacles and red arrow shows the position objective. Black area represent the inflation around obstacles for the cost function that guarantees collision avoidance

denote the Cartesian coordinate vectors of anchor points B_{11} to B_{42} in \mathcal{F}_0 . ${}^0\mathbf{u}_{11}$ to ${}^0\mathbf{u}_{42}$ denote the unit vector alongs cable \mathcal{C}_{11} to \mathcal{C}_{42} . ${}^0\mathbf{p}$ is the Cartesian coordinate vector of the geometric center of the moving-platform expressed in frame \mathcal{F}_0 .

8.3.1 First Order Kinematic Model of FASTKIT

The twist ${}^0\mathbf{t}_P^j$ of the moving-platform due to the cables and the mobile bases is expressed as [24]:

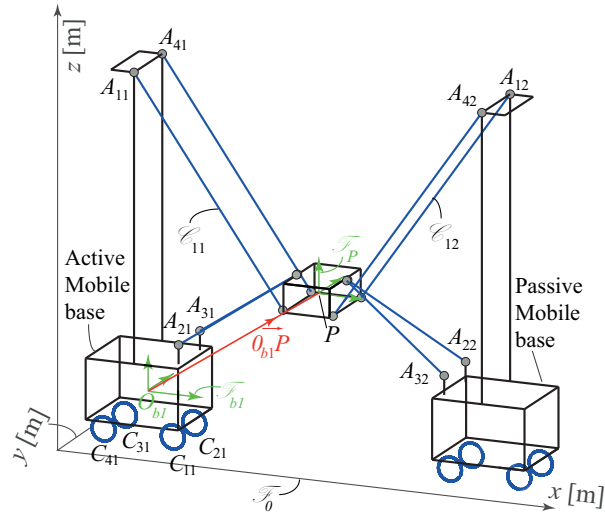
$$\begin{bmatrix} \mathbf{A}_1 \\ \mathbf{A}_2 \end{bmatrix} \mathbf{t}_P = \begin{bmatrix} \mathbf{A}_1 {}^{b1}\mathbf{Ad}_P \mathbf{J}_{b1} & \mathbf{0} \\ \mathbf{0} & \mathbf{A}_2 {}^{b2}\mathbf{Ad}_P \mathbf{J}_{b2} \end{bmatrix} \begin{bmatrix} \dot{\mathbf{q}}_{b1} \\ \dot{\mathbf{q}}_{b2} \end{bmatrix} + \begin{bmatrix} \mathbf{i}_1 \\ \mathbf{i}_2 \end{bmatrix}, \quad (8.4)$$

where ${}^{b1}\mathbf{Ad}_P$ (${}^{b2}\mathbf{Ad}_P$, resp.) is called the adjoint matrix, which represents the transformation matrix between twists expressed in \mathcal{F}_{b1} (\mathcal{F}_{b2} , resp.) and twist expressed in \mathcal{F}_P ,

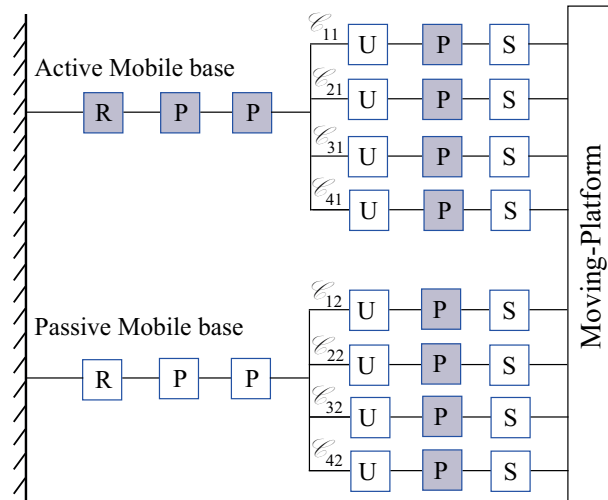
$${}^{b1}\mathbf{Ad}_P = \begin{bmatrix} \mathbf{I}_3 & \mathbf{0}_3 \\ -{}^{b1}\hat{\mathbf{r}}_P & \mathbf{I}_3 \end{bmatrix}, \quad {}^{b2}\mathbf{Ad}_P = \begin{bmatrix} \mathbf{I}_3 & \mathbf{0}_3 \\ -{}^{b2}\hat{\mathbf{r}}_P & \mathbf{I}_3 \end{bmatrix} \quad (8.5)$$

${}^{b1}\hat{\mathbf{r}}_P$ (${}^{b2}\hat{\mathbf{r}}_P$, resp.) is the cross-product matrix of vector $\overrightarrow{O_{b1}P}$ ($\overrightarrow{O_{b2}P}$, resp.) expressed in \mathcal{F}_0 shown in Fig. 12(a). From Eq. (8.4), $\dot{\mathbf{q}}_{b1}$ ($\dot{\mathbf{q}}_{b2}$, resp.) is the three-dimensional joint velocity vector of the virtual RPP kinematic chain for the active (passive, resp.) mobile base, expressed as:

$$\dot{\mathbf{q}}_{b1} = \begin{bmatrix} \dot{\theta}_1 \\ \dot{\rho}_{11} \\ \dot{\rho}_{21} \end{bmatrix}, \quad \dot{\mathbf{q}}_{b2} = \begin{bmatrix} \dot{\theta}_2 \\ \dot{\rho}_{12} \\ \dot{\rho}_{22} \end{bmatrix} \quad (8.6)$$



(a) FASTKIT Parameterization



(b) Kinematic diagram of FASTKIT: active and passive joints are highlighted in gray and white, respectively

Fig. 8.12: FASTKIT kinematics

\mathbf{J}_{b1} (\mathbf{J}_{b2} , resp.) is the (6×3) serial Jacobian matrix of the active (passive, resp.) mobile base, namely,

$$\mathbf{J}_{b1} = \begin{bmatrix} \mathbf{k}_0 & \mathbf{0}_3 & \mathbf{0}_3 \\ \mathbf{k}_0 \times^0 \mathbf{p} & {}^0\mathbf{R}_{b1}\mathbf{i}_0 & {}^0\mathbf{R}_{b1}\mathbf{j}_0 \end{bmatrix}, \quad \mathbf{J}_{b2} = \begin{bmatrix} \mathbf{k}_0 & \mathbf{0}_3 & \mathbf{0}_3 \\ \mathbf{k}_0 \times^0 \mathbf{p} & {}^0\mathbf{R}_{b2}\mathbf{i}_0 & {}^0\mathbf{R}_{b2}\mathbf{j}_0 \end{bmatrix} \quad (8.7)$$

where $\mathbf{i}_0, \mathbf{j}_0$ and \mathbf{k}_0 denote the unit vector along x_0, y_0 and z_0 axes, respectively. ${}^0\mathbf{R}_{b1}$ (${}^0\mathbf{R}_{b2}$, resp.) is the rotation matrix between frame \mathcal{F}_0 and frames \mathcal{F}_{b1} (\mathcal{F}_{b2} , resp.). Equation (8.4) can be expressed in a matrix form as:

$$\mathbf{A}t_P = \mathbf{B}_b \dot{\mathbf{q}}_b + \dot{\mathbf{i}} \quad (8.8)$$

$$\mathbf{A}t_P = \mathbf{B}\dot{\mathbf{q}} \quad (8.9)$$

where $\mathbf{B} = [\mathbf{B}_b \quad \mathbf{I}_m]$ is a (8×14) matrix while $\dot{\mathbf{q}} = [\dot{\mathbf{q}}_b \quad \dot{\mathbf{i}}]^T$ is a fourteen-dimensional vector containing all joint velocities. As a result, Eq. (8.9) represents the first order kinematic model of FASTKIT.

8.3.2 FASTKIT Available Twist Set

The Available Twist Set (ATS) is used to characterize the twist capabilities of the moving-platform. The ATS of FASTKIT is obtained from its joint velocity limits and first order kinematic model. The joint velocity limits of the active mobile base are the following:

$$-0.2 \text{ rad.s}^{-1} \leq \dot{\theta}_1 \leq 0.2 \text{ rad.s}^{-1} \quad (8.10)$$

$$-0.2 \text{ m.s}^{-1} \leq \dot{\rho}_{11} \leq 0.2 \text{ m.s}^{-1} \quad (8.11)$$

$$-0.2 \text{ m.s}^{-1} \leq \dot{\rho}_{21} \leq 0.2 \text{ m.s}^{-1} \quad (8.12)$$

Once FASTKIT is deployed, its passive trailer is stabilized and does not move. Therefore, its linear and angular velocities are null, i.e.,

$$\dot{\theta}_2 = 0 \text{ rad.s}^{-1} \quad (8.13)$$

$$\dot{\rho}_{12} = 0 \text{ m.s}^{-1} \quad (8.14)$$

$$\dot{\rho}_{22} = 0 \text{ m.s}^{-1} \quad (8.15)$$

From Tab. 8.1, the cable velocity limits are the following:

$$-2 \text{ m.s}^{-1} \leq \dot{l}_{11}, \dot{l}_{21}, \dot{l}_{31}, \dot{l}_{41}, \dot{l}_{12}, \dot{l}_{22}, \dot{l}_{32}, \dot{l}_{42} \leq 2 \text{ m.s}^{-1} \quad (8.16)$$

From the ATS of FASTKIT in the configuration shown in Fig.12(a), the maximum angular (linear, resp.) velocities of the MP about (along, resp.) x, y and z axes are shown in Fig. 8.13. It is noteworthy that the twist capacity of the moving-platform is higher when the MBs are moving than when the MBs are fixed.

8.4 Wrench Feasibility

The classical techniques used to analyze the workspace of CDPRs are wrench-closure workspace (WCW) [25, 26] and wrench-feasible workspace (WFW) [27, 28]. To analyze the workspace of FASTKIT, WFW has been chosen as it is more relevant from a practical viewpoint. WFW is defined as the set of platform poses for which the required set of wrenches can be balanced with

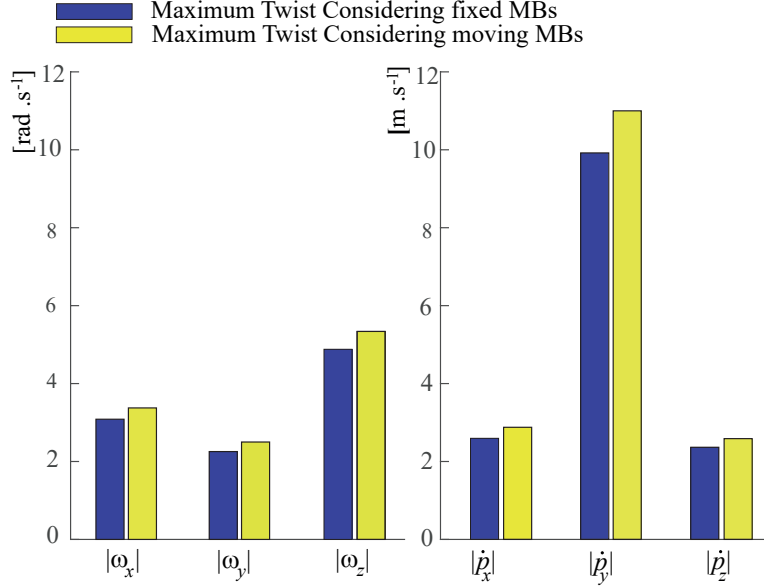


Fig. 8.13: Kinematic performance of FASTKIT

wrenches generated by the cables, while maintaining the cable tension within the defined limits [27]. For a given pose, the set of wrenches a mechanism can generate is defined as available wrench set (AWS), denoted as \mathcal{A} .

The AWS for CDPRs only takes into account the Static Equilibrium (SE) of the moving-platform. In contrast, for FASTKIT to be in SE, both mobile bases and the moving-platform should be in SE [31]. Its a necessary and a sufficient condition for the FASTKIT to be in SE. Thus this section aims at presenting the AWS of FASTKIT by taking into account the SE of both the moving platform and the mobile bases.

8.4.1 Static Equilibrium of the Moving-Platform

The Static Equilibrium (SE) of the moving platform is expressed as [29, 30]:

$$\mathbf{W}\mathbf{t} + \mathbf{w}_e = \mathbf{0}, \quad (8.17)$$

where \mathbf{W} is a (6×8) wrench matrix mapping the cable tension vector $\mathbf{t} \in \mathbb{R}^8$ onto the wrench applied by the cables on the end-effector expressed as:

$$\mathbf{W} = \begin{bmatrix} \mathbf{u}_{11} & \mathbf{u}_{21} & \mathbf{u}_{31} & \mathbf{u}_{41} & \mathbf{u}_{12} & \mathbf{u}_{22} & \mathbf{u}_{32} & \mathbf{u}_{42} \\ \mathbf{r}_{11} \times \mathbf{u}_{11} & \mathbf{r}_{21} \times \mathbf{u}_{21} & \mathbf{r}_{31} \times \mathbf{u}_{31} & \mathbf{r}_{41} \times \mathbf{u}_{41} & \mathbf{r}_{12} \times \mathbf{u}_{12} & \mathbf{r}_{22} \times \mathbf{u}_{22} & \mathbf{r}_{32} \times \mathbf{u}_{32} & \mathbf{r}_{42} \times \mathbf{u}_{42} \end{bmatrix} \quad (8.18)$$

\mathbf{r}_{11} to \mathbf{r}_{42} are the vectors pointing from the reference point P of the moving platform to the cable anchor points B_{11} to B_{42} . \mathbf{w}_e denotes the external wrench applied to the end effector expressed as:

$$\mathbf{w}_e = \begin{bmatrix} \mathbf{f}_e \\ \mathbf{m}_e \end{bmatrix} \quad (8.19)$$

where $\mathbf{f}_e = [f_e^x, f_e^y, f_e^z]^T$ and $\mathbf{m}_e = [m_e^x, m_e^y, m_e^z]^T$ respectively denote the external forces and moment applied by the MP. The cable tension vector is bounded between a minimum tension vector $\underline{\mathbf{t}}$ and a maximum tension vector $\bar{\mathbf{t}}$,

$$\underline{\mathbf{t}} \leq \mathbf{t} \leq \bar{\mathbf{t}}. \quad (8.20)$$

8.4.2 Static Equilibrium of the Mobile Bases

The SE of both the mobile bases is defined by the moment generated at the boundaries of the mobile base footprint formed by their respective wheels, referred to as the tipping constraints. For the active mobile base, the footprint is formed by joining the contact points of the wheels with the ground C_{11} to C_{41} in ascending order of the wheels numbering (See Fig. 8.12a). Similarly, the footprint of the passive mobile base is formed by joining the contact points C_{12} to C_{42} in ascending order.

Let $\mathcal{L}_{C_{11}}$ denote the boundary of the footprint between the two consecutive contact points of the wheels C_{11} and C_{21} . Let $\mathbf{u}_{C_{11}}$ be the unit vector along $\mathcal{L}_{C_{11}}$. For the active mobile base to be in SE, the moment $m_{C_{11}}$ generated about $\mathcal{L}_{C_{11}}$ should be always lower than zero, namely,

$$m_{C_{11}} = \mathbf{u}_{C_{11}}^T ((\mathbf{g}_1 - \mathbf{c}_{11}) \times \mathbf{w}_{g1}) + \mathbf{u}_{C_{11}}^T ((\mathbf{c}_{11} - \mathbf{b}_{11}) \times \mathbf{t}_{11}) + \mathbf{u}_{C_{11}}^T ((\mathbf{c}_{11} - \mathbf{b}_{21}) \times \mathbf{t}_{21}) + \mathbf{u}_{C_{11}}^T ((\mathbf{c}_{11} - \mathbf{b}_{31}) \times \mathbf{t}_{31}) + \mathbf{u}_{C_{11}}^T ((\mathbf{c}_{11} - \mathbf{b}_{41}) \times \mathbf{t}_{41}) \leq 0, \quad (8.21)$$

where \mathbf{c}_{11} and \mathbf{g}_1 denote the Cartesian coordinate vectors of contact point C_{11} and the center of gravity G_1 , respectively. \mathbf{w}_{g1} denotes the weight vector of the active mobile base. Similarly for the active mobile base to be in SE, the moment generated about each boundary of the footprint must be negative. Therefore, the tipping conditions of the active mobile base are expressed as follows:

$$\begin{bmatrix} m_{C_{11}} \\ m_{C_{21}} \\ m_{C_{31}} \\ m_{C_{41}} \end{bmatrix} = \begin{bmatrix} \mathbf{u}_{C_{11}}^T ((\mathbf{g}_1 - \mathbf{c}_{11}) \times \mathbf{w}_{g1}) + \mathbf{u}_{C_{11}}^T ((\mathbf{c}_{11} - \mathbf{b}_{11}) \times \mathbf{t}_{11}) + \mathbf{u}_{C_{11}}^T ((\mathbf{c}_{11} - \mathbf{b}_{21}) \times \mathbf{t}_{21}) \\ + \mathbf{u}_{C_{11}}^T ((\mathbf{c}_{11} - \mathbf{b}_{31}) \times \mathbf{t}_{31}) + \mathbf{u}_{C_{11}}^T ((\mathbf{c}_{11} - \mathbf{b}_{41}) \times \mathbf{t}_{41}) \\ \mathbf{u}_{C_{21}}^T ((\mathbf{g}_1 - \mathbf{c}_{21}) \times \mathbf{w}_{g1}) + \mathbf{u}_{C_{21}}^T ((\mathbf{c}_{21} - \mathbf{b}_{11}) \times \mathbf{t}_{11}) + \mathbf{u}_{C_{21}}^T ((\mathbf{c}_{21} - \mathbf{b}_{21}) \times \mathbf{t}_{21}) \\ + \mathbf{u}_{C_{21}}^T ((\mathbf{c}_{21} - \mathbf{b}_{31}) \times \mathbf{t}_{31}) + \mathbf{u}_{C_{21}}^T ((\mathbf{c}_{21} - \mathbf{b}_{41}) \times \mathbf{t}_{41}) \\ \mathbf{u}_{C_{31}}^T ((\mathbf{g}_1 - \mathbf{c}_{31}) \times \mathbf{w}_{g1}) + \mathbf{u}_{C_{31}}^T ((\mathbf{c}_{31} - \mathbf{b}_{11}) \times \mathbf{t}_{11}) + \mathbf{u}_{C_{31}}^T ((\mathbf{c}_{31} - \mathbf{b}_{21}) \times \mathbf{t}_{21}) \\ + \mathbf{u}_{C_{31}}^T ((\mathbf{c}_{31} - \mathbf{b}_{31}) \times \mathbf{t}_{31}) + \mathbf{u}_{C_{31}}^T ((\mathbf{c}_{31} - \mathbf{b}_{41}) \times \mathbf{t}_{41}) \\ \mathbf{u}_{C_{41}}^T ((\mathbf{g}_1 - \mathbf{c}_{41}) \times \mathbf{w}_{g1}) + \mathbf{u}_{C_{41}}^T ((\mathbf{c}_{41} - \mathbf{b}_{11}) \times \mathbf{t}_{11}) + \mathbf{u}_{C_{41}}^T ((\mathbf{c}_{41} - \mathbf{b}_{21}) \times \mathbf{t}_{21}) \\ + \mathbf{u}_{C_{41}}^T ((\mathbf{c}_{41} - \mathbf{b}_{31}) \times \mathbf{t}_{31}) + \mathbf{u}_{C_{41}}^T ((\mathbf{c}_{41} - \mathbf{b}_{41}) \times \mathbf{t}_{41}) \end{bmatrix} \leq \mathbf{0}_4, \quad (8.22)$$

where $\mathbf{u}_{C_{21}}$, $\mathbf{u}_{C_{31}}$, and $\mathbf{u}_{C_{41}}$ are the unit vectors along the lines $\mathcal{L}_{C_{21}}$, $\mathcal{L}_{C_{31}}$ and $\mathcal{L}_{C_{41}}$, respectively. Similarly, for the passive mobile base to be in SE, the tipping conditions takes the form:

$$\begin{bmatrix} m_{C_{12}} \\ m_{C_{22}} \\ m_{C_{32}} \\ m_{C_{42}} \end{bmatrix} = \begin{bmatrix} \mathbf{u}_{C_{12}}^T ((\mathbf{g}_2 - \mathbf{c}_{12}) \times \mathbf{w}_{g1}) + \mathbf{u}_{C_{12}}^T ((\mathbf{c}_{12} - \mathbf{b}_{12}) \times \mathbf{t}_{12}) + \mathbf{u}_{C_{12}}^T ((\mathbf{c}_{12} - \mathbf{b}_{22}) \times \mathbf{t}_{22}) \\ + \mathbf{u}_{C_{12}}^T ((\mathbf{c}_{12} - \mathbf{b}_{32}) \times \mathbf{t}_{32}) + \mathbf{u}_{C_{12}}^T ((\mathbf{c}_{12} - \mathbf{b}_{42}) \times \mathbf{t}_{42}) \\ \mathbf{u}_{C_{22}}^T ((\mathbf{g}_2 - \mathbf{c}_{22}) \times \mathbf{w}_{g1}) + \mathbf{u}_{C_{22}}^T ((\mathbf{c}_{22} - \mathbf{b}_{12}) \times \mathbf{t}_{12}) + \mathbf{u}_{C_{22}}^T ((\mathbf{c}_{22} - \mathbf{b}_{22}) \times \mathbf{t}_{22}) \\ + \mathbf{u}_{C_{22}}^T ((\mathbf{c}_{22} - \mathbf{b}_{32}) \times \mathbf{t}_{32}) + \mathbf{u}_{C_{22}}^T ((\mathbf{c}_{22} - \mathbf{b}_{42}) \times \mathbf{t}_{42}) \\ \mathbf{u}_{C_{32}}^T ((\mathbf{g}_2 - \mathbf{c}_{32}) \times \mathbf{w}_{g1}) + \mathbf{u}_{C_{32}}^T ((\mathbf{c}_{32} - \mathbf{b}_{12}) \times \mathbf{t}_{12}) + \mathbf{u}_{C_{32}}^T ((\mathbf{c}_{32} - \mathbf{b}_{22}) \times \mathbf{t}_{22}) \\ + \mathbf{u}_{C_{32}}^T ((\mathbf{c}_{32} - \mathbf{b}_{32}) \times \mathbf{t}_{32}) + \mathbf{u}_{C_{32}}^T ((\mathbf{c}_{32} - \mathbf{b}_{42}) \times \mathbf{t}_{42}) \\ \mathbf{u}_{C_{42}}^T ((\mathbf{g}_2 - \mathbf{c}_{42}) \times \mathbf{w}_{g1}) + \mathbf{u}_{C_{42}}^T ((\mathbf{c}_{42} - \mathbf{b}_{12}) \times \mathbf{t}_{12}) + \mathbf{u}_{C_{42}}^T ((\mathbf{c}_{42} - \mathbf{b}_{22}) \times \mathbf{t}_{22}) \\ + \mathbf{u}_{C_{42}}^T ((\mathbf{c}_{42} - \mathbf{b}_{32}) \times \mathbf{t}_{32}) + \mathbf{u}_{C_{42}}^T ((\mathbf{c}_{42} - \mathbf{b}_{42}) \times \mathbf{t}_{42}) \end{bmatrix} \leq \mathbf{0}_4, \quad (8.23)$$

where $\mathbf{u}_{C_{12}}$, $\mathbf{u}_{C_{22}}$, $\mathbf{u}_{C_{32}}$, and $\mathbf{u}_{C_{42}}$ are the unit vectors along the lines $\mathcal{L}_{C_{12}}$, $\mathcal{L}_{C_{22}}$, $\mathcal{L}_{C_{32}}$ and $\mathcal{L}_{C_{42}}$, respectively.

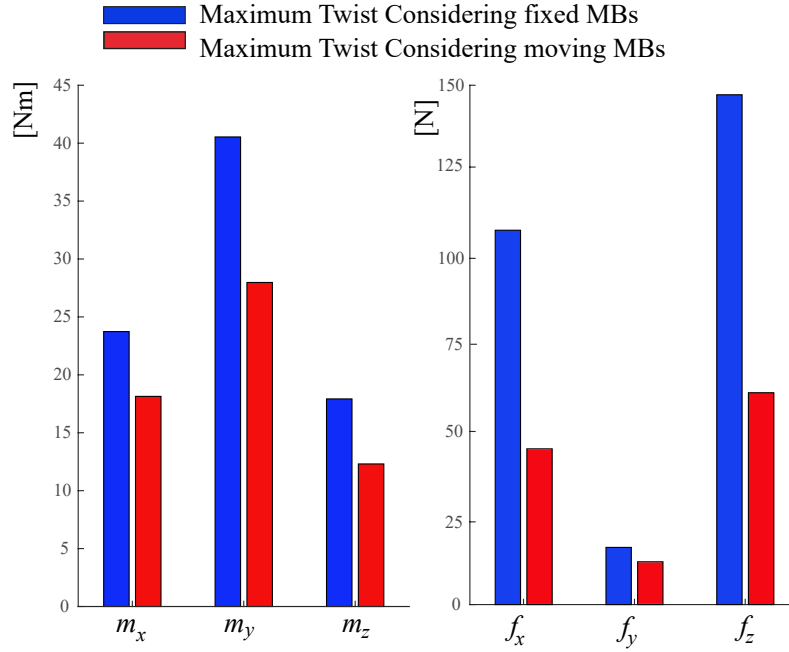


Fig. 8.14: Wrench capability of FASTKIT

8.4.3 Available Wrench Set of FASTKIT

The AWS (\mathcal{A}) of FASTKIT is defined by Eq. (8.17), respecting the cable tension limits (Eq. 8.20) and the tipping conditions defined by Eqs. (8.22) and (8.23). There \mathcal{A} can be expressed as:

$$\mathcal{A} = \left\{ \begin{bmatrix} \mathbf{f} \\ \mathbf{m} \end{bmatrix} \in \mathbb{R}^6 \mid \begin{bmatrix} \mathbf{f} \\ \mathbf{m} \end{bmatrix} = \mathbf{W}\mathbf{t}, \underline{\mathbf{t}} \leq \mathbf{t} \leq \bar{\mathbf{t}}, m_{C11} \leq 0, m_{C21} \leq 0, m_{C31} \leq 0, \right. \\ \left. m_{C41} \leq 0, m_{C12} \leq 0, m_{C22} \leq 0, m_{C32} \leq 0, m_{C42} \leq 0 \right\}. \quad (8.24)$$

where $\mathbf{f} = [f^x, f^y, f^z]^T$ and $\mathbf{m} = [m^x, m^y, m^z]^T$ denote the forces and moments exerted by the cables onto the moving platform, namely,

$$\mathbf{f} = -\mathbf{f}_e, \mathbf{m} = -\mathbf{m}_e. \quad (8.25)$$

From the AWS of FASTKIT in the configuration shown in Fig.12(a), the maximum absolute moments (forces, resp.) that the platform can support about (along, resp.) x , y and z axes are illustrated in Fig. 8.14. It can be noted that the wrench capability of the moving-platform is lower when the MBs are moving than when the MBs are fixed.

8.5 Conclusions and Future Work

This paper dealt with the design, modeling and performance analysis of a Mobile Cable-Driven Parallel Robot (MCDPR), named FASTKIT, developed in the framework of ECHORD++ FASTKIT project. FASTKIT project addressed an industrial need for fast picking and kitting operations in existing storage facilities while being easy to install, keeping existing infrastructures and covering large areas. The FASTKIT prototype consists of two mobile bases that carry the exit points of the CDPR.

FASTKIT is capable of autonomously navigating in its environment to reach the task location referred to as a navigation mode. During this mode, the two Mobile Bases (MBs) are coupled together and act as a single working unit while the MP is fixed on the two MBs. The twist of the MP and the passive mobile base is equal to the twist generated by the active mobile base. No cable motion is generated during the navigation mode. The second working mode, referred to as the task mode, deploys the system at the desired location such that the desired pick or/and place operation is achievable within the defined workspace. During this mode, the passive mobile base is static while the motion of the cables and the active mobile base is used to deploy the complete system. It should be noted that during the task mode, FASTKIT is kinematically redundant due to the additional mobility of the active mobile base as explained in [12].

The main components, the control strategy and the architecture of the navigation stack of FASTKIT were presented in this paper. Both the hardware design and the software architecture of the prototype were discussed. First, the Cable-Driven Parallel Robot (CDPR) and mobile based were studied separately. It turns out that the combination of a CDPR with two mobile bases leads to several issues such as: (i) the hardware + software assembly of the CDPR with the mobile bases; (ii) the definition of a control law to properly manage the robot motion in all its phases, and notably the deployment phase.

The main outcome of this paper is the demonstrator of a MCDPR. This demonstrator is capable of navigating in unknown environments, positioning in front of the shelves and picking some boxes on the shelf. The kinematic performance and the wrench capability of FASTKIT have also been assessed in some specific configurations.

Therefore, a compact and reconfigurable CDPR that can work both in a fully constrained configuration and in a suspended configuration have been developed. Customized pulleys for the CDPR have designed and realized to reduce cable friction. Two electromagnetic links between the two mobile bases that rigidly connect them during the navigation phase were also implemented. From a software view point, a navigation algorithm for the mobile CDPR based on existing open-

source libraries was written. A global control law that synchronizes the CDPR actuators with the active mobile base during the deployment phase was synthesized too.

There are still several open issues to be solved in the future such as: (i) the kinematic redundancy planning of FASTKIT and (ii) the wrench analysis of MCDPRs while considering both tipping and sliding conditions of their mobile bases.

Acknowledgements This research work is part of the European Project ECHORD++ “FASTKIT” dealing with the development of collaborative and Mobile Cable-Driven Parallel Robots for logistics. Moreover, Centrale Nantes is dutifully acknowledged for the doctorate thesis financial support provided to the second author of the paper.

References

1. Albus, J., Bostelman, R., Dagalakakis, N.: The NIST spider, a robot crane. *J. of Research of the Nat. Inst. of Standards and Technology* **97**(3), 373–385 (1992)
2. Holland, C., Cannon, D.: Cable array robot for material handling (2004)
3. Bruckmann, T., Lalo, W., Sturm, C., Schramm, D., Hiller, M.: Design and realization of a high rack and retrieval machine based on wire robot technology (2013)
4. Pott, A., Meyer, C., Verl, A.: Large-scale assembly of solar power plants with parallel cable robots. In: *Proc. of the Int. Symp. on Robotics and 6th German Conf. on Robotics (ISR/ROBOTIK 2010)*, pp. 1–6. Munich, Germany (2010)
5. Kamawura, S., Kino, H., Won, C.: High-speed manipulation by using parallel wire-driven robots. *Robotica* **18**(1), 13–21 (2000)
6. Fortin-Coté, A., Cardou, P., Gosselin, C.: An admittance control scheme for haptic interfaces based on cable-driven parallel mechanisms. In: *Proc. of the IEEE Int. Conf. on Robotics and Automation (ICRA 2014)*, pp. 819–925. Hong Kong (2014)
7. P. Miermeister et al., The CableRobot simulator large scale motion platform based on cable robot technology. 2016 IEEE/RSJ International Conference on Intelligent Robots and Systems (IROS), 3024–3029. Daejeon (2016)
8. Merlet, J.P., Daney, D.: A portable, modular parallel wire crane for rescue operations. In: *Proc. of the IEEE Int. Conf. on Robotics and Automation (ICRA 2010)*, pp. 2834–2839. Anchorage, AK (2010)
9. Bostelman, R., Jacoff, A., Proctor, F., Kramer, T., Wavering, A.: Cable-based reconfigurable machines for large scale manufacturing. In: *Proc. of the 2000 Japan-USA Symp. on Flexible Automation*. Ann Arbor, MI (2000)
10. Izard, J.B., Gouttefarde, M., Michelin, M., Tempier, O., Baradat, C.: A reconfigurable robot for cable-driven parallel robotic research and industrial scenario proofing. In: *Cable-Driven Parallel Robots, Mechanisms and Machine Science*, **12**, pp. 135–148 (2013)
11. Gagliardini, L., Caro, S., Gouttefarde, M., Girin, A.: Discrete reconfiguration planning for cable-driven parallel robots. *Mechanism and Machine Theory* **100**, 313–337 (2016)
12. Rasheed, T., Long, P., Marquez-Gamez, D., Caro, S.: Optimal Kinematic Redundancy Planning For Planar Mobile Cable Driven Parallel Robots. *Proceedings of the ASME 2018 International Design Engineering Technical Conferences & Computers and Information in Engineering Conference IDETC/CIE 2018*, 26–29, Quebec City, Canada, (2018)
13. Rasheed, T., Long, P., Marquez-Gamez, D. and Caro, S.: Tension Distribution Algorithm for Planar Mobile Cable-Driven Parallel Robots. *Cable-Driven Parallel Robots. Mechanisms and Machine Science*, **53**, 268–279 (2018)
14. Lamaury, J., Gouttefarde, M.: A tension distribution method with improved computational efficiency. *Cable-driven parallel robots*, 71–85 (2013)
15. Mikelsons, L., Bruckmann, T., Hiller, M., Schramm, D.: A real-time capable force calculation algorithm for redundant tendon-based parallel manipulators. *Proceedings of the 2008 IEEE International Conference on Robotics and Automation (ICRA 2008)*, 3869–3874 (2008)

16. Quigley, M., Conley, K., Gerkey, B.P., Faust, J., Foote, T., Leibs, J., Wheeler, R., Ros, A.Y.N.: An open-source robot operating system. ICRA Workshop on Open Source Software (2009)
17. Eskandarian, A.: Handbook of intelligent vehicles. Springer, London (2012)
18. Philippsen, R., Jensen, B., Siegwart, R.: Autonomous navigation in dynamic environments. Springer Tracts on Advanced Robotics (2006)
19. Brady, M.: Robot motion: Planning and control. MIT press (1982)
20. Choset, H.M.: Principles of robot motion: theory, algorithms, and implementation. MIT press (2005)
21. LaValle, S.M.: Planning algorithms. Cambridge university press (2006)
22. Roberts, R. G., Graham, T., Lippitt, T., Girin, A.: On the inverse kinematics, statics, and fault tolerance of cable-suspended robots. *Journal of Field Robotics*, **15**(10), 581–597 (1998)
23. Lessanibahri, S., Gouttefarde, M., Caro, S., Cardou, P.: Twist Feasibility Analysis of Cable-Driven Parallel Robots. *Cable-Driven Parallel Robots. Mechanisms and Machine Science*, **53**, 128–139 (2018)
24. Rasheed, T., Long, P., Gamez, D. M., Caro, S.: Kinematic modeling and twist feasibility of mobile cable-driven parallel robots. *Advances in Robot Kinematics* (2018)
25. Gouttefarde, M. and Gosselin, C.M.: Analysis of the wrench-closure workspace of planar parallel cable-driven mechanisms. *IEEE Transactions on Robotics*, **22**(3), 434–445 (2006)
26. Lau, D., Oetomo, D., Halgamuge, S.K.: Wrench-Closure Workspace Generation for Cable Driven Parallel Manipulators using a Hybrid Analytical-Numerical Approach. *ASME J. Mech. Des.*, **133** (2011)
27. Gouttefarde, M., Daney, D., Merlet, J.P.: Interval-analysis-based determination of the wrench-feasible workspace of parallel cable-driven robots. *IEEE Transactions on Robotics*, **27**(1), 1–13 (2011)
28. Cruz Ruiz, A. L., Caro, S., Cardou, P., Guay, F.: ARACHNIS : Analysis of Robots Actuated by Cables with Handy and Neat Interface Software. *Cable-Driven Parallel Robots, Mechanisms and Machine Science*, **32**, 293–305 (2015)
29. Kawamura, S., Ito, K.: A new type of master robot for teleoperation using a radial wire drive system. *Proceedings IEEE/RSJ Intelligent Robots and System (IROS)*, **1**, 55–60 (1993)
30. Hiller, M., Fang, S., Mielczarek, S., Verhoeven, R., Franitza, D.: Design, analysis and realization of tendon based parallel manipulators. *Mechanism and Machine Theory*, **40**(4), 429–445 (2005)
31. Rasheed, T., Long, P., Gamez, D.M., Caro, S.: Available wrench set for planar mobile cable-driven parallel robots. *IEEE International Conference on Robotics and Automation* (2018).

Chapter 9

Heuristic Planning for Rough Terrain Locomotion in Presence of External Disturbances and Variable Perception Quality

Michele Focchi, Romeo Orsolino, Marco Camurri, Victor Barasuol, Carlos Mastalli, Darwin G. Caldwell and Claudio Semini

Abstract

The quality of visual feedback can vary significantly on a legged robot meant to traverse unknown and unstructured terrains. The map of the environment, acquired with online state-of-the-art algorithms, often degrades after a few steps, due to sensing inaccuracies, slippage and unexpected disturbances. If a locomotion algorithm is not designed to deal with this degradation, its planned trajectories might end-up to be inconsistent in reality. In this work, we propose a heuristic-based planning approach that enables a quadruped robot to successfully traverse a *significantly* rough terrain (*e.g.* stones up to 10 cm of diameter), in *absence* of visual feedback. When available, the approach allows also to leverage the visual feedback (*e.g.* to enhance the stepping strategy) in *multiple ways*, according to the *quality* of the 3D map. The proposed framework also includes reflexes, triggered in specific situations, and the possibility to estimate *online* an unknown time-varying disturbance and compensate for it. We demonstrate the effectiveness of the approach with experiments performed on our quadruped robot *HyQ* (85 kg), traversing different terrains, such as: ramps, rocks, bricks, pallets and stairs. We also demonstrate the capability to estimate and compensate for external disturbances by showing the robot walking up a ramp while pulling a cart attached to its back.

9.1 Introduction

Legged robots are mainly designed to traverse unstructured environments, which are often demanding in terms of torques and speeds. Trajectory optimization [1, 2, 3, 4, 5] can be used to

Michele Focchi, Romeo Orsolino, Marco Camurri, Victor Barasuol, Carlos Mastalli, Darwin G. Caldwell, Claudio Semini

Dynamic Legged Systems lab, Istituto Italiano di Tecnologia, Genova, Italy e-mail: {michele.focchi, romeo.orsolino, victor.barasuol, darwin.caldwell, claudio.semini}@iit.it

Marco Camurri

Oxford Robotics Institute, University of Oxford, Oxford, UK e-mail: mcamurri@robots.ox.ac.uk

Carlos Mastalli

LAAS-CNRS, Toulouse, France e-mail: carlos.mastalli@laas.fr

generate dynamically stable body motions, taking into account: robot dynamics, kinematic limits, leg reachability for motion generation and foothold selection. In particular, motion planning enables the necessary *anticipative* behaviors to address appropriately the terrain. These include: obstacle avoidance, foothold selection, contact force generation for optimal body motion and goal-driven navigation (*e.g.* [3, 6]). Furthermore, when the flat terrain assumption is no longer valid, a $3D/2.5D$ map of the environment is required, to appropriately address uneven terrain morphology, through optimization.

Despite the considerable efforts and recent advances in this field [4, 3, 7, 8], optimal planning that takes into account terrain conditions is still far from being executed *online* on a real platform, due to the computational complexity involved in the optimization. These optimization problems are strongly nonlinear, prone to local minima, and require a significant amount of computation time to be solved [7]. Some improvements have been recently achieved by computing convex approximations of the terrain [5] or the dynamics [8].

Most of these approaches optimize for a whole time horizon and then execute the motion in an “open loop” fashion, rather than optimizing *online*. Depending on the complexity of terrains and gaits, Aceituno *et al.* [5] managed to reduce the computation time (for a locomotion cycle) in a range between 0.5 s and 1.5 s, while the approach by Ponton *et al.* [8] requires 0.8 s to 5 s to optimize for a 10 s horizon. Therefore, it is still not possible to optimize *online* and perform replanning (*e.g.* through a Model Predictive Control (MPC) strategy).

We believe that replanning is a crucial feature to intrinsically cope with the problem of error accumulation in real scenarios. These errors can be caused by delays, inaccuracy of the 3D map, unforeseen events (external pushes, slippages, rock falling), or dynamically changing and deformable terrains (*e.g.* rolling stones, mud, etc.).

The sources of errors in locomotion are many: a premature/delayed touchdown due to a change in the terrain inclination, external disturbances, wrong terrain detection. Other source of errors include: tracking delays in the controller, sensor calibration errors, filtering delays, offsets, structure compliance, unmodeled friction and modeling errors in general. These errors can make the actual robot state diverge from the original plan. Moreover, in the prospect of tele-operated robots, the user might want to modify the robot velocity during locomotion, and this should be reflected in a prompt change in the motion plan.

As mentioned, a significant source of errors can come from non-modeled disturbances, such as external pushes. A possible solution to this particular issue is implementing a disturbance observer [9]. Engelsberger *et al.* [10] proposed a Momentum Based Disturbance Observer (MBDO) for pure linear force disturbances. In his thesis, Rotella and *et al.* [11], implemented an external wrench estimator for a humanoid robot, based on an Extended Kalman Filter. Besides that, he was also compensating for the estimated wrench in an inverse dynamics controller. However the experimental tests on the real robot were limited to a static load, acting on the legs while performing a switch of contact between the two feet. In a separated experiment, he also tested against impulsive disturbance without any contact change. We extend this work by presenting a MBDO capable of estimating both linear and angular components of external disturbance wrenches, of variable amplitude, applied on the robot during the execution of a walk.

Even though a disturbance observer can improve the tracking against external disturbances, *online replanning* is still required for rough terrain locomotion, because it constitutes the basic mechanism to adapt to the terrain (*terrain adaptation*), promptly recover from planning errors and handle environmental changes, while simultaneously accommodate for the user set-point. In particular, the planning horizon should be large enough to execute the necessary *anticipative* body motions, but at the same time the replanning frequency should be high enough to mitigate the accumulation of errors.

Bledt *et al.* [12] implemented online replanning, by introducing a policy-regularized model-predictive control (PR-MPC) for gait generation, where a heuristic policy provides additional information for the solution of the MPC problem. The authors found that regularizing the optimization with a policy it improves the cost landscapes and decreases the computation time. However, this work has not been demonstrated experimentally.

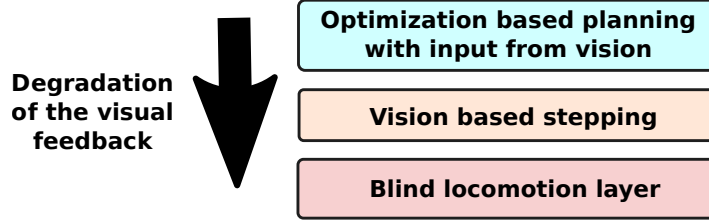


Fig. 9.1: Locomotion layers for different quality of the visual feedback. The bottom layer is purely reactive (blind) locomotion. The vision-based stepping allows the robot to quickly adapt to local terrain conditions. Then, the motion planning provides the level of anticipation needed in locomotion over challenging terrain.

A MPC-based approach has been successfully implemented for a real humanoid in the past. In his seminal work, Wieber [13] addressed the problem of strong perturbations and tracking errors, yet limiting the application to flat terrains.

In the quadruped domain, Cheetah 2 has shown running/jumping motions over challenging terrains using a MPC controller [14]. More recently, Bellicoso *et al.* [15, 16] implemented a 1-step replanning strategy, based on Zero Moment Point (ZMP) optimization, on the quadruped robot ANYmal.

Most vision-based approaches [3, 6, 17] require reasonably accurate 3D maps of the environment [18]. However, the accuracy of a 3D map strongly depends on reliable state estimation [19, 20, 21], which involves complex sensor fusion algorithms (inertial, odometry, LiDAR, cameras). Typically, these algorithms involve the fusion of high-frequency proprioceptive estimates from inertial and leg odometry [19], with low-frequency pose correction from visual odometry [22]. The proprioceptive estimate (and, indirectly, the pose correction) can be jeopardized by unforeseen events such as: slippage, unstable footholds, terrain deformation, and compliance of the mechanical structure. For the above reasons, we envision different locomotion layers, according to the quality of the perception feedback available, as depicted in Fig. 9.1.

At the bottom layer we have a *blind* reactive strategy, always active. This strategy does not require any vision feedback. The layer mainly contains basic terrain adaptation mechanisms and reflex strategies. Motion primitives are triggered to override the planner in situations where the robot could be damaged (*e.g.* stumbling).

In cases when the vision feedback is denied (*e.g.* foggy, smoky, poorly lit areas), a *reactive strategy* is preferred [23], [24]. On the other hand, when a degraded visual feedback is available, this can still be usefully exploited for 1-step horizon planning (middle block in Fig. 9.1) [25]. When the vision feedback is instead reliable, it can be used for more sophisticated terrain assessment [26, 27].

In this work, we present a motion control framework for rough terrain locomotion. The terrain adaptation and the mitigation of tracking errors is achieved through a 1-step *online* replanning strategy, which can work either blindly or with visual feedback.

This work builds upon a previously presented statically stable *crawl* gait [28], where the main focus was on whole-body control. Hereby, our focus is mainly on the capability to adapt to rough terrains during locomotion. We incorporate a number of features to increase the robustness of the locomotion, such as slip detection and two reflex strategies, previously presented in [29], [30]. The reflexes are automatically enabled to address specific situations such as: loss of mobility (in cases of abrupt terrain changes, see *height reflex* in [29]) and unforeseen frontal impacts (see *step reflex* in [30]).

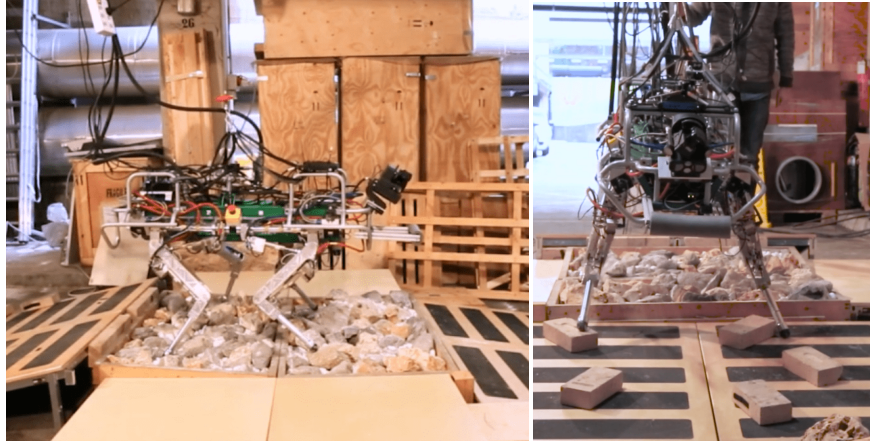


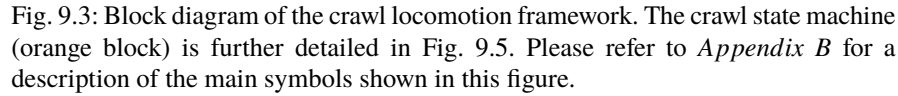
Fig. 9.2: HyQ crawling on a rough terrain playground: (left) lateral and (right) frontal view. Our locomotion framework can deal with moving rocks and various terrain elevation changes.

9.1.1 Contribution

The main contributions of this article are *experimental*:

- We show that with the proposed approach the Hydraulically actuated Quadruped (HyQ) robot [31] can successfully negotiate different types of terrain templates (ramps, debris, stairs, steps), some of them with a significant roughness¹ (Fig. 9.2). The size of the stones are up to 12 cm (diameter) that is about 26% of the retractable leg length. We also applied this strategy, with little variations (see Section 9.7.2), to the task of climbing up and down industrial-size stairs (14cm x 48cm), also performing 90° turns while climbing the stairs in simulation.
- We validate *experimentally* our MBDO for quadrupedal locomotion. We are able to compensate for the disturbances *online* and in close-loop during locomotion. Additionally, while planning the trajectories, we also consider the shift of the ZMP due to the estimated external disturbance. We show HyQ walking up a 22° inclined ramp, while pulling a 12 kg wheelbarrow attached to his back with a rope. The wheelbarrow is also impulsively loaded up to 15 kg of extra payload, incrementally added during the experiment. The robot is able to crawl robustly on a flat terrain while leaning against a constant horizontal pulling force of 75 N. To the authors knowledge, this is the first time such tasks are executed on a real quadruped platform.
- As a marginal contribution, we introduce a *smart terrain estimation* algorithm, which improves the state-of-the-art terrain estimation and adaptation of [15]. This is particularly beneficial in some specific situations (*e.g.* when one stance foot is considerably far from the plane fitted by the other three stance feet).

¹ See accompanying video of rough terrain experiments: <https://www.youtube.com/watch?v=TC8HoUBXy54>



This work is part of the Echord++ HyQ-REAL experiment, where novel quadrupedal locomotion strategies are being developed to be used on newly designed hydraulic robots. At the time of writing this manuscript, the HyQ-REAL robot was not yet fully assembled. Therefore, the framework is demonstrated on its predecessor version, HyQ. The major improvements of HyQ-REAL over HyQ are: more powerful actuators, full power autonomy (no tethers), greater range of motion, self-righting capabilities, fully enclosed chassis. The presented software framework can be easily run on both platforms, thanks to the kinematics/dynamics software abstraction layer presented in [32].

The remainder of this paper is detailed as follows. In Section 9.2 we briefly present our statically stable gait framework; Sections 9.3 and 9.4, detail the body motion and swing motion phases of the gait, respectively; Section 9.4 is particularly focused on the different stepping strategies, depending on the presence of a visual feedback; Section 9.5 describes the reactive modules for robust rough terrain locomotion; in Section 9.6, we present an improved terrain estimator; Section 9.7 shows a strategy for stair climbing based on the proposed framework; in Section 9.8, we describe the implementation of our disturbance observer; in section 9.9 we address the conclusions.

In this section, we briefly illustrate our *statically* stable crawling framework, (previously presented in [28]), enriched with additional features specific for rough terrain locomotion. Fig. 9.3 shows the block diagram of the framework. The core module is a state machine (see [28] for details) which

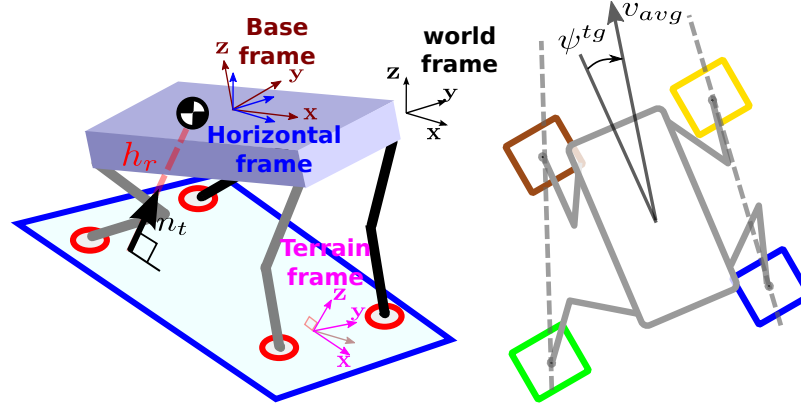


Fig. 9.4: (left) Definition of the relevant reference frames and of the terrain plane (light blue) used in the locomotion framework and (right) computation of the target ψ^{tg} for the robot yaw.

orchestrates two temporized/event-driven locomotion phases: the *swing phase*, and the *body motion phase*. In the former, the robot has three legs in stance, while in the latter it has four legs in stance.

During the *body motion phase*, the robot Center of Mass (CoM) is shifted onto the *future* support triangle, (opposite to the *next* swing leg, in accordance to a user-defined foot sequence). As default footstep sequence we use: RH, RF, LH, LF².

The CoM trajectory is generated after the terrain inclination is estimated (see Section 9.3). At each touchdown, the inclination is updated by fitting a plane through the actual stance feet positions. When the terrain is uneven (and the feet are not coplanar), an *average* plane is found.

The *swing phase* is a swing-over motion, followed by a linear searching motion (see Section 9.4) that terminates with a *haptic* touchdown. The haptic touchdown ensures that the swing motion does not stop in a prescheduled way; instead, the leg keeps extending until a new touchdown is established.

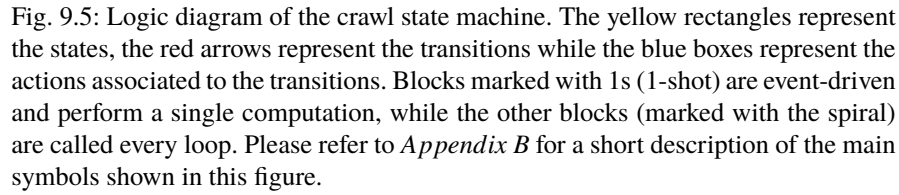
When a contact is detected (either by thresholding the Ground Reaction Force (GRF), or directly via a foot contact sensor [33, 34]), the touchdown is established. A searching motion with *haptic* touchdown is a key ingredient to achieve robust *terrain adaptation*. Indeed, haptic touchdown is important to mitigate the effect of tracking errors, because it allows to trigger the stance only when the contact is truly stable. This is important whenever there is a discrepancy between the plan and the real world. This typically happens when a vision feedback is used to select the foothold (see Section 9.4.2), because the accuracy of a height map is typically in the order of centimeters [27, 35].

The vision feedback can be also used to estimate the direction of the normal of the terrain under the foot, in order to set the searching, or reaching, motion direction. Both the body and the swing trajectories are generated as quintic polynomials.

The body trajectory is always expressed in the *terrain frame*, which is aligned to the terrain plane (see Fig. 9.4 (left)). The terrain frame has the Z-axis normal to the terrain plane, while the X-axis is a projection of the X-axis of the base on the terrain plane, and the Y-axis is chosen to form a right hand side system of coordinates. The swing trajectory is expressed in the *swing frame*, which can be either coincident with the terrain frame (section 9.4.1) or set independently for each foot (section 9.4.2), depending on the stepping strategy adopted.

The *Whole Body Control* module (also known as *Trunk Controller* [28]) computes the torques required to control the position of the robot CoM and the orientation of the trunk. At the same time,

² LH, LF, RH and RF stands for Left-Hind, Left-Front, Right-Hind and Right-Front legs, respectively.



To address unpredictable events (*e.g.* limit slippage on an unknown surface, whenever the optimized force is out of the real (unknown) friction cone), we implemented an impedance controller at the joint level [36]³ in parallel to the whole-body controller. The impedance controller computes the feedback joint torques $\tau_{fb} \in \mathbb{R}^n$ (where for HyQ $n = 12$ is the number of active joints) to track reference joint trajectories ($q_d^j, \dot{q}_d^j \in \mathbb{R}^n$).

Note that the impedance controller should receive position and velocity set-points that are consistent with the body motion, to prevent conflicts with the Trunk Controller. To achieve this, we map the CoM motion into feet motion (see Section 9.3) to provide the correspondent joint references q_j^d , \dot{q}_j^d .

³ Without any loss of generality, the same controller can be implemented at the foot level. However, to avoid non collocation problems due to leg compliance, it is safer to close the loop at the joint level.

9.3 Body Motion Phase

When traversing a rough terrain, unstable footholds (*e.g.* stones rolling under the feet), tracking errors, slippage and estimation errors can create deviations from the original motion plan. These deviations require some corrective actions in order to achieve *terrain adaptation*. In our framework, these actions are taken both at the beginning of *swing* and *body motion* phases. The body motion phase starts with a foot touchdown and ends when the next foot in the sequence is lifted off the ground. After each touchdown event, we compute the target for the CoM position x_{com}^{tg} and the body orientation Φ^{tg} from the *actual* robot state. This feature prevents error accumulation and, together with the haptic touchdown, constitutes the core of the *terrain adaptation* feature.

To avoid hitting kinematic limits, the robot's orientation should be adapted to match the terrain shape. Indeed, some footholds can only be reached by tilting the base. On the other hand, constraining the base to a given orientation restricts the range of achievable motions.

We parametrize the trajectory for the trunk orientation with Euler angles⁴ $\Phi^d(t) = [\phi(t), \theta(t), \psi(t)]$ (*i.e.* roll, pitch and yaw respectively). The trajectories are defined by quintic 3D polynomials connecting the actual robot orientation (at the beginning of the phase, namely the touchdown) $\Phi^d(0) = [\phi_{td}, \theta_{td}, \psi_{td}]$ with the desired orientation $\Phi^d(T_{mb}) = \Phi^{tg} = [\phi^{tg}, \theta^{tg}, \psi^{tg}]$, where T_{mb} is the duration of the *move body phase*. To match the inclination of the terrain, the target roll and pitch are set equal to the orientation of the terrain plane that was updated at the touchdown ($\phi^{tg} = \phi_t, \theta^{tg} = \theta_t$). The target yaw ψ^{tg} is computed to align the trunk with an average line v_{avg} from the ipsi-lateral⁵ legs (see Fig. 9.4 (right)). This is somewhat similar to a heading controller that makes sure that the trunk “follows” the motion of the feet (the feet motion is driven by the desired velocity from the user).

Similarly to the angular case, the CoM trajectory is initialized with the *actual* position of the CoM⁶, while the target x_{com}^{tg} can be computed with different stability criteria (*e.g.* ZMP-based [1] or wrench-based [37, 38]). Henceforth, the vectors are expressed in the world (fixed) frame \mathcal{W} , unless otherwise specified.

Since the crawl does not involve highly dynamic motions, a heuristic *static* stability criterion can also be used and in particular, our strategy consists in making sure that the projection of the CoM target x_{comp}^{tg} always lies inside the future support triangle [28]. The robustness (in terms of stability margin) can be regulated by setting the projected CoM target at a distance d , on the support plane, from the middle point of the segment connecting the diagonal feet (see Fig. 9.6 (right)). We define the *robot height* $h_r \in \mathbb{R}$ as the distance between the CoM and the *terrain plane* (see Fig. 9.4 (left)). This is computed by averaging the actual positions of the feet $b_{x_{fi}}$ in contact with the ground (stance feet):

$$h_r = e_z^T \frac{1}{c_{st}} \sum_{i=1}^{c_{st}} {}_tR_b(b_{x_{fi}} + b_{x_{com}}) \quad (9.1)$$

where c_{st} is the number of stance feet, $b_{x_{com}} \in \mathbb{R}^3$ is the CoM offset with respect to the base origin, ${}_tR_b \in SO(3)$ maps vectors from base to the terrain frame and $e_z \in \mathbb{R}^3$ selects the Z component of 3D vectors. In general, the robot height should be kept constant (or it could vary with the cosine of the terrain pitch θ_t on ramps) during locomotion. If the above-mentioned heuristics is used for planning, the CoM target x_{com}^{tg} can be obtained by adding the height vector expressed in the world frame $h_r n_t$ (where n_t is the normal to the terrain) to the projection x_{comp}^{tg} coming from the heuristics.

Note that, on an inclined terrain, to have the CoM above the desired projection and the distance of the CoM from the terrain plane equal to h_r , the following scaling should be applied (see Fig. 9.6 (left)):

⁴ This is a reasonable choice because the robot is unlikely to reach singularity (*i.e.* 90° pitch).

⁵ Belonging to the same side of the body.

⁶ We found experimentally that using the *desired* feet position instead of the *actual* one to compute the CoM target would make the robot's height gradually decrease.

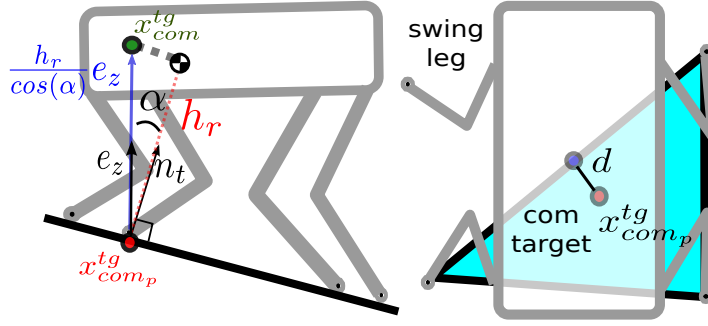


Fig. 9.6: Heuristic generation of the CoM target. (left) planning on inclined terrain, (right) the future support polygon is depicted in light blue while the projection x_{comp}^{tg} of the com target on the polygon is a red dot.

$$\begin{aligned} \cos(\alpha) &= e_z^T n_t \\ x_{com}^{tg} &= x_{comp}^{tg} + \frac{h_r}{\cos(\alpha)} e_z \end{aligned} \quad (9.2)$$

where α is the angle between the unit vectors e_z and n_t .

Now, similarly to the orientation case, we build a quintic polynomial $x_{com}^d(t)$ to connect the *actual* CoM at the beginning of the motion phase (namely at the touchdown) $x_{com,td}$ to the computed target x_{com}^{tg} .

To determine the 6 parameters of each quintic, in addition to the initial/final positions, we force the initial/final velocities and accelerations to zero, both for CoM and Euler angles. This ensures *static stability*⁷ and implies that the robot's trunk does not move when one leg is lifted from the ground (*i.e.* during the swing phase).

Alternatively, if a wrench-based optimization is used, as in [37], the robot height should be constrained (*e.g.* to be constant) and the CoM X, Y trajectory will be a result of the optimization.

As mentioned in the previous section, it is convenient to provide desired joint positions (for the stance legs) that are consistent with the body motion. We first map the body motion into feet motion. This mapping is linear in the velocity domain and can be computed independently for each stance foot i as:

$$\dot{x}_{f_i}^d[k] = -\dot{x}_{com}^d[k] - \omega[k] \times (x_{f_i}^d[k-1] - x_{com}([k])) \quad (9.3)$$

where the desired position of the foot $x_{f_i}^d[k-1]$ at the previous controller loop is used. Then, $x_{f_i}^d[k]$ is obtained by integrating the velocity $\dot{x}_{f_i}^d[k]$ (*e.g.* with a trapezoidal rule). Afterwards, we compute the corresponding desired joint positions $q_i \in \mathbb{R}^3$ through inverse kinematics: $q_i = IK(x_{f_i})$ and the joint velocities as:

$$\dot{q}_i^d = J(q_i)^{-1} \dot{x}_{f_i} \quad (9.4)$$

where $J_i \in \mathbb{R}^{3 \times 3}$ is the Jacobian of foot i ⁸.

⁷ Statically stable gaits are convenient for locomotion in dangerous environments (*e.g.* nuclear decommissioning missions) because the motion can be stopped at any time. However, without loss of generality, the final velocity can be set to any other arbitrary value other than zero.

⁸ Note that we performed a simple inversion since in our robot we have point feet and 3 Degree of Freedom (DoF) per leg, thus the Jacobian matrix is squared.

9.4 Swing phase

The swing phase of a leg starts with the foot liftoff and ends with the foot touchdown. The obvious goal of the leg's swing phase is to establish a new foothold. Then, an *interaction force* drives the robot's trunk towards the desired direction. The swing phase has two main objectives: 1) attaining enough clearance to overcome potential obstacles (so as to avoid *stumbling*) and 2) achieving a stable contact.

9.4.1 Heuristic Stepping

In this section, we illustrate the heuristic *stepping strategy* we use for *blind* locomotion. The goal is to select the footholds to track a *desired* speed from the user when no map of the surroundings is available.

First, we compute the default step length (for the swing leg) from the desired linear and heading velocities $v_{xy}^r \in \mathbb{R}^2$, $\psi^r \in \mathbb{R}$. For sake of simplicity, *only in this section* the vectors are expressed in the *horizontal frame* \mathcal{H} ⁹ (instead of the *world frame* \mathcal{W}), unless otherwise specified. Expressing the default step in a *horizontal frame* allows to formulate the swing motion independently from the orientation of both terrain and trunk.

The swing trajectory consists of a parametric curve, whose four main parameters are: the linear foot displacement $\Delta L_{x0}, \Delta L_{y0}$, the angular foot displacement ΔH_0 (see Fig. 9.7), and the default swing duration T_{sw} . These quantities can be computed from the nonlinear mapping $F(\cdot)$:

$$[\Delta L_{x0} \ \Delta L_{y0} \ \Delta H_0 \ T_{sw}] = F(v_{xy}^r, \psi^r) \quad (9.5)$$

$F(\cdot)$ makes sure that the step length increments linearly with the desired velocity, but only at low speeds (see *compute step length* block in Fig. 9.5). When the step length approaches the maximum value, the cycle time T_{cycle} (sum of swing and stance time of each leg) is decreased, and the stepping frequency $f_s = 1/T_{cycle}$ is increased accordingly to avoid hitting the kinematic limits. For instance, for the X component, we can use the following equation:

$$A = \frac{2\Delta L_{x0}^{max}}{\pi} \quad (9.6)$$

$$G = \frac{\Delta L_{x0}^{tr}}{\Delta L_{x0}^{max} v_{tr}} \quad (9.7)$$

$$\Delta L_{x0} = A \cdot \arctan(G v_x^r) \quad (9.8)$$

where ΔL_{x0}^{max} is the maximum allowable step length in the X direction.

According to Eq. (9.8), ΔL_{x0} linearly increases with velocity up to the transition point ΔL_{x0}^{tr} , which corresponds to the user-defined value v_{tr} . Then, the step length is increased sub-linearly with velocity (because the stepping frequency is also increased), up to the saturation point ΔL_{x0}^{max} . After this point, only the frequency increases. Similar computations are performed for ΔL_{y0} and ΔH_0 . Since it is possible to set different values for heading and linear speed, the cycle time (and so the stepping frequency) is adjusted to the minimum coming from the three velocity components:

$$T_{cycle} = \min \left(\frac{\Delta L_{x0}}{v_x^r}, \frac{\Delta L_{y0}}{v_y^r}, \frac{\Delta H_0}{\dot{\psi}^r} \right) \quad (9.9)$$

⁹ The horizontal frame \mathcal{H} is the reference frame that shares the same origin and yaw value with the base frame but is aligned (in pitch and roll) to the world frame, hence horizontal (see Fig 9.4 (left)).

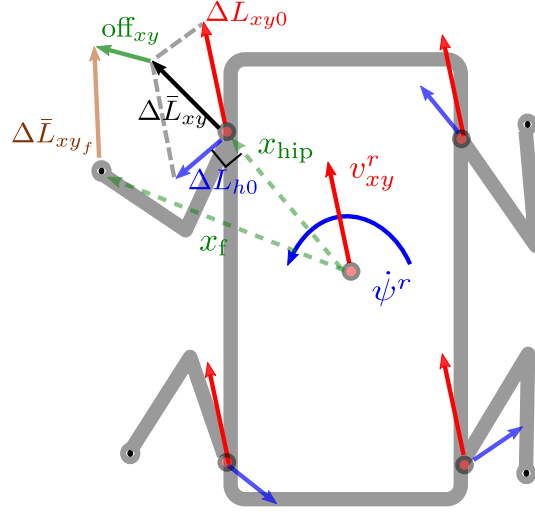


Fig. 9.7: Vector definitions for the heuristic stepping strategy. Red arrows represent the desired linear velocity v_{xy}^r and the linear component ΔL_{xy0} of the default step. In blue is the desired heading velocity ψ^r and the angular component ΔL_{h0} of the default step $\Delta \bar{L}_{xy0}$ that is in black. The offset to increase/decrease the stance size is in green, The step about the foot ΔL_{xy} is depicted in brown.

When a new value of T_{cycle} is computed, the durations of the body and swing trajectories are recomputed as $T_{mb} = (T_{cycle} - T_{lu})D$ and $T_{sw} = (T_{cycle} - T_{lu})(1 - D)$ respectively, according to the duty factor D [39].

The variable T_{lu} represents the cumulative duration of the load/unload phases. As explained in [28], we remark that a load/unload phase at the touchdown/liftoff events is important to avoid torque discontinuities. In particular, a *load phase* at the touchdown allows the Trunk Controller to redistribute smoothly the load on all the legs. At the same time, it ensures that the GRF always stay inside the friction cones, thus reducing the possibility of slippage.

Note that a heading displacement ΔH_0 can be converted into a X, Y displacement of the foot, as shown in Fig. 9.7, by:

$$\Delta L_{h0} = E_{xy} \begin{bmatrix} 0 & 0 & \Delta H_0 \end{bmatrix}^T \times x_{hip} \quad (9.10)$$

where $x_{hip} \in \mathbb{R}^3$ is the vector from the origin of the base frame to the hip of the swinging leg, and $E_{xy} \in \mathbb{R}^{2 \times 3}$ selects the X, Y components. Then, the default step becomes:

$$\Delta \bar{L}_{xy0} = \Delta L_{xy0} + \Delta L_{h0}. \quad (9.11)$$

Note that we defined the *default* step about the hip rather than the foot position (see Fig. 9.7). This is crucial to avoid inconvenient kinematic configurations while walking (*e.g.* stretched or “crouched” configuration), thus degenerating the support polygon. Indeed, if we refer each step to the previous foot position, an anticipated/delayed touchdown would produce unexpected step lengths. This would make the stance feet closer/farther over time¹⁰.

¹⁰ As a matter of fact, if the support polygon shrinks, the robustness decreases. In particular, CoM tracking errors and external pushes can move the ZMP very close to the boundary of the support

Since the swing polynomial is defined at the foot level, we have to determine the step $\Delta L_{xy} \in \mathbb{R}^2$ from $\Delta \tilde{L}_{xy0}$, to express it about the actual foot position:

$$\Delta L_{xy} = \Delta \tilde{L}_{xy0} + E_{xy}(\text{off}_{xy} + x_{hip} - x_f), \quad (9.12)$$

where off_{xy} is a parameter to adjust the average size of the stance polygon.

In delicate situations, it might be useful to walk with the feet more outward to increase locomotion stability at the price of a bigger demanded torque at the Hip Abduction/Adduction (HAA) joint.

As a final step, it is convenient to express the swing motion in the *swing plane* (see Fig. 9.8)¹¹. This means we need to express the above quantities in the swing frame S^{12} .

We set quintic 3D polynomials $p(t) \in \mathbb{R}^3$ of duration T_{sw} , where the X, Y components go from $(0,0)$ to ${}_s\Delta L_{xy}$, while for the Z component we set two polynomials such that the swing trajectory passes by an intermediate *apex* point at a time $T_{sw}\chi$. At the apex, the Z component is equal to the step height ${}_s\Delta L_z$ and $\chi \in [0,1]$ represents the apex ratio that can be adjusted to change the apex location (see Fig. 9.8). Hence, the swing foot reference trajectory is computed from the *actual* foot position at the instant of liftoff to the desired foothold as:

$$x_{fsw}^d(\bar{t}) = x_{fsw,lo} + p(\bar{t}), \quad (9.13)$$

where $\bar{t} \in [0, T_{sw}]$, T_{sw} is the swing duration, and the final target is defined as $x_{fsw}^{tg} = x_{fsw,lo} + p(T_{sw})$.

Remark: the *swing frame* (unless specified) is always aligned with the *terrain frame*. Consequently, we have an initial *retraction* along the normal to the *terrain plane* (thus avoiding possible trapping or stumbling of the foot), while the step is performed *along* the terrain plane. A swing motion expressed in this way allows to adjust the step clearance simply with the step height ${}_s\Delta L_z$. This parameter regulates the maximum retraction from the terrain (apex point). In general, the apex is located in the middle of the swing, but it can be parametrized to shape differently the swing trajectory.

Definition: *Searching motion.* A *haptic* triggering of the touchdown allows to accommodate the shape of the terrain by stopping the swing motion either before or after the foot reaches the target x_{fsw}^{tg} .

If the touchdown is deemed to happen after the target is reached, the trajectory is continued with a leg extension movement that we name *searching motion*: the swing foot keeps moving linearly along the direction of the terrain plane normal n_t (see Fig. 9.8) until it touches the ground or eventually reaches the workspace (WS) limit. In this way, the stance is triggered in any case. To avoid mobility loss, a height reflex can be enabled to aid the *search* motion with the other stance legs (see section 9.5.2).

9.4.2 Vision Based Stepping

The *terrain plane* is a very coarse approximation of the terrain. If a vision feedback is available, it is advisable to exploit this information, which allows to:

polygon. This would result in a situation where not all the contact feet are “pushing” on the ground (*e.g.* the robot starts tipping about the line connecting two feet).

¹¹ We call the *swing plane* the plane passing through the X-Z axes of the swing frame.

¹² The *swing frame*, in general, is aligned with the *terrain frame* unless a vision based stepping strategy is used. In this case, the swing frame is computed *independently* for each foot (as explained in Section 9.4.2) from the visual input.

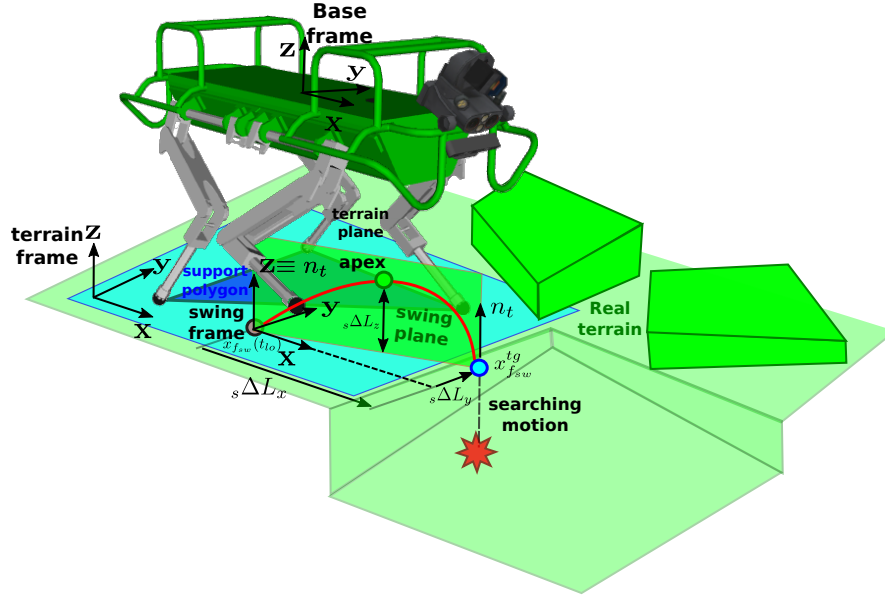


Fig. 9.8: Swing frame and terrain frame definition for the heuristic-based stepping strategy used in blind locomotion. The terrain presents a decrease in elevation, haptically handled by the searching motion.

1. compute the target foothold on the *actual* terrain rather than on its planar approximation (see Fig. 9.9). This allows to increase the overall swing *clearance* (cf. blind stepping in Fig. 9.8 with vision based stepping in Fig. 9.9).
2. set a different swing frame for each foot instead of having the *swing frame* always coincident to the *terrain frame*. This enables the swing on different planes per each leg (essential for climbing though difficult terrain configurations such as V-shaped walls [28]).

To implement the first point, we first compute a step (along the terrain plane) using the heuristic-based stepping strategy. This is meant to realize the user velocity. Then, the height map of the terrain is queried at the target location, and the Z component of the target is corrected to have it on the real terrain (X, Y components remain unchanged):

$$\tilde{x}_c^g = H \left(E_{xy} x_{fsw}^g \right) \quad (9.14)$$

where $E_{xy} \in \mathbb{R}^{2 \times 3}$ selects the X, Y components, and $H(\cdot)$ is a function that queries the terrain elevation for a certain (X, Y) location on the $X-Y$ plane¹³.

As a final step, we compute the Z axis \hat{a}_{swz} of the swing frame such that its X axis \hat{a}_{swx} is aligned with the segment connecting the actual foot position to the corrected foothold \tilde{x}_{fsw}^g (see Fig 9.10):

¹³ Being the map expressed in a (fixed) world frame, it is necessary to apply appropriate kinematic conversions to this frame before evaluating the map.

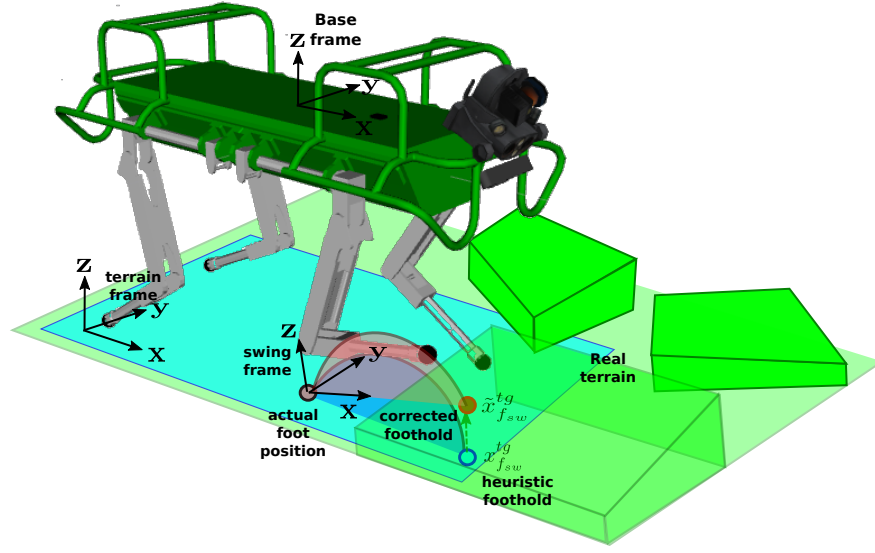


Fig. 9.9: Swing frame definition for the vision-based stepping strategy. Blue and red shaded area represent the swing in the heuristic and the vision-based cases, respectively. In this case the terrain elevation is higher than the foot location at the liftoff and the target foot-hold (blue dot) computed with heuristics, is corrected by vision (red dot) to lay on the real terrain. The swing frame is also adjusted accordingly.

$$\begin{aligned}
 a_{swz} &= (\hat{x}_{fsw}^{tg} - x_{fsw}) \times ({}_wR_b e_y), \\
 \hat{a}_{swz} &= \frac{a_{swz}}{\|a_{swz}\|}, \\
 \hat{a}_{swy} &= \hat{a}_{swz} \times e_x, \\
 \hat{a}_{swx} &= \hat{a}_{swy} \times \hat{a}_{swz},
 \end{aligned} \tag{9.15}$$

where the $\hat{(\cdot)}$ represents unit vectors and e_x, e_y are the base frame axes expressed in the world frame. This correction allows for more clearance around the actual terrain during the swing motion and reduces the chances of stumbling.

The first consequence is that the swing frame is no longer aligned with the terrain frame, and the swing trajectory is laying on the plane $\hat{a}_{swx}/\hat{a}_{swz}$.

Additionally, if the normal n_r of the *actual* terrain is available from the visual feedback [27], we can exploit it to further correct the swing plane, in order to have the swing-down tangent to that normal. This is particularly useful when the robot has to step on a laterally slanted surface (e.g. like in [28]).

In our experience, however, we noticed that on the sagittal direction, maximizing clearance has more priority. Therefore, we remove the component of n_r along the X axis computed in Eq. (9.15) ($\hat{a}_{swz}^v = n_r - \hat{a}_{swx}^T n_r \hat{a}_{swx}$) and use as the new swing Z axis. The new vision-corrected Z -axis of the *swing frame* becomes n_{rp} (see Fig. 9.10), while the other axes should be recomputed accordingly as in Eq. (9.15).

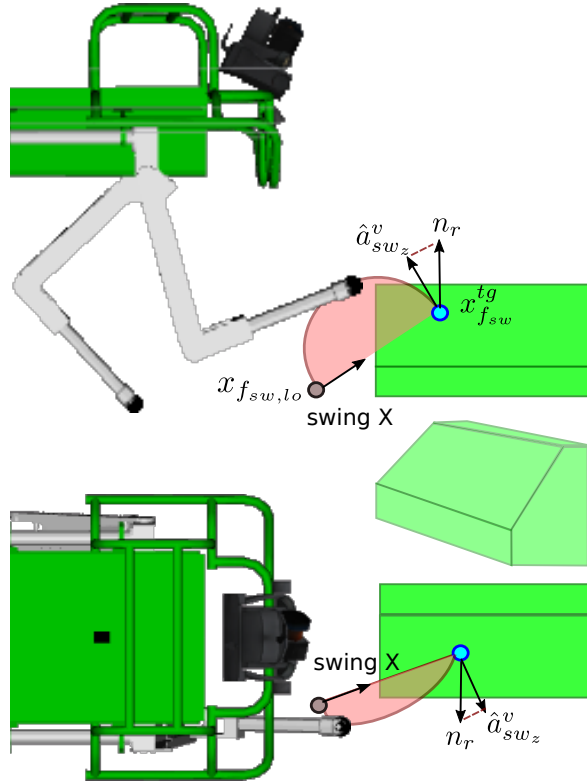


Fig. 9.10: Vision based adjustment of the target foothold Z coordinate. Top and lateral views of the swing plane on a slanted terrain.

9.4.3 Clearance Optimization

If the quality of the map is good enough, the *apex* (point of maximum clearance) and the step height ${}_s\Delta L_z$ can be adjusted in accordance with the point of maximum asperity of the terrain, so as to maximize clearance. To some extent, this can be considered a simple adaptation of the swing to the terrain shape. First, we take a slice of the map and evaluate the height of the terrain on the line segment of direction \hat{b} connecting the actual foot location with the target \hat{x}_{fsw}^{tg} (see Fig. 9.11). With a discretization of N points, we then follow the steps below:

$$\begin{aligned}
1) \quad s_k &= \tilde{x}_{fsw}^g \frac{k}{N} + \tilde{x}_{fi} \left(1 - \frac{k}{N}\right), \quad k = 1 \dots N, \\
2) \quad h_k &= H(E_{xy} s_k), \\
3) \quad \delta_k &= \mathcal{P}_+(h_k - e_z^T s_k), \\
4) \quad \delta_k^\perp &= \left\| [0 \ 0 \ \delta_k]^T - ([0 \ 0 \ \delta_k] \hat{b}) \hat{b} \right\|, \\
5) \quad [{}_s \Delta L_z \ k_{max}] &= \max_k \delta_k^\perp,
\end{aligned} \tag{9.16}$$

where 1) is a discretization of the line segment; 2) is the evaluation of the height map on the discretized points; 3) $\mathcal{P}_+(\cdot) : \mathbb{R} \rightarrow \mathbb{R}$ is a function that sets negatives values to zero; in 4) we project the δ_k onto the swing Z axis, getting δ_k^\perp ; in 5) we set the step height ${}_s \Delta L_{fsw}$ as the maximum value among the δ_k^\perp where k_{max} is its index. Finally, the apex can be set to k_{max}/N . This reshapes the swing in a conservative way, by adjusting the apex according to the terrain feature.

9.4.4 Time Rescheduling

In our state-machine-based framework, a change in locomotion speed corresponds to changing the duration of the swing/body phases. However, to change speed promptly (without waiting until the end of the current phase) it is necessary to reschedule the polynomials of the active phase (swing or body motion). As a consequence, we compute a new duration T_f' (where T_f is the previous duration). Setting a new duration for a (previously designed) polynomial is equivalent to finding the *initial point* of a new polynomial that: 1) has the new duration T_f' and 2) is passing through the same point at the moment of the rescheduling. We know that a quintic polynomial can be expressed as:

$$p(t) = a^T \mu(t), \quad \dot{p}(t) = a^T \dot{\mu}(t), \quad \ddot{p}(t) = a^T \ddot{\mu}(t) \tag{9.17}$$

where:

$$\begin{aligned}
a^T &= [a_5 \ a_4 \ a_3 \ a_2 \ a_1 \ a_0], \\
\mu(t) &= [t^5 \ t^4 \ t^3 \ t^2 \ t \ 1], \\
\dot{\mu}(t) &= [5t^4 \ 4t^3 \ 3t^2 \ 2t \ 1 \ 0], \\
\ddot{\mu}(t) &= [20t^3 \ 12t^2 \ 6t \ 2 \ 0 \ 0].
\end{aligned} \tag{9.18}$$

Setting the initial/final boundary conditions for position, velocity and acceleration: $p_0 = a^T \mu(0)$, $\dot{p}_0 = a^T \dot{\mu}(0)$, $\ddot{p}_0 = a^T \ddot{\mu}(0)$, $p_f = a^T \mu(T_f)$, $\dot{p}_f = a^T \dot{\mu}(T_f)$, $\ddot{p}_f = a^T \ddot{\mu}(T_f)$ is equivalent to solving a linear system of 6 equations that allows us to find the a_i parameters:

$$\begin{aligned}
a_0 &= p_0, \\
a_1 &= \dot{p}_0, \\
a_2 &= 0.5\ddot{p}_0, \\
a_3 &= \frac{1}{2T_f^3} [20p_f - 20p_0 + T_f(-12\dot{p}_0 - 8\dot{p}_f) + T_f^2(-3\ddot{p}_0 + \ddot{p}_f)], \\
a_4 &= \frac{1}{2T_f^4} [30p_0 - 30p_f + T_f(16\dot{p}_0 + 14\dot{p}_f) + T_f^2(3\ddot{p}_0 - 2\ddot{p}_f)], \\
a_5 &= \frac{1}{2T_f^5} [12p_f - 12p_0 + T_f(-6\dot{p}_0 - 6\dot{p}_f) + T_f^2(-\ddot{p}_0 + \ddot{p}_f)],
\end{aligned} \tag{9.19}$$

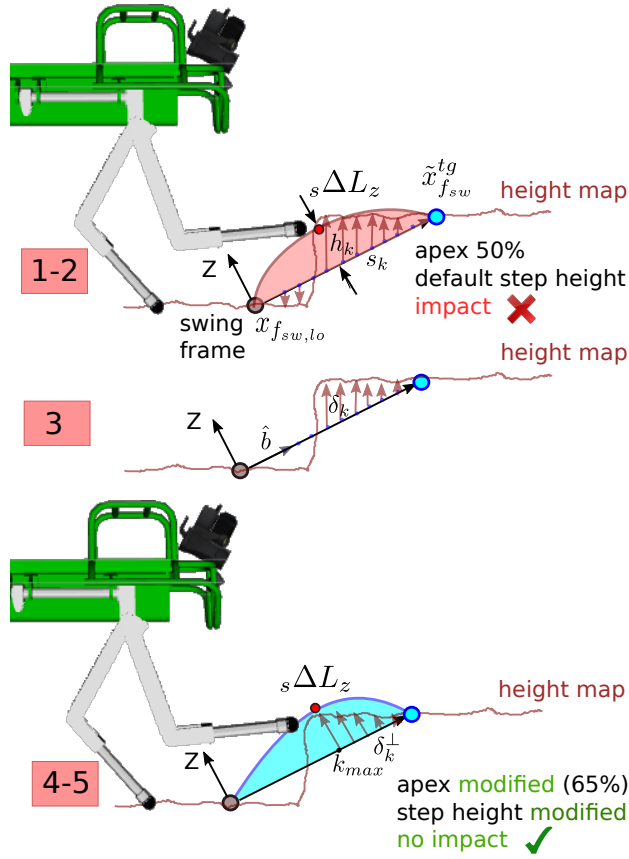


Fig. 9.11: Clearance optimization. The grey dot represents the actual foot location at liftoff, the blue dot the foot target while the red dot the apex location. The numbers in the red rectangles are related to the steps in Eq. (9.16).

with a similar criterion, to ensure continuity in the position, we can compute the new initial point p'_0 such that:

$$a'\mu(\bar{t}) = p(\bar{t}), \quad (9.20)$$

where \bar{t} is the time elapsed (from 0) at the moment of the rescheduling, and a' are the coefficient of the new polynomial of duration T'_f . Then, collecting p_0 from all the parameters in Eq. (9.19), we can obtain a closed form expression for it:

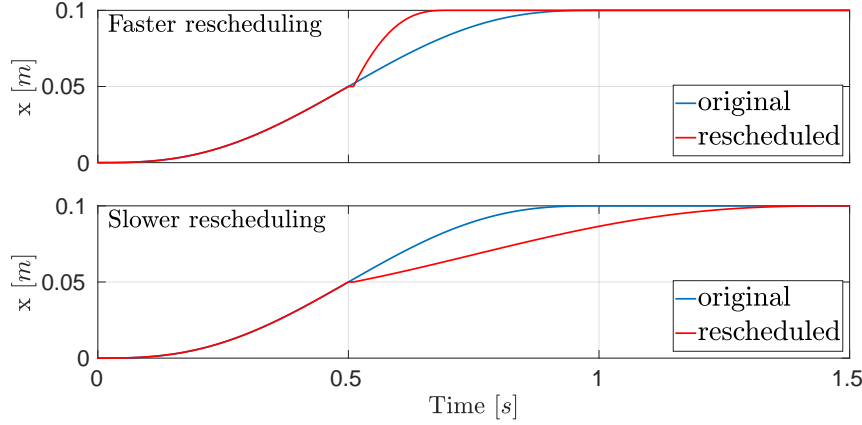


Fig. 9.12: Time rescheduling. The original trajectory (blue) at $\bar{t} = 0.5s$ is rescheduled into a new trajectory (red) of duration of (Upper plot) $0.7s$ or (lower plot) $1.5s$.

$$\begin{aligned}
 \beta_1 &= \frac{1}{2T_f^3} [20p_f + T_f(-12\dot{p}_0 - 8\dot{p}_f) + T_f^2(-3\ddot{p}_0 + \ddot{p}_f)], \\
 \beta_2 &= \frac{1}{2T_f^4} [-30p_f + T_f(16\dot{p}_0 + 14\dot{p}_f) + T_f^2(3\ddot{p}_0 - 2\ddot{p}_f)], \\
 \beta_3 &= \frac{1}{2T_f^5} [12p_f + T_f(-6\dot{p}_0 - 6\dot{p}_f) + T_f^2(-\ddot{p}_0 + \ddot{p}_f)], \\
 \beta_4 &= 1 - 10T_f^3\bar{t}^3 + 15T_f^4\bar{t}^4 - 6T_f^5\bar{t}^5, \\
 p_0 &= \frac{1}{\beta_4} [p(\bar{t}) - a_1\bar{t} + a_2\bar{t}^2 + \beta_1\bar{t}^3 + \beta_2\bar{t}^4 + \beta_3\bar{t}^5] \quad (9.21)
 \end{aligned}$$

Now, exploiting Eq. (9.21) for the computation of p_0 , the new polynomial parameters can be recomputed as in Eq. (9.18) while keeping the other boundary conditions unchanged. This will result in a polynomial that *continues* from \bar{t} with a new duration T_f' .

In Fig. 9.12, we show an example of time rescheduling happening at $0.5s$, where the duration of an original trajectory $T_f = 1s$ is reduced to $T_f' = 0.7s$ (fast scheduling) or increased to $T_f' = 1.5s$ (slower scheduling).

9.5 Reactive Behaviors

In this section, we briefly describe the framework's reactive modules for robust locomotion. These modules implement strategies to mitigate the negative effects of unpredictable events, such as: 1) slippage (Section 9.5.1); 2) loss of mobility (Section 9.5.2); 3) frontal impacts (see Section 9.5.3) and 4) unexpected contacts (*e.g.* shin collisions, see Section 9.5.4).

9.5.1 Slip Detection

The causes of slippage during locomotion can be divided into three categories: 1) wrong estimation of the terrain normal; 2) wrong estimation of the friction coefficient; 3) external disturbances.

In our previous work [24], we addressed the first and the second categories. In particular, we proposed a slippage detection algorithm which estimates *online* the friction coefficient and the normal to the terrain. After the estimation, the coefficient were passed to the whole-body controller (see slip detection and recovery module in Fig. 9.3).

Concerning the third category, an external push can create a loss of contact. This can cause a sudden inwards motion of the foot. For instance, the trunk controller can create internal forces, depending on the regularization used. When there is loss of contact, these internal forces can make the foot move away from the desired position, leading to large tracking error and catastrophic loss of balance. Thanks to the impedance controller (a PD running in parallel to the Trunk Controller), the tracking error will be limited, and it will be recovered at the next replanning stage (see Section 9.3).

9.5.2 Height Reflex

The *height reflex* is a motion generation strategy for all the robot's feet. It redistributes the *swing* motion onto the *stance* legs, with the final effect of "lowering" the trunk to assist the foothold *searching* motion.

The *height reflex* is useful when the robot is facing considerable changes in the terrain elevation (e.g. stepping down from a high platform) [29]. In such situations, the swing leg can lose mobility, causing issues during the subsequent steps (e.g. walking with excessively stretched legs). For this reason, the height reflex is most likely to be activated when stepping down.

9.5.3 Step Reflex

The *step reflex* [30] is a local elevation recovery strategy, triggered in cases of frontal impacts with an obstacle during the swing up phase.

This reflex is key in cases of visual deprivation (e.g. smoky areas or thick vegetation): it allows the robot to overcome an obstacle and establish a stable foothold at the same time, without *stumbling*.

Since the step reflex can be enabled only during the *swing* phase, it is important to set its duration T_{rfx} to stop concurrently with the end of the default swing duration:

$$T_{\text{rfx}} = T_{\text{sw}} - \bar{t}, \quad (9.22)$$

where \bar{t} is the time elapsed from the beginning of the swing until the moment the reflex is triggered (the searching motion will be still possible to accommodate for further errors).

The angle of retraction α_{rfx} (see Fig. 9.13) depends on the distance r_x (along the swing X axis \hat{a}_{sw_x} of the swing frame) already covered by the swing foot:

$$r_x = \hat{a}_{\text{sw}_x}^T (x_{f_{\text{sw}}}^d(\bar{t}) - x_{f_{\text{sw}}}^d(0)), \quad (9.23)$$

and the reflex maximum vertical retraction r_z :

$$\alpha_{\text{rfx}} = \text{atan2}(r_z, r_x).$$

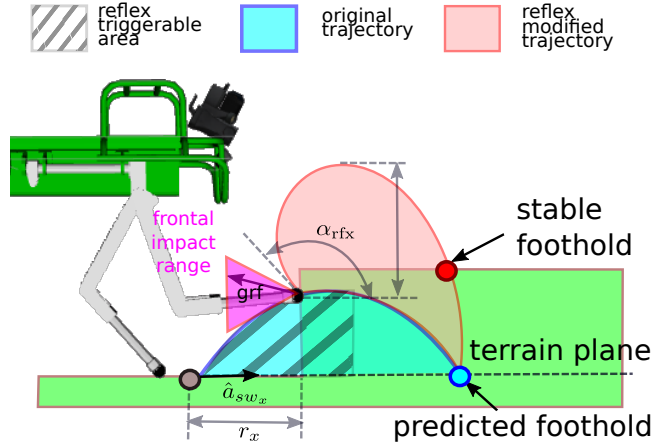


Fig. 9.13: Step Reflex. In shaded blue the original trajectory while in shaded red is the modification due to the reflex. The red cone, shows the range of GRF that are eligible as frontal impacts. Out of this cone the GRF will be used to trigger the stance. Area of possible activation along the trajectory, is depicted with stripes.

The maximum vertical retraction r_z is an input parameter related to the step height and the roughness of the terrain. Note that the step reflex is also conveniently generated in the *swing frame*.

The reflex can be triggered only when the impact is frontal (GRF in the purple cone of Fig. 9.13), and only during the swing *up* phase (*e.g.* before the apex point). The reason for these constraints is twofold:

1. a force from a frontal impact is larger (and pointing downwards) if the impact occurs in the swing up phase; in contrast, it is lower (and pointing upwards) in the swing down phase. Therefore, a small and upward force would cause an increment of false positives for a regular touchdown detection.
2. the time available for a reflex after the swing apex is more limited and would require significantly higher accelerations to be executed.

Missed reflex: If a frontal impact is detected in the swing down phase, the reflex is not triggered immediately, but it is scheduled for the beginning of the next swing phase.

The accompanying video¹⁴ shows a simulation where the robot performs a blind stair ascent, using the heuristic-based stepping strategy as described in Section 9.4.1). Even if the swing leg stumbles against the step, the robot is still able to climb the stairs, thanks to the step reflex. In contrast, when the step reflex is *disabled*, the robot gets stuck.

Remark: the reflex is omni-directional and depends on the desired locomotion speed. For instance, if the robot walks sideways, the step will be triggered along the swing-plane, which will be oriented laterally.

¹⁴ Step reflex video: <https://www.youtube.com/watch?v=TC8HoUBXy54&t=2m33s>

9.5.4 Shin Collision

The foot might not be the only point of contact with the terrain. For certain configurations, the shin of a quadruped robot can collide as well (as shown in this simulation ¹⁵). Since contact forces directly influence the dynamics of the robot, we take this into account in the trunk controller, *i.e.* with an appropriate weight redistribution after updating the number and location of the contact points. The detection of the contact point location can be done either with a dedicated sensor or an estimation algorithm. On the same line, the contact points are updated during the generation of body trajectories.

9.5.5 Experimental Results

In this section, we present the experiments carried out on our robotic platform HyQ, to show the effectiveness of the proposed reactive behaviors framework in addressing rough terrain locomotion. All the experiments have been carried out on HyQ, a 85 kg, fully-torque controlled, hydraulically actuated quadruped robot [40].

HyQ is equipped with a variety of sensors¹⁶, including: precision joint encoders, force/torque sensors, a depth camera (Asus Xtion), a combined (stereo and LiDAR) vision sensor (MultiSense SL), and a tactical grade Inertial Measurement Unit (KVH 1775).

The size of HyQ is $1.0\text{ m} \times 0.5\text{ m} \times 0.98\text{ m}$ ($L \times W \times H$). The leg's length ranges from 0.339 m to 0.789 m and the hip-to-hip distance is 0.75 m.

HyQ has two onboard computers: a real-time compliant (Xenomai-Linux) used for locomotion and a non-RT machine to process vision data. The RT PC processes the low-level controller (hydraulic actuator controller) at 1 kHz and communicates with sensors and actuators through EtherCAT. Additionally, this PC runs the high-level controller at 250 Hz and the state estimation at 500 Hz. The non-RT PC processes the exteroceptive sensors to generate a 2.5-D terrain map [42] with 4 cm resolution and $3\text{ m} \times 3\text{ m}$ size, surrounding the robot.

The template terrain used for the experiments is shown in Fig. 9.2. It is composed by: 1) ascending ramp; 2) a step-wise elevation change; 3) area with big stones (diameter up to 12 cm); 4) another step-wise elevation change; 5) a descending ramp with random bricks. Walking on stones and bricks is challenging from the locomotion point of view: the stones can collapse or roll away, causing a loss of balance, if specific strategies are not implemented. This video¹⁷ shows the robot successfully traversing the template terrain. The terrain adaptation capabilities (*e.g.* haptic feedback, searching motion) are mostly demonstrated when the robot is walking on rocks. The changes in elevation (where the *height reflex* is triggered) prevents the swing leg from losing mobility.

The importance of replanning is particularly evident during the stair descent, where the robot steps on bricks rolling away under a foothold. The pitch error caused by the rolling bricks is recovered in the next step. Since the crawl is statically stable, the robot can move in extremely cluttered environments, almost at ground level. In the last scene of the video, we show a simulation with the second generation of our robots, HyQ2Max [43]. Thanks to its increased range of motion with respect to HyQ, this robot is able to crawl with a very low desired body height and is thus able to walk through 45 cm wide duct.

¹⁵ Shin coll. video: <https://www.youtube.com/watch?v=TC8HoUBXy54&t=4m04s>

¹⁶ For a complete description of the sensor setup, see [41], Chapter 3

¹⁷ Rough terrain experiments:

<https://www.youtube.com/watch?v=TC8HoUBXy54&t=0m10s>

9.6 Terrain Estimation

The terrain estimation module (see Fig. 9.3) estimates the *terrain plane*, which is a linear approximation of the terrain enclosed by the stance feet.

The inclination of the terrain plane (ϕ_t, θ_t) is updated at each *touchdown* event (*e.g.* a when a foot is “sampling” the terrain). Typically, this is done by fitting a plane through the stance feet and computing the principal directions of the matrix containing the feet positions. The fitting plane can be found in two ways:

- **Vertical Fit:** it minimizes the “distance” along the *vertical* component, between the fitting plane ($\Pi : ax + by + cz + d = 0$) and the set of points represented by the feet position;
- **Affine Fit:** it minimizes the Euclidean distance (along the terrain plane normal) between the feet and the plane.

In the first case, we have to solve a linear system, while the second is an *eigenvalue* problem.

9.6.1 Vertical Fit

The “vertical” distance can be minimized by setting the c coefficient to be equal to 1 and solve a *linear system* for the $x = [a \ b \ d]$ parameters:

$$x = A^\# b, \quad (9.24)$$

where the positions of the stance feet have been collected in:

$$A = \begin{bmatrix} x_{f1x} & x_{f1y} & 1 \\ x_{f2x} & x_{f2y} & 1 \\ x_{f3x} & x_{f3y} & 1 \\ x_{f4x} & x_{f4y} & 1 \end{bmatrix}, \quad b = \begin{bmatrix} -x_{f1z} \\ -x_{f2z} \\ -x_{f3z} \\ -x_{f4z} \end{bmatrix}. \quad (9.25)$$

and where $[\cdot]^\#$ is the Moore-Penrose pseudoinverse operator. Then, the normal to the terrain plane n_t and the corresponding roll/pitch angles ϕ_t, θ_t (in ZYX convention), can be obtained as¹⁸:

$$\begin{aligned} n_t &= [a \ b \ 1]^T / \| [a \ b \ 1] \|, \\ \theta_t &= \text{atan}(n_{tx} / n_{tz}), \\ \phi_t &= \text{atan}(-n_{ty} \sin(\theta_t) / n_{tx}). \end{aligned} \quad (9.26)$$

9.6.2 Affine Fit

In the affine case, we first need to reduce the feet samples by subtracting their average \bar{x} (belonging to the fitting plane):

$$R = \begin{bmatrix} x_{f1}^T - \bar{x}^T \\ x_{f2}^T - \bar{x}^T \\ x_{f3}^T - \bar{x}^T \\ x_{f4}^T - \bar{x}^T \end{bmatrix}, \quad \bar{x} = \frac{1}{4} \sum_{i=1}^4 x_{fi}. \quad (9.27)$$

¹⁸ Note that the normal vector $[a, b, 1]$ should be normalized for the computation of ϕ_t, θ_t .

The principal directions of this set of samples are the eigenvectors of $R^T R$:

$$\begin{aligned} [V \ D] &= \text{eig}(R^T R) \\ n_t &= S_1 V \end{aligned} \quad (9.28)$$

where V is the matrix of the eigenvectors and D the diagonal matrix of the eigenvalues of $R^T R$.

We can obtain the terrain normal n_t by extracting the first column from the eigenvector matrix (e.g. the eigenvector associated to the smallest eigenvalue). Then, similarly to the vertical fit case, Eq. (9.26) can be applied to find the terrain parameters. Note that the result is slightly different from the vertical fit case. Indeed, in the affine fit case, we minimize the Euclidean distance, while in the vertical fit case we minimize the distance along the z direction. On the other hand, the two approaches give the same result if the feet are coplanar.

It is noteworthy that the affine approach does not provide meaningful results when $R^T R$ is rank deficient. However, this happens only when (at least) three feet are aligned, which is a very unlikely situation.

9.6.3 Correction for Rough Terrain

There are some situations where just fitting an average plane is not the ideal thing to do during a statically stable motion. For instance, when the robot has three feet on the ground and one on a pallet, the *average* (fitting) plane is not horizontal. In this case, moving the CoM projection along the terrain plane (to enter in the support triangle) results in an inconvenient “up and down” motion. This happens because the robot tries to follow the orientation of the terrain plane with its torso. In this case, it would be preferable to keep the posture horizontal until *at least* two feet are on the pallet.

In this section, we propose a more robust implementation of the terrain estimation strategy, which allows to address these particular situations. The idea is to have the terrain plane fitting the *subset* of the stance feet that are closer to be *coplanar*. In this case, the influence of the “outlier” foot (e.g. the one on the pallet) would be reduced. For more dynamic gaits, where the CoM trajectory is not planned (e.g. like trotting [23]), a low-pass filtering of the terrain estimate would be sufficient to mitigate the effect of the outliers. However, since the crawl makes heavily use of the *terrain plane* to change the pose of the robot, a different strategy has been adopted.

A preliminary step (after computing the terrain normal n_t as in Section 9.6.1) is to compute the norm of the least square errors vector. This can be easily done by exploiting the matrix computed in Eq. (9.25): $e_{LS} = \|Ax - b\|_2$. If e_{LS} (Least Square error) is bigger than a certain (user defined) threshold, it means that the feet are not *coplanar*, and n_t should be corrected.

First, we compute the normal vectors in common to all the combinations of two adjacent edges (l_i, l_j) , (sorted in Counter Clock Wise (CCW) order, see Fig. 9.14):

$$n_{ij} = l_i \times l_j \quad (i, j) \in C, \quad (9.29)$$

where C is the set of all the combinations of two adjacent edges (sorted in CCW order). In our case, C has 4 elements. Since any couple of (intersecting or parallel) lines defines a plane, we associate each normal n_{ij} to one support triangle (e.g. two edges of the support polygon, see Fig. 9.14 (left)).

The corrected terrain normal is a *weighted* average of n_{ij} , where the weights are inversely proportional to the distance of each normal n_{ij} from the terrain plane normal, computed at the previous touchdown event n_{old} .

$$\cos(\alpha_{ij}) = n_{old}^T n_{ij}. \quad (9.30)$$

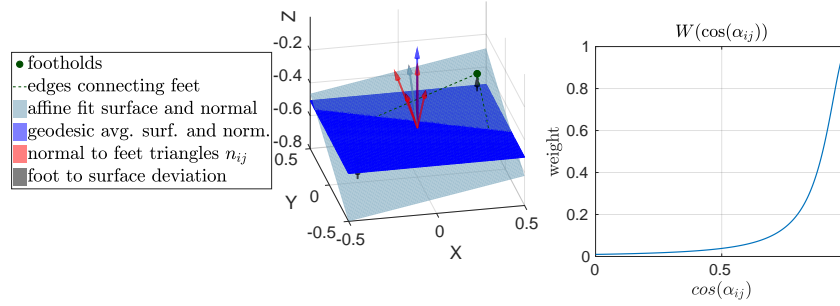


Fig. 9.14: Smart height correction. (Left) the blue arrow represent the corrected normal while the grey arrow the not corrected one (computed with the affine fit method). In this case the corrected normal is almost coincident to one of the red arrows representing the normals n_{ij} to the triangles defined by three stance feet; (right) weight function (W) of the angular distance (*e.g.* cosine) w.r.t $n_{t_{old}}$.

We compute the weight w_{ij} associated to each normal n_{ij} through the nonlinear function $W(\cdot) \in \mathbb{R} \rightarrow \mathbb{R}$ (Fig. 9.14 (right)), in accordance to its angular distance from $n_{t_{old}}$.

$$\begin{aligned} W(x) &= 1 / (1 + s(x - 1)^p), \\ w_k &= W(\cos(\alpha_{ij})), \end{aligned} \quad (9.31)$$

where k is the index of the ij -th element of the set C ; and s is a sensitivity factor proportional to the LS error e_{LS} .

According to Eq. (9.31), the normals closer to $n_{t_{old}}$ (*e.g.* cosine close to 1) are assigned a bigger weight (the weight is bounded to 1 by construction of $W(\cdot)$). The exponent p allows us to adjust the degree of nonlinearity of $W(\cdot)$ and the degree of correction (in our case $p = 2$ was sufficient).

Since the normals n_{ij} are directly affected by the position of their corresponding feet on the pallet, a weighted average of the normals (with weights inversely proportional to the distance from the previous estimation) allows to naturally reduce the influence of the “outlier” foot. This discourages the terrain estimator from modifying too much the previous estimate when a foot position is far away from the previous fitting plane.

Note that, since we are aiming at “averaging” orientations, we need to perform a Spherical Linear interpolation (SLERP) using geodesic curves [44] (see *Appendix A*).

9.6.4 Experimental Results

The terrain estimation video¹⁹ shows how the smart terrain estimator improves locomotion by removing undesired up/down motions.

¹⁹ Terrain estimation video: www.youtube.com/watch?v=TC8HoUBXy54&t=5m01s

With reference to our initial example, as long as the robot has one foot on the pallet, the normal is closer to the one provided by the other stance feet — which in turn are closer to the previous estimation with all the feet on the flat ground (see Fig. 9.14).

When the robot steps with the two lateral feet on the pallet, the fitting error e_{LS} is reduced (the feet are more coplanar) and an inclined terrain plane is estimated.

The approach can address situations with non coplanar feet (*e.g.* support has a “diamond” shape, shown later in the video). In this case, the terms from the feet on the pallet cancel each other, keeping the previous terrain plane estimate unchanged, which is the desirable behavior. For the single pallet example, we have $e_{LS} = 0.02$ (for the “diamond” shape $e_{LS} = 0.031$), therefore we set the threshold of intervention for the terrain correction to 0.002.

Since we want a stronger correction when the LS error increases, we make the sensitivity factor s of the function $W(\cdot)$ proportional to e_{LS} .

9.7 Stair climbing

Stair climbing is an essential skill in the for a legged robot. Indeed, a *versatile* legged robot should be able to address both *unstructured* and *structured* environments, such as the one we can find in a disaster scenario.

The problem of stair climbing can be addressed through foothold planning, to avoid collisions with the step edges. An optimization taking into account the full kinematic of the robot could possibly solve the problem, but it is currently hard to be performed *online*.

Moreover, as previously mentioned, a full optimization approach that plans for a whole staircase is prone to tracking errors, which might eventually end up in missing a step and fall.

An alternative strategy is to conservatively select the foothold in the middle of the step (depth-wise). However, depending on the inclination of the stairs and on the step-size, the robot can end up in inconvenient configurations from the kinematic point of view (*e.g.* with degeneration of the support triangle and associated loss of mobility).

In the case of HyQ, the kinematic limits at the Hip-Flexion-Extension joints (*i.e.* hip joints rotating around the Y -axis, see [40]) are likely to be hit during the *body motion* phase²⁰.

According to our experience, keeping the joint posture as close as possible to the *default* configuration²¹ it improves mobility, and is an important factor for the robustness of locomotion. Our heuristic approach, rather than avoiding potentially dangerous situations (*e.g.* missed steps, collisions), aims to be robust enough to cope with them.

In particular, we show that our vision-based stepping approach, with minor modifications (see section 9.7.2), is sufficient to successfully climb up/down industrial-size stairs. In case the *vision based swing strategy* is not sufficient to avoid frontal impacts (*e.g.* against one step), the *step reflex* is triggered to achieve a stable foothold and prevent the robot from getting stuck.

²⁰ We adopt a “telescopic strut” strategy as in [45], which means that, on an inclined terrain, the vector between each stance foot and the corresponding hip aiming to be maintained parallel to gravity. On one hand, this improves the margin for a static equilibrium. On the other hand, for high stair inclinations, it can result in bigger joint motions, where the kinematic limits are most likely hit.

²¹ As the one shown in Fig. 9.2 (left), where the joints are in the middle of their range of motion

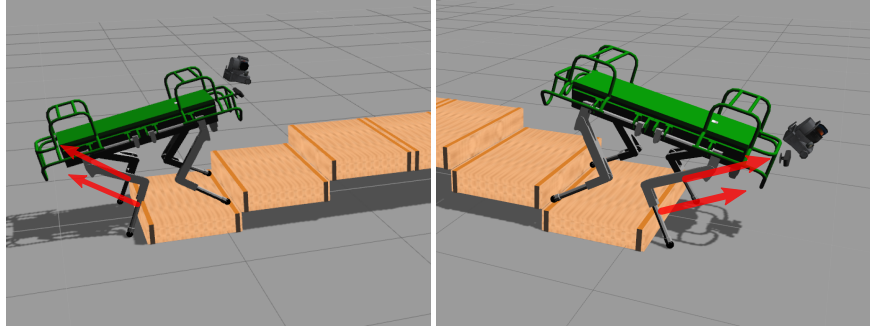


Fig. 9.15: Comparison of KBB and KBF configurations during stair climbing. In the KBF while climbing up the GRF point against the direction of motion making the robot get stuck.

9.7.1 Influence of the knee configuration

The probability of “getting stuck” when climbing stairs depends on the knee configuration (bent backwards or forward). In particular, when the leg has a Knee Bent Backward (KBB) configuration, it is more prone to have shin collision when climbing *downstairs*. Conversely, a Knee Bent Forward (KBF) configuration increases the risk of shin collision when climbing *upstairs*. These are important aspects for the design of robots that are expected to climb stairs.

Note that the contact forces at the shin are *in* the direction of motion when the configuration is KBB and the robot is climbing downstairs, whereas they point *against* the motion with the KBF configuration and the robot climbs upstairs (see Fig. 9.15). In the former case we might have slippage, but the robot eventually moves forward, while in the latter case the robot might get stuck or fall backwards, unless these situation are properly dealt with (see Section 9.5.4).

9.7.2 Stair locomotion mode

The *stair locomotion mode* can be triggered either by the user or by a dedicated stair detection algorithm [46]. It consists in the activation of three features (relevant for the task of climbing stairs) on top of the vision-based stepping strategy:

1. **Rescheduling of the gait sequence:** the kinematic configurations that cause mobility loss are undesired. To avoid them, it is important to climb stairs with both front feet (or back feet) on the same step. Specifically, the *next* foot target is checked at each touchdown (*i.e.* before the *move body* phase). If this is on a different height than the foot on the opposite side, we perform a rescheduling of the gait sequence.
For instance, if the last swing foot was the right front (*RF*) then, according to our *default* configuration (*RH, RF, LH, LF*)²² the next leg to swing would be the *LH*. However, if the left-front (*LF*) foot is on a different height (*e.g.* still on the previous step), the whole sequence is rescheduled to move the *LF* instead. The same applies for the back feet.
2. **Conservative stepping:** taking inspiration from the ideas presented in [25], this module corrects the foot location to step far away from an edge. The terrain flatness is checked along

²² This sequence is the one animals employ that reduces the backward motions [47].

the direction of motion and the foothold is corrected (along the swing plane) in order to place it in a more conservative location (*i.e.* away from the step edge).

3. **Clearance optimization:** this feature (presented in Section 9.4.3) is useful to avoid the chance of stumbling against the step's edge. It adjusts the swing apex and the step height to maximize the clearance from the step.

9.7.3 Experimental Results

We successfully applied the reactive modules of our framework to the problem of climbing up (and down) stairs, in simulation, with our quadruped robot, HyQ²³. In the video, we show that HyQ is able to climb up and down industrial size stairs (step raise 14 cm) and climbing up a staircase with a 90° turn.

The approach is generic enough to be used also with irregular stair patterns (different step raise) and turning stairs. The user provides only a reference speed and heading.

In the simulation video we show the advantage of activating the stair locomotion mode and the importance of using a vision based stepping strategy.

In the 90° staircase, we demonstrate omni-directional capability of our statically stable approach, which allows to move backwards on the staircase.

9.8 Momentum Based Disturbance Observer

A significant source of error might come from unmodeled disturbances, such as an external push. Specifically, in the case of a model-based controller (*e.g.* our Whole Body controller [28]), inaccurate model parameters cause a wrong prediction of the joint torques. This shifts the responsibility of the control to the feedback-based controllers, thus increasing tracking errors and delays. However, if a proper identification is carried out *offline*, these model inaccuracies are mainly restricted to the trunk. Indeed, in the case of our quadruped robot, the leg inertia does not change significantly, but the trunk parameters are instead strongly dependent on robot payload (*e.g.* a backpack, an additional computer, different sets of cameras for perception, *etc.*).

In [48], we presented a *recursive* strategy which performs *online* payload identification to estimate the new CoM position of the robot's trunk. The updated model is then used for a more accurate inversion of the dynamics [28, 3]. Even though this approach is effective to detect constant payload changes, it is not convenient to estimate *time-varying* unknown external forces, which might change both in *direction* and *intensity*. Indeed, this kind of disturbances can dramatically increase the tracking errors and jeopardize the locomotion, unless they are compensated *online*.

In the following, we mention two scenarios where an external disturbance observer is useful: 1) the robot is required to pull a cart or a load (*e.g.* with some delicate material inside); and 2) the robot is requested to pull up a payload from underneath with a hoist mounted on the torso (see 9.16).

In this section, we present a MBDO able to estimate an external *wrench* (*e.g.* cumulative effect of all the disturbance forces and moments). We also show how this *wrench* is compensated during the locomotion, thus improving tracking accuracy and locomotion stability.

Our approach builds on top of the one described in [10], which is designed to estimate an external *linear* force acting on the robot base. We extended this work to the angular case, estimating the full wrench at the CoM.

²³ Stair climb video:

<https://www.youtube.com/watch?v=TC8HoUBXy54&t=7m19s>

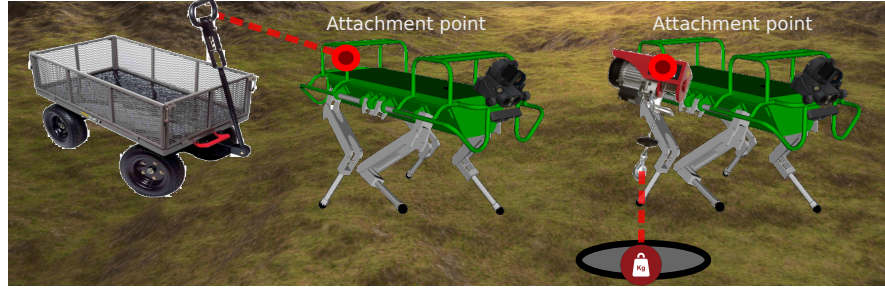


Fig. 9.16: Use cases for load estimation: (left) the robot is pulling a cart, (right) the robot is pulling up a payload.

Since our robot has a non negligible angular dynamics, estimating only a *linear* force has limited effectiveness. Unless the force is applied at the CoM, the *application point*, then the moment about the CoM must be worked out. Our approach is more general as it does not require the application point to estimate the full wrench.

The idea underlying the estimation is that any external *wrench*²⁴ $W_{ext} \in \mathbb{R}^6$ has an influence on the *centroidal* momentum (*i.e.* linear and angular momentum at the CoM) [50].

We observe that the discrepancy between the predicted (centroidal) spatial momentum $\hat{h}(t) \in \mathbb{R}^6$, based on *known* forces (*e.g.* gravity and GRF), and the measured one $h(t)$, based on proprioceptive estimation of the CoM twist²⁵, in absence of modeling errors is caused only by an external wrench W_{ext} ²⁶. We can exploit this fact to design an observer.

To obtain a prediction of $\hat{h}(t) = [\hat{p}_G(t) \ \hat{k}_G(t)]$, we exploit the centroidal dynamics (*e.g.* Newton-Euler equations)[50]:

$$\begin{cases} \hat{p}_G(t) = mg + \underbrace{\sum_{i=1}^c f_i(t)}_{f_{\text{known}}} + \hat{f}_{ext}(t) \\ \hat{k}_G(t) = \underbrace{\sum_{i=1}^c (x_{f_i}(t) - x_c(t)) \times f_i(t)}_{\tau_{\text{known}}} + \hat{\tau}_{ext}(t) \end{cases} \quad (9.32)$$

where $\hat{p}_G(t) \in \mathbb{R}^3$ and $\hat{k}_G(t) \in \mathbb{R}^3$ are the linear and angular momentum rate, respectively; $\hat{W}_{ext}(t) = [\hat{f}_{ext}(t) \ \hat{\tau}_{ext}(t)]$ is a prediction of the wrench disturbance at time t , expressed at the CoM point.

Starting from an initial measure of the momentum $h_0 = [p_{G0} \ k_{G0}] = [m\dot{x}_{com}(0) \ I_{com}(0)\omega(0)]$, we can get the predicted $\hat{h}(t)$, at a given time t , by integration of Eq. (9.32):

²⁴ Henceforth, for simplicity, we talk about coordinate vectors and not spatial vectors, that is why $W_{ext} \in \mathbb{R}^6$ rather than $W_{ext} \in F^6$ [49]

²⁵ The twist (*i.e.* 6D spatial velocity) is usually computed by a state estimator, which merges Inertial Measurement Unit (imu), encoder and force/torque sensors [19].

²⁶ It is well known that it is impossible to distinguish between a CoM offset and an external wrench [11]. Therefore our starting assumption is that there are no modeling errors (*i.e.* a preliminary trunk CoM identification has been carried out previously using [48]).

$$\begin{cases} \hat{p}_G(t) = p_0 + \int_0^t (mg + \sum_{i=1}^{c_{st}} f_i(t) + \hat{f}_{ext}(t)) dt \\ \hat{k}_G(t) = k_0 + \int_0^t (\sum_{i=1}^{c_{st}} (x_{f_i}(t) - x_{com}(t)) \times f_i(t) + \hat{\tau}_{ext}(t)) dt \end{cases} \quad (9.33)$$

Then, the discrepancy between the measured and the predicted momentum can be used to estimate the external wrench disturbance, leading to the following observer set of equations:

$$\begin{cases} \hat{f}_{ext}(t) = G_{lin} (m\dot{x}_{com}(t) - \hat{p}_G(t)) \\ \hat{\tau}_{ext}(t) = G_{ang} (I_{com}(t)\omega(t) - \hat{k}_G(t)) \end{cases} \quad (9.34)$$

where the gains $G_{lin}, G_{ang} \in \mathbb{R}^{3 \times 3}$ are user-defined positive definite matrices, which describe the observer's dynamics, and $I_{com}(t) \in \mathbb{R}^{3 \times 3}$ is the rotational inertia of the robot (as a rigid body) computed at time t . On the other hand, Eq. (9.32) can be rewritten using spatial algebra [49], considering the whole robot as a rigid body:

$$\dot{h} = \frac{d}{dt} (\bar{I}_{com} v) = \bar{I}_{com} \dot{v} + v \times \bar{I}_{com} v = W_{known} + \hat{W}_{ext} \quad (9.35)$$

where $v = [\dot{x}_{com} \ \omega] \in \mathbb{R}^6$ is the measured CoM twist composed of CoM linear velocity and robot angular velocity (for simplicity of notation, we omit henceforth the dependency on t); $\bar{I}_{com} \in \mathbb{R}^{6 \times 6}$ is the composite rigid body inertia (expressed in an inertial frame attached to the CoM), evaluated at each loop at the actual configuration of the robot; $W_{known} = [f_{known} \ \tau_{known}]$ is the wrench due to contacts and gravity.

Using Eq. (9.35), it is possible to formulate a wrench observer where the nonlinear term $v \times \bar{I}_{com} v$ is compensated:

$$\begin{cases} \bar{I} \hat{v} = \bar{I}_0 v_0 + \int_0^t (W_{known} + \hat{W}_{ext} - v \times \bar{I}_{com} v) dt \\ \hat{W}_{ext} = G \bar{I} (v - \hat{v}) \end{cases} \quad (9.36)$$

where $G = \text{diag}(G_{lin}, G_{ang}) \in \mathbb{R}^{6 \times 6}$ is the observer gain matrix.

At each control loop, after the *estimation* step, we perform *online* compensation of the estimated disturbance wrench \hat{W}_{ext} in the whole-body Trunk Controller [28] (see Fig. 9.3):

$$W^d = W_{vm} + W_g - \hat{W}_{ext} \quad (9.37)$$

where $W^d \in \mathbb{R}^6$ is the desired wrench (expressed at the CoM), mapped to desired joint torques by the Trunk Controller; $W_g, W_{vm} \in \mathbb{R}^6$ are the gravity compensation wrench and the virtual model attractor (which tracks a desired CoM trajectory) wrench, respectively.

9.8.1 ZMP compensation

Compensating for the external wrench is not sufficient to achieve stable locomotion. During a static crawl, the accelerations are typically small, and the ZMP mostly coincides with the projection of the CoM on the support polygon. However, this does not hold if an external disturbance is present. In this case, the ZMP can be shifted. If this is not properly accounted for in the body motion planning, the locomotion stability might be at risk.

Knowing that the ZMP is the point on the support polygon (or, better, the line) where the tangential moments nullify, the shift Δx_{com} can be estimated by computing the equilibrium of moments about this point (see Fig. 9.17):

$$\underbrace{(x_{com} - x_{zmp})}_{\Delta x_{com}} \times (mg + f_{ext}) + \tau_{ext} = 0 \quad (9.38)$$

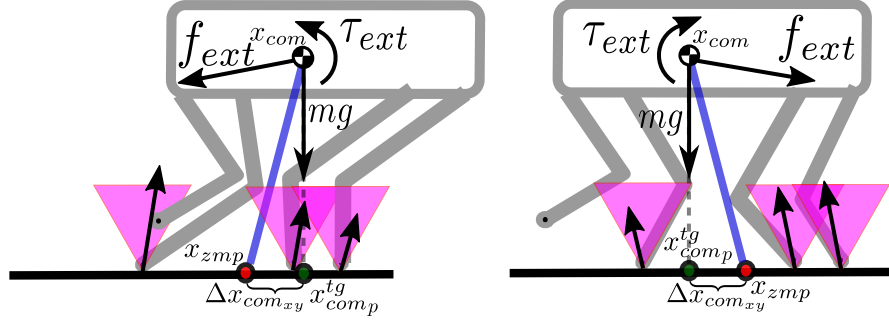


Fig. 9.17: Diagram for the computation of the ZMP due to external disturbances. Left and right figures show different values of $\Delta x_{com_{xy}}$ for different external disturbances.

where Δx_{com} is the vector going from the ZMP to the CoM²⁷. Rewriting Eq. (9.38) in an explicit form²⁸, we get [51]:

$$\begin{cases} \Delta x_{com_x} = \frac{1}{f_{ext_z} - mg} [f_{ext_x}(x_{com_z} - x_{zmp_z}) + \tau_{ext_y}] \\ \Delta x_{com_y} = \frac{1}{f_{ext_z} - mg} [f_{ext_y}(x_{com_z} - x_{zmp_z}) - \tau_{ext_x}] \end{cases} \quad (9.39)$$

then, the new target computed at the beginning of the base motion will account for this term:

$$x_{com_{xy}}^{tg} = x_{com_{xy}}^{tg} + \Delta x_{com_{xy}} \quad (9.40)$$

9.8.2 Stability Issues

Any observer/state feedback arrangement can lead to some stability issues if the gains are not set properly (e.g. by separation principle). We did not carried out a system stability analysis, since a proper evaluation of the stability region (and an improved implementation taking care of this aspects) is an ongoing work and it is out of the scope of this paper. However, we noticed that there are some combinations of gains for which the system becomes unstable.

In the experiments, we decided to be conservative and set lower gains than in simulation. We also did not see a significant improvement in using the implementation Eq. (9.36) instead of Eq. (9.34).

9.8.3 Simulations

To evaluate the quality of the *estimation*, we inject in simulation a known disturbance: a pure force to the back of the robot (with application point ${}_b x_p = [-0.6, 0.0, 0.08] m$, expressed in the base frame), while the robot is standing still. Specifically, we generate a time-varying perturbation force f_{ext} with random stepwise changes both in *magnitude* (between 40 N and 200 N) and *direction*, with

²⁷ Note that only gravity and the external wrench have an influence on $\Delta x_{com_{xy}}$, because the resultant of the GRF passes through the ZMP point, by definition.

²⁸ Note that computing this equations as $\Delta x_{com} = [mg + f_{ext}] \times \tau_{ext}$ where $[\cdot]_{\times}$ is the skew symmetric operator associated to the cross product, returns inaccurate results because $[\cdot]_{\times}$ is rank deficient.

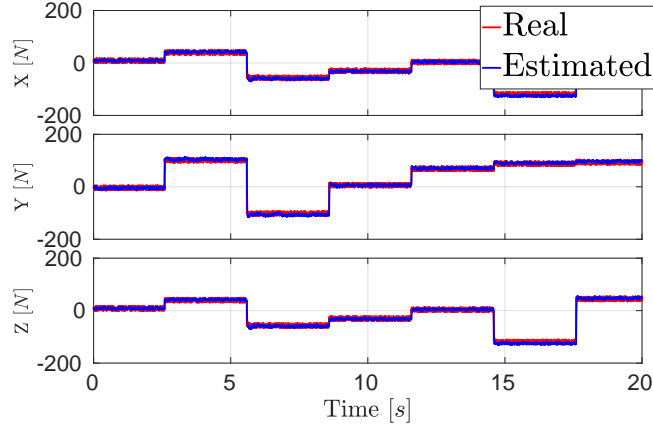


Fig. 9.18: Simulated estimation of a time-varying external force.

additive white Gaussian noise $n \in \mathcal{N}(0, 20)\text{N}$. The gains used in the observer are the following: $G_{ang} = \text{diag}(100, 100, 100)$, $G_{ang} = \text{diag}(10, 10, 10)$.

The result of the estimation is shown in Fig. 9.18: the estimator is able to follow promptly the step changes with the gains set, while a small filtering effect of the noise is given by the observer dynamics.

To evaluate the effectiveness of the *compensation*, we observe that an external force not properly compensated (*e.g.* by the Trunk Controller) results in GRF which differ from the desired ones (outputs of the optimization), even in absence of modeling errors. This can create slippages and loss of contact, as shown in the accompanying video²⁹.

Therefore, a good metric to assess the effectiveness of the compensation is the norm of the GRF tracking error $\|f\|$.

Figure 9.19 shows that the compensation improves significantly the GRF tracking by almost two orders of magnitude.

The video also shows a simulation of the robot pulling a wheelbarrow, illustrating the GRF (green arrows) and the location of the ZMP (purple sphere). In the simulation the robot “leans forward”, compensating for the offset in the ZMP created by the pulling force, while the back legs are more loaded (*i.e.* with larger GRF) with respect to the front ones, due to the weight of the wheelbarrow.

9.8.4 Experimental Results

To demonstrate the effectiveness of our approach, we designed several test scenarios in which the robot is walking and compensating a time-varying disturbance force³⁰. In all the experiments, we set the gains to $G_{lin} = \text{diag}(10, 10, 10)$, $G_{ang} = \text{diag}(1, 1, 1)$.

²⁹ MBDO simulations: <https://www.youtube.com/watch?v=TC8HoUBXy54&t=9m20s>

³⁰ MBDO experiments: <https://www.youtube.com/watch?v=TC8HoUBXy54&t=9m51s>

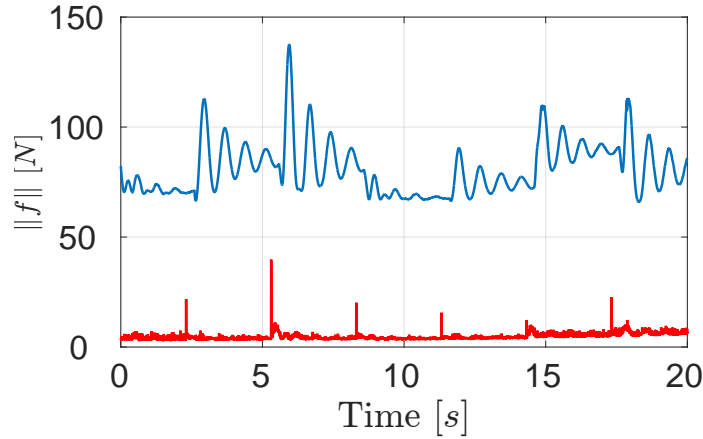


Fig. 9.19: Norm of tracking error the with (red) and without (blue) compensation of the external wrench.

Experiment 1 - Pulling a Wheelbarrow

pulling a wheelbarrow on a ramp is an interesting experimental scenario for our MBDO.

This task poses several challenges: 1) the wheelbarrow attached with a rope (intermittent unilateral pull constraint) creates a disturbance force which has a constant vertical component (to counteract wheelbarrow gravity) and a time-varying component (due to horizontal accelerations); 2) The motion of the wheel barrow results in potential unload of the rope that causes discontinuity in the force; 3) a walking gait involves a mutable contact condition, implying that the compensation force must be exerted by different legs at different times, without discontinuities. 4) the additional loading of the wheelbarrow is done *impulsively*; 5) walking on a ramp shrinks the support polygon and reduces the stability margin, requiring a high accuracy in the estimation/compensation pipeline.

The accompanying video shows the robot walking on a ramp while pulling a 12 kg wheelbarrow. We performed different trials, with the disturbance wrench compensation enabled, adding 10 kg and 5 kg supplementary weights (on top of the wheelbarrow), in different stages of the walk. Being the total weight of 27 kg equally shared between the robot and the wheels of the cart, we estimate the total load to be 13.5 kg. With the compensation enabled, the robot is able to smoothly climb the ramp while dragging this extra weight. Without the compensation, the robot was struggling to maintain the support polygon even with 5 kg of extra weight (for a total load of approximately 8.5 kg hanging from the robot). With 15 kg it was unable to climb the ramp.

Figure 9.21 shows the components of the estimated wrench. As expected, the most relevant ones are f_{ext_x} , which is time varying, and f_{ext_z} , which is mostly the constant and vertical component of the disturbance force. Note how the vertical component f_{ext_z} changes when two different loads are added to the wheelbarrow. The wheelbarrow is attached to the back of the robot, hence it also exerts a constant negative moment around the Y direction.

Since the interaction force with the wheelbarrow is unknown, again the GRF tracking is the only metric available to assess the quality of the compensation. Figure 9.22 shows the pitch variation (upper plot) while walking first horizontally and then up the slope. The GRF tracking for the LH leg is also shown (lower plot). Thanks to the compensation, the tracking error is always below 40 N for the Z component (about 5 % of the total robot's weight) and 20 N for the X component.

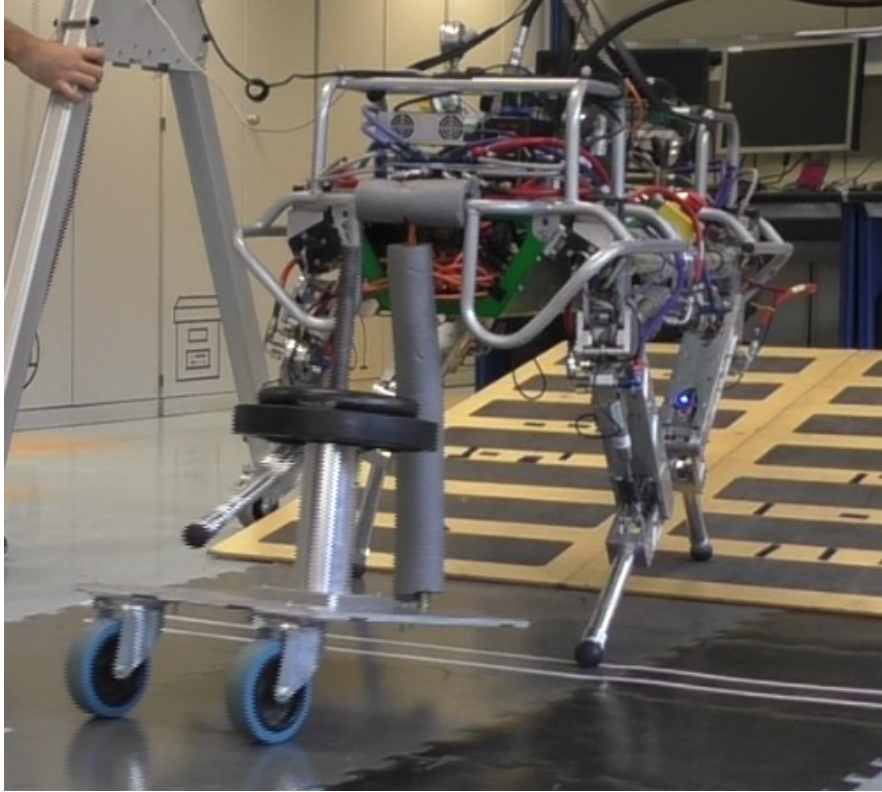


Fig. 9.20: HyQ quadruped robot pulling a wheelbarrow (of 12 kg) loaded with 15 kg of additional weight. The total vertical force acting on the robot is about 13.5 kg. The cart is attached to the robot through a rope.

Experiment 2 - Leaning Against a Pulling Force

In this experiment, a 15 kg load is attached to the back of the robot with a rope. An intermediate pulley transforms the gravitational load into a horizontal force. This test allows to evaluate the effectiveness of the estimation/compensation pipeline in presence of disturbance forces mostly *horizontal*. In the experiments, the robot is able to pull 15 kg when walking with the compensation enabled. When the estimation is disabled, the controller accumulates errors and suffers from instability. Figure 9.24 shows that the only significant component in the estimated wrench is along the X direction (horizontal). The force increases, while the robot walks, because the load is pulled up gradually (see video), until it reaches the steady value of 75 N (*i.e.* the 15 kg load halved by the pulley).

). The RViz visualization in the accompanying video shows that the GRF have a constant component along the X direction (*e.g.* pointing forward) to compensate for the backward pulling force. At the same time, when the compensation is active, the ZMP is shifted forward.

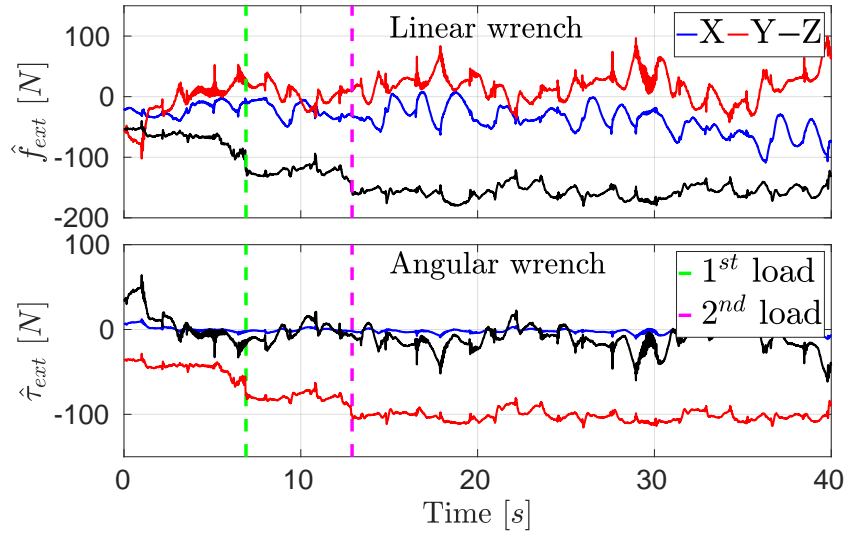


Fig. 9.21: Wheelbarrow experiments. Estimated wrench in real experiments while the robot carries out a wheelbarrow on rough terrain, (upper plot) linear part (lower plot) the angular one. The two vertical lines represent the moments where the 1-st (10 kg) and 2-nd (5 kg) load were applied.

9.9 Conclusions

In this work we addressed the problem of locomotion on rough terrain. We proposed a 1-step *receding horizon* heuristic planning strategy that can work with variable levels of exteroceptive feedbacks.

When no exteroceptive perception is available (and no map of the environment is given to the robot) the locomotion framework presented in this paper is still capable of traversing challenging terrains. This is possible thanks to its capability to *blindly* adapt to the terrain, mainly because of the 1-step re-planning and of the *haptic* touchdown.

When a map of the surrounding world is available, the proposed locomotion framework can exploit this information by including the actual terrain height and orientation in the planning, thus decreasing the chances of stumbling and allowing to traverse more difficult situations (*e.g.* climbing stairs).

With the proposed approach we were able to achieve several experimental results, such as traversing a template rough terrain made of ramps, debris and stairs. We have also shown our quadruped walking while compensating for external *time-varying* disturbance forces caused by a load up to 15 kg, using the MBDO that we proposed. All these tasks were performed with the same locomotion strategy that we presented in this paper.

Future works involve an extensive analysis of the stability of the MBDO, considering its interactions with the Trunk Controller loop. Based on these results, we intend to implement improved observer that maximizes the stability region. Our future research directions also include extending the navigation capabilities of HyQ to more complex environments made of rolling stones and big size obstacles (>12 cm diameter). For these scenarios, we envision the need to develop a shin collision detection algorithm capable of kino-dynamic proprioception using a foot-switch sensor[34]. Finally, we plan to carry out extensive stair climbing experiments with the proposed approach.

Appendix A

This appendix shows how to compute the weighted average of N orientation vectors.

Because finite rotations do not sum up as vectors do, it is not possible to apply ordinary laws of vector arithmetic to them. Specifically, the task of averaging orientations (described in the algorithm 1 written in pseudo-code) is equivalent to average points on a sphere, where the line is replaced with a spherical geodesic (arc of a circle)³¹.

Algorithm 1 compute geodesic average

```

1:  $w_1 \leftarrow 1$ 
2:  $\bar{n} \leftarrow n_1$ 
3: for  $k = 2$  to  $N$  do
4:    $\theta_k = \text{acos}(\text{dot}(\bar{n}, n_k))$ 
5:    $\bar{\theta}_k = \theta_k \frac{\sum_{p=1}^{k-1} w_p}{\sum_{p=1}^k w_p}$ 
6:    $\bar{n} \leftarrow \text{rotate } n_k \text{ towards } \bar{n} \text{ by angle } \bar{\theta}_k$ 
7: end for
  
```

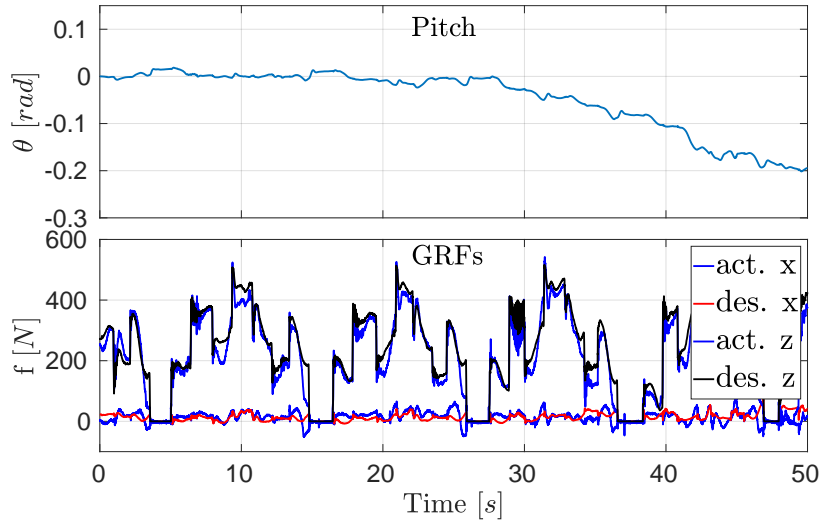


Fig. 9.22: Wheelbarrow experiments: (upper plot) trunk pitch angle and (lower plot) tracking of the Z component of the GRF of the *LH* leg, while the robot carries the wheelbarrow on ramp.

³¹ The geodesic distance is the length of the shortest curve lying on the sphere connecting the two points.

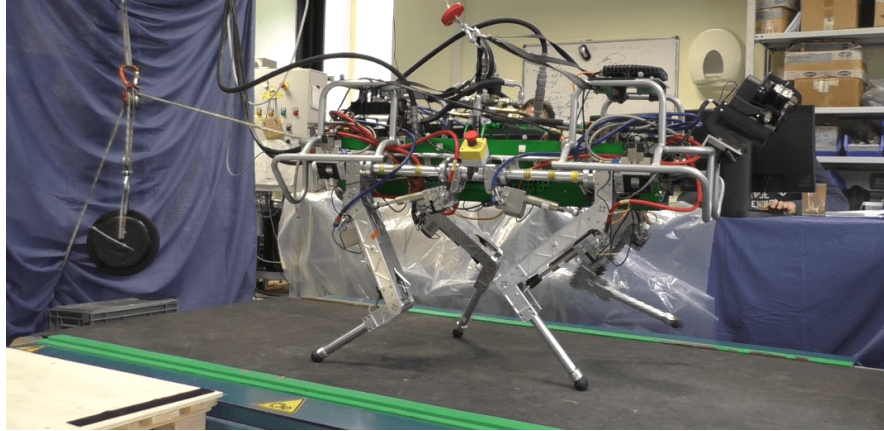


Fig. 9.23: HyQ quadruped robot dragging a $75N$ horizontal disturbance force (15 kg load on a pulley) to testing the performances of the MBDO.

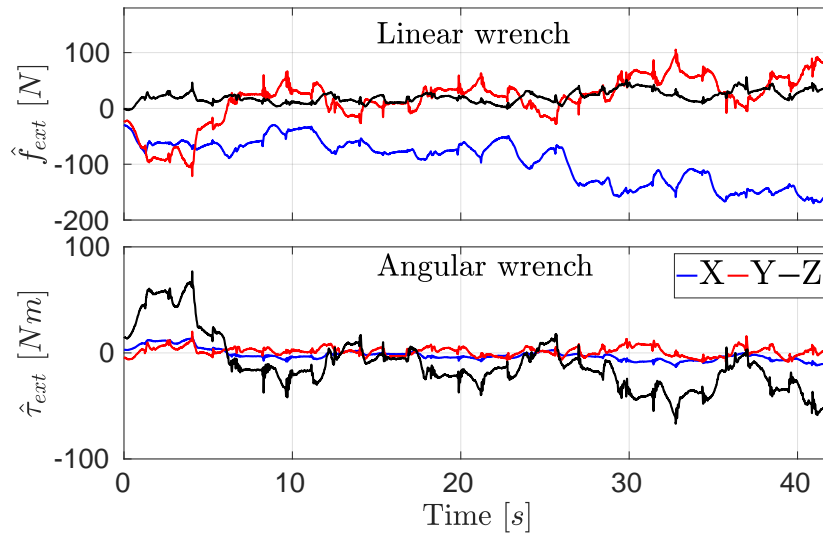


Fig. 9.24: Curling experiments. Estimated wrench: (upper plot) linear part, the load is mainly along the X component (horizontal) (lower plot) angular part, all the moments are oscillating around zero, showing that the interaction force direction is passing close to the CoM.

The iterative procedure illustrated above is generic and can be used to obtain the average of N directional vectors n_k , even though at each iteration we are only able to directly compute the average of two. After the initialization, at each loop the actual average \bar{n} is updated with the next normal n_k . To do so, we first compute the angle θ_k between n_k and the actual average \bar{n} . Then we scale this angle, according to the (accumulated) weight of \bar{n} . Finally, n_k is rotated by the scaled angle θ toward \bar{n} and the result is assigned back to \bar{n} .

Appendix B

List of the main symbols used throughout the paper:

Symbol	Description
$x_{com} \in \mathbb{R}^3$	coordinates of the CoM of the robot
$x_{fi}, \dot{x}_{fi} \in \mathbb{R}^3$	positions and velocities of the i^{th} foot
$f_i \in \mathbb{R}^3$	contact forces of the i^{th} stance foot
n	number of active joints of the robot
$q_j^d, \dot{q}_j^d \in \mathbb{R}^n$	joint reference positions and velocities
$\tau_{ff}^d \in \mathbb{R}^n$	feedforward torque command
$\tau_{pd}^d \in \mathbb{R}^n$	impedance torque command
$\tau^d \in \mathbb{R}^n$	total reference torque command
ϕ	roll angle of the robot's trunk
θ	pitch angle of the robot's trunk
ψ	yaw angle of the robot's trunk
$\Phi = [\phi, \theta, \psi]$	actual orient. of the robot's trunk
$\Phi^d = [\phi^d, \theta^d, \psi^d]$	desired orient. of the robot's trunk
$\Phi^d(0) = \Phi$	des. orient. at the start of the move base
Φ^{tg}	target orient. at the end of the move base
x_{com}^{tg}	target CoM position of the trunk
x_{comp}^{tg}	projection of x_{com}^{tg} on the terrain plane
h_r	robot's height
f_{ext}, τ_{ext}	external disturbance force and torque

Acknowledgement

This work was supported by Istituto Italiano di Tecnologia (IIT), with additional funding from the European Union's Seventh Framework Programme for research, technological development and demonstration under grant agreement no. 601116 as part of the ECHORD++ (The European Coordination Hub for Open Robotics Development) project under the experiment called *HyQ-REAL*.

References

1. Bretl, T., Lall, S.: Testing static equilibrium for legged robots. *IEEE Transactions on Robotics* **24**, 794–807 (2008)

2. Pardo, D., Möller, L., Neunert, M., Winkler, A.W., Buchli, J.: Evaluating Direct Transcription and Nonlinear Optimization Methods for Robot Motion Planning. *IEEE Robotics and Automation Letters* **1**(2), 946–953 (2016)
3. Mastalli, C., Focchi, M., Havoutis, I., Radulescu, A., Calinon, S., Buchli, J., Caldwell, D. G., Semini, D. G.: Trajectory and foothold optimization using low-dimensional models for rough terrain locomotion. In: *IEEE International Conference on Robotics and Automation (ICRA)* (2017)
4. Winkler, A. W., Bellicoso, C. D., Hutter, M., Buchli, J.: Gait and Trajectory Optimization for Legged Systems through Phasebased End-Effector Parameterization. *IEEE Robotics and Automation Letters*, 1–1 (2018)
5. Aceituno-Cabezas, B., Mastalli, C., Hongkai, D., Focchi, M., Radulescu, A., Caldwell, D. G., Cappelletto, J., Grieco, J. C., Fernando-Lopez, G., Semini, C.: Simultaneous Contact, Gait and Motion Planning for Robust Multi-Legged Locomotion via Mixed-Integer Convex Optimization. *IEEE Robotics and Automation Letters*, 1–8 (2018)
6. Mastalli, C., Winkler, A.W., Havoutis, I., Caldwell, D. G., Semini, C.: On-line and On-board Planning and Perception for Quadrupedal Locomotion. In: *IEEE International Conference on Technologies for Practical Robot Applications (TEPRA)* (2015)
7. Dai, H., Tedrake, R.: Planning robust walking motion on uneven terrain via convex optimization. *2016 IEEE-RAS International Conference on Humanoid Robots* (2016)
8. Ponton, B., Herzog, A., Del Prete, A., Schaal, S., Righetti, L.: On Time Optimisation of Centroidal Momentum Dynamics. <https://arxiv.org/abs/1709.09265> (2017)
9. Stephens, B. J.: State estimation for force-controlled humanoid balance using simple models in the presence of modeling error. In: *2011 IEEE International Conference on Robotics and Automation*, pp. 3994–3999 (2011)
10. Engelsberger, J., Mesesan, G., Ott, C.: Smooth trajectory generation and push-recovery based on divergent component of motion. In: *IEEE International Conference on Intelligent Robots and Systems (IROS)*, pp. 4560–4567 (2017)
11. Rotella, N.: Estimation-based control for humanoid robots. In: *PhD Thesis, University of Southern California (USC)* (2018)
12. Bledt, G., Wensing, P. M., Kim, S.: Policy-regularized model predictive control to stabilize diverse quadrupedal gaits for the MIT cheetah. *IEEE/RSJ International Conference on Intelligent Robots and Systems (IROS)*, 4102–4109 (2017)
13. Wieber, P-B.: Trajectory Free Linear Model Predictive Control for Stable Walking in the Presence of Strong Perturbations Trajectory Free Linear Model Predictive Control for Stable Walking in the Presence of Strong Perturbations. *IEEE-RAS International Conference on Humanoid Robots* (2006)
14. Park, H-W., Wensing, P., Kim, S.: Online Planning for Autonomous Running Jumps Over Obstacles in High-Speed Quadrupeds. *Robotics: Science and Systems XI* (2015)
15. Bellicoso, C. D., Gehring, C., Hwangbo, J., Fankhauser, P., Hutter, M.: Perception-less terrain adaptation through whole body control and hierarchical optimization. In: *2016 IEEE-RAS 16th International Conference on Humanoid Robots (Humanoids)*, pp. 558–564. (2016)
16. Bellicoso, C. D., Jenelten, F., Fankhauser, P., Gehring, C., Hwangbo, J., Hutter, M.: Dynamic Locomotion and Whole-Body Control for Quadrupedal Robots. *IEEE/RSJ International Conference on Intelligent Robots and Systems (IROS)*, 3359–3365 (2017)
17. Fankhauser, P., Bjelonic, M., Bellicoso, C. D., Miki, T., Hutter, M.: Robust rough-terrain locomotion with a quadrupedal robot. *IEEE International Conference on Robotics and Automation (ICRA)* (2018)
18. Fallon, M., Marion, P., Deits, R., Whelan, T., Antone, M., McDonald, J., Tedrake R.: Continuous humanoid locomotion over uneven terrain using stereo fusion. In: *2015 IEEE-RAS 15th International Conference on Humanoid Robots (Humanoids)*, pp. 881–888 (2015)
19. Camurri, M., Fallon, M., Bazeille, S., Radulescu, A., Barasuol, V., Caldwell, D.G., Semini, C.: Probabilistic Contact Estimation and Impact Detection for State Estimation of Quadruped Robots. *IEEE Robotics and Automation Letters* **2**, 1023–1030 (2017)

20. Bloesch, M., Hutter, M., Hoepflinger, M.H., Gehring, C., David Remy, C., Siegwart, R.: State estimation for legged robots: Consistent fusion of leg kinematics and IMU. *MIT Press Journals* **8**, 17–24 (2013)
21. Xinjilefu, X., Feng, S., Huang, W., Atkeson, C.G.: Decoupled state estimation for humanoids using full-body dynamics. In: 2014 IEEE International Conference on Robotics and Automation (ICRA), pp. 195–201 (2014)
22. Nobili, S., Camurri, M., Barasuol, V., Focchi, M., Caldwell, D., Semini, C., Fallon, M.: Heterogeneous Sensor Fusion for Accurate State Estimation of Dynamic Legged Robots. *Robotics: Science and Systems XIII* (2017)
23. Barasuol, V., Buchli, J., Semini, C., Frigerio, M., De Pieri, E.R., Caldwell, D.G.: A reactive controller framework for quadrupedal locomotion on challenging terrain. *Proceedings - IEEE International Conference on Robotics and Automation*, 2554–2561 (2013)
24. Focchi, M., Barasuol, V., Frigerio, M., Caldwell, D.G., Semini, C.: Slip Detection and Recovery for Quadruped Robots. *Cham: Springer Proceedings in Advanced Robotics* **3**, 185–199 (2018)
25. Barasuol, V., Camurri, M., Bazeille, S., Caldwell, D., Semini, C.: Reactive trotting with foot placement corrections through visual pattern classification. In: *IEEE/RSJ International Conference on Intelligent Robots and Systems (IROS)* (2015)
26. Belter, D., Skrzypczyński, P.: Rough terrain mapping and classification for foothold selection in a walking robot. *Journal of Field Robotics* **28**(4), 497–528 (2011)
27. Mastalli, C., Havoutis, I., Focchi, M., Caldwell, D.G., Semini, C.: Motion planning for quadrupedal locomotion: coupled planning, terrain mapping and whole-body control. HAL id: hal-01673438v2 (2018)
28. Focchi, M., Del Prete, A., Havoutis, I., Featherstone, R., Caldwell, D.G., Semini, C.: High-slope terrain locomotion for torque-controlled quadruped robots. *Autonomous Robots*, **41**(1), 259–272, (2017)
29. Focchi, M., Featherstone, R., Orsolino, R., Caldwell, D.G., Semini, C.: Viscosity-based height reflex for workspace augmentation for quadrupedal locomotion on rough terrain. In: *IEEE/RSJ International Conference on Intelligent Robots and Systems (IROS)* (2017)
30. Focchi, M., Barasuol, V., Havoutis, I., Buchli, J., Semini, C., Caldwell, D.G.: Local reflex generation for obstacle negotiation in quadrupedal locomotion. In: *Int. Conf. on Climbing and Walking Robots (CLAWAR)* (2013)
31. Semini, C., Tsagarakis, N., Guglielmino, E., Focchi, M., Cannella, F., Caldwell, D.: Design of HyQ – a Hydraulically and Electrically Actuated Quadruped Robot. *J. of Systems and Control Eng.* (2011)
32. Frigerio, M., Buchli, J., Caldwell, D.G., Semini, C.: RobCoGen: a code generator for efficient kinematics and dynamics of articulated robots, based on Domain Specific Languages **7**(1), 36–54, (2016)
33. Tar, A. S., Cserey, G. G., Veres, J.: Patent N. WO 2013072712 A1 (May 2014)
34. Gao, Y., Semini, C., Focchi, M., Caldwell, D.G.: Patent N. IT 102018000002407 (February 2018)
35. Winkler, A., Mastalli, C., Havoutis, I., Focchi, M., Caldwell, D.G., Semini, C.: Planning and execution of dynamic whole-body locomotion for a hydraulic quadruped on challenging terrain. In: *IEEE International Conference on Robotics and Automation (ICRA)* (2015)
36. Boaventura, T., Buchli, J., Semini, C., Caldwell, D. G.: Model-based hydraulic impedance control for dynamic robots. *IEEE Transactions on Robotics* **31**, 1324–1336 (2015)
37. Orsolino, R., Focchi, M., Mastalli, C., Dai, H., Caldwell, D. G., Semini, C.: Application of Wrench based Feasibility Analysis to the Online Trajectory Optimization of Legged Robots. *IEEE Robotics and Automation Letters (RA-L)* (2018)
38. Audren, H., Kheddar, A.: 3D robust stability polyhedron in multicontact. Submitted to *IEEE Transactions On Robotics (TRO)* (2017)
39. Alexander, R. M.: *Principles of animal locomotion*. Princeton University Press (2003)
40. Semini, C., Tsagarakis, N.G., Guglielmino, E., Focchi, M., Cannella, F., Caldwell, D.G.: Design of hyq - a hydraulically and electrically actuated quadruped robot. *IMechE Part I: Journal of Systems and Control Engineering* **225**(6), 831–849 (2011)

41. Camurri, M.: Multisensory State Estimation and Mapping on Dynamic Quadruped Robots. PhD thesis, Istituto Italiano di Tecnologia (IIT) and University of Genoa. <http://iit-dlslab.github.io/papers/camurri17phd.pdf> (2017)
42. Fankhauser, P., Hutter, M.: A Universal Grid Map Library: Implementation and Use Case for Rough Terrain Navigation. In: A. Koubaa, editor, Robot Operating System (ROS) – The Complete Reference **1**, ch. 5. Springer (2016)
43. Semini, C., Barasuol, V., Goldsmith, J., Frigerio, M., Focchi, M., Gao, Y., Caldwell, D.G.: Design of the hydraulically-actuated, Torque-controlled quadruped robot hyq2max. *IEEE/ASME Transactions on Mechatronics* **PP(99)**, 1–1 (2016)
44. Gramkow, C.: On averaging rotations. *Journal of Mathematical Imaging and Vision* **15(1-2)**, 7–16 (2001)
45. Gehring, C., Coros, S., Hutler, M., Dario Bellicoso, C., Heijnen, H., Diethelm, R., Bloesch, M., Fankhauser, P., Hwangbo, J., Hoepflinger, M., Siegwart, R.: Practice Makes Perfect: An Optimization-Based Approach to Controlling Agile Motions for a Quadruped Robot. *IEEE Robotics and Automation Magazine* **23(1)**, 34–43 (2016)
46. Oßwald, S., Gutmann, J.S., Hornung, A., Bennewitz, M.: From 3D point clouds to climbing stairs: A comparison of plane segmentation approaches for humanoids. In: 2011 11th IEEE-RAS International Conference on Humanoid Robots, pp. 93–98 (2011)
47. Pongas, D., Mistry, M., Schaal, S.: A Robust Quadruped Walking Gait for Traversing Rough Terrain. In: Proceedings 2007 IEEE International Conference on Robotics and Automation, pp. 1474–1479 (2007)
48. Tournois, G., Focchi, M., Del Prete, A., Orsolino, R., Caldwell, D.G., Semini, C.: Online payload identification for quadruped robots. In: IEEE/RSJ International Conference on Intelligent Robots and Systems (IROS) (2017)
49. Featherstone, R.: Rigid Body Dynamics Algorithms. Springer US, Boston, MA (2008)
50. Orin, D. E., Goswami, A., Lee, S-H.: Centroidal dynamics of a humanoid robot. *Autonomous Robots* **35**, 161–176 (2013)
51. Popovic, M. B., Goswami, A., Herr, H.: Ground reference points in legged locomotion: Definitions, biological trajectories and control implications. *The International Journal of Robotics Research* **24(12)**, 1013–1032 (2005)

Chapter 10

EXOtrainer Project

Clinical Evaluation of Gait Training with Exoskeleton in Children with Spinal Muscular Atrophy

Daniel Sanz-Merodio, Gonzalo Puyuelo, Amartya Ganguly, Elena Garces, Ane Goñi and Elena Garcia

Abstract Life expectancy of the children affected with Spinal Muscular Atrophy (SMA), an autosomal recessive hereditary disease, is considerably reduced by the onset of the respiratory problems induced by the scoliosis. It is hypothesized that maintaining walking would significantly reduce or delay the appearance of related complications, which would increase life expectancy and in addition would improve the quality of life. This paper presents the challenges and main features of the ATLAS 2020, an active paediatric exoskeleton developed in the frame of the EXOtrainer project. The result of the evaluation of ATLAS 2020 exoskeleton in the clinical trials performed in the hospital Sant Joan de Deu in Barcelona (Spain) during three months are summarized. This evaluation was carried out with 7 children with Spinal Muscular Atrophy (SMA). The study evaluates the performance and safety of the exoskeleton from psychological and physiological perspective. The evaluation was successfully passed. ATLAS 2020 gait trainer exoskeleton is expected to reduce and delay the side effect of the disease and increase these children's quality of life.

10.1 Introduction

Spinal muscular atrophy (SMA), is an autosomal recessive hereditary disease. It is caused by mutations that affects the survival of the moto neuron SMN 1 gene, and it is characterized by the degeneration of the alpha motor neurons in the spinal cord. This degeneration results in a progressive proximal muscle weakness and paralysis in the people affected by this disease [1]. With an incidence of 1 in 6,000 to 1 in 10,000 live births, it is the most common fatal autosomal recessive disorder [2].

In most cases, the disease results from the homozygous deletion of the SMN gene at the 5q13 locus. This SMN gene is presented in the form of two copies on each chromosome 5, designated SMN1 and SMN2. There is an important correlation between the number of copies of the SMN2 protein and the severity of the disease [3].

D. Sanz-Merodio, G. Puyuelo, A. Ganguly, E. Garces
Marsi Bionics SL, 28805 Alcala de Henares, Madrid, Spain e-mail: daniel.sanz@marsibionics.com

A. Goñi, E. Garcia
Centre for Automation and Robotics, CSIC-UPM, 28500 Arganda del Rey, Madrid, Spain

There is currently no cure for SMA and the pathogenesis of the disease is not completely understood. Current research is focusing mainly on the development of drugs to achieve increased SMN or improve the activity of SMN-2, in gene therapy and the study of treatments based on the use of stem cells [3].

The clinical spectrum of SMA varies from a severe muscle weakness that appears from birth and that causes infant death, to patients who can have a normal adult life with only slight signs of weakness [4].

The disease has been classified into three main categories: SMA Type I, Type II and Type III. SMA Type I is the most severe form of the disease and is called “Werdnig-Hoffman” disease. It is the most common type of SMA (50% of cases). The first signs of the disease appear before 6 months of age. These children never get to sit on their own without support, and without intervention they usually do not survive beyond two years of life. SMA Type II is the intermediate form in terms of affection and severity. In this type of SMA, the first signs of weakness usually appear between 7 and 18 months of age. These children can sit alone without any support and some can stand up, but they are not able to walk independently. SMA Type III is the mildest form of the disease, also called “Kugelberg-Welander” disease, which have heterogeneous clinical features. While some people need to use a wheelchair, others have productive adult lives with only a slight weakness [4].

Children with SMA suffer from hypotonia, a proximal and progressive weakness that affects the lower limbs more than the arms, and also intercostal muscles weakness. Other complications are poor postural control, scoliosis, hip dislocation, foot and chest deformities, contractures, osteoporosis and fractures [5]. Although difficulty swallowing is not common, weakness of the chewing muscles may affect the ability to eat. Their body mass index is usually low and as these patients have low mobility and can barely move, therefore they are at high risk of overweight. Finally, the weakness of the respiratory muscles, combined with the scoliosis they develop, results in a restrictive pulmonary disease when they get older, which requires the use of mechanical ventilatory support [3].

Survival of children with SMA Type II has been estimated at 98.5% at the age of 5 years, and 68.5% at the age of 25 years. Some can live until their thirties but their life expectancy is low due to the risk of infections and respiratory compromise in general [3].

A proper care, focused on preventing, treating or avoiding complications of the disease, is a key aspect to get the best possible quality of life for these patients. Respiratory care is mainly directed to keep the airway clean of secretions and possible obstructions, to assess and maintain adequate ventilation, and to prevent or treat infectious respiratory diseases. Gastrointestinal and nutritional care are focused on assessing the adequate supply of food for proper nutrition and avoiding excess or defect in weight, detecting signs of weakness in mastication, treating digestion problems and the appearance of reflux. Chronic constipation is a common elimination problem, due to immobility, which must be prevented and treated. Parents and non-professional caregivers of these children should be provided with the information and skills necessary for the continuity of care in their homes to be carried out in an appropriate manner. Including palliative care in the last phase of the disease [6].

The increase of a person's degree of disability has a direct impact on their social participation, and conditions their perception of their quality of life. The quality of life is not determined by a single area, but is multifactorial, and is influenced by the physical, psychological and social functioning of the person [7]. People who have a disability due to the significant limitation of mobility in lower limbs, use wheelchairs as a way to compensate for this limitation of mobility. But wheelchairs do not allow the individual to walk. Medical gait exoskeletons are presented as a very promising alternative to the wheelchair, since they would allow functional walking of the patient [8].

The ATLAS 2020 active lower-limb exoskeleton, designed specifically for SMA type II kids, provides intensive walking exercise in order to improve the patient's health, enhance the overall motor system, delay and reduce the onset of scoliosis and increase the quality of life and life expectancy.

The EXOtrainer project focuses on the following goals in order to achieve the expected results:

- Identify requirements of wearable exoskeletons for SMA.
- Develop an exoskeleton for SMA children.
- Perform a clinical evaluation of the developed device to assess and demonstrate its usability for gait assistance of SMA patients.
- Transfer the research results to the market.

This paper presents the multidisciplinary work carried out in the EXOtrainer project. After the presentation of a background in exoskeletons, the ATLAS 2020 exoskeleton, see Figure 10.1, for the therapy of SMA Type II, is described. Then, the clinical evaluation data, obtained at the Sant Joan de Deu Hospital, are detailed. Finally, the results and the conclusions of the project are presented.

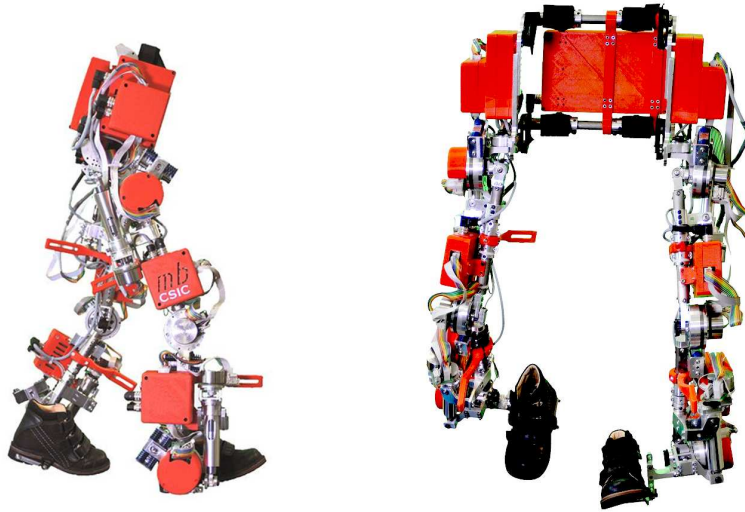


Fig. 10.1: General view of the ATLAS 2020 paediatric gait exoskeleton.

10.2 Background

Lower limb exoskeletons for physical therapy are an increasing research topic in the field of robotics. There are currently some commercially available wearable devices intended for adult patients with stroke or spinal cord injury, such as Lokomat by HOCOMA [9] and EksoGT by Ekso Bionics [10]. However, the use of these devices is restricted to the hospital or rehabilitation center. This issue limits the use of the exoskeleton for each patient to usually once a week, while medical professionals strongly recommend treating SMA patients with rehabilitation every day. In addition, commercial exoskeletons have only two actuated joints, which is not enough to provide balance during standing and walking. Consequently, patients need to use crutches or a walker together with the exoskeleton in order to keep balance. Furthermore, since these joints are actuated in the sagittal plane, they cannot turn, and it is the user who has to manoeuvre with the crutches to turn. Children suffering from SMA are affected by weakness not only in their legs but in their entire body, thus they do not have sufficient strength in their arms and hands to use crutches. On top of that, the stiff actuators

used in these devices are not suitable for SMA patients due to the degeneration of strength as the disease progresses; compliant actuation is required. Finally, commercially available exoskeletons are not suitable for children since the minimum height required to wear them is 1.54m. Lokomat has a paediatric model but its use is not indicated for all neuromuscular diseases [9]. For all the mentioned reasons, there is currently no robot-assisted gait training method to treat children with Type II SMA. The aim of the EXOtrainer project is to adapt an exoskeleton [11] designed at the Center of Robotics and Automatics of the Spanish National Research Council (CSIC) for children with SMA and perform clinical trials to evaluate its usability.

10.3 ATLAS 2020 description

Children affected by Spinal Muscular Atrophy (SMA) have mobility limitations. The design of the wearable gait exoskeleton ATLAS 2020 is adapted to these SMA children's mobility characteristics. ATLAS 2020 is a lightweight exoskeleton (12 kg) with 10 active degrees of freedom (DOF). Figure 10.2 resumes the main components and dimensions of the exoskeleton.

10.3.1 Mechanical structure

ATLAS 2020 has been designed to fit to the dimensions of SMA children from 4 to 12 years old. Five degrees of freedom drive each leg, two DOF at the hip in flexion-extension and abduction-adduction, one at the knee in flexion-extension and another two at the ankle in flexion - extension and eversion - inversion. Table 10.1, details the distribution and range of motion of these DOF. The motion of the hip, knee and ankle joints is driven by rotational series elastic actuators (rSEA), based on the ARES development[12]. While the motion in the hip abduction and the ankle eversion/inversion joints is driven by a linear actuator [13]. An important research has been made in the orthotics of the structure. The orthotics must hold the user properly maintaining alignment of the joints of the exoskeleton children without the fastenings disturbed. The structure is attached to the user through a custom-made corset and the legs are supported by comfortable cuffs.

10.3.2 Electronic architecture

ATLAS 2020 measures joint angles and torques in each joint and measures body inertia through IMUs in each link. The electronic architecture is divided in two interconnected systems:

1. The high-level controller is based on a real time processor and a Field Programmable Gate Array (FPGA). This main controller generates synthetic trajectory through the information received from the user interface. The high-level controller provides Wi-Fi communication so the main parameters can be changed by a smart device like a tablet. Calculating the inverse kinematic the angle trajectory of each joint is sent to the motor low-level controller.
2. The low-level control systems communicate with the main controller. This system receives the desired position and closes the loop with the position measured in each joint. The springs included in the rSEA actuator design provides the measurement of the torque. The position and the torque exerted by each joint is sent to the high-level controller. This system incorporates and measures the information of an inertial measurement unit (IMU), which also is sent to the main controller. Each low-level system fully controls two joints.

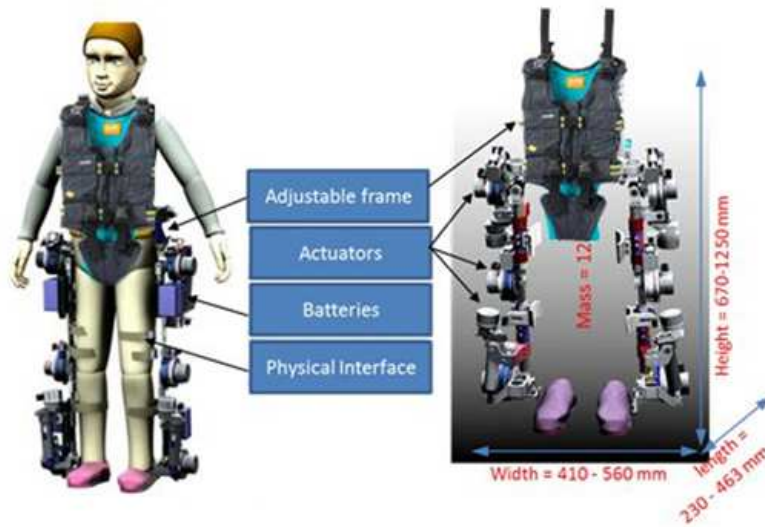


Fig. 10.2: ATLAS 2020 concept and main dimensions

Table 10.1: ATLAS 2020 degrees of freedom and range of motion

Joint / Degrees of freedom	Exoskeleton parameters for each limb	
	Actuated joints	Range of motion°
Hip / 2	Hip flexion	110°/-30°
	Hip abduction	25°/-10°
Knee / 1	Knee flexion	120°/0°
Ankle / 2	Ankle dorsiflexion	30°/-30°
	Ankle eversion/ inversion	16°/-16°

The power system, including three packs of Li-ion batteries distributed in the back and the legs, provides up to 2.5 hours in continuous operation.

10.3.3 Control system

According to the patient's features and joint limitations, (the distance of the link for each segment, hip, knee and ankle flexors), and the gait features (step length, step height, advancement of the leg, gait speed), the main controller provides synthetic trajectories to stand up, sit down and walk. Figure 10.3 shows the synthetic trajectory obtained with the parameters of an SMA patient compared with obtained in the Clinical Gait Analysis (CGA) of healthy people. Note in this Figure, with the blue lines, how the hip and knee flexors are limited.

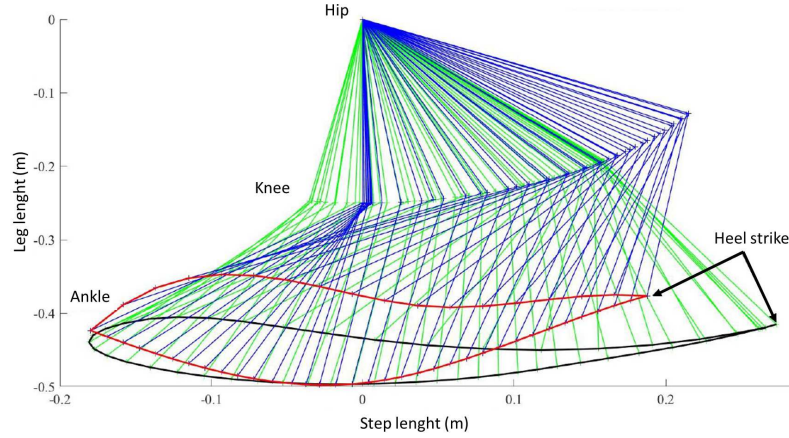


Fig. 10.3: The black ellipse is the ankle motion of a healthy child. The red ellipse is the synthetic trajectory obtained with the parameters of a SMA patient. The green and blue lines shown the position of each link following the trajectory for a healthy participant and a SMA patient respectively.

These angular positions of each joint, calculated by the high-level controller in real time, together with the desired torque value is sent to the low-level system that controls each joint.

The Jacobian matrix J is used to calculate the torque that each joint must do to achieve the force in the Cartesian place F_{des} :

$$\tau_{des} = J^T F_{des} \quad (10.1)$$

The torque exerted in a joint, according with the position θ and the speed $\dot{\theta}$ of the joint as

$$\tau_{des} = K\theta + B\dot{\theta} \quad (10.2)$$

where B is the virtual damping and K is the virtual joint stiffness.

Each low-level control receives the desired angular position (θ_{des}) and the stiffness and damping (B, K) values from the high-level controller. The final position (θ_{final}) applied in the inner-control is:

$$\theta_{final} = \theta_{des} + \Delta\theta \quad (10.3)$$

where

$$\Delta\theta = \frac{\tau - B\dot{\theta}}{K} \quad (10.4)$$

The feedforward speed $\dot{\theta}_{FF}$ is obtained from the known trajectory and with the value θ_{final} obtained in the force-position control, the desired joint speed $\dot{\theta}_{des}$ is sent to the motor position controller. Figure 10.4 details the control diagram of each joint.

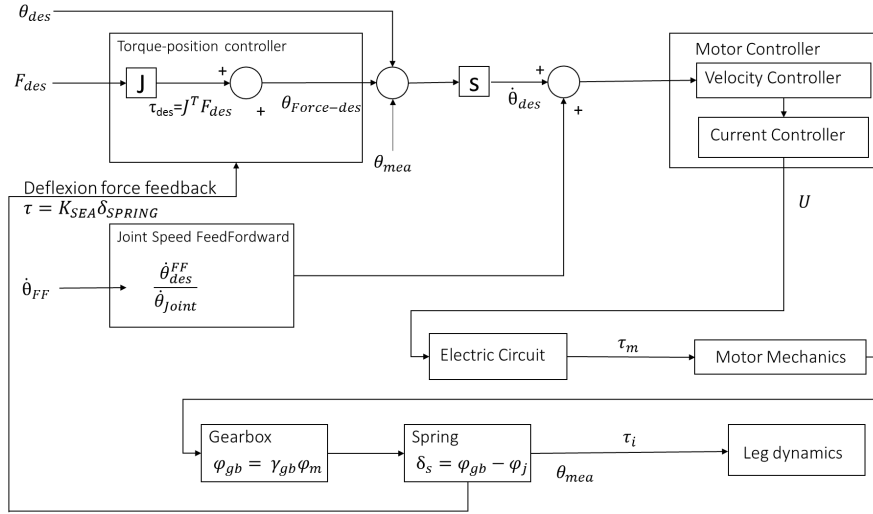


Fig. 10.4: Control scheme used in the ATLAS 2020 exoskeleton. θ_{des} is the reference angular position. $\dot{\theta}_{FF}$ is the feedforward speed. F_{des} is the force in the Cartesian place. J is the Jacobian matrix. U is the motor voltage. τ_m is the motor torque. φ_m is the motor angle, φ_{gb} is the angle at the output of the gearbox, δ_{gb} is the gearbox transmission ratio. δ_s is the spring deflection. K_{SEA} is the equivalent constant of the actuator springs. φ_j is the joint angle. τ_i is the torque measured by the springs.

10.4 Clinical evaluation

The clinical trial entitled “Clinical Evaluation of Gait Training with Exoskeleton for Children with Spinal Muscular Atrophy (SMA)”, is part of the European project EXO-TRAINER coordinated by ECHORD ++. The ATLAS 2020 performance and usage, when standing and walking, with patients affected by SMA type II is the goal of the present paper. In order to assess the device, security, skin tolerance, blood pressure, respiratory frequency and cardiac frequency were taken by a health professional with expertise in paediatric population. The clinical evaluation was performed at Rehabilitation Service of Childrens Hospital Sant Joan de Deu (Barcelona, Spain) assessing the usability of the ATLAS 2020 paediatric gait exoskeleton. This clinical evaluation can be divided into 2 parts: the first one, the pre-clinical phase, was aimed to adapt the exoskeleton to each of the patient, s functional alterations. The second part, the clinical phase, consisted in training sessions using the exoskeleton to perform standing and walking actions with the SMA type II patients. This second part was aimed to assess if there was an improvement in functional, joint and muscular force. Also, measurements regarding blood pressure, heart rate, breathing rate, oxygen saturation, recommended hip abduction angle to avoid hip dislocation and fatigue assessed by the OMNI scale were taken in order to ensure the patient, s safety and wellbeing. The ethics committee at Hospital Sant Joan de Deu approved the initial trial along with the written informed consent of the parents or legal guardians. All data is stored and protected according to Directive (EU) 2016/680 of the European Parliament with regard to the processing of personal data. Table 10.2 shows the main characteristics of the patients involved in the clinical trial:

Table 10.2: Main characteristics of the patients involved in the clinical trial

Number of patients	7
Median age (years)	6
Age range (years)	3-9
Percentage of males and females	42.9% 57.1%
Median weight (kg)	21
Weight range (kg)	14.0 – 46.3
Median height (cm)	115
Height range (cm)	101 – 140
Hip width range (cm)	19 - 38
Thigh length (cm)	22 - 32
Shank length (cm)	21- 31
Foot size (Europe)	25 - 33
Knee Flexo (° deg)	15 - 30
Hip Flexo (° deg)	0 - 30

10.4.1 Clinical sessions

The clinical sessions consisted of an ergonomic evaluation regarding all the participants in the study and walking tests. A total of 8 clinical sessions are conducted with 7 children. At the 3rd session, 3 kids were removed from the clinical trial due to joints Range Of Motion (ROM) limitations, which made the walking activity not possible. A total amount of 30 sessions were performed. As the clinical sessions were aimed to measure differences in functional, joint and muscular force changes, a series of tests were administered to assess these differences. These tests were the Hammersmith Functional Motor Scale for SMA (HFMS), Brook scale and maximum expiratory and inspiratory pressure. Also, walking time and distance was recorded. The HFMS test is widely used in patients with SMA disease in order to assess general mobility [14]. It has 20 items where the patient is asked to perform a posture or activity, and a given score (from 0 to 2 for each item) is given according to their performance. A higher score represents better functional ability. The Brooke scale measures upper limb function [15]. The patient is asked to touch their hands by a full abduction shoulder movement. According to their performance, a score from 1 to 6 is given. A lower score represents better performance of the test. The maximum expiratory and inspiratory pressure measure the respiratory muscle's force. This measurement, obtained in cmH₂O, is directly related to the patient's breathing performance, which is altered due to the muscle degeneration caused by the SMA pathology. A higher score would represent a better muscle function regarding breathing ability, therefore the risk of breathing related complications are less frequent. These tests were administered by healthcare professionals from the Hospital Sant Joan de Déu, with wide expertise in the field of paediatric neuromuscular patients.

Figure 10.5 shows the process carried out with the children to test the exoskeleton.

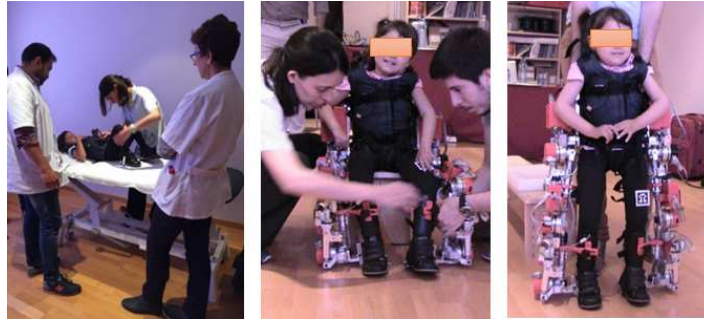


Fig. 10.5: Complete process carried out in the test: Stretching exercises, placement of the exoskeleton and lifting to standing position.

During each trial, the child's physical condition was checked regarding respiratory frequency, blood pressure, heart rate and recommended hip abduction angle in the case of hip dislocation in order to ensure patient's safety. Prior to the walking test, a experienced physiotherapist performed stretching and mobilization exercises to facilitate leg movement in the exoskeleton. Then, the child was placed inside the exoskeleton. Once the patient was secured and its safety was ensured, the exoskeleton proceeded to stand up. An ergonomic verification was performed once the kid was standing up. In addition, measurements regarding points of contact with the exoskeleton at the thigh, shinbone and foot were recorded. When the safety was ensured in standing position, the walking test started. During these tests, the children's comfort and safety was ensured, and if a problem was detected, the trial was interrupted. When the walking test was finished, a final verification of the skin integrity, OMNI auto-perceived fatigue, blood pressure, heart rate and breath rate were checked again. After the session, distance walked, total amount walking time and number of rests needed during the walking phase were recorded. When the clinical sessions finished, the Hammersmith scale, Brook scale and maximum expiratory and inspiratory pressure were measured again.

10.4.2 Results of ergonomics and safety measures

The exoskeleton placement was reduced from 8 minutes in the initial sessions, to 3 minutes in the last ones, and its operation was adequate. Regarding the blood pressure, heart rate and breath rate there were no significant differences between the start and the end of the trial. In addition, the pressures recorded on the thighs and legs during the process of getting up and sitting down are acceptable for manoeuver. There were minor displacements between the hip joint center and the engine center at each joint, during the process of getting up and sitting, which were acceptable for this manoeuver. The total amount of sessions in which skin bruises occurred was 6 of the 30 sessions (20%). Nevertheless, the skin bruises were present in 57% of the initial trials held by each kid, to 0% of them at the last trial. The attitude of the children and their opinion about the device was always cheerful, ready to cooperate and with the intent of continuing in the next session.

10.4.3 Results of clinical measures

Regarding the heart rate, blood pressure, breathing rate and oxygen saturation there were no significant differences between the results obtained prior at the end of each trial. The distance walked (Figure 10.6), measured in meters, was recorded in 23 of the sessions, being the median distance walked 6 meters. This parameter ranged from a median of 1.5 meters in the first session, to 12.4 meters in the last one. The walking time (Figure 10.7), measured in minutes, was done in 20 of the sessions. Regarding the number of rests needed during a session (Figure 10.8), it was evaluated in 29 of the sessions, where in 23 sessions (79.3%), no rests were needed. The degree of fatigue (Figure 10.9) was assessed asking the participants to score their fatigue from 0 to 10, being 0 not fatigued at all, and 10 extremely fatigued, following the OMNI scale guidelines. The degree of fatigue was recorded in 25 sessions. The Hammersmith scale (Figure 10.10) and the Brook scale (Figure 10.11) were recorded at the basal and final time of the clinical sessions. Caused by the 3 participants drop out, at the end of the trial there are only 4 measures recorded. There was 1 point in increment in the median at the final measure in each scale, showing the functional benefit in 15 weeks of training in the participants which remained until the end of the trial. The maximum expiratory pressure in mouth (Figure 10.12) median was 34.0 at the basal measurement, ranging from 15 cmH₂O to 120 cmH₂O. At the final one, the median was 26.5 cmH₂O, ranging from 15 cmH₂O to 64 cmH₂O. The maximum inspiratory pressure in the mouth (Figure 10.13) median was 29 cmH₂O at the basal visit, ranging from 17 cmH₂O to 67 cm H₂O. At the final visit, the median was 26 cmH₂O, ranging from 20 cmH₂O to 34 cmH₂O. The results from the maximum expiratory and inspiratory force are shown in Table 10.3. The deviation from initial to final examinations, regarding maximum expiratory and inspiratory pressure, are not significant enough to be considered as improvements due to the use of the exoskeleton.

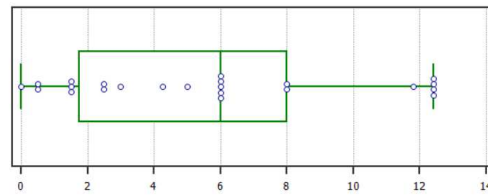


Fig. 10.6: Distance walked in meters.

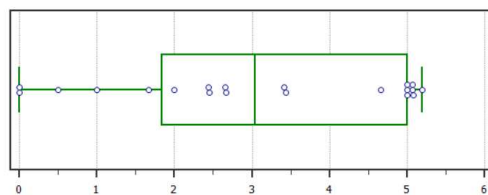


Fig. 10.7: Walking time, in minutes.

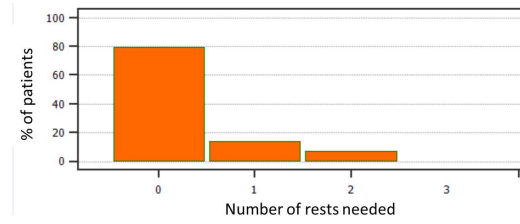


Fig. 10.8: Number of rests needed during a session.

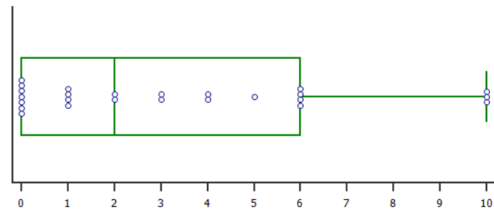


Fig. 10.9: Degree of fatigue, from 0 to 10.

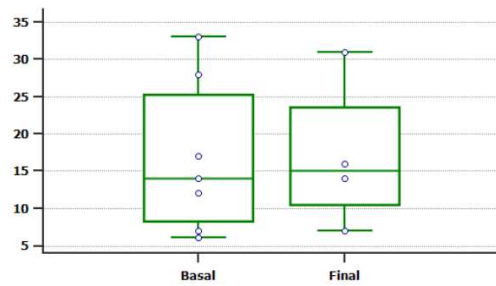


Fig. 10.10: HFMS scale, at the beginning and the end of the trial.

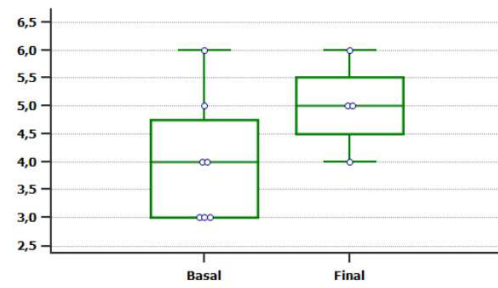


Fig. 10.11: The Brook scale, at the beginning and the end of the trial.

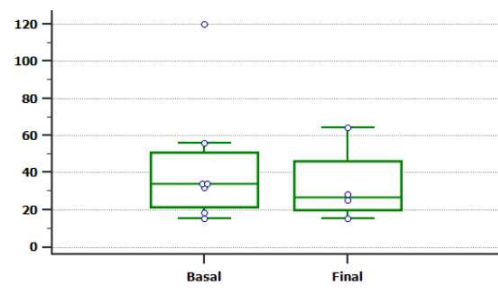


Fig. 10.12: The maximum expiratory pressure in mouth, at the beginning and the end of the trial.

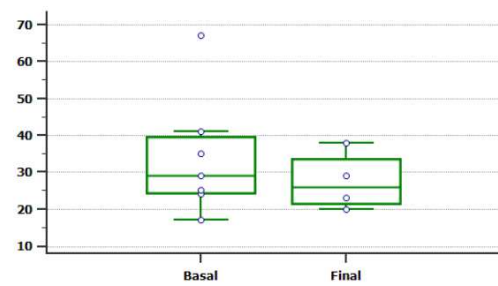


Fig. 10.13: The maximum inspiratory pressure in mouth, at the beginning and the end of the trial.

Table 10.3: Maximum expiratory and inspiratory pressure in mouth (measured in cmH₂O), at the beginning and the end of the trial.

	Maximum inspiratory pressure		Maximum expiratory pressure	
	Beginning	End	Beginning	End
Median	29	26	34	26.5
Range	17-67	20-34	15-120	15-64

10.5 Discussion

At our knowledge, there is no other exoskeleton aimed to assist gait to pediatric neuromuscular patients. Therefore, comparisons between other similar devices are not possible. Regarding the ergonomy results, only skin bruises were observed. Nevertheless, this skin redness disappeared in the last session, showing that the kids adapted correctly to the exoskeleton,s ergonomy. The patient tolerated the exoskeleton usage, and patient adhesion to the intervention was achieved, showing also that the ATLAS2020 is safe to use in this population. Regarding functional and muscular results, we can observe little or no difference between the baseline and the final measurement of the HFMS and maximum inspiratory and expiratory pressure. Nevertheless, there are differences regarding the Brooke scale, number of rests needed, walking distance and time. As expected, this might be related to the patient adaptation to the exoskeleton based therapy. The results related to physical rehabilitation outcomes obtained in this study may not be conclusive due to the limited population and time of exoskeleton usage. In other studies, regarding strength improvement in SMA patients, the therapy consisted of sessions from 5 to 3 times per week [16, 18, 17]. Their population study consisted of 9 to 14 patients, and the intervention lasted from 3 to 12 months. In our study, the exoskeleton use was once a week, for 3 months and 4 patients finished the trial. We consider that we achieved a correct ergonomy adaptation of the exoskeleton in order to optimize the patient comfort and wellbeing when placed inside the exoskeleton. For next trials focusing on measuring physical rehabilitation outcomes, we propose to increment the time, patients and frequency using the exoskeleton in order to provide significant outcomes in physical rehabilitation measures.

10.6 Conclusions and future works

This paper presents the results of the EXOtrainer project. In this project, the first wearable gait training exoskeleton, ATLAS 2020, has been developed for children with SMA type II. The research has focused on adapting the robotic device to physical therapy with a multidisciplinary approach. ATLAS 2020 is adjustable in size and includes 10 active degrees of freedom. Algorithms for the generation of synthetic trajectories have been developed to manage with the patient,s joints limitations. Impedance control allows detecting user intention for an assist as needed training. The clinical evaluation of the exoskeleton has been carried out in the Sant Joan de Deu hospital in Barcelona with 7 patients in a range of ages from 3 to 9 years of age. From this clinical trial, the inclusion criteria have been modified, since children with a very pronounced scoliosis and a range of motion in the hip, knees and ankle (flexor greater than 20°), had difficulties in using the exoskeleton. Of the 7 patients that started the clinical evaluation, 3 were excluded during the progress of the evaluation and 4 of them finalized the evaluation successfully. Therefore, the exoskeleton ATLAS 2020 is a device focused on the early stages of the disease, with the aim of delaying the onset of complications. Future experiments are focused on demonstrating the hypothesis that the children

recover or at least don't lose strength in their lower limbs while increases range of motion in their leg joints.

10.7 Acknowledgements

This work has been partially funded by the Spanish Ministry for Economy and Competitiveness through grant DPI2013-40504-R, EU FP7 Echord++ Exp 401 EXOTrainer, EXORAPI RTC-2016-4728-1 and by Marsi Bionics funds.

References

1. Mercuri, E., Bertini, E., Iannaccone, S.T.: Childhood spinal muscular atrophy: controversies and challenges. *The Lancet Neurology* **11**(5), 443–452 (2012)
2. Prior, T.W., Snyder, P.J., Rink, B.D., Pearl, D.K., Pyatt, R.E., Mihal, D.C., Conlan, T., Schmalz, B., Montgomery, L., Ziegler, K.: Newborn and carrier screening for spinal muscular atrophy. *American journal of medical genetics Part A* **152**(7), 1608–1616 (2010)
3. Markowitz, J.A., Singh, P., Darras, B.T.: Spinal muscular atrophy: a clinical and research update. *Pediatric neurology* **46**(1), 1–12 (2012)
4. Wang, C.H., Finkel, R.S., Bertini, E.S., Schroth, M., Simonds, A., Wong, B., Aloysius, A., Morrison, L., Main, M., Crawford, T.O.: Consensus statement for standard of care in spinal muscular atrophy. *Journal of child neurology* **22**(8), 1027–1049 (2007)
5. Mercuri, E., Finkel, R.S., Muntoni, F., Wirth, B., Montes, J., Main, M., Mazzone, E.S., Vitale, M., Snyder, B., Quijano-Roy, S.: Diagnosis and management of spinal muscular atrophy: Part 1: Recommendations for diagnosis, rehabilitation, orthopedic and nutritional care. *Neuromuscular Disorders* **28**(2), 103–115 (2018)
6. Finkel, R.S., Mercuri, E., Meyer, O.H., Simonds, A.K., Schroth, M.K., Graham, R.J., Kirschner, J., Iannaccone, S.T., Crawford, T.O., Woods, S.: Diagnosis and management of spinal muscular atrophy: Part 2: Pulmonary and acute care; medications, supplements and immunizations; other organ systems; and ethics. *Neuromuscular Disorders* **28**(3), 197–207 (2018)
7. Piccininni, M., Falsini, C., Pizzi, A.: Quality of life in hereditary neuromuscular diseases. *Acta neurologica scandinavica* **109**(2), 113–119 (2004)
8. Esquenazi, A., Talaty, M., Jayaraman, A.: Powered exoskeletons for walking assistance in persons with central nervous system injuries: a narrative review. *PM&R* **9**(1), 46–62 (2017)
9. Westlake, K., Patten, C.: Pilot study of Lokomat versus manual-assisted treadmill training for locomotor recovery post-stroke. *Journal of NeuroEngineering and Rehabilitation* **6**(1), 18 (2009)
10. Kolakowsky-Hayner, S.A., Crew, J., Moran, S., Shah, A.: Safety and feasibility of using the eksotm bionic exoskeleton to aid ambulation after spinal cord injury, pages 001–003 (2013)
11. Sanz-Merodio, D., Cestari, M., Arevalo, J.C., Garcia, E.: A lower-limb exoskeleton for gait assistance in quadriplegia. In: *IEEE International Conference on Robotics and Biomimetics*. Guangzhou, China (2012)
12. Cestari, M., Sanz-Merodio, D., Arevalo, J.C., Garcia, E.: An adjustable compliant joint for lower-limb exoskeletons. *IEEE/ASME Transactions on Mechatronics*, 889–898 (2015)
13. Sancho-Perez, J., Perez, M., Garcia, E., Sanz-Merodio, D., Plaza, A., Cestari, M.: Mechanical description of atlas 2020, a 10-dof pediatric exoskeleton. In: *Advances in Cooperative Robotics*, pp 814–822. World Scientific (2017).

14. Main, M., Kairon, H., Mercuri, E., Muntoni, F.: The Hammersmith functional motor scale for children with spinal muscular atrophy: a scale to test ability and monitor progress in children with limited ambulation. *European journal of paediatric neurology: EJPN: official journal of the European Paediatric Neurology Society* **7(4)**, 155-159 (2003)
15. Henricson, E.K., Abresch, R.T., Cnaan, A., Hu, F., Duong, T., Arrieta, A., Han, J., Escolar, D.M., Florence, J.M., Clemens, P.R., Hoffman, E.P., McDonald, C.M.: The cooperative international neuromuscular research group duchenne natural history study: glucocorticoid treatment preserves clinically meaningful functional milestones and reduces rate of disease progression as measured by manual muscle testing and other commonly used clinical trial outcome measures. *Muscle and nerve* **48(1)**, 55-67 (2013)
16. Lewelt, A., Krosschell, K.J., Stoddard, G.J., Weng, C., Xue, M., Marcus, R.L., Gappmaier, E., Viollet, L., Johnson, B.A., White, A.T., Viazzo-Trussell, D., Lopes, P., Lane, R.H., Carey, J.C., Swoboda, K.J.: Resistance strength training exercise in children with spinal muscular atrophy. *Muscle & Nerve* **52(4)**, 559-567 (2015).
17. Montes, J., Garber, C.E., Kramer, S.S., Montgomery, M.J., Dunaway, S., Kamil-Rosenberg, S., Carr, B., Strauss, N.E., Sproule, D., De Vivo, D.C.: A Randomized, Controlled Clinical Trial of Exercise in Patients with Spinal Muscular Atrophy: Methods and Baseline Characteristics. *Journal of Neuromuscular Diseases* **1(2)**, 151-161 (2014)
18. Montes, J., Garber, C.E., Kramer, S.S., Montgomery, M.J., Dunaway, S., Kamil-Rosenberg, S., Carr, B., Cruz, R., Strauss, N.E., Sproule, D., De Vivo, D.C.: Single-Blind, Randomized, Controlled Clinical Trial of Exercise in Ambulatory Spinal Muscular Atrophy: Why are the Results Negative?. *Journal of Neuromuscular Diseases* **2(4)**, 463-470 (2015)

Chapter 11

Technology for assisting during the Comprehensive Geriatric Assessment process: the ASSESSTRONIC project

Giuseppe Palestra, Consuelo Granata, Isabelle Hupont and Mohamed Chetouani

Abstract Comprehensive Geriatric Assessment (CGA) is a powerful tool to have a complete and exhaustive knowledge of patients' cognitive and physical health. The use of technology to conduct CGA would: i) reduce the time spent by clinicians; ii) increase the objectiveness and the transparency of the results. In this paper, we present the architecture of the ASSESSTRONIC platform, which aims to develop a robotic platform able to autonomously carry out and assist the caregivers during the CGA process. Two main aspects have been treated: the interaction for the cognitive tests and the mobility of the platform for the physical tests. Preliminary results of usability evaluation and reliability of cognitives and physical tests are given.

11.1 Introduction

The average age of the global population continues to grow thanks to a longer life expectancy. The World Health Organization (WHO) calculates that between 2015 and 2050, the world's population over 60 years of age will double [1]. Therefore, the global healthcare system has to adapt to the new demographic conditions.

In Echord++, the Public end-user Driven Technological Innovation (PDTI) in Healthcare is seeking for technical solutions to improve the Comprehensive Geriatric Assessment (CGA). CGA is a multidimensional, multidisciplinary diagnostic instrument designed to collect data on the medical, psychosocial and functional capabilities of elderly patients for diagnosis, treatment development and long-term follow-up plans. It is performed in medical offices and inpatient units by professionals involved in elderly people care, namely geriatricians, physiotherapists, occupational therapists, nurses, social workers, psychologists and neuropsychologists. CGA is a powerful tool to have a complete and exhaustive knowledge of patients' functional capabilities and cognitive and physical health and it can provide all the information required for adequate individualized care plans. However, the professionals have pointed out some issues that put at risk the efficiency and the accuracy of this assessment process.

Giuseppe Palestra, Isabelle Hupont, Mohamed Chetouani
Sorbonne Université, Institut des Systèmes Intelligents et de Robotique CNRS UMR7222, 4 Place Jussieu 75252 Paris Cedex 05, FRANCE e-mail: giuseppepalestra@gmail.com

Consuelo Granata
ACETIAM, 11 Rue du Bois de Soeuvres, 35770 Vern-sur-Seiche, FRANCE e-mail: consuelo.granata@gmail.com

A CGA well performed takes approximately 2.5 hours and a periodical review is needed (approximately every 6 months). Thus, considering also the increasing demand, it is very expensive for the care providers and requires a lot of resources involved. That is why most geriatric assessments, performed under the constraints of time and money, tend to be less comprehensive and accurate [2].

Usually, the process requires professionals' to use supporting devices (frequently a computer) or to take note of the observations, which sometimes had a negative impact on the quality of interaction between health professionals and patients/relatives because of the visual contact loosing. The communication is frequently interrupted, and the patients feel that health professionals are more focused on their computer or notes than to them.

Some of the CGA standard tests require the health professional to interpret the results because of the lack of objective and quantitative parameters for scoring the patient's status. The same test, for the same patient, can have different results if performed by different health professionals.

Additionally, some patients experience discomfort and stress while performing a test in presence of a doctor because they feel judged and under exam. Many patients tend to overestimate or underestimate their actual daily life capabilities because of shame or simply lack of objectiveness [3]. Frequently, the results from questionnaires about daily activities filled-in by the patients and by their relatives/carers do not match at all.

On the one hand, an automation of the process achieved by using a technology solution is highly suitable for absorbing the demand without compromising on the quality of the assessment and containing the costs. The use of technology to conduct CGA would considerably reduce the time spent by professionals with mechanistic tasks such as filling questionnaires while leaving more time to develop individualized care plans for their patients. An automatic approach is suitable for the parallelization of the tests as well. For instance, the patient and the relative can perform the requested tests without the need of involving members of the medical staff.

On the other hand, the use of an automated system instead of a human being should be felt as more neutral and not judgmental, which would have a positive impact on the exactness of the results and on the level of stress of the patients. Furthermore, an assessment made by a machine capable of collecting quantitative parameters for scoring the patients' performances, would increase the objectiveness and the transparency of the results.

Additionally, the use of sophisticated algorithms for the analysis of relevant signals such as voice, gaze and facial expressions, can provide rich and extremely meaningful information that it is not objectively observable by a human being.

Currently, although the efforts of many researchers in the fields [4], to the best of our knowledge, there is no robotic system on the market able to assist clinicians in taking CGA. Only few web applications have been introduced [5], but most of them are just limited to questionnaire-like forms and they require the online availability of the health professional. The functional tests (such as Tinetti and Berg tests, that measure a person's static and dynamic balance abilities), cannot be performed through these platforms as the professional needs to be physically close to the patient for a successful assessment.

Mobile applications are also available in the literature and they are usually used for cognitive evaluation [6], [7]. In Zorluoglu *et al.* [8] cognitive tests are implemented as an application for mobile devices that operates on Android OS.

These systems, mobile or online applications, are restricted to cognitive tests or physical tests. None of the proposed approach, in the recent literature, is able to address the CGA requirements to assist clinicians.

Along with ASSESSTRONIC project, Echord++ is financing CLARC project [9] to address the same issues related to the CGA process. CLARC consortium proposed a completely different approach compared to us [10]. They proposed a system composed of a mobile robot to assist health professionals during cognitive and physical tests and capable of moving into the environment autonomously.

ASSESSTRONIC approach is completely different because it finds all its powerful and efficiency on the modularity, the simplicity and the cost-effectiveness. The idea is to allow the use of the technology that is strictly necessary for each test, avoiding unnecessary complexity (and consequently costs). For instance, there is not need to use a complex and expensive mobile robot to

perform a cognitive-based test. The use of a mobile platform is strictly necessary for physical-based tests which require displacements bigger than 3 m (because of the limitations of the camera field of view). Besides, the need of having a robot with navigation capability has never been expressed by the clients, so we decided to not add any unnecessary complexity, and so unreliability, and unneeded extra-costs.

With this mindset, the ASSESSTRONIC consortium uses benefits of information and robotic technologies to make the execution of CGA process easier, faster, more accurate, traceable and repeatable. It focuses on providing added-value outputs in different, more objective and subtle dimensions, by analyzing the verbal (voice contents) and non-verbal (facial expressions and gaze) behavior of the subject while performing cognitive and physical tests. The outcome of the project could have a real impact on the geriatric community by offering a more efficient way of detecting and assessing fragile/dependent persons and partially address the dilemma of a growing aging population with less medical resources and/or insufficient funding/staffing.

The rest of the paper is further organized as follows. Section 2 provides a hardware and software overview of the ASSESSTRONIC platform. Section 3 and Section 4 present respectively cognitive and physical tests. Section 5 describes the experiments and the experimental results. Finally, conclusion are given in Section 6.

11.2 ASSESSTRONIC Platform Overview

The general requirement of a system for the CGA challenge is the ability to help the health professionals to decrease the amount of time spent on the clinical interviews (first phase of the CGA process) and on the geriatrics tests (second phase of the CGA process). This can be achieved by providing a completely autonomous solution, when feasible, and an efficient assistant, when the nature of the test compulsorily requires the presence of the health professional.

The ASSESSTRONIC platform is designed to perform autonomously or assist the caregivers during the CGA process for assessing medical, psychosocial and functional capabilities of elderly patients through physical and cognitive tests. We designed a modular solution consisting on several sub modules of different complexity both in terms of hardware and software. The idea is to allow the use of the technology that is strictly necessary for each test avoiding unnecessary complexity and consequently costs.

The ASSESSTRONIC platform is structured on 4 modules (see Fig. 11.1):

- the tablet PC where the ASSESSTRONIC Android app is installed. The app is the interface used by the health professionals, patients and relatives for performing the tests and accessing to patients' data;
- the workstation, a compact device for performing physical-based tests. It is used to perceive the patient's body movements;
- the mobile platform, embedding the workstation module. This allows the use of the the system for performing physical tests requiring big displacements of the patient (more than 3 meters);
- the server, which is where the intelligence of the system is located. The analysis of the collected data is performed by the server. Additionally, the server is used as database to store both processed and raw data.

With these 4 separate components, the system is highly modular and allow a very efficient tests parallelization optimizing the costs. In fact, 3 different configurations are available. The simplest (and cheaper) configuration of the system is composed of the tablet PC running the ASSESSTRONIC Android app and the access to the server. With this only 2 elements all the cognitive tests can be performed, and all patients' data can be processed, safely stored and accessible.

An intermediary configuration is composed of the tablet PC, the server and the workstation. It allows all the cognitive and physical tests, the latter, if the required movements are not bigger than 3 m (because of the camera field of view constraint).



Fig. 11.1: The 4 modules composing the ASSESSTRONIC platform: the tablet PC for interaction, the workstation for perception of the patients' movements, the mobile platform for physical-based tests requiring big displacements and the server, which store all data and runs analysis algorithms.

The most complex configuration consists of the use of all the modules shown in Fig. 11.1. The use of the mobile platform add a certain level of complexity and make the system costs increase, but it allows all the cognitive and physical tests.

The tablet PC communicates with the server to upload the data to store (tests results and raw collected data) and to load the data of the patients (results and personal/medical information). It also communicates with the workstation module to manage the physical-based tests. The workstation module communicate with the server as well to upload the information about the patient's movements and also with the mobile platform, when used, to control its displacement according to the patient's position. All the necessary back-end services for client software are provided as web API in REST style (see Fig. 11.2).

11.2.1 Tablet PC

The user interface is runnable on Android tablets. The app can be run on 3 different modes: Patient mode, to present the survey forms to be filled by the patient himself; Relative mode, to present the forms to be filled by the patient's relative; Physician mode, to present the survey forms to be filled by health professionals, to consult the tests results and configure the sequence of tests to be performed by each patient.

Also, the interfaces is used to display the tests results, to customize the tests sequence and to create new tests have been designed by following an user-centered approach. The doctors validated

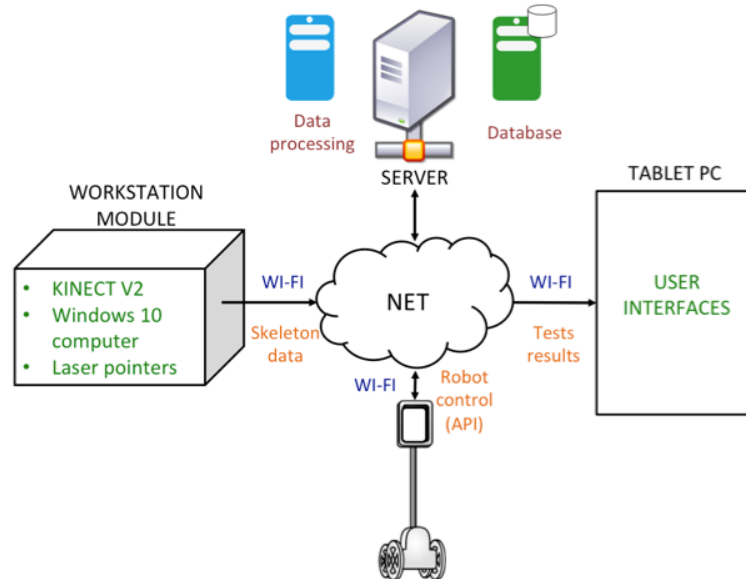


Fig. 11.2: Overview of the architecture of communication between the ASSESSTRONIC platform modules.

the proposed graphics aspects, the code colors to track the patient evolution and the edit system was considered ideal.

11.2.2 Workstation

The workstation module (see Fig. 11.3) includes a powered 3D camera (Kinect v2), a processor and a couple of laser pointers (with adjustable orientation) for running physical-based tests. The skeleton data provided by the Kinect is collected by the processor integrated on the workstation sent to the server for storage and analysis.

11.2.3 Mobile platform

In line with the requirement of keeping the costs of the system as low as possible, we have designed and developed a mobile platform capable of making mobile most of medical carts existing on the market. The design of this platform has been conceived in order to make it compatible with the majority of carts currently used worldwide. The idea is that this platform can be easily attached on the bottom of the cart, between the wheels (see Fig. 11.4), to lead the cart movements and that the workstation module is placed on the top table of the cart. In this configuration, the workstation processor, considering the position of the patient during the test, can control the platform movements



Fig. 11.3: The workstation module, used for perceiving patients' body movements during physical-based tests.

in order to optimize the perception of the patient's body during tests requiring significant movements (more than 3 m).



Fig. 11.4: From left to right: the ASSESSTORNIC mobile platform, a typical medical cart used in hospitals and the ASSESSTRONIC mobile platform mounted on a medical cart.

11.2.4 Server

The server is used both as database to store raw and processed data (videos, audio tracks, tests results etc.) and as processor to perform the analysis of the collected data (to compute both the physical and cognitive tests results).

11.2.5 Fulfilled Functions

The system has been designed and implemented in order to fulfill the following functions:

- Questionnaires-based tests. The solution is able to carry out autonomously or semi-autonomously (when the nature of the test compulsorily requires the presence of the health professional) the CGA questionnaire-based tests.
- Physical-based tests. The solution is able to track the patients' movements and to evaluate their performance during physical-based tests such as the Get Up & Go and the Tinetti tests. The parameters useful for evaluating the quality of the motion (i.e. speed, number of step, step length, frequency and so on) are collected, interpreted and stored.
- Dashboard. Health professionals can display raw and processed data, manually modify or correct tests scores, select the sequence of tests to include in an individual CGA, easy configure and add new tests.
- Data Management. Both raw and processed are stored safely, in an open format (also other than text) and are readable from free non-proprietary software (e.g. XML or CSV).

11.3 CGA cognitive-based tests

The patients' cognitive status is evaluated in CGA through several questionnaire or interview based tests. This assessment needs to be updated periodically (usually every 6 months), which means the monitoring of a patient is very time and resources consuming (between 2 and 3 hours per patient are needed to complete it). The automatization of these tests can bring many advantages to the medical staff: time saving, easy traceability of the status evolution, richer range of information (voice, facial expression, and gaze estimation). But there are also very delicate issues to handle carefully in particular because the end users are elderly people, often with cognitive troubles.

In order to evaluate specific aspects of the patient, five tests are included in the ASSESSTRONIC platform:

1. the Mini-Mental State Examination (MMSE) [11] is a test widely used in clinical evaluation to assess cognitive functioning taking into account age and education of the person;
2. the Barthel scale [12] measures performance or dependence in activities of daily living;
3. the Mini Nutritional Assessment (MNA) [13] is composed of brief questions and it provides an evaluation of nutritional condition in seniors persons;
4. the Geriatric Depression Scale (GDS) [14] is used to measure severity of depression in older adults;
5. the mini-Zarit [15] is a validated short version of the Zarit Burden Inventory and it is used to assess the subjective caregiver burden.

The cognitive tests are implemented in the Android app and it is installed on the tablet of the ASSESSTRONIC platform (see Fig. 11.5). Both the vocal and the graphic interfaces designs have followed an user-centered approach, taking into account main stakeholders: patients (i.e. elderly persons), relatives, and clinicians:

- basic usability/accessibility questions: elements and colors to be used, fonts and their size;
- design of the virtual character: they advised us to use a male embodied virtual character, dressed with clinician clothes (white coat), as it would result more reassuring and trustworthy to the user;
- sentences formulation: they checked every test question formulation, in order to reduce as much as possible any possible feeling of stress or being judged. E.g. for Barthel test questions, they proposed to replace the formulation "I am capable of [e.g. using the toilet]" by "I can [e.g. use the toilet]";

- voice interaction: for every test question and situation, they helped us to define the most appropriate timeline for voice interaction. E.g. what has to be said by the virtual character at each moment, how much time to wait for the user answer, how many times to repeat an instruction for some questions, etc.



Fig. 11.5: Screenshots of the ASSESSTONIC app during two cognitive tests.

A voice synthesis module serves, e.g., to guide patients through the accomplishment of the different tests via audio channel (OUTPUT). A voice detection module that allows detecting natural verbal answers (based on key-words detection) and interaction commands from the patients (INPUT).

Besides, language and touch, our solution is able to analyze in background (i.e. in a transparent manner for the user) other non-verbal relevant information, such as gaze behavior and facial expressions. This allows, e.g., to automatically detect the percent of time where the user focus of attention was in the test or elsewhere (quantitative measure of concentration/engagement), situations of stress, pain, depression, or the number hesitations while answering questions.

11.4 CGA physical-based tests

The Get Up and Go [16] test is one of the physical tests used in CGA for assessing physical mobility. It is considered useful in clinical assessment of change in functional status and in risk of fall estimation. The patient is asked to perform the following actions:

1. Sit comfortably in a straight-backed chair
2. Rise from the chair
3. Stand still momentarily
4. Walk a short distance (approximately 3 meters)
5. Turn around

6. Walk back to the chair
7. Turn around
8. Sit down in the chair

The health professional observes the patient's movements and gives a score from 1 to 5 using the following scale: 1 = Normal; 2 = Very slightly abnormal; 3 = Mildly abnormal; 4 = Moderately abnormal; 5 = Severely abnormal.

Such approach is certainly easy to set up, but, obviously, it lacks of accuracy, objectiveness and transparency. This problem has been partially addressed with the introduction of the Timed Get Up and Go test (TUG), which consists of considering the total time spent to achieve the 8 tasks as quantitative parameter to mark the performance. With the TUG, the assessment of the quality of the patients' movements is still based just on the personal judgment of the observer. Recent researches introduced sensor based methods for quantitative analysis of movement during the TUG [17]. These methods produce different ranges of parameters quantifying various attributes and phases of the TUG test.

Echord++ asked for a solution able to perform autonomously the Get Up and Go test in a non invasive, objective and repeatable fashion. The ASSESSTRONIC consortium proposed a Microsoft Kinect based solution, that is low-cost, non invasive at all for the patient and easy to set up. The 3-dimensional position of 25 body joints are extracted and used as input for the analysis algorithm. In order to keep the patient in the field of view of the Kinect, the sensor is embedded on a mobile platform (see Fig. 11.6) able to track his body during his displacements. The robotic platform is completely autonomously in performing this tracking task and any intervention of the medical staff is required.



Fig. 11.6: The mobile platform used for the digital physical tests.

Raw and processed data is recorded during the test in order to allow further analysis and to verify the results given by the algorithm in any moment.

The data collected all the test long is analyzed and used first of all to identify the different phases of the test. We have defined the 5 phases shown in Fig. 11.7:

- Phase 1 (P1): getting up from the chair

- Phase 2 (P2): standing before walking
- Phase 3 (P3): walking forward
- Phase 4 (P4): walking back
- Phase 5 (P5): sitting back on the chair

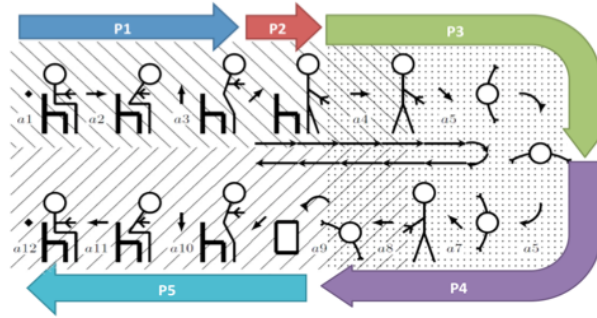


Fig. 11.7: The different phases we defined for the analysis of the patient's performance during the Get Up & Go test.

Then, the phases are analyzed separately considering different factors for the score computation (depending of the nature of the task): time (in relation to the patient's age), steps length, number of steps, steps frequency, velocity gait, arms swing amplitude and upper-lower body synchrony. Eventually, the overall performance is scored with the mentioned scale from 1 to 5.

Besides the observed patient's motion behavior, the performance could be analyzed by taking into account other sensorimotor and psychological factors. For instance, the patient's visual condition (acuity, contrast sensitivity and depth perception) as well as mood, pain, anxiety and depression have been proved to have a significant impact on the standing movement performance. Knowing these patient's details, the overall assessment of his mobility condition could be even more accurate.

Our system follows the standard for data protection, privacy and patient rights. The CGA platform meets the HIPAA (US) et EC requirements including the French laws for Hosting Health Data (Décret Hébergement Données de Santé).

11.5 Preliminary Results

This section is devoted to provide a first assessment of the ASSESSTRONIC platform. This evaluation consists of: i) a qualitative pilot study in order to assess the system usability during cognitive-based tests; ii) a quantitative experiment in order to evaluate the reliability and efficiency of the system performing physical-based tests.

11.5.1 Cognitive-based tests

Seniors are not familiar with new technologies such as tablets or robots. These difficulties in the use of technologies lead to a pilot study. The system usability, according to the user-centered design methodology, has been evaluated with a formative usability test. The scope of the pilot study is to collect feedback on the cognitive tests from participants of this phase. The test consisted in carrying out a session with the system to evaluate the cognitive tests implemented in the ASSESSTRONIC platform.

Initially, the system has been tested with 3 healthy graduate participants. All the participants were trying the system for the first time, after being properly informed, they had familiarity with tablets and robots. All participants have completed the three sessions successfully. Several suggestions about the Android app have been raised.

Furthermore, in order to perform a qualitative evaluation of the cognitive-based tests in a real environment, 3 experimental sessions have been performed involving all relevant stakeholders including the patients, relatives and clinicians. The experiments were carried out at an outpatient clinic in Paris where participants were recruited. Three participants were recruited: one patient, one relative (the husband of the patient), and one clinician. Generally speaking, the system was able to operate well in real environment for all the experimental sessions. The system usability has been evaluated thanks to the System Usability Scale (SUS). In total, 10 Likert-type items with a score ranging from 1 (strongly disagree) to 5 (strongly agree) were administered. At the end of the questionnaire, a debriefing was given to participants that stated suggestions to improve the app. Therefore, results, reported in in table 11.1, are expressed with SUS score that represents a composite measure of the overall usability of the cognitive-based tests of the system. Results can be considered as satisfactory for the first cognitive-based tests evaluation taking into account that SUS scores ranging from 0 to 100.

Table 11.1: Cognitive-based tests usability evaluation.

	Patient	Relative	Clinician
SUS Score	65	90	82.5
Age	78	80	—

11.5.1.1 Facial Expression Recognition

During cognitive-based tests the ASSESSTRONIC platform is able to recognize facial expressions.

Our facial expression recognition algorithm is able to identify six basic emotions: anger, disgust, fear, happiness, sadness, and neutral. The algorithm processes, frame by frame, the video recorded by the camera of the tablet PC. The pipeline of our algorithm is composed of several modules following the approach described in Palestra et al. [18]. As a first step, a face is detected and then facial key points are detected. Once the facial key points are detected, they are given as input to extract the facial features and finally the features are used to classify the facial expression. In order to implement this pipeline, the first step uses the well-know Viola and Jones face detector [19], that achieves high detection performance. Then, facial key points detection based STaked Active Shape model (STASM) [20], an approach for locating key points of human faces, is used. STASM uses Active Shape Model for locating facial landmarks with a simplified form of SIFT descriptors and Multivariate Adaptive Regression Splines (MARS) [20] for descriptor matching. 77 key points are detected and they are used to localize important regions of the face, such as: eyes, eyebrows,

nose, and mouth. Subsequently, the facial key points are employed to compute 41 geometrical facial features. The algorithm uses 4 types of geometrical features: linear, polygonal, elliptical, and angular (see Fig. 11.8). They describe and represent the face and are used to classify facial expression.

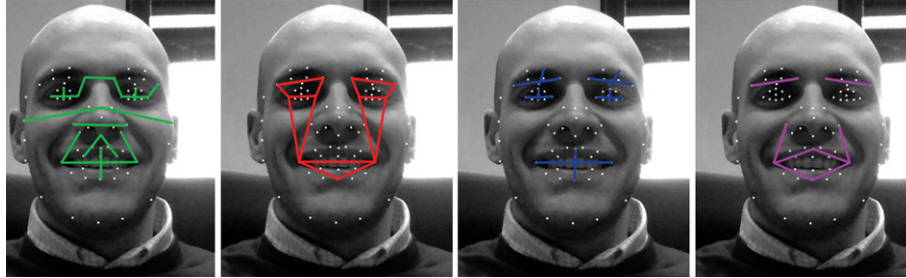


Fig. 11.8: Geometrical facial features that describe the face (from left to right): linear, polygonal, elliptical, and angular.

In order to train and test our classifier two datasets have been used: the Extended Cohn-Kanade (CK+) dataset [21] and the FACES dataset [22]. To obtain a balanced dataset anger, disgust, fear, happiness, sadness, and neutral image emotions have been extracted for both datasets. From the former dataset, that comprising 123 (18 to 50 years of age) individuals performing facial expressions, all individuals were selected. Because of the specific application of the algorithm (facial expression recognition during cognitive-based tests with seniors), from the latter dataset 57 older women and men ($M=73.2$ years, $SD=2.8$; age range=69 - 80) were selected for training and test our classifier.

The algorithm reached an average recognition rate of 70% using Multi Support Vector Machines classifier implemented in the LIBSVM library with a Radial Basis Function (RBF) kernel (penalty parameter $C = 1000$ and $\gamma = 0.5$).

11.5.2 Physical-based tests

The performance of the system in perceiving and analyzing body movements during the Get Up and Go test have been evaluated with 4 healthy adults. Each participant has been asked to perform the test 3 times. For each trial, we imposed the step length by spotting the exact distance between each stride with colored tape on the floor. Also the frequency has been imposed by using a metronome. In total, 3 different step lengths and 3 different frequencies have been tested. All the sessions have been filmed in order to have a ground truth time wise.

The goal of the experiment is to assess the performances of the algorithm to compute the following parameters:

1. duration of the 5 phases (see Fig. 11.7);
2. average steps length;
3. number of steps;
4. average steps frequency.

The real duration of each phase has been measured manually directly from the video. The frequency, step length and the number of steps have been imposed with metronome and tape (the number of steps can be observed directly from the video as well).

The average errors for all the analyzed parameters and the standard deviations are shown in Fig. 11.9. We discussed these results with health professionals and they considered totally acceptable the output of the system. They judged the system very accurate and fulfilling their expectations.

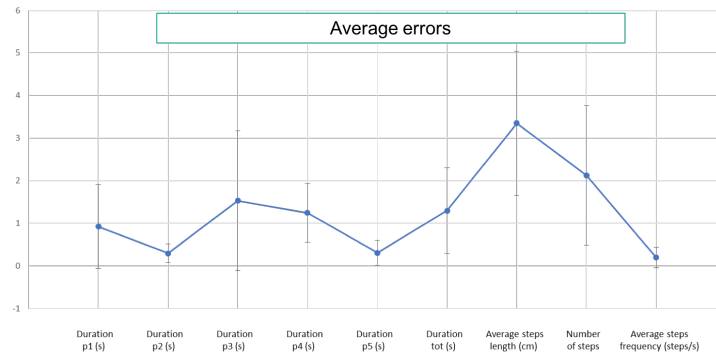


Fig. 11.9: Average errors with standard deviation for all the analyzed parameters.

In order to have an even more accurate assessment of the system performance during the physical-based tests, we are planning additional tests using a MoCap system, the CodaMotion [23], to evaluate the accuracy of the parameters indicated above, but also other such as the arms swing amplitude. The global score issued from the algorithm need also to be compared with the marks from different health professionals in order to verify the consistency of the system.

11.6 Economic viability

A question widely ignored from the academic side of social robotics/agents, but that has nevertheless a great impact in Society, is how to transform academic findings into real market opportunities. To ensure that ASSESSTRONIC platform can be used in the real world and meet the market demands, the economic implications of implementing and operating a machine for assisting during the CGA process have been carefully discussed with health professionals from France and Spain.

11.6.1 Key features

The principal key features that have been tackled are:

- **User Experience and Social Acceptance.** The solution is not invasive for the patient: the patient's position and orientation during the tests cannot be constraint too much, he/she doesn't have to wear special equipment such particular clothes, wristbands, etc. The system usability and accessibility have been assessed and validated by a multidisciplinary team made of engineers, psychologists, psychiatrists, geriatricians and neuropsychologists.
- **Portability.** The solution is manageable by one person to be moved around at the clinic.

- Modularity and scalability. The solution is modular and scalable in order to facilitate an international deployment as potential extent.
- Mobility. The mobile platform guarantees the constant visibility of the patient to increase the quality of the information (signal / noise ratio) gathered by the sensors, which would also simplify the signals processing and improve the algorithms performances.

11.6.2 Impact

The outcome of the project could have an impact on the geriatric community by offering a more efficient way of detecting and assessing fragile or dependent persons and partially address the dilemma of a growing aging population with less medical resources or insufficient funding and staff. Given the poor financial capabilities of the institutions in charge of elderly dependent persons, and/or the low level of reimbursement of medical acts, commercial plan for this technology will focus on:

- obtaining support from the geriatric community as a new standard for Geriatric Assessment;
- obtaining public financing to equip the thousands of french institutions dedicated to dependent elderly people;
- negotiating with the few major players in France that operate Private Care institutions;
- convincing Private Health Insurances companies to co-fund large deployment programs;

Also, to avoid distribution barriers due to costly solutions, our approach will leverage existing low-cost technologies (such as cameras, Kinect systems, standards computers and devices).

11.6.3 Targeted market segment

We also plan to expend the commercial scope of this technology beyond the Hospitals and the institutions in charge of elderly dependent persons by addressing other market segments:

- the Home Care emerging segment by coming up with cost effective / software based only application of this technology;
- the international geriatric market through distribution agreements;
- as an add-on to telemonitoring solutions through licensing of the technology;
- creating new evaluation approaches leveraging the latest technologies;
- integration into other geriatric assessments solutions.

It came out that the economic sustainability is ensured with a solution that does not exceed 8K €. The first developed prototype costs 7K €. This price will considerably decrease for larger production (a reasonable estimation of the final hardware costs is around 2.5K €). We can estimate that the final cost of a platform including costs for software licenses will not exceed 3K €.

11.7 Conclusions and future work

In this paper we presented the ASSESSTRONIC project, which aims in developing a system able to autonomously carry out and assist the caregivers during the CGA process. Two main aspects have been treated: the interaction for the cognitive tests and the mobility of the system for the physical

tests. The interfaces for the cognitive tests consist on a combination of voice recognition and GUI for allowing a natural and reliable interaction with the patients.

A reliable motion analysis based on a low-cost and non invasive sensor (Kinect) is performed with a mobile robotic platform. The current version of the analysis algorithm is able to analyze some quantitative parameters to give an objective score to the quality of the patients' movements. Besides the observed patient's motion behavior, the performance has to be analyzed by taking into account other sensorimotor and psychological factors. For instance, the patient's visual condition (acuity, contrast sensitivity and depth perception) as well as mood, pain, anxiety and depression have been proved to have a significant impact on the standing movement performance. The data protection system of the solution is already conform with the international standard rules.

In future work, we will investigate if the tests made with the ASSESSTRONIC platform give the same results of the traditional CGA. An additional effort in the development of the results display and the global integration of all the functionalities on the same platform needs to be done.

Acknowledgements This work has been partially funded by the European Union ECHORD++ project (FP7-ICT-601116).

References

1. World Health Organization. "Fact sheet 404 september 2015". <http://www.who.int/mediacentre/factsheets/fs404/en/> Retrieved April 24, 2018
2. World Health Organization et al.: Global strategy on human resources for health: workforce 2030 (2016)
3. Lachman, M.E., Jelalian, E.: Self-efficacy and attributions for intellectual performance in young and elderly adults. *Journal of Gerontology*, **39**(5), 577-582 (1984)
4. Wrobel, J., Pino, M., Wargnier, P., Rigaud, A.S.: Robots and virtual agents to assist older adults: A review of present day trends in gerontechnology. *NPG Neurologie-Psychiatrie-Gériatrie* **14**(82), 184-193 (2014)
5. Rocha, A., Martins, A., Freire, J.C., Boulos, M.N.K., Vicente, M.E., Feld, R., van de Ven, P., Nelson, J., Bourke, A., ÓLaighin, G., et al.: Innovations in health care services: The caalyx system. *International journal of medical informatics* **82**(11) (2013)
6. Areán, P.A., Ly, K.H., Andersson, G.: Mobile technology for mental health assessment. *Dialogues in clinical neuroscience* **18**(2), 163 (2016)
7. Laput, V., Berauk, A., Murugiah, M.K., Soh, Y.C., Sheng, Y.C., Wong, T.W., Chiau Ming, L.: Mobile health applications for caring of older people: Review and comparison. *Therapeutic Innovation & Regulatory Science*, page 2168479017725556 (2017)
8. Zorluoglu, G., Kamasak, M.E., Tavacioglu, L., Ozanar, P.O.: A mobile application for cognitive screening of dementia. *Computer methods and programs in biomedicine* **118**(2), 252-262 (2015)
9. Bandera, A., Bandera, J.P., Bustos, P., Calderita, L.V., Duenas, A., Fernández, F., Fuentetaja, R., Garcia-Olaya, A., Garcia-Polo, F.J., González, J.C. et al: Clarc: a robotic architecture for comprehensive geriatric assessment. In: *Proceedings of the 17th Workshop of Physical Agents (WAF)*, pp 1-8 (2016)
10. Ting, K.L.H., Voilmy, D., Iglesias, A., Pulido, J.C., García, J., Romero-Garcés, A., Bandera, J.P., Marfil, R., Dueñas, A.: Integrating the users in the design of a robot for making comprehensive geriatric assessments (cga) to elderly people in care centers. In: *Robot and Human Interactive Communication (RO-MAN)*, 2017 26th IEEE International Symposium on, pp 483-488 (2017)

11. Folstein, M.F., Folstein, S.E., McHugh, P.R.: “Mini-mental state”: a practical method for grading the cognitive state of patients for the clinician. *Journal of psychiatric research* **12**(3), 189-198 (1975)
12. Mahoney, F.I., Barthel, D.: Functional evaluation: the barthel index. *Maryland State Medical Journal* **14**, 56-61 (1965)
13. Vellas, B., Guigoz, Y., Garry, P.J., Nourhashemi, F., Bennahum, D., Lauque, S., Albarede, J.L.: The mini nutritional assessment (mna) and its use in grading the nutritional state of elderly patients. *Nutrition* **15**(2), 116-122 (1999)
14. Sheikh, J.I., Yesavage, J.A.: Geriatric depression scale (gds): recent evidence and development of a shorter version. *Clinical Gerontologist: The Journal of Aging and Mental Health* (1986)
15. Zarit, S.H., Todd, P.A., Zarit, J.M.: Subjective burden of husbands and wives as caregivers: a longitudinal study. *The Gerontologist* **26**(3), 260-266 (1986)
16. Podsiadlo, D., Richardson, S.: The timed “up & go”: a test of basic functional mobility for frail elderly persons. *Journal of the American geriatrics Society* **39**(2), 142-148 (1991)
17. Sprint, G., Cook, D.J., Weeks, D.L.: Toward automating clinical assessments: A survey of the timed up and go. *IEEE reviews in biomedical engineering* **8**, 64-77 (2015)
18. Palestra, G., Pettinicchio, A., Del Coco, M., Carcagnì, P., Leo, M., Distant, C.: Improved performance in facial expression recognition using 32 geometric features. In: *International Conference on Image Analysis and Processing*, pages 518–528. Springer (2015)
19. Jones, M., Viola, P.: Fast multi-view face detection. *Mitsubishi Electric Research Lab TR-20003-96* **3**(14), 2 (2003)
20. Milborrow, S.: Active shape models with stasm. *Stasm Version 3* (2009)
21. Lucey, P., Cohn, J.F., Kanade, T., Saragih, J., Ambadar, Z., Matthews, I.: The extended cohn-kanade dataset (ck+): A complete dataset for action unit and emotion-specified expression. In: *Computer Vision and Pattern Recognition Workshops (CVPRW)*, 2010 IEEE Computer Society Conference on, pp 94-101 (2010)
22. Ebner, N.C., Riediger, M., Lindenberger, U.: Faces—a database of facial expressions in young, middle-aged, and older women and men: Development and validation. *Behavior research methods* **42**(1), 351-362 (2010)
23. Codamotion system: <http://www.codamotion.com/> Accessed: 2016-09-06.

Chapter 12

ARSI: An Aerial Robot for Sewer Inspection

François Chataigner, Pedro Cavestany, Marcel Soler, Carlos Rizzo, Jesús Pablo Gonzalez, Carles Bosch, Jaume Gibert, Antonio Torrente, Raúl Gomez and Daniel Serrano

Abstract In this chapter we present the Autonomous Robot for Sewer Inspection (ARSI), a robotic system designed to make the work of inspection brigades safer and more efficient. ARSI uses an autonomous Micro Air Vehicle (MAV) to collect HD imagery and structural data in the sewers, while operators remain on the surface to supervise missions.

Our compact quadrotor design is lightweight and robust, with a flight autonomy of 15 minutes and a payload capacity of 1kg. It can be deployed without any special equipment, and operates in sewer tunnels as narrow as 80cm. The sensor payload collects inspection data as well as inputs for the onboard software, allowing the ARSI MAV to follow pre-planned inspection paths autonomously. User-friendly interfaces are provided to plan, execute, and monitor sewer inspections. Data collected by the MAV onboard sensors is processed by our offline algorithms to generate detailed 3D models of the sewers, and perform automatic visual and structural analysis. Our data analysis software allows ARSI users to review all information and generate inspection reports for their clients. Our system was tested and validated during rigorous field tests in the city of Barcelona, Spain.

Key words: autonomous, robot, sewer, inspection, MAV, drone, structural defects, detection, communications

12.1 Introduction

The sewer network is one of the essential infrastructures of a city, which must be inspected methodically to monitor for structural defects such as fissures or breaks in the walls. However, sewer inspections are notoriously hazardous and time-consuming tasks. Inspection brigades work in darkness and high humidity, surveying vast tunnel networks where low ceilings often cause posture-related injuries, potentially in the presence of toxic or explosive gases.

ECHORD++, the European Coordination Hub for Open Robotics Development, in collaboration with BCASA¹ in Barcelona, Spain, proposed to develop a robotic system to increase the safety and efficiency of sewer inspections. Under the Urban Robotics PDTI² (Public end-user Driven Technological Innovation program), ECHORD brought together researchers, industrial partners and

EURECAT Technology Center, Barcelona, Spain
www.eurecat.org

¹ www.bcasa.cat

² www.echord.eu/pdti/pdti-urban-robotics-sewer-inspection

end-users with the goal of transferring research technology into applicable, tested sewer inspection solutions ready to be deployed on the market.

In this chapter we present the Aerial Robot for Sewer Inspection (ARSI), which addresses this challenge using an autonomous Micro-Air Vehicle (MAV). The key advantage of our system is that it can be operated from the surface, so that inspection brigades are no longer exposed to the hazards of work in the sewers. We begin by describing the state of the art of the research in this area. In this section we make clear what are our main contributions to the literature. In the following section we detail our Concept of Operations, developed in close collaboration with inspection professionals to ensure that our system is practical and adapted to real-world sewer environments.

Sewer tunnels are challenging environments for MAVs to navigate, due to the total darkness, the narrow dimensions of the tunnels, and the ubiquity of sewage water. Furthermore, external localisation systems such as GPS do not reach the sewers, and their topology makes localisation a complex task due to the scarcity of structural features.

In the rest of this work we present our solutions to each of these challenges, in particular our quadrotor design which meets the operational requirements while remaining compact, robust and lightweight. We present our sensor payload for data collection, localisation and navigation; as well as the onboard algorithms which allow our MAV to execute mission plans autonomously. We describe our offline algorithms to process sensor data collected by the MAV in the sewers and generate new data products, such as 3D models and automated structural analysis. Finally we present our visualisation interface, which allows ARSI users to review and analyse all inspection data in order to generate comprehensive inspection reports for their clients.

We conclude this chapter by presenting results from the field trials and validation tests carried out in Barcelona, and we outline our future work for the remainder of this project.

12.2 Related work

In recent years, the application of Unmanned Aerial Vehicles (UAV) for inspection and asset monitoring has been confirmed as a cost-effective, safe, and efficient approach in the infrastructure inspection industry. The importance for inspection of robotics systems is exemplified by the growing number of startups and companies which offer UAV-based asset monitoring solutions in a large range of critical areas: Microdrones, DroneViewTech, Sky-Futures [1], Industrial SkyWorks [2], Cyberhawk [3], etc. Cyberhawk remarkably covers hazardous environments and has developed an asset management software. Sky-Futures and Industrial SkyWorks make use of AI applied to imagery to generate industrial inspection analytics from UAV data. However, the majority of UAV-based service providers perform manually controlled missions. Autonomous navigation is yet to be settled in this sector, even though it would multiply the service and simplify its operation. An example of this is AIRobotics [4], which proposes an all-in-one autonomous UAV solution for periodical industrial surveying and inspection in open spaces.

Another evidence of the assimilation of UAV to the inspection industry is the celebration of a variety of contests and challenges in this respect. Specifically, the ARGOS challenge [5] with the involvement of ground robots, and the European Robotics Challenge (EuRoC) [6], in particular Challenge 3 addressing industrial site inspection with autonomous drones. Recently UAV have even been equipped with active tools for tasks of maintenance, as two European Projects, AEROARMS [7] and AEROWORKS [8], demonstrate. They develop the idea of UAV with manipulating skills that can work collaboratively in a team. In the context of inspection and monitoring of confined spaces, ROBO-SPECT European project [9] adapts recent research in robotics and computer vision to automatically assess tunnels stability, by means of a ground robot with an automatic robotic arm.

Sewers are a critical infrastructure for the good functioning of cities, and they must be maintained and supervised periodically. There is an established industry that deploys ground robots for assessing sewers of small diameter. EnviroSight [10], IBAK [11] and Aries Industries [12] are leaders in the sector with their tethered robots, which are capable of issuing full inspection reports. However,

untethered robotic systems (and therefore, autonomous) provide more functionality. RedZone has launched SOLO [13], a non-tethered robot that navigates autonomously based on image sensors and makes use of a specific software to plan a given mission inspection. Moreover, there exists robots able to perform small repairs in sewers, like KA-TE [14], a filler robot which realises root removal and crack repair in small sewers. Such a great demand for defect inspection in water infrastructures has recently fostered automated solutions based on deep learning techniques to detect anomalies in sewer pipes, such as the system presented by Inloc Robotics [15]. Alongside software solutions, the utility of UAV in spaces of difficult access has been acknowledged by the industry as well. SafeFlight [16] and DJI Aerial solutions [17] are companies specialised in confined space drone inspections, however their missions are executed by manual navigation. Autonomous navigation in pipes has been addressed by GRASP laboratory (University of Pennsylvania, USA) with an autonomous UAV which navigates and maps penstocks (3-5m diameter) [18].

In this work we present an autonomous UAV capable of navigating narrow sewers, equipped with sensors to generate imagery and 3D maps of the inspected area, while keeping a visual data link with the operator. Our solution also includes software to detect structural and volumetric defects in the sewers.

12.3 Concept of operations

In Barcelona, the standard procedure for sewer inspection is that brigades are assigned series of sewer sections that they should visit each day, to perform visual inspection of structural defects such as fissures or cracks and report any anomaly. For safety reasons, inspectors must travel the sewers in pairs while two colleagues follow them on the surface, opening and closing manholes along their route to provide ventilation as well as an exit in case of an emergency, in particular if dangerous gas concentrations are detected using hand-held monitors.

In the ARSI Concept of Operations, inspection brigades do not need to travel in the sewers, other than to briefly enter manholes to replace the MAV battery between flights. Risks of exposure to toxic gases are therefore greatly minimised, as are posture-related injuries which are frequent due to the narrow dimensions and low ceilings of most sewer tunnels. Each day, an ARSI team is assigned a series of flights (or *missions*) to execute with the MAV. These missions are planned in advance to divide inspection work for a given area between brigades over a number of days. Each flight starts and ends at an entry point into the sewers (typically a manhole).

At the beginning of the day, the team deploys the ARSI MAV in the sewers via a manhole. This does not require any special equipment, since the platform is lightweight and compact (see section 12.4.2). A WiFi access point is also deployed in the manhole and connected to the Operator Console on the surface.

The console is divided into various panels allowing operators to monitor the progress of the ARSI MAV along the mission path, as well as battery status and live video feedback transmitted over the WiFi link (see figure 12.1). Operators can perform high-level actions such as starting the mission (take-off), or pausing the flight to observe and report a possible structural defect. Low-level navigation and execution of the missions is carried out autonomously onboard the MAV.

After each flight, the MAV automatically lands below the chosen entry point in the sewer. A team member then enters the sewer (typically via a manhole) to change the battery and perform a rapid sanity check of the platform. The team member then returns to the surface and proceeds to executing the next flight from the Operator Console. Only two team members are required to operate the ARSI system.

All inspection data generated by the onboard sensors during ARSI missions is stored on high-capacity SD cards. The inspection data is passed on to the data analysis team back at base for analysis using our post-processing tools, to generate data products and inspection outputs for the clients (see section 12.5). Inspection data formats were chosen to be easily stored by sewer maintainers in a database, so that the evolution of the sewer network may be tracked and documented.

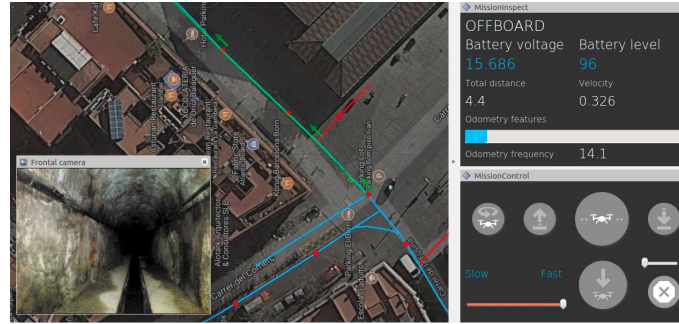


Fig. 12.1: ARSI Operator Console with video feedback, mission status and flight controls

12.4 Autonomous Navigation in sewers

Piloting a MAV manually in narrow sewer tunnels is very difficult even for experienced operators, due to the minimal clearance and low ceilings, the darkness, and additional complexities such as manhole ladders or service pipes obstructing the flight path. The ARSI MAV must therefore be able to operate autonomously to follow predefined inspections plans.

In this section, we present the different hardware and software elements of our strategy for autonomous navigation, from the platform design and sensor payload, to the real-time planners and obstacle avoidance.

12.4.1 Sensor payload

Our inspection payload comprises two Intel Realsense RGB-D (colour and depth) cameras, mounted at the front and back of the MAV, as well as two lateral HD cameras with fisheye lenses dedicated to the detection of defects on the sewer walls. Since our system normally operates in total darkness, each camera has its own set of LED lights for illumination. Other sensors can seamlessly be included in the payload to meet client requirements, within the weight capacity of our platform. For example, gas detectors could be added to measure concentrations of toxic gases such as hydrogen sulphide or carbon monoxide, which are frequently found in sewer tunnels.

The RGB-D cameras are also used as navigation sensors, providing visual and depth information for path planning, visual odometry and obstacle avoidance. They are complemented by a 2D laser providing close-range information about the immediate surroundings of the MAV, and compensating for the narrower field of view of the RGB-D cameras. Finally, a high-frequency infrared sensor provides ground range measurements for altitude control. Our payload has a total weight of 1kg, including an Intel NUC computer for onboard processing, a Pixhawk autopilot for low-level control, plus all cables and electrical components.

12.4.2 MAV design

Even though battery technology is improving rapidly, MAV systems are often limited by their relatively short flight autonomy. In this project in particular, the narrow sewer tunnels impose that our MAV platform remains very compact, which in turn restricts the propellers size and motors available to us, and therefore the weight capacity of the system. Other robotics systems such as ground robots have fewer weight limitations, allowing them to carry multiple batteries and operate for several hours.

Furthermore, having to change batteries affects sewer inspection brigades, since it requires that operators access the MAV in the sewers via a manhole which typically involves interrupting road traffic. Flight autonomy is therefore critical for the viability of operations with ARSI: by increasing autonomy we allow operators to choose the best access points for their missions, and to improve the overall inspection efficiency.



Fig. 12.2: ARSI quadrotor design with overlapping propellers

In partnership with drone manufacturer DroneTools³, we developed the innovative quadrotor design shown in figure 12.2. DroneTools used 13-inch propellers and powerful motors to deliver a flight autonomy of 15 minutes with a payload capacity of 1kg. The propellers have a 40% overlap so that the platform remains very compact; and a lightweight carbon fibre frame provides full protection against contact with the sewer walls. A central area provides mounting space on two levels for the onboard PC, the Pixhawk autopilot, and other electronic components. This central area is designed to protect critical components from exposure to dust or sewage water. A 6-cell 7000mAh lithium-polymer (LiPo) battery is mounted in a protective case underneath the platform.

Our MAV design is 62cm wide and 81cm long and has a total weight of 3.5kg including payload and battery, so that it can be deployed easily through standard manholes without any special equipment. It is able to navigate in all tunnels at least 80cm wide, which represents 39% of all sewers in Barcelona, covering a total of 612km. Another 23% of sewers in Barcelona (covering 360km) are >80cm at their widest point but narrower in other parts, typically at ground level (many sewer sections have slanted walls, see for example figure 12.3). As our system becomes more robust, we hope to extend our inspection capability to a large portion of these narrower tunnels.

Both the MAV frame and sensor payload are symmetrical, so that our system can seamlessly navigate forwards or backwards. This capability will give inspection brigades flexibility when

³ www.dronetools.es

planning flights, for example to simplify operations by having the MAV return to the deployment point, even in a sewer tunnel too narrow for the platform to perform a turn.

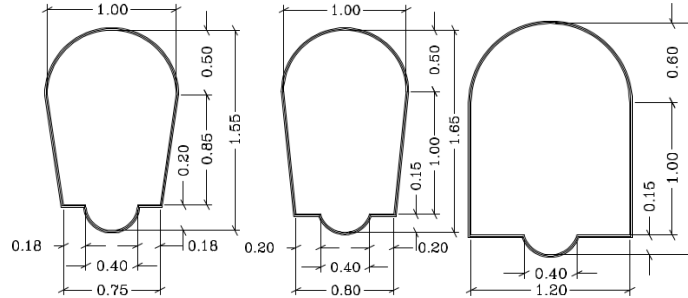


Fig. 12.3: Sewer section types encountered during our tests in Barcelona.

12.4.3 Communications

Propagation in tunnels differs from regular indoor and outdoor scenarios. For operating frequencies high enough with free space wavelength much smaller than the tunnel cross-section dimensions, tunnels behave as hollow dielectric waveguides. This allows extending the communication range, but affects the signal with the appearance of strong spatial fadings. Depending on the transmitter-receiver setup (i.e. frequency, position), these spatial fadings can be predictable and periodic, which subsequently can be used for network planning and deployment, navigation under connectivity constraints, and even for localisation purposes. For a detailed explanation about this phenomenon, see [19, 20].

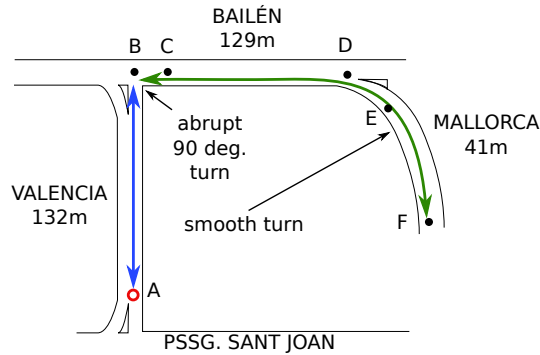


Fig. 12.4: Sewer environment for the communications tests.

In this section we summarise the results of extensive communications field tests carried out in a sewer scenario in Barcelona. A detailed analysis of the results presented here can be found in [21].

In our tests we established an ad-hoc network to collect information about the measured received power and bandwidth. The communication nodes (base station - tx and, mobile receiver - rx) are composed of a laptop with an external WiFi network card (Ralink rt2770 chipset), with a sensitivity of -95 dBm. The tests were conducted at 2.4 and 5.2 GHz, with the transmitter broadcasting frames every 5ms at a power of 20 dBm. All antennas used were dipoles, with a 2.15 dBi gain. The transmitter was placed at different points according to the test, and will be specified in each case. The test scenario is shown in figure 12.4.

12.4.3.1 Propagation along straight segments

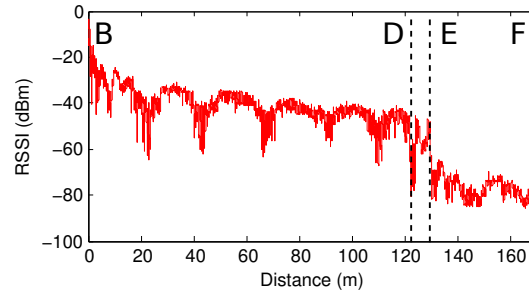


Fig. 12.5: Measured Received Power at 2.4 GHz along different segments of the sewer.

At first, the transmitter was placed at point B (see figure 12.4), and the receiver was displaced from point B to point F , along more than 150 meters from the transmitter, logging the RSSI. Results are shown in figure 12.5. In the straight segment (from B to D), we can appreciate spatial fadings with a period of about 22m, and an attenuation of about 9 dB in 100m. The free space path loss at 2.4 GHz is approximately 82 dB for a 132m long path.

With these results, we corroborate both the waveguide behaviour, which allows to greatly extend the coverage in comparison to free space, and the presence of fadings.

12.4.3.2 Propagation across smooth turns

Along the smooth turns (D to F in figure 12.4), it can be seen that at point E (where the LoS with the transmitter is lost), the signal suffers great attenuation. Nevertheless, the received signal still remains above the sensitivity of the receiver. This means that the smooth turn guides the wave softly, making it able to provide communication coverage with a perpendicular street.

12.4.3.3 Propagation across 90 degree abrupt turns

Following the previous test, the receiver was moved from point B to point C , while the transmitter was kept at point A . In this condition, we have non LoS between the transmitter and the receiver. As soon as the receiver loses the LoS with the transmitter, the connectivity is lost (in less than 3

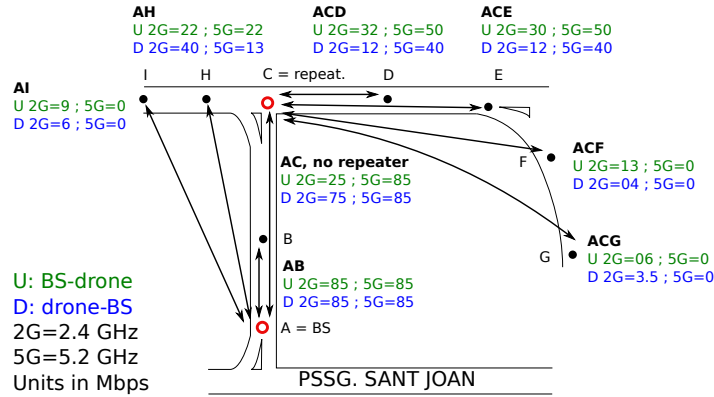


Fig. 12.6: Bandwidth measurements results. The letter U represents the BS-drone link, while letter D represents the contrary. 2G and 5G represent the frequency, 2.4 and 5.2 GHz respectively. The units are represented in Mbps and the bold letters represent the path.

meters). No results are shown, due to the fact that if a frame is not received, the RSSI cannot be determined (i.e. non-existence of RSSI=0).

12.4.3.4 Bandwidth Measurement

Following the wireless propagation characterisation, an extensive measurement campaign was performed to determine the bandwidth of the link between the robot (drone) and the base station (BS) ($tx \rightarrow rx$, $rx \rightarrow tx$), specifically in eight strategic points (A to I in Fig. 12.6), under LoS and N-LoS conditions, with and without the use of a network repeater to overcome the problems related to the 90 degrees abrupt turns. Two frequencies were tested: 2.4 GHz and 5.2 GHz.

To measure the bandwidth, the JPERF software was used⁴, which generates traffic to measure the capacity of the link by estimating the time required to send and receive large amounts of data. In each of the points, a sequential bi-directional link bandwidth measurement was performed. The drone was left static for a period of 120 seconds. In the first 60 seconds, the bandwidth of the BS-drone link was measured, followed by the drone-BS link. The base station was kept fixed at point A, and the repeater at point C. The drone was moved from point B through I.

Results are showed in Fig. 12.6. The letter U represents the upload link (BS-drone), while letter D represents the contrary. 2G and 5G represent the frequency, 2.4 and 5.2 GHz respectively. The units are represented in Mbps. As an example, U 2G=85 means BS-robot link, at 2.4 GHz, and the obtained mean bandwidth was 85 Mbps. Finally, the bold letters represent the path (eg. **AH** is the link between points A and H without using the repeater, while **ACG** is the link between A and G, passing through the repeater located at C).

⁴ <https://iperf.fr>

12.4.3.5 Summary

After the tests performed, we can summarise that:

- Under LoS conditions, the bandwidth is higher at 5.2 GHz compared to 2.4 GHz.
- As in the previous section, the signal is not able to make the abrupt 90 degree turn (point *C* + 3m towards point *D* in Fig. 12.6), at 2.4 GHz nor at 5.2 GHz.
- At 2.4 GHz, the smooth curved structure is able to guide the signal to the perpendicular street (point *A* to point *H* and *I*, or point *C* to point *F* and *G*).
- At 5.2 GHz, the signal is not guided by the smooth turn. This can be explained by the fact that the wavelength of the signal is much smaller and gets affected by surface irregularities and roughness.

These results demonstrate that, similar to road tunnels, periodic fadings are also observed inside sewers networks, with an attenuation that would allow the signal to cover several hundreds of meters at 2.4 and 5.2 GHz. Our bandwidth measurements also showed that the curvature radius in smooth turns, which are common in sewers network as they guide water towards a collection point, is large enough to softly guide propagation and overcome the turn for several meters. This allows operators to plan missions beyond intersections without requiring extra equipment such as WiFi repeaters. However this does not happen at a higher frequency (5.2 GHz), which might be due to fact that the wavelength of the signal is smaller and gets affected by the structure.

12.4.4 Localisation

In this section we present our strategy for real-time localisation of the ARSI quadrotor during operation. Knowing the location of the MAV is required both to execute pre-planned missions, and to allow geo-referencing of inspection data such as video, 3D reconstructions, or reported structural defects.

Note that sewer networks are deprived of external information such as GPS or cell towers, and that the permanent installation of localisation devices is not permitted. MAV localisation must therefore rely entirely on onboard sensors and static geo-referenced information such as maps or GIS databases provided by clients.

12.4.4.1 Multi-sensor estimation

Our main localisation sensors are 2 Intel Realsense RGB-D cameras mounted at the front and back of the MAV platform. The high-definition colour and depth streams generated by the cameras are used by an RGB-D visual odometry algorithm to estimate the robot velocity and trajectory in real time.

In this project, we used the open-source RTABMAP library [22] for RGB-D visual odometry. The algorithm extracts visual features from the colour stream and matches them against a cached keyframe using ORB descriptors [23]. Keyframes are updated when the distance travelled by the MAV exceeds a certain threshold. RTABMAP estimates the transform between these sets of matches using an iterative optimisation of 3D-2D point correspondences, from which the estimated MAV trajectory and instant velocity are derived.

The odometry solution generated from the RGB-D cameras is then fused with information from the other onboard sensors (accelerometers and gyroscopes in the Pixhawk autopilot, ground ranges from the infrared sensor) using a statistical filter included in the Pixhawk firmware [24].

12.4.4.2 Geo-localisation against GIS data

The MAV trajectory generated using RTABMAP and sensor fusion is relative to the initial position and orientation of the MAV at takeoff, while ARSI missions are planned referencing real-world GIS information (in particular sewer sections and access points). In this section we describe our method to relate the MAV-centric odometry to geo-referenced information extracted from maps or GIS databases of the sewer networks.

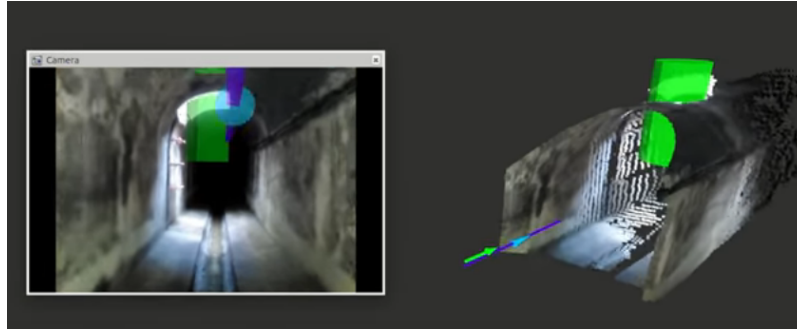


Fig. 12.7: Automatic manhole detection (in green) from RGB-D point clouds.

Sewer tunnels are a challenging environment for localisation because they are largely featureless, apart from sporadic landmarks such as manholes or intersections which are referenced in the GIS data provided by the clients. Manholes in particular are interesting features because of their standardised dimensions and relative frequency. We model manholes using a pattern comprising an empty volume (the manhole chute) and 4 non-empty volumes (the surrounding walls or roof). This pattern is matched against the depth data from the RGB-D camera, clustering consistent detections together. This algorithm was very successful in our test data (see figure 12.7), however some manholes were missed due to being outside the field of view of the forward RGB-D camera.

We use a particle filter approach to model the MAV location as it executes a mission. Since sewer networks are well-mapped and confined environments, we simplify the localisation problem by limiting the propagation of our particles to a graph of the network (see figure 12.8). Particles are displaced and spread based on odometry information, and their weight is recalculated when a salient feature is detected. Monte-Carlo resampling is then used to only retain particles that are consistent with the GIS information.

12.4.5 Navigation

In this section we give a top-down presentation of the navigation and control algorithms which allow the ARSI quadrotor to autonomously execute the predefined flight plan for each inspection mission. The task is complex because many tunnels are narrow and the clearance from the MAV to the sewer walls is often less than 10cm.

12.4.5.1 Mission planning

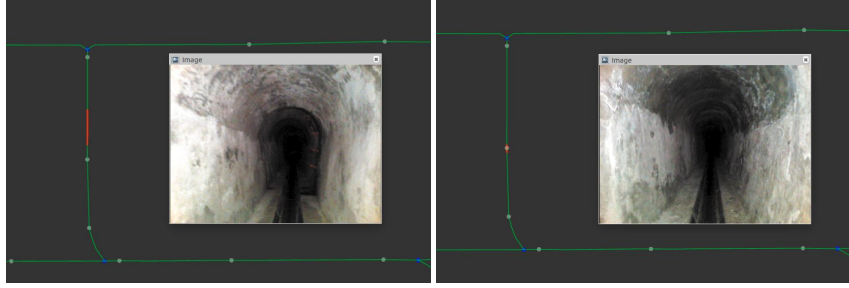


Fig. 12.8: Particles (in red) on the GIS map (in green) during localisation. Left: in the absence of features, the particles spread according to the uncertainty of the localisation solution. Right: the particles are weighted and re-sampled after a manhole (in grey) has been detected, and the localisation error is reduced.

In our Concept of Operations, mission planning is carried out by inspection specialists using maps and GIS databases of the sewer network as well as reports from previous inspections. This planning is manual as it requires knowledge of the types of defects previously seen in an area, the accessibility of entry points given road traffic, as well as an understanding of the MAV limitations, in particular flight autonomy and WiFi coverage.

We provide a Planning Interface to facilitate this task and generate ARSI mission files that inspection brigades take with them on the field. Missions are verified and uploaded onto the MAV from the Operations Console before being executed.

12.4.5.2 Local planning

Given a series of sewer sections to inspect, our onboard local planner is responsible for generating high-frequency control commands to the Pixhawk autopilot. It allows the MAV to navigate autonomously towards each goals whilst staying at safe distance of the sewer walls and any other obstacle.

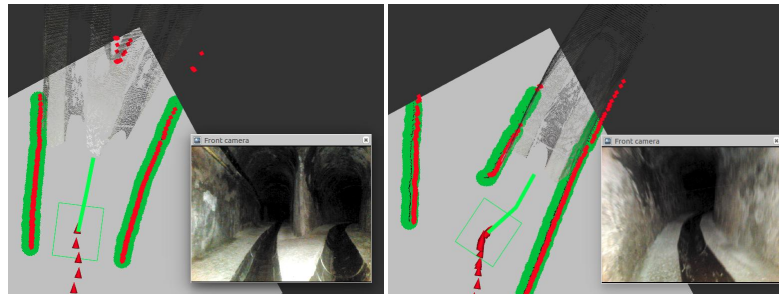


Fig. 12.9: Local plan (in green) using a 2D occupancy map guiding the MAV through an intersection into a narrow tunnel

Our method is inspired by the Dynamic Window Approach (DWA) path planner [25], where the 2D space is scanned to generate path candidates ranked using the following criteria: 1) distance from the path vertices to any obstacle and 2) distance from the path vertices to the global goal. These criteria are weighted and combined to assign a score to each path candidate.

Our local planner searches for the optimal safe path towards a given mission goal by building a local occupancy map using laser and depth data, and estimating the distance from each map pixel to the nearest obstacle. Path candidates are generated iteratively by adding segments until a given planning range is reached. Only the optimal path (with the smallest score) is retained at each planner iteration.

This approach was successfully tested in real sewers as narrow as 80cm, featuring corners and intersections. We ran this algorithm on 4x4m occupancy maps with a 1cm resolution, generating local paths at a frequency of 20Hz. The control requests were then issued to the Pixhawk autopilot onboard the MAV using the ROS-Mavlink interface Mavros.

12.4.5.3 Obstacle avoidance



Fig. 12.10: ARSI MAV avoiding a service pipe crossing a sewer tunnel

A MAV solution is advantageous in the sewers because it can carry out inspections unaffected by the state of the sewer floors, which are often irregular or obstructed by obstacles or sewage water. However, our solution must handle possible obstacles obstructing its flight path. Figure 12.10 for example depicts a situation encountered during our field tests in Barcelona, where a series of service pipes crossing the sewer sections only left 60cm of clearance underneath for our MAV to fly.

We overcame these obstacles using a semi-autonomous approach, where operators used our Operations Console to trigger a change in flight altitude near these obstacles so that the MAV was able to fly underneath despite the minimal clearance (see figure 12.10). Once the obstacle was cleared, the MAV returned to its normal flight altitude and completed its mission. We are currently developing an automated solution to obstacle avoidance using a 3D local planning approach based on potential fields (see section 12.7).

12.4.5.4 Flight control

The safe trajectories calculated in real-time by our local planner are broken into a series of setpoints issued at high-frequency to the Pixhawk autopilot, which runs highly configurable cascaded control loops to convert them into individual low-level commands for each of the 4 motors.

While Pixhawk provides a default configuration, it is recommended that users tune the control loops to achieve the desired flight dynamic for their specific application and quadrotor platform. The tuning process is particularly important in this project, given the extremely narrow margins around the MAV in sewer tunnels. Another important factor is that sewers are confined spaces, so that the air flow generated by the ARSI quadrotor generates turbulences which add instability to the flight.

During our 2017 field trials, we tuned both the outer (position) and inner (velocity) control loops in real sewer environments. An important observation that we made during our tuning process is that a trade-off must be found between the reactivity of the control and the effects of rapid movements on sensor data. While reactive control is required to navigate curves or intersections in narrow tunnels, rapid changes, particularly in yaw, introduce blur in the RGB-D camera images which is detrimental to feature detection and therefore to the quality of the visual odometry solution. This in turn results in poor velocity estimation, reducing the capacity of the Pixhawk control loops to control yaw error. Moreover, large yaw errors in narrow tunnels imply that the MAV is facing towards a wall and given the short distances, direct illumination from the MAV LEDs can saturate the images, which is also detrimental to visual odometry and velocity estimation.

For yaw in particular, we found that an aggressive inner loop combined with a slower outer loop provided the required control accuracy and reactivity to turbulences, whilst ensuring smooth video data and visual odometry.

12.5 Sewer monitoring

While a robotic tool like ARSI represents an important step towards safety and more efficient inspections, the goal of any sewer management system must be to provide an assessment of the structural integrity of the network, so that necessary repairs are executed before serious damage occurs. To this end, the ARSI consortium applied state-of-the-art Computer Vision techniques to render 3D models of the sewers from data generated by the RGB-D sensors and the localisation software described in section 12.4. These 3D models are instrumental in the development of software tools which provide the main outcomes of an inspection mission: serviceability assessments and defect inspection reports. A user-friendly GUI was also developed to visualise the results of these software tools, and to help operators review inspection missions to compile inspection reports.

12.5.1 Inspection reports

The inspection results produced by the ARSI software, which was designed in close relationship with inspection professionals and public entities, cover the expected goals of sewer maintenance: serviceability assessment and structural defect inspection. These concepts are described here for clarity.

12.5.1.1 Serviceability assessment

The serviceability of a sewer is determined by the ability of wastewater to flow through it. For cities like Barcelona, where the sewer network is used both for wastewater and rainwater, serviceability

is defined by how free from obstacles the sewer is across the section, as water under pressure may flow in the sewer during heavy rainfalls. In this context, an obstacle can be a pipe or cable crossing the section, voluminous objects in the way, dirt, etc. Figure 12.11-left depicts a sewer with a serviceability failure. Serviceability reports indicate whether the water is able to run through the sewer, and to identify the profile type of the sewer sections for documentation purposes. A complete serviceability assessment also surveys the location of manholes, inlets, scuppers and sewer junctions.

12.5.1.2 Structural defect detection

Structural defect inspection consists in scanning sewer sections in search of faulty elements or failures in the structure. The most relevant structural defects are as follows:

- Surface scaling: due to action of water the wall and ground coating may be removed and the filling arid appears to sight.
- Faulty gutters and inlets: they may be deteriorated, deformed (not cylindrical), out of place in the section (located too high on the wall or even on the ceiling) or protruding in it.
- Structural failures: cracks, fractures, breaks (with or without loss), sinkholes, wall displacements or even collapses of ceiling/walls (see figure 12.11-right)
- Deformations: ground pressures and settlements provoke changes of shape in the profile of the sewer section.



Fig. 12.11: Examples of sewer defects. Left: serviceability of sewer compromised by sediments. Right: structural viability of the sewer affected by sinkhole on the ground.

Apart from surface scalings, which are detected using image processing and deep learning techniques, these structural defects can be all detected by analysing the geometry and volume of the sewer section. The necessary prior for this type of analysis is thus a 3D map of the sewer, and the ARSI consortium made significant efforts to generate accurate 3D models of the sewers from RGB-D data and MAV pose information.

12.5.2 3D reconstruction

Our 3D reconstruction pipeline combines the camera poses generated by our localisation algorithms (see section 12.4.4) with the camera images to optimise the pose estimation by means of openMVG

[26], a multiple view geometry open-source library. The optimised pose information is then integrated with the depth data produced by the RGB-D sensors to obtain a coherent data arrangement of camera pose and 3D structure for each mission. Subsequently we generate the 3D dense map by applying an open-source, state-of-the-art 3D dense reconstruction system. The pipeline finishes with the rendering of 3D surfaces from the 3D point clouds.

We benchmarked a number of 3D dense reconstruction libraries in order to maximise the accuracy of our 3D models: MVE [27], RTABMAP [22] and Look@U⁵ amongst others. Our 3D reconstruction library currently uses RTABMAP as it best suits the input data of the 3D system. Figure 12.12 depicts samples of 3D models produced with this pipeline.



Fig. 12.12: 3D reconstruction samples of the sewer via current RGBD sensors and RTABMAP. Left: outside view. Right: inside view.

An accurate 3D reconstruction of a sewer segment, along with the corresponding imagery, constitutes the baseline of our post-processing tools that perform the inspection reports.

12.5.3 Post-processing tools

In order to produce a comprehensive inspection report of the sewer, our platform is equipped with 2 lateral HD colour cameras with 185 degrees FOV fisheye lenses, to ensure full coverage of the sewer sections. We developed two separate image processing algorithms to produce the inspection assessments: a volumetric analysis of the computed 3D models, and a texture classification of the mission imagery.

12.5.3.1 Volumetric analysis

The volumetric analysis software fits the sewer section profile provided by the GIS database to the reconstructed 3D model by applying a 2D shape matching approach [28]. It first computes the curve generated by the longitudinal axis of the reconstructed sewer segment (originated from the visual odometry drift, see section 12.4.4). With the prior knowledge from the GIS of the topology of the sewer segment, our software rectifies the computed curve and subsequently the full mesh. It then performs the section fitting automatically over the course of the rectified sewer and creates a heat map of the divergences between the 3D model and the theoretical profile section. It also notifies at what angle on the section and position along the sewer a divergence occurs. Figure 12.13 shows

⁵ Look@U is a GPU-based 3D dense reconstruction software system developed by Eurecat.

how the 3D models are rectified (fig. 12.13-top) and the heat map of divergences generated for a 3D model (fig. 12.13-bottom)

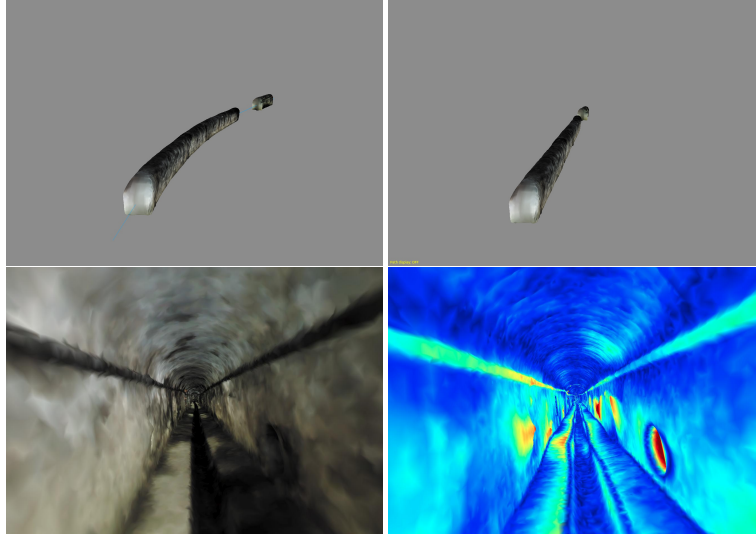


Fig. 12.13: Results output by volumetric analysis module. Top left: Curved 3D reconstruction of sewer caused by visual odometry drift. Top right: 3D reconstruction rectified. Bottom left: 3D sample of sewer. Bottom right: heatmap of divergences with expected section profile applied on this 3D sample.

This method allows us to classify sewer section profiles and to detect any obstacle which might obstruct the clean section. These features, along with the manhole detection described in section 12.4.4.2, comprise the necessary analysis for a serviceability assessment. It also detects differences with the theoretical profile due to deformations or any deviation from the original shape in the form of structural defects or obstacles. In addition, it detects scuppers, inlets and gutters, as they are reflected in the 3D models. It therefore covers all the structural defects mentioned in section 12.5.1.2.

12.5.3.2 Texture classification

Some defects might not be detected by means of the volumetric analysis approach. In particular, the type of defect labelled as “surface scaling” in section 12.5.1.2 will appear as an irregular texture over the wall of the sewer without enough deviation from its expected profile. We apply the latest techniques in machine learning for image understanding [29] in order to detect these kinds of defects. Specifically, semantic segmentation of sewer images is employed by means of fully Convolutional Neural Networks (CNN) [30]. These CNN are trained using a large set of manually-labelled representative defect samples and deployed to produce a heat map which encodes the probability for each recorded pixel to be part of a defect. In Figure 12.14 we show a validation example of an image taken from the platform and its corresponding heat map. The area of the surface scaling is correctly identified by our classifier.

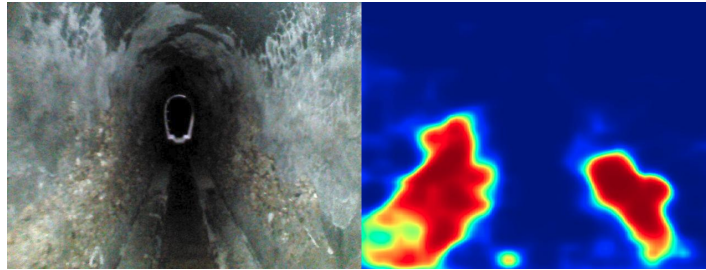


Fig. 12.14: Surface scaling defect detected by CNN-powered texture classifier.

The post-processing tools need to be supported by a visualisation app so that their outputs can be presented in a user-friendly manner. This role is undertaken by the ARSI GUI app.

12.5.4 Visualisation interface

This app provides an incidence notification system and a visualisation space for all the imagery captured by the image sensors, along with the output from the post-processing tools. It shows, in a coherent and synchronised fashion, a timeline of the mission on which the incidences are tagged. This timeline is coupled with the mission image sequence and a GIS representation, on which it is possible to track the location of the MAV at any given moment of the flight. It also visualises the 3D maps and the outputs of the processing tools.

The design philosophy of this app is to save time to the operator in the analysis of the mission. By notifying with tags when and where each incidence occurred in the mission, the operator does not have to go through the entire mission, but only to the isolated tags along the timeline, or specific stretches that he or she might want to go through. The operator can then add, edit or remove incidence tags at will. When finished tagging, the app will produce a serviceability and inspection report for documentation purposes.

12.6 Field validation

As part of the ECHORD++ monitoring process, the ARSI system was evaluated by inspection professionals and ECHORD evaluators in real sewers in Barcelona, Spain, where 650m of sewers had to be inspected with our system (see figure 12.16). The area presented several complexities, including narrow sewer sections (see figure 12.3), sewage water running from service pipes on the walls, dust and spiderwebs, as well as a series of service pipes crossing the sewer sections.

The entire area was successfully inspected under 3 hours as required by the evaluators, with an inspection brigade operating from the street to execute a series of 7 flights shown in figure 12.17. Note that the MAV used in the evaluation had a shorter flight autonomy (7 minutes) than our new platform (15 minutes), so that fewer flights would now be required. During the inspection, our MAV successfully flew underneath 4 services pipes as shown in figure 12.10). Video data was transmitted back to the Operators Console on the surface at all times during the inspection, taking advantage of the propagation properties of several smooth turns (see section 12.4.3). Inspection data collected

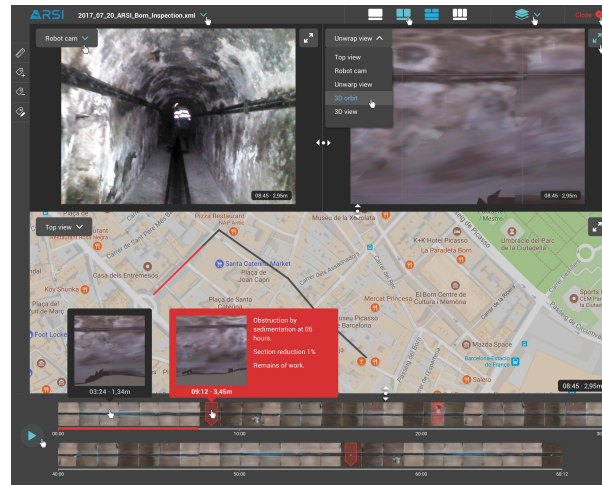


Fig. 12.15: Overview of the visualisation interface. The top area allocates images and 3D reconstruction views of the point marked on the timeline (bottom area). In the middle area the segment covered by the MAV up to this point is marked on the path of the mission. Defect tags pop up on the timeline.

onboard the MAV was post-processed to generate 3D models of the sewer sections visited (see fig. 12.12).

Figure 12.18 shows the variation in roll during a 40m flight carried out during the evaluation. Throughout the flight in this narrow tunnel (90cm wide), the vehicle roll remains within ± 2 degrees despite the turbulences caused by the MAV motors in a confined space. This illustrates the flight stability of our prototype, allowing us to generate high-quality video data for sewer inspection.

Figure 12.19 depicts the ranges to the left and right walls, as well as the range difference, estimated from our onboard laser data during a flight in the same narrow tunnel. This result shows that the trajectory generated autonomously by our real-time path planner keeps the MAV largely within 10cm of the centre of the tunnel throughout the flight, despite the turns and irregularities. Note that some of the higher range differences are due to side entries or pipes in the tunnel walls.

12.7 Conclusions and Future Work

In this chapter we presented the ARSI system, which helps inspection brigades carry out safer and more efficient sewer inspections using an autonomous Micro Air Vehicle. Developed in close collaboration with inspection professionals, our solution proved intuitive to use and was tested over numerous field trials in real sewers in Barcelona. Several other field demonstrations in different areas of Barcelona have already been planned by evaluators from ECHORD and BCASA, where we will validate new functionality, refine our Concept of Operations, and verify that our system can cope with the variability of the sewer networks.

Other tasks remain for the remainder of this project, in particular with our new MAV prototype (see section 12.4.2) where we will iterate with our partners at DroneTools to improve aspects such as the landing gear and the electronic integration for protection against dust and water. Our onboard software will be upgraded to include a new 3D local planner based on potentials fields [31]. The

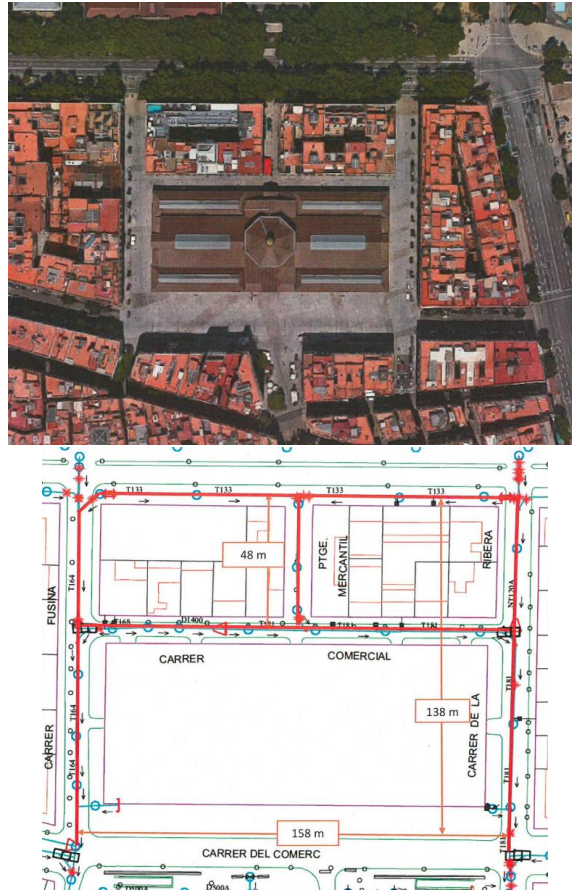


Fig. 12.16: Validation area in Mercado del Borne, Barcelona. The sewers marked in red had to be inspected with our system

planner derives a safe flight path from a set of simulated attractive and repulsive forces, so that the MAV navigates around obstacles autonomously, without requiring input from the operator. Work on our geo-localisation algorithm will also continue, in particular by attempting to detect new GIS features such as intersections and manhole ladders.

Since our RGB-D sensors were recently upgraded to the new Intel Realsense D400 cameras (replacing the Orbbec Astra camera used in previous phases), our benchmarking of 3D dense reconstruction libraries (see section 12.5.1.2) will be revisited to take advantage of the improved image resolution and camera field of view. Colour information will also be included in the 3D reconstruction process to improve 3D surface textures in the rendering step.

Finally, work will continue on our user interfaces, building on feedback from our inspection partners, to ensure that they meet all the needs of our end-users for tasks such as mission planning, monitoring and data analysis.

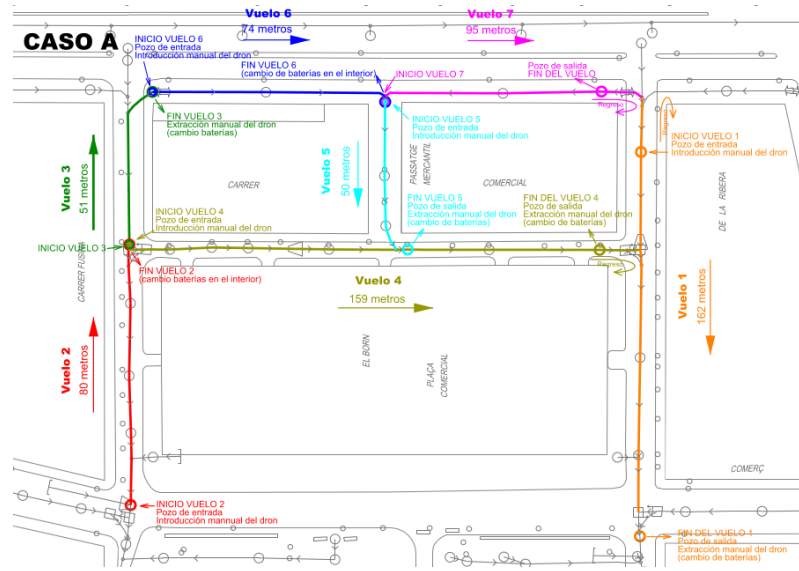


Fig. 12.17: Mission flights executed during the evaluation in Mercado del Borne, Barcelona.

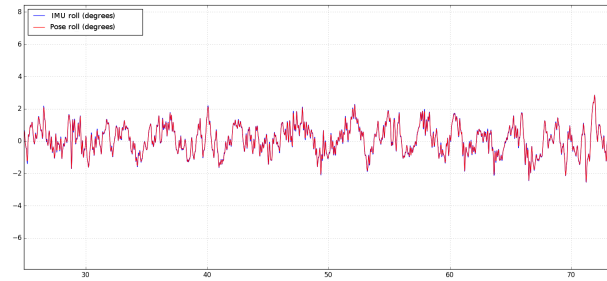


Fig. 12.18: Vehicle roll in degrees during a flight in a narrow tunnel (Passatge Mercantil). We can see that the roll remains within 2 degrees, indicating a stable flight for video data capture.

Acknowledgements

This work has received funding from the European Union's Seventh Framework Programme for research, technological development and demonstration under grant agreement No 601116. The authors would like to thank Mr. Raul Hernandez and the whole team at FCC (Fomento de Construcciones y Contratas) for their logistic support during the numerous field tests.

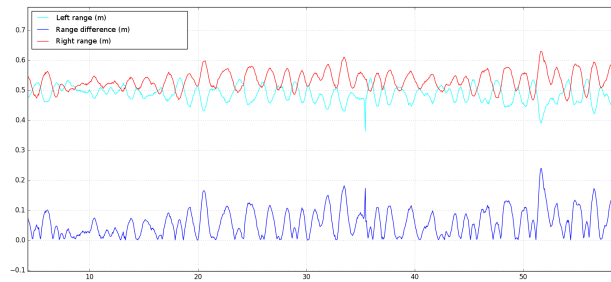


Fig. 12.19: Ranges to left and right walls, and range difference, measured from laser data in a narrow tunnel. We can see that the MAV remains with 10cm of the centre of the tunnel throughout the flight.

References

1. Skyfuture company. <https://www.sky-futures.com/> Accessed: 2018-10-04
2. Industrialskyworks company. <https://industrialskyworks.com/> Accessed: 2018-10-04
3. Cyberhawk company. <https://www.thecyberhawk.com/> Accessed: 2018-10-04
4. Airobotics company. <https://www.airoboticsdrones.com/> Accessed: 2018-10-04
5. Argos challenge. www.argos-challenge.com Accessed: 2018-10-04
6. European robotics challenge. <http://www.euroc-project.eu/> Accessed: 2018-10-04
7. Aeroarms European project. <https://aeroarms-project.eu/> Accessed: 2018-10-04
8. Aeroworks European project. <http://www.aeroworks2020.eu/> Accessed: 2018-10-04
9. Robo-spect European project. <http://www.robo-spect.eu/> Accessed: 2018-10-04
10. EnviroSight company. <https://www.envirosight.com/> Accessed: 2018-10-04
11. Ibak company. <https://www.ibak.de/en/homepage/> Accessed: 2018-10-04
12. Aries Industries company. <https://international.ariesindustries.com/> Accessed: 2018-10-04
13. SOLO from redzone company. <https://www.redzone.com/technology/solo> Accessed: 2018-10-04
14. KA-TE company. <http://ka-te.ch/en/startseite-2/> Accessed: 2018-10-04
15. Inloc robotics company. <http://inlocrobotics.com/>, Accessed: 2018-10-04
16. SafeFlight company. <http://www.safeflightservices.com/> Accessed: 2018-10-04
17. DJM Aerial Solutions company. <https://djm-aerial.com/> Accessed: 2018-10-04
18. Özaslan, T., Loianno, G., Keller, J., Taylor, C.J., Kumar, V., Wozencraft, J.M., Hood, T.: Autonomous navigation and mapping for inspection of penstocks and tunnels with mavs. *IEEE Robotics and Automation Letters* **2**(3), 1740-1747 (2017)
19. Rizzo, C., Lera, F., Villarroel, J.L.: Transversal fading analysis in straight tunnels at 2.4 GHz. In: ITS Telecommunications (ITST), 13th International Conference. pp. 313-318 (2013)
20. Rizzo, C., Sicignano, D., Riazuelo, L., Tardioli, D., Lera, F., Villarroel, J.L., Montano, L.: Guaranteeing Communication for Robotic Intervention in Long Tunnel Scenarios. In: Robot 2015: Second Iberian Robotics Conference, *Advances in Robotics* **1**, pp. 691-703 (2016)
21. Rizzo, C., Cavestany, P., Chataigner, F., Soler, M., Moreno, G., Serrano, D., Lera, F., Villarroel, J.L.: Wireless propagation characterization of underground sewers towards autonomous inspections with drones. In: ROBOT 2017: Third Iberian Robotics Conference, pp. 849-860 (2018)
22. Labb, M., Michaud, F.: Online global loop closure detection for large-scale multi-session graph-based slam. (2014)

23. Rublee, E., Rabaud, V., Konolige, K., Bradski, G.: Orb: An efficient alternative to sift or surf (2011)
24. Meier, L., Honegger, D., Pollefeys, M.: PX4: A node-based multithreaded open source robotics framework for deeply embedded platforms (2015)
25. Gerkey, B., Konolige, K.: Planning and control in unstructured terrain (2008)
26. Moulon, P., Monasse, P., Marlet, R., et al.: Openmvg. an open multiple view geometry library <https://github.com/openMVG/openMVG>
27. Fuhrmann, S., Langguth, F., Goesele, M.: A multi-view reconstruction environment. In: Eurographics Workshop on Graphics and Cultural Heritage, Darmstadt, Germany (2014)
28. Belongie, S., Malik, J., Puzicha, J.: Shape matching and object recognition using shape contexts. *IEEE Transactions on Pattern Analysis and Machine Intelligence* **24**(4), 509-522 (2002)
29. LeCun, Y., Bengio, Y., Hinton, G.: Deep learning. *Nature* **521**(7553), 436-444 (2015)
30. Shelhamer, E., Long, J., Darrell, T.: Fully convolutional networks for semantic segmentation. *IEEE Trans. Pattern Anal. Mach. Intell.* **39**(4), 640-651 (2017)
31. Nieuwenhuisen, M., Droschel, D., Holz, D., Behnke, S.: Omnidirectional obstacle perception and collision avoidance for micro aerial vehicles. (2013)

Chapter 13

SIAR: A ground robot solution for semi-autonomous inspection of visitable sewers

David Alejo, Gonzalo Mier, Carlos Marques, Fernando Caballero, Luís Merino and Paulo Alvito

Abstract The SIAR platform is a six-wheeled ground robot with differential kinematic configuration and automatic width adjustment developed for the ECHORD++ Challenge on Urban Robotics: “Robots For The Inspection And The Clearance Of The Sewer Network In Cities”. This challenge proposes the development of a wireless robotic platform for long range inspection of large city sewers, which are currently not addressed by commercial solutions. SIAR leverages RGBD data for affordable and high-resolution 3D perception of its surroundings. This information is internally used for robot localization and safe navigation. Moreover, this information is also employed in high-level functionalities such as automatic defect inspection, the detection of serviceability losses and the generation of global 3D reconstructions of the environment. This chapter describes the main software and hardware architecture of the system. It also details the advances made over state-of-the-art techniques in order to take into account the particularities of this environment, i. e., localization in a GPS-denied area, navigation or communications, to name a few. Finally, the chapter presents experimental results on real sewers of Barcelona to demonstrate the reliability and suitability of the proposed solution.

13.1 Introduction

Sewers represent a very important infrastructure of cities. The state of the sewer network has to be continuously assessed in order to intervene if damages, blockages and other hazards are discovered. This is a labour intensive task. For instance, the city of Barcelona has a 1532 km long network, in which 50% can be visited by operators. Furthermore, sewer inspections require many people to work in risky and unhealthy conditions. Sewers are classified as confined spaces which require special health and safety measures, in addition to other risks present like slippery sections, obstacles or biological risks from the potential contact with wastewater.

These features make the process of sewer inspection a risky and expensive process that requires improvements urgently. Therefore, introducing a robotic solution in this process aims at reducing the

D Alejo, G. Mier, F. Caballero and L. Merino
Service Robotics Laboratory, Universidad Pablo de Olavide, Seville, Spain. e-mail: {daletei, gmiermun, fcaballero, lmercab}@upo.es

C. Marques and P. Alvito
IDMind. IDMind, Lisbon, Portugal.
e-mail: {cmarques, palvito}@idmind.pt

labour risks, improving the precision of sewer inspections and optimizing sewer cleaning resources of the city. This is the objective of the ECHORD++ Public end-user Driven Technological Innovation challenge for urban robotics [1]. The goal is to have a semi-autonomous robotic platform, able to operate in sewers with a diameter larger than 80 cm, without a communication infrastructure. The robot should be able to self-localize in the network, provide visual imaging with artificial illumination and 3D information, air and waste samples, as well as automatic inspection capabilities, like defects and serviceability reduction detections.

Autonomous sewer inspection by robots is a harsh task in many senses: the environment is very aggressive with a high level of humidity and potential toxic gases; the robot should move in very narrow spaces with almost no place for maneuvering; and communications are very restricted due to lack of direct line of sight (NLOS). In addition, the robot needs to carry a wide range of sensors for all the previous functionalities. These sensors increase the weight of the system and also drain the power of the robot with the corresponding impact in battery life and autonomy.

Payload, autonomy (in terms of battery life and traversed distance) and harsh environment altogether conform a working framework in which ground robots seem to be the best solution [2]. Additional options include the use of micro aerial vehicles (MAVs) based on multi-rotors, given their small size and maneuverability. On the other hand, submarine or boat robots [3] are discarded because the water level into the sewage network is expected to be low during inspection and monitoring tasks and the inspection capabilities from inside the water are very limited. Thus, ground robots are the good choice if long-term and high maneuverability are required, as they can be built waterproof and sensors of different size and weight can be installed on-board.

There are a wide variety of robotic platforms for gallery inspection already in the market. In particular, the sewer inspection scene can be divided in two fields: pipe inspection performed by small robots which can fit inside pipes; and sewer inspection performed by medium to big sized robots which move inside galleries. Pipe inspection can be purely remote controlled, e.g., Alligator, Minigator, Multigator and Flexigator wheeled robots from IBAK [4] or Geolyn's tracked robots [5], but it can be also autonomous, e.g., Solo tracked robots from REDZone [6] or Makro's wheeled worm type robot [7]. In sewer inspection is also possible to find teleoperated solutions, e.g., PureRobotics' Pipeline Inspection tracked robot [8], and autonomous solutions, e.g., ServiceRoboter wheeled solution from Fraunhofer IFF [9]. However, they have been designed in order to inspect small pipes and sewers or larger environments than the visitable and semi-visitable sewers.

The SIAR (Sewer Inspection Autonomous Robot) solution seeks to solve the problem by the creation of a semi-autonomous ground robot, which has an option of fully manually control in case of need or emergency. By using a wireless communication system, augmented by the deployment of self-powered wireless repeaters, it is possible to transmit bidirectional data between robot and an external operator, allowing the operator to change the mission in real time, instead of having to wait for the end of the sewer exploration to identify problems on the sewer system.

The SIAR system goes beyond existing solutions through the inclusion of some innovative features, while maintaining affordable costs: locomotion system with variable length/width of the traction system; reliable navigation system based on data fusion from low-cost commercial RGB-D cameras, IMU and encoders, performing accurate localization and navigation on the sewer system; and automatic inspection capabilities. The chapter summarizes the main elements of the solution. First, Section 13.2 describes the hardware aspects. Then, Section 13.3 presents the software architecture. Sections 13.4 and 13.5 present the techniques for autonomous localization and navigation in the sewer network, respectively. Section 13.6 describes the automatic inspection capabilities of the robot. Section 13.7 presents results obtained in experiments in sewers in Barcelona. Finally, Section 13.8 discusses lessons learned and potential future works.



Fig. 13.1: Left: the SIAR platform in the sewer. Right: the robot being introduced in the manhole.

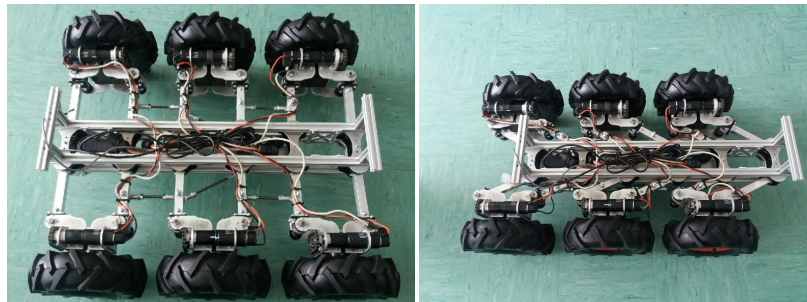


Fig. 13.2: The width adaptation mechanism in its two extreme configurations. Left: maximum width. Right: maximum width.

13.2 Description of the SIAR platform

A new ground robot has been developed to tackle the requirements of the sewer inspection application [1]. The main elements are the robotic platform, the sensor payload, and the communications system.

13.2.1 The robotic platform

The SIAR robot is a six-wheeled differential robot that includes a width adjustment mechanism (see Fig. 13.1). The wheel traction system is composed by 6 sets of independent motors, a 90° gearbox and a 260 mm off-road wheel. Each of these sets has a independent suspension arm that connects to the central robot frame. A central structural frame is used to connect the motorized wheel traction system, the width adjustment mechanism and to carry the payload equipment and electronics.

Due to the specifications of the problem, the robot must be introduced through a manhole, which is noticeably smaller than the width of the tunnels (see Fig. 13.1, right). Furthermore, the robot

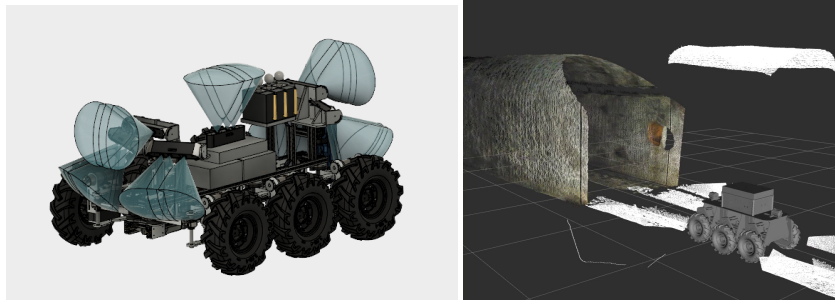


Fig. 13.3: The robot carries 7 RGBD cameras (left). These cameras provides high-resolution 3D point clouds of the environment (right), used for navigation and inspection.

should negotiate sewer sections and gutters of different widths. The width adjustment mechanism (see Fig. 13.2) improves the robot adaptability to these different structural changes in the working environment. This mechanism allows to vary the width of the robot by means of a change in the position of the wheels. It showed to be very important and effective in the sewer environment. It allows the robot to adjust its width in order to pass through sections of different width and at the same time change the center of gravity of the robot. This feature is also very helpful when crossing bifurcations, allowing the robot to maintain the balance and also to overcome large gaps in the sewer.

In order to protect the electronic components from the dirt and liquids present in the environment, precautions has been taken. All electrical components are inserted in a fiberglass box located at the center of the robot (see Fig. 13.1, left). The box has a cover made of transparent polycarbonate. On the cover there are two IP67 buttons to connect the motors and the electronics. A water foam sealer was applied between the box and the cover to prevent water to enter the box. The geometry of the box was designed to minimize the volume of the robot and to allow the suspension movement without interferences with the box. All components connected to the box have IP67 or IP68 connectors.

13.2.2 Sensor payload

The robot is equipped with a set of navigation and environmental perception sensors. The main element of the sensor payload is a set of seven RGB-D cameras¹ that provide visual and depth information. The cameras are placed symmetrically as presented in Fig. 13.3, left. There are three RGB-D cameras looking forward, three backwards and one upwards. The three cameras located in each direction of the x-axis have a camera parallel to the ground to detect damage in the tunnel and to illustrate the operator controlling the robot, and two cameras facing downwards and sideways to visualize possible obstacles and improve control over the position of the wheels. The upward camera is placed over the center of the robot. This camera is used to detect flaws in the tunnel dome and elements of the sewers such as manholes.

At full resolution, the 7 cameras are able to provide 3D point clouds of nearly 1,000,000 points per scan at 30 Hz (see Fig. 13.3, right). These cameras, because they have no moving parts, are able to produce these scans without requiring the robot to stop. And while the robot carries illumination devices, it could even provide these data without illumination.

¹ From Orbbec <https://orbbec3d.com>

For navigation the robot also uses encoders to control the velocity of the traction motors and an encoder plus a potentiometer to control the position and velocity of the platform width actuator. The robot is also equipped with an inertial sensor and gas and water measurement devices.

13.2.3 Communications

One of the main requirements of the robot is the capability of receiving commands from the operator, who, at the same time, should receive images and other data from the robot [1]. The SIAR communication system is based on wireless communications to provide the platform with continuous connection with the base station, even without direct line of sight (LoS) and with a long distance between the robot and the base station (hundreds of meters).

Wireless communications in the sewage system is an open issue. Most of current robotic solutions use tethers and cables, which limit the distances that the robot can explore [2]. The design of a wireless communication system inside the sewer system involves a great challenge due to the harsh environmental conditions and its architecture. In fact, it is common to find 100% humidity condition. Another major issue is the presence of obstacles, such as walls, pipes or garbage which would not allow LoS transmission between the robot and the base.

The proposed system is based on the use of robust 2.4 GHz WiFi communication repeaters² that can extend the communication range even in presence of non-line of sight. These repeaters form an ad-hoc network. The use of multi-hop ad-hoc networks have been shown [10] as an potential solution in similar scenarios.

In the current solution, the repeaters are manually deployed through manholes. The places for deployment are part of the planning for the mission. As it will be seen in the experiment section, with careful planning, it is possible to cover large sewer scenarios with a small number of repeaters.

13.3 Software Architecture

The SIAR software architecture is a set of modules that make use of the robot platform, sensors and communications, described in the previous sections, to develop the required functionalities (self-localization, navigation, inspections, etc). This architecture is implemented under the Robotic Operating System (ROS [11]) framework, using the ros-indigo distribution under Ubuntu 14.04. These modules³ are the following:

- **SIAR driver:** Software that interfaces with the hardware board of the robot, and offers a standard ROS commands and services for easy integration of the robot with the rest of the system.
- **Sensor drivers:** These packages capture the data from the main sensors (IMU, gas sensor and cameras) and offer them to the rest of the system. They provide different filtering and configuration functionalities.
- **Enhanced Odometry:** This package provides enhanced odometry estimates by fusing IMU and encoders measures with visual odometry estimates. In this way, the SIAR platform is able to precisely and robustly estimate a 6-DOF odometry.
- **Localization:** The precise odometry estimations are used by this module in order to estimate the global position of the platform. The details of the odometry and localization modules are given in Section 13.4.

² <http://www.microhardcorp.com/nVIP2400.php>

³ All the code is open-source and can be found in https://github.com/robotics-upo/siar_packages

- **Navigation:** This module is in charge of the semi-autonomous navigation mode, described in Section 13.5.
- **Local 3D mapping** (Section 13.6.1): This package gets the enhanced odometry outputs and uses them to integrate the measurements from the different RGB-D sensors disposed over the SIAR robot. This allows the operator to have a precise 3D local reconstructions of the sewer in real-time. With the localization outputs, these local maps can be referred to the global sewer network.
- **Map Analysis** (Section 13.6.3): This module provides the high level automatic inspection capabilities. It receives the local 3D maps and analyzes them to extract sewer elements, estimate the serviceability and inspect critical defects.
- **Control Station:** This module sends alerts to the operator when critical conditions occur. These conditions can include automatic detection of structural defects, bad state of the radio links, low battery indicator, the robot has lost traction and should be recovered, among others. It also displays the localization of the robot and the images from the on-board cameras in real-time.
- **Communication block:** This modules enables the communication between the robot and control station through the network described in Section 13.2.3. Even though ROS offers a middleware for inter-process communication, we experienced that it was not very optimized for real-time transmissions where the delay should be as low as possible. Therefore, we opted to bring up two independent ROS cores in both the robot and the base station and to design and implement new ROS modules that would act as bridges between the different ROS cores in the system.

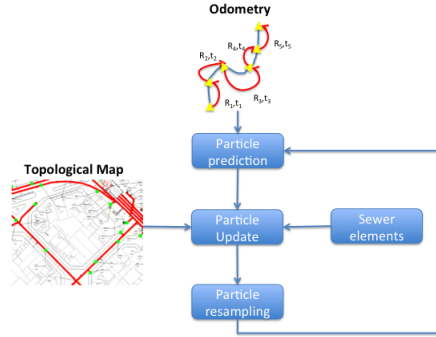
13.4 Robot Localization

According to the requirements on [1], one of the main functionalities required from SIAR is the registration of the monitored elements on the sewer network. This requires a localization system able to estimate the robot's position with respect to a previously existing map of the sewer system. Moreover, this system is vital in case of issues in the communication. In this way, the robot could navigate to the manhole were it was deployed in case of losing communication with the base station.

The proposed localization system is based on the integration of Visual Odometry (VO), visual detection of sewer elements and Monte-Carlo map-based localization. A brief description of the main functional blocks of the proposed approach is introduced below (see Fig. 13.4). For further information, the reader is directed to [12].

- **RGBD Odometry.** While the robot provides wheel odometry, due to the typical slippage of the environment, the values are not reliable. Thus, the main odometry source is a VO method [21] developed for stereo-vision and adapted to RGBD. This block takes as input the RGB and depth flows of the frontal camera of the robot, matches robust features from consecutive or closely spaced frames and then obtains the relative pose between cameras that minimizes the re-projection error.
- **Topological Map.** The map used by the localization module is a topological map. It consists of a graph that contains manhole vertices, where a manhole detection can be performed; and fork vertices, in which whether the several sewers converge, or the sewer starts to turn to another direction. These vertices are joined with edges that indicate traversable paths between them. Also, additional information regarding to section types, and metrical information like distances is added to the edges. A module obtains the topological map from the GIS data given by the local authority.
- **Manhole detector.** This module will check whether the robot is under a manhole or not based on the depth images gathered by a camera pointed upwards (see Fig. 13.3). A machine learning approach is employed to robustly perform this classification (see Section 13.6.2).

Fig. 13.4: Topological map based localization approach. The detected sewer elements, like manholes, and a map of the sewer network including such elements are used to provide a global localization tracking within this map.



- **Localization module.** A particle filter [14] is used to combine all the previous elements. The module integrates the odometry measurements through time, performing corrections according to the *a priori* topological map and the manhole detector. As a result, the localization of the robot within the map is stochastically approximated as a particle cloud, which englobes several hypotheses. Further details can be found in [12].

13.5 Robot Navigation

In the current version, SIAR operates in semi-autonomous mode. In this mode, the operator just selects the exploration direction (forwards or backwards) and the desired speed. With the proposed navigation modules, the robot is able to follow these commands without falling into the gutter, negotiating obstacles and avoiding collisions and getting stuck.

The first step of the module is to combine the information of the on-board cameras and process it into a obstacle map that indicates zones with positive or negative obstacles (see Section 13.5.1). Then, a set of candidate trajectories are tested against the obstacle map to see whether they are traversable or not and to rank them according to their safety. Please refer to [15] for a review on traversability methods for ground robots. Two different traversability analyses have been implemented in the proposed system. First, the basic navigation module, described in Section 13.5.2 which allows the platform to operate into linear galleries. The second mode allows the robot to negotiate forks and bifurcations, which typically require the capability of performing complex maneuvers in which some part of the robot are allowed to enter the gutter. In this case, the operator should also select the new exploration direction from the available possibilities in the fork. This is explained in Section 13.5.3.

13.5.1 Obstacle Map

The depth images obtained by the front and rear cameras (six in total) are combined and processed in order to obtain an altitude map of the environment close to the robot. This is done in real time at

a frequency of 10 Hz. Then, this altitude map is further processed to define the areas with positive or negative obstacles.

To date we have empirically set a threshold of 7.5 cm as the maximum step that can be safely negotiated by the platform. Moreover, the parts of the maps are given a safety penalty which decays exponentially with the distance of the closest detected obstacle. This way, the robot can be aware of the parts of the floor near to obstacles, avoiding them as much as possible. Fig. 13.5 shows a obstacle map obtained from an experiment in a real sewer scenario. Note that the analysis distinguishes between positive and negative obstacles.

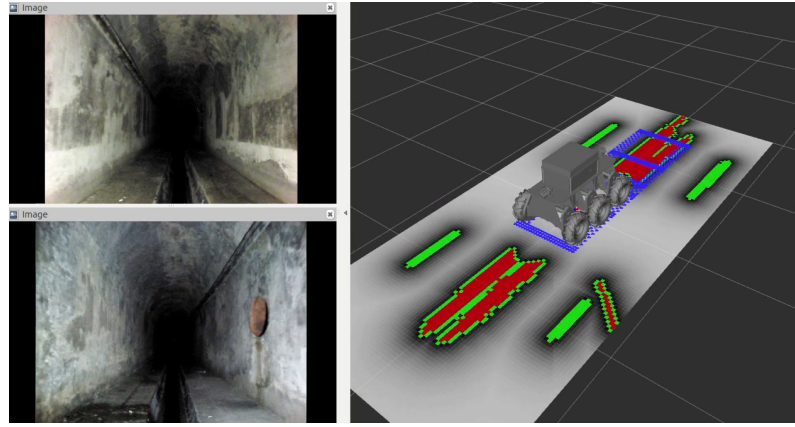


Fig. 13.5: Left: Pictures obtained from rear and front cameras. Right: Obstacle map. Positive obstacles in green (walls), negative obstacles in red (gutter). Gray zones obstacle-free, the intensity indicates the associated cost (the lighter the lower). In blue the best trajectory is represented.

13.5.2 Basic Local Navigation

The obstacle map described in the previous section is used for computing safe trajectories when the robot operates in semi-autonomous mode. This module uses a variation of the Dynamic Window Approach [16]. In the proposed method, the basic local navigation module gets the desired command given by the operator and then evaluates commands in the desired direction of travel. There is one command for each curvature in the set to be tested and the maximum speed depends on the curvature of the tested command.

For each command, the module predicts the trajectory of the robot during the next T seconds. At each timestep, the traversability is evaluated. Even though most methods consider the robot as a point and then enlarge the obstacles to detect untraversable zones, we carefully consider the geometry of the robot, distinguishing two main parts of the robot: the wheels and the robot frame. To evaluate the traversability, we check whether the robot traverses obstacles or not.

In particular, the robot frame is allowed to enter into negative obstacle zones, but the trajectory is discarded if it passes through a positive obstacle. In contrast, the wheels are not allowed to collide to neither positive nor negative obstacles. Therefore, in this mode, the wheels are always touching

the floor and therefore the stability of the platform is guaranteed at any moment. Fig. 13.5 (right) represents the footprint of the wheels of the robot for the tested predicted trajectories by the module.

The remaining traversable trajectories that are being tested are then ranked according to the following formula:

$$J = \int_0^T P(t) dt \quad (13.1)$$

where $P(t)$ is the safety penalty obtained when the wheel footprint is applied to the traversability map at time t .

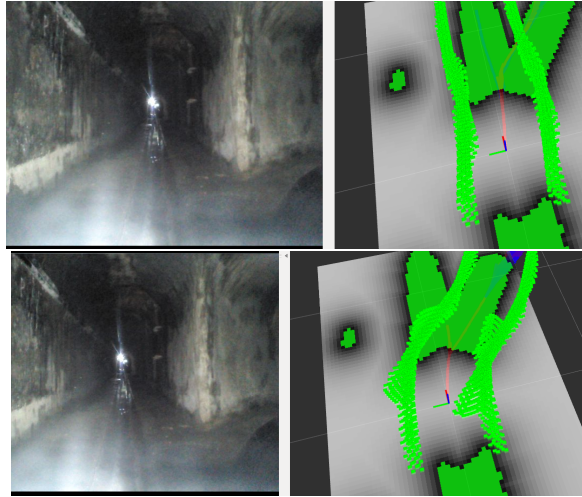
Finally, the trajectory with lowest rank is kept and its related command is sent to the controller of the robot. The best trajectory is marked in blue in Fig. 13.5 (right). This operation is also performed at a frequency of 10 Hz. Note that it is possible that all trajectory are considered as non-traversable. In these cases, the robot could not advance in the desired direction and other navigation modes described in Section 13.5.3 should be employed.

13.5.3 Local Navigation in the presence of forks

Even though the local basic navigation module has proven its reliability on several experiments, by safely traversing hundreds of meters in areas of the sewers without forks, it was not designed to be able to let the robot traverse a fork. The reason is quite simple: when the robot has to traverse a fork some of the wheels should be allowed to enter the gutter during the maneuver. Unfortunately, the local navigation module bases its reliability in not letting any wheel to enter the gutter.

The aforementioned automatic control of the position of the robot with respect to the gutter can be modified in a way that lets the robot not only cross the gutter in presence of forks but also change the direction whenever required. To this end, we modified the concept of traversable areas including the following different traversability definitions as a function of the action being performed by the robot as follows.

Fig. 13.6: Trajectories for choosing direction. (a) Up: goes to the left-most gallery with the keep left mode. (b) Down: goes to the right-most gallery with the keep right mode.



If the robot is commanded to go to the left fork, the left wheels are not allowed into a negative obstacle, whereas the right wheels can enter but keeping at least one of the three wheels on the

floor. This ensures that the robot does not fall into a unrecoverable situation inside the gutter. We empirically test the platform in such situations and verified that the neither the roll nor pitch angles of the platform surpassed levels that made the platform dynamically unstable, as suggested in [17]. This mode is useful to choose the leftmost option whenever a fork is detected (Fig. 13.6a).

If the robot is commanded to go to the right fork, the roles of right and left set of wheels are reversed. Therefore, this mode is useful to choose the rightmost option whenever a fork is detected (Fig. 13.6b).

In addition we designed a recovery mode. In this mode, we extend the definition of traversable areas to other configurations that have also empirically contrasted to be stable. In any case, due to the high cost that is given to areas with obstacles, the natural behavior of the robot in this mode will be to reach a state with all wheels on the floor as soon as possible.

13.6 Inspection functionalities

The robotic solution also offers the following automatic sewer inspection capabilities [1]:

- Providing 3D local scanning data.
- Sewer map building: build 3D reconstructions of the sewer.
- Sewer elements localization: determine the localization of elements of interest, like manholes, inlets and others.
- Sewer serviceability inspection: determine when there is debris in the gutters and floor that may obstruct the sewer.
- Structural defects inspection: determine the presence of cracks, fractures, breaks and collapses in the structure of the sewers.

The methods employed are summarized next:

13.6.1 3D data and map building

The RGBD sensor payload described in Section 13.2.2 provides 3D scanning data. This data can be accumulated in time to build 3D local maps of the sewer, which are the basis for automatic inspection of the sewer. These local maps can be used to analyze the sewer serviceability, as will be described below. The 3D reconstruction can be also compared with pre-computed 3D models of the gallery in order to detect possible defects.

The 3D scans can be also used to build a global 3D map reconstruction of the sewer, typically offline once a mission has finished. This can be used to update old maps, mission analysis, etc. Next subsections will provide some details about the 3D local and global mapping process.

13.6.1.1 Local mapping

The main purpose of the 3D local mapping module is to provide a locally coherent 3D map of the robot environment online. For this purpose two elements will be used as inputs: 3D point-clouds provided by RGBD cameras mounted in the robot and an accurate robot odometry for the integration of the point-cloud information through time.

Fig. 13.7 shows the different stages of the local 3D mapping process. As previously introduced, the main inputs of the system are a single point-cloud provided by the RGB-D sensors and the estimated translation since last map update given by the visual odometry system mentioned in

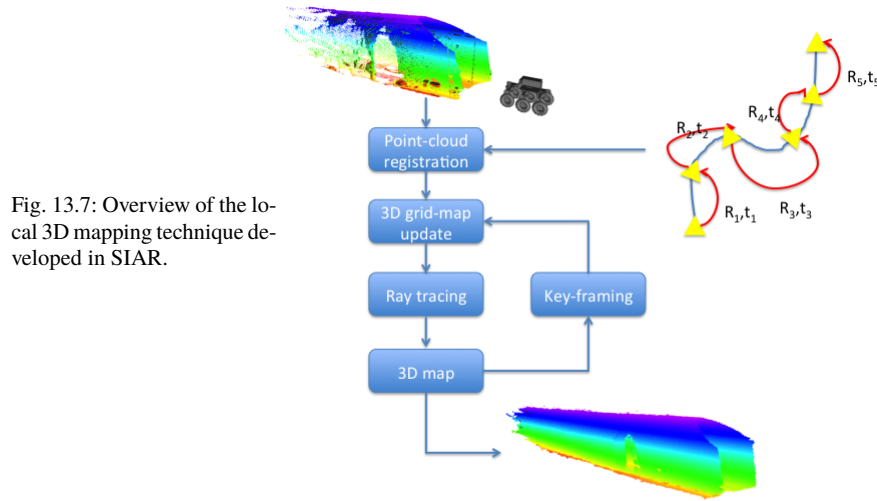


Fig. 13.7: Overview of the local 3D mapping technique developed in SIAR.

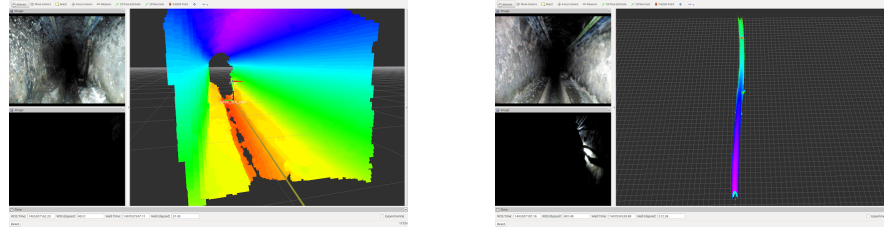


Fig. 13.8: 3D local map reconstruction of a 50 meters long section of Valencia Street sewer (Barcelona).

Section 13.4. With this information the point-cloud is aligned with the current map so that it can be merged with it.

The local map is represented as a 3D occupancy grid that stores the probability of cell of having an obstacle. This 3D occupancy grid has a predefined resolution of 25 mm and a fixed size around the robot that can be adjusted depending on the requirements. The occupancy grid is implemented as an octomap [18] in order to make a very efficient use of the computer memory.

The motion of the robot is checked in order to detect a new key-frame position. If the robot moves more than a given threshold, a new key-frame is added and all the map points are translated to the reference of the new key-frame. This method allows reducing the computational requirements for map building and map representation.

This system has been intensively tested in real experiments with the robot. Fig. 13.8 shows the local 3D reconstruction of Valencia Street. The map shows a 50 m long local map build during one of the experiments in Barcelona. It can be seen how the structure is very clear locally and how the map diverges slowly.

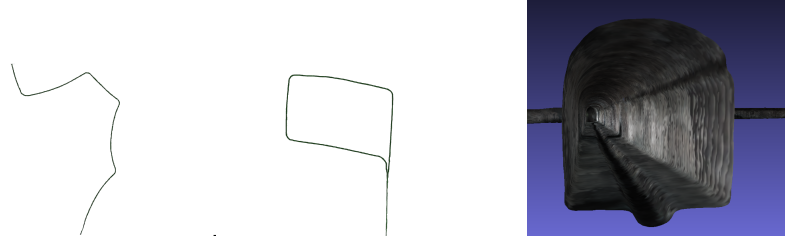


Fig. 13.9: Optimization process over a real trajectory (400 m long approximately). Left: Original trajectory computed based on visual odometry. Center: Obtained trajectory after non-linear optimization using manholes to detect close-loops. Right: Mesh built from the final 3D map.

13.6.1.2 Global mapping

The local maps described above can be used online for serviceability inspection, situation awareness, etc. However, due to the lack of global references, the map will eventually diverge due to cumulative errors. We have extended this functionality to be able to also provide full global 3D maps of the inspected area offline.

The SIAR approach for global 3D reconstruction is based on the application of an off-line robot trajectory optimization. It considers the information provided by the sewer elements automatically detected (presented in next sections) by the robot to correct the errors of the visual odometry and 3D local maps described above.

A pose-SLAM [19] system based on off-line nonlinear optimization has been implemented. This system tries to optimize the following elements:

- The relative position between consecutive poses given by the visual odometry.
- The position of the manholes automatically detected and matched.
- The alignment of the 3D point-clouds gathered by the robot in each pose of the graph.

Fig. 13.9 shows the original graph computed with the visual odometry. The figure also shows the estimated trajectory once the optimization has been performed over the whole trajectory. In this experiment the robot traversed approximately 400 m, then returning to the starting point. A couple of manholes located at the beginning of the trajectory were used to close-loop the pose-SLAM and to rectify the trajectory.

The outcome of the previous optimization will be a globally consistent trajectory. Now we can perform automatic loop-closing detection on the RGB-D data, based on different approaches as visual place recognition or scan matching. This approach implements a massive scan-matching process among all the poses that fall within a given search radius. This loop-closing detection will add new constraints among the robot poses [19]. However, the approach goes one step forward and takes into account a different type of constraint as the usual transform between poses, so that we can optimize the alignment between the point-clouds directly into the optimizer, as in [20, 13]. As a result, a global 3D map can be obtained (see Fig. 13.9, right).

13.6.2 Sewer Elements Location

An additional required functionality is the localization of sewer elements, like manholes, inlets, crossings and others. Detecting those elements can be based on a geometric analysis of the 3D local

maps described above, considering the typical geometry of the elements. However, there can be subtle differences between instances of the same element. Also, it is not straightforward to define precisely all the elements that can be found, and this is difficult to extend. Thus, we have developed an initial system based on training, in which exemplar (depth) images of the elements are used to teach the system to detect elements of interest.

We use Convolutional Neural Networks (CNNs) for the detection of manhole elements from depth images coming from the camera pointing upwards. CNNs seem a good option as they have been extensively used for image classification purposes in last years with great success. In particular, we use a similar architecture to *AlexNet* [22].

We summarize here first results on the detection of manholes because of their particular shape, as they break with the uniformity of the gallery ceiling which might simplify its detection. Also, this is used for the localization and mapping modules described above. However, we consider that a similar method could easily be used for detecting other types of elements such as forks and inlets without any trouble. The reader is referred to [12] for more details on the detection system.

The CNN has been trained and validated with a dataset that is composed by 40,000 depth image samples with resolution 80x60 gathered from two experiments at the “Mercat del Born” on the 17th of January, 2017. Each sample integrates a label that indicates if the image contains a manhole or not. From these samples, 21,000 are used to validate the CNN and are not included into training process.

After the training process, we performed a validation experiment. The obtained detection accuracy is roughly a 96%. These results are very satisfactory, taking into account that different types of galleries visited and that there were opened and closed manholes. The false positive rate is approximately of a 2%. On the other hand, the false negative rate is bigger, going up to a 10%. This indicates the probability of missing one manhole by considering one image. However, as the robot traverses a manhole, it can take tens of images of the manhole. Therefore, the probability of missing a manhole is much lower.

13.6.3 Serviceability and defects inspection

The system should be able to determine if the serviceability of the sewer has been reduced, raising alarms in case this occurs. This requires to distinguish waste on the sewers, of different sizes. Furthermore, different critical defects have to be detected, from cracks and fractures to collapses.

The module for structural defects inspection should automatically analyze the 3D information to search for such defects and then alert the operator, who can then confirm the defect. From the local sensors on the robot, it is possible to determine if the defect is located in the vault, the walls or the floor. The information from the localization module is used to provide the distance to the closest manhole of the defect and the position in the general GIS.

For the automatic detection of serviceability reduction and of defects, we used a model-based approach considering the known geometry of sewers. The different sections are included in the GIS, and have a known metric shape. From this known shape, it is possible to generate artificial point clouds, as shown in Fig. 13.10, left.

The current procedure aligns, by using Iterative Closest Point (ICP) matching [23, 24], the virtual model with the current point cloud gathered by the cameras on-board the robot (see Fig. 13.10, center), if the section is provided by the GIS. The system can also look for the most-likely section by aligning the current point-cloud to the different section models and selecting the one with the smallest error.

The alignment is then used to determine the residuals between the actual point cloud and the model. The differences are thresholded to determine potential defects in 3D, that are then presented to the operator in real-time (see Fig. 13.10, right). Spatial and temporal filters are used to eliminate spurious detections.

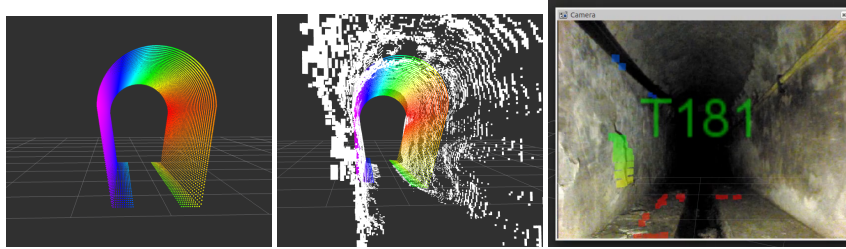


Fig. 13.10: Inspection of defects. Left: a 3D virtual model of a particular section type. Center: alignment of the model over the actual 3D data. Right: estimated section type and potential defects overlaid on a live image from the robot.



Fig. 13.11: Experimental setup of the presented experiments. Planned trajectory of the platform (red line) and visited manholes (marked with yellow stickers). Disposition of the repeaters with manhole deployment, depicted as black boxes with gray grippers. Reported defects found during the inspection marked in red exclamation signs. Finally, we deployed the robot over the manhole marked with a picture of the platform.

13.7 Experimental Results

In the context of the ECHORD++ project, several experiments and demonstrations have been performed in real sewers of the city of Barcelona. This section summarizes the results obtained in a exemplar mission with the robot.

13.7.1 Mission setup

The experiment consisted of the semi-autonomous exploration of a section of the sewer network with a total longitude of 640 m., located at the Mercat del Born in Barcelona (see Fig. 13.11).

The mission setup starts with the definition of the location of the base station and the manhole for robot deployment, and the definition of the manholes where the communications devices have to be deployed. Three wireless repeaters were deployed in the sewers in those manholes by fixing them to the stairs. The base station communication module was carried by one operator inside the sewer together with the robot and deployed at a fork to improve its coverage. With this disposition of the repeaters, shown in Fig. 13.11, we obtained network coverage over the whole demonstration area.

The route to be followed by the robot is also determined and then the mission starts.

13.7.2 Mission execution



Fig. 13.12: The SIAR robot is operated from outside of the sewers.

The robot is operated from the control station located at street level (see Fig. 13.12). With the repeaters configuration, the operator was able to receive real-time images from up to four cameras (three in the direction of travel and the upper camera) simultaneously (RGB and Depth) without a noticeable lag. This allowed us to safely operate the platform over all the inspection area.

In these experiments, the basic semi-autonomous mode presented in Section 13.5.2 is used. The robot navigated semi-autonomously in almost all the test area, with the operator only indicating the direction (forward or backwards) and speed of motion. The robot behaved well in all curves and all the straight sections of many different types (including pipes). The manual mode was only used in the cross-sections, as the fork managing method was yet to be implemented at this time. The robot was also correctly localized during the whole mission using the methods summarized in Section 13.4.

During the whole experiment, the serviceability and defect inspection module detailed in Section 13.6.3 was active and highlighted potential defects in real time. An inspection report was generated during the execution of the mission. This report includes images of areas that were highlighted by the module and then confirmed as defects by the operators. The location where the different defects



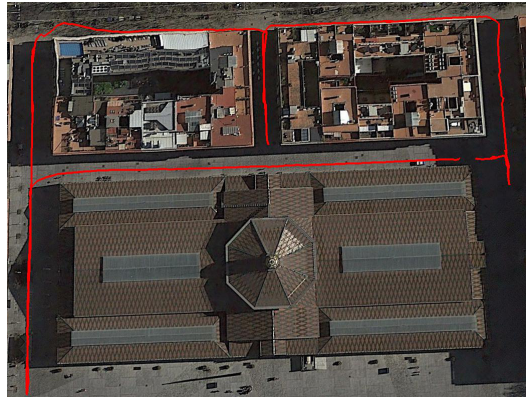
Fig. 13.13: Alert ID 1. This alert was generated as evident defects on the left wall can be found (right with the rear camera). Also sediments on the floor had been detected. Images obtained from front camera (left) and rear camera (right). Location: $41.386359^{\circ}\text{N}$, 2.183163°E . Local Time: 2017-10-17 10:58:15

were detected (provided by the localization module) is labeled with an alert sign in Fig. 13.11. As an example, the detailed information gathered by the robot in one of the defects is shown in Fig. 13.13.

13.7.3 Localization experiments

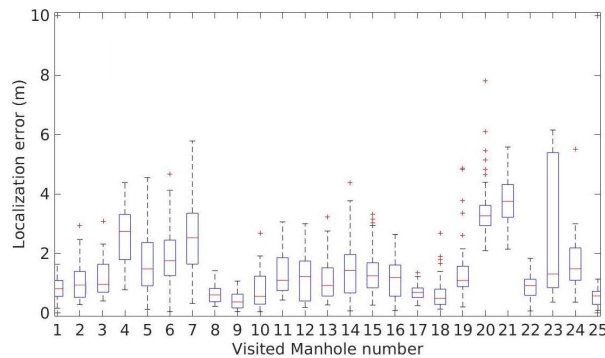
Different experiments have been also carried out to analyze the different subsystems of the solution. In this section, we provide additional localization results with the data acquired in one of those experiments at Mercat del Born.

Fig. 13.14: Localization results of the robot's position in the experiments of September, 21st.



The estimated trajectory of the robot is detailed in Fig. 13.14. Fig. 13.15 represents the distribution of the mean error of the estimated position of the robot whenever it passed below a manhole (whose positions are known). Due to the stochastic nature of the localization algorithm, the distribution of the error over 50 runs is represented.

Fig. 13.15: Distribution of the localization error whenever the platform reached a manhole.



The results are quite good in the majority of the experiment, with the exception of a small fraction that corresponds with visited manholes 20 and 21. In these cases, the particle filter for localization held more than one hypotheses. Therefore the mean is not a good representation of the information in the cloud. Nevertheless, the system was able to properly localize the robot during all the experiment without the need of manually resetting the position hypothesis.

13.8 Conclusions

The SIAR project has successfully designed, developed, tested and experimented a new robotic platform that is able to inspect real visitable and semi-visitable sewers with minimal intervention of the operator.

The robot has been tested in experiments carried out in operational scenarios. These experiment shows that the platform is close of reaching the final goal of the Challenge; that is, having a fully-operative prototype being able of semi-autonomously navigate through visitable sewers while at the same time being capable of detecting defects in the sewer system, and providing monitoring real-time images to the operator.

However, there are still work that remains to be done. First, the semi-autonomous navigation system should be refined to increase its reliability in the presence of forks. Moreover, in the current stage of the project the system is being tested in different scenarios, in which the adaptability of the platform would be challenged. Finally, the automatic defect inspection has to be polished to further diminish the workload of the operator.

References

1. ECHORD++: Utility infrastructures and condition monitoring for sewer network. Robots for the inspection and the clearance of the sewer network in cities. http://echord.eu/public/wp-content/uploads/2015/11/20141218_Challenge-Brief_Urban_Robotics.pdf (2014)
2. Mirats-Tur, J., Garthwaite, W.: Robotic devices for water main in-pipe inspection: A survey. *Journal of Field Robotics*, 491–508 (2010)
3. Walter, C., Saenz, J., Elkmann, N., Althoff, H., Kutzner, S., Stuerze, T.: Design considerations of robotic system for cleaning and inspection of large-diameter sewers. *Journal of Field*

- Robotics **29**(1), 186-214
4. Ibak. <http://www.ibak.de/>
5. Geolyn. <http://www.geolyn.ca/>
6. Solo tracked robots from redzone. <http://www.redzone.com/products/solo-robots/>
7. Makro's. wheeled worm robot http://www.inspector-systems.com/makro_plus.html
8. Purerobotics' pipeline inspection. <http://www.puretechltd.com/services/robotics/>
9. Serviceroboter. <https://www.iff.fraunhofer.de/en/business-units/robotic-systems/sewer-inspection-svm.html>
10. Tardioli, D.: A proof-of-concept application of multi-hop robot teleoperation with online map building. In: Proceedings of the 9th IEEE International Symposium on Industrial Embedded Systems (SIES 2014), pp. 210–217. IEEE (2014)
11. Quigley, M., Gerkey, B., Conley, K., Faust, J., Foote, T., Leibs, J., Berger, E., Wheeler, R., Ng, A.: ROS: an open-source Robot Operating System. In: Proc. of the IEEE Intl. Conf. on Robotics and Automation (ICRA) Workshop on Open Source Robotics. Kobe, Japan (2009)
12. Alejo, D., Caballero, F., Merino, L.: RGBD-based Robot Localization in Sewer Networks. In: IEEE/RSJ International Conference on Intelligent Robots and Systems (IROS), pp.4070-4076 (2017)
13. Perez-Grau, F., Caballero, F., Merino, L., Viguria, A.: Multi-modal mapping and localization of unmanned aerial robots based on ultra-wideband and RGB-D sensing. In: 2017 IEEE/RSJ International Conference on Intelligent Robots and Systems, IROS 2017, Vancouver, BC, Canada, September 24-28, 2017, pp. 3495-3502 (2017).
14. Thrun, S., Fox, D., Burgard, W., Dellaert, F.: Robust Monte Carlo localization for mobile robots. *Artificial intelligence* **128**(1-2), 99-141 (2001)
15. Papadakis, P.: Terrain traversability analysis methods for unmanned ground vehicles: A survey. *Engineering Applications of Artificial Intelligence* **26**(4), 1373-1385 (2013)
16. Fox, D., Burgard, W., Thrun, S.: The dynamic window approach to collision avoidance. *IEEE Robotics Automation Magazine* **4**(1), 23-33 (1997)
17. Krüsi, P., Furgale, P., Bosse, M., Siegwart, R.: Driving on point clouds: Motion planning, trajectory optimization, and terrain assessment in generic nonplanar environments. *Journal of Field Robotics* **34**(5), 940-984
18. Hornung, A., Wurm, K.M., Bennewitz, M., Stachniss, C., Burgard, W.: OctoMap: An efficient probabilistic 3D mapping framework based on octrees. *Autonomous Robots* (2013). <http://octomap.github.com>. Software available at <http://octomap.github.com>
19. Grisetti, G., Kummerle, R., Stachniss, C., Burgard, W.: A tutorial on graph-based slam. *IEEE Intelligent Transportation Systems Magazine* **2**(4), 31-43 (2010)
20. Pérez-Lara, J., Caballero, F., Merino, L.: Enhanced monte carlo localization with visual place recognition for robust robot localization. *Journal of Intelligent and Robotic Systems* **80**, 641-656 (2015)
21. Perez-Grau, F.J., Fabresse, F.R., Caballero, F., Viguria, A., Ollero, A.: Long-term aerial robot localization based on visual odometry and radio-based ranging. In: Proceedings of the 2016 International Conference on Unmanned Aerial Systems. Arlinton, USA (2016)
22. Krizhevsky, A., Sutskever, I., Hinton, G.E.: Imagenet classification with deep convolutional neural networks. In: Advances in Neural Information Processing Systems (2012)
23. Besl, P.J., McKay, N.D.: A method for registration of 3-d shapes. *IEEE Transactions on Pattern Analysis and Machine Intelligence* **14**(2), 239-256 (1992)
24. Rusu, R.B., Cousins, S.: 3D is here: Point Cloud Library (PCL). In: 2011 IEEE International Conference on Robotics and Automation, pp. 1-4 (2011)

Chapter 14

Public Entity role in Robotic Innovation Barcelona participation in Echord++ PDTI Project for Urban Challenges

Javier Varela, Ma José Chesa, Lina Martinez, Silvia Burdons and Josep Garriga

Abstract In 2014, the European project ECHORD++ made a call for challenges in cities that could be solved by robotics. Among the fourteen challenges proposed, Barcelona presented four challenges from which the "Robots for the Inspection and Clearance of the Sewer Network in Cities" was the selected challenge. Introducing a robotics solution in sewer inspections aims at reducing the labour risks and optimize resources since sewer inspections require humans to work in risky and unhealthy conditions. Barcelona City Council, through its public body Barcelona Cicle de l'Aigua SA (BCASA), is playing an active role in guiding innovation by: identifying the public body needs; solving doubts about requirements of the service; providing existing information of the sewer network and the service offered; supporting ECHORD++ coordinators and external evaluators through evaluations; identifying feasible locations for each testing stage; and supporting access to sewers for testing and evaluations. Next actions will be take advantage from the knowledge and products developed during the project and continuing to spread teachings from this project about innovation through Barcelona City Council departments.

14.1 Barcelona City Council and Innovation

Barcelona City Council has long experience in innovation. Many initiatives had been developed both explaining city's challenges to be solved by innovation and helping developers to test their products or services making Barcelona a "city lab". Some initiatives are described by Vara and Van der Most [1] including the following:

- In 2008, Barcelona Urban Lab facilitated the use of public spaces to carry out tests and pilot programs on products and services with an urban impact, which were in the pre-market stage and in line with the Barcelona City Council's aims, priorities and lines of action. The idea was to use the city as an urban laboratory.
- In 2012, Eindhoven, Birmingham and Barcelona participated in the Smart Procurement European Alliance (SPEA) project that focused on improving energy efficiency in municipal buildings in order to incorporate energy saving and renewable energy to these buildings and to develop sustainable management procedures.

Javier Varela, Ma José Chesa, Lina Martinez, Silvia Burdons and Josep Garriga
Barcelona Cicle de l'Aigua. Ajuntament de Barcelona. Carrer de l'Acer 16, Barcelona 08038
e-mail: {[jvarela](mailto:jvarela@bcn.cat), [mjchesa](mailto:mjchesa@bcn.cat), [lmartinez](mailto:lmartinez@bcn.cat), [sburdons](mailto:sburdons@bcn.cat), [jgarriga](mailto:jgarriga@bcn.cat)}@bcn.cat

- In 2014, before the civil works for redevelopment of the Diagonal Avenue, the city council asked for a specific cobblestone. Innovation was done in the component materials used (recycled) and other characteristics as more resistance, ease of cleaning and less risk of slipping.
- In the same year, the Barcelona Open Challenge made it possible to invite local and international companies to present innovative solutions to six city's explicit challenges, and to steer the solutions by means of municipal purchasing of services.
- Form its creation in 2002; the public company Barcelona Serveis Municipals (BSM) manages diverse city services including parking zones, mobility regulation and cultural installations. Among other initiatives for innovation, BSM has used alternative procedures in procurement like dialogues with the market in order to find the best solution for the analysis of its surveillance cameras.

Thanks to City council efforts, Barcelona was awarded as European Capital of Innovation (iCapital) in 2014 for "introducing the use of new technologies to bring the city closer to citizens" [2]. Aligned with the European Strategy for innovation not only in the services offered but in procurement procedures as well, Barcelona City Council approved in 2017 criteria guides for social, environmental and innovation enhancement through public procurement. Through this guides, Barcelona City Council aims to help create employment and growth in the city, strengthen its social and environmental values, and support innovative companies that are focused on solving the problems of citizenship [3].

Meanwhile, The FP7 European Union's Research and Innovation funding program for 2007-2013 begun to run including the robotics research project European Coordination Hub for Open Robotics Development (ECHORD++). ECHORD++ promotes the interaction between robot manufacturers, researchers and users. This program has developed three branches of action called Experiments (Exp), Robotic Innovation Facilities (RIF) and Public end-user Driven Technological Innovation (PDTI). In particular, the PDTI scheme offers research consortia funding to develop robotics technology for real use-cases including city necessities. This aim matches along with the European Commission objective of making from public procurement a basic tool for supporting innovation [4]. Two application areas for PDTI application have been identified: Healthcare and Urban Robotics. A summary of the fourteen urban challenges (technology needs) proposed by cities can be found in [5] including four challenges from Barcelona city related to infrastructures and pedestrian areas. Selected challenge for urban robotics was "Robots for the Inspection and Clearance of the Sewer Network in Cities" proposed by the city of Barcelona

14.2 Public entity role in PDTI procedure

As stated by Puig-Pey *et al.* [5], PDTI procedure develops two main phases: Activities for public demand knowledge and Activities for research and technical development of pre-commercial products. Both phases demand implication from the end-user in order to achieve technologies that fulfills its necessities.

In this case, the end-user is Barcelona City Council through its public company Barcelona Cicle de l'Aigua SA (BCASA). BCASA has long experience as sewer network operator among other activities related to urban water cycle. The ongoing PDTI project for urban robotics implicated different departments from the public body in order to obtain a global solution. BCASA tasks have been the following (see Figure 14.2):

- A. Challenge's call Questionnaire: answering the questionnaire BCASA set out an early description of the challenge and expected impact. Public body experience and existing knowledge was key for determine the current state of the service and the future needs to be solved by robotic technology.
- B. Challenge Brief's written up: the Challenge Brief includes detailed description of the public body needs and service requirements. During this stage, BCASA and ECHORD++ coordina-



Fig. 14.1: Barcelona Urban Lab and BCN Open Challenge. Source: Barcelona City council

tors set down evaluation criteria about innovation, functions and conditions of the technology. Some of these performance indicators were related to existing indicators of the service. Furthermore, it includes a study of the state of the art about the existing technology, and about other possible sites and situations where the developed technology could be applied.

- C. Consortia support: BCASA as public service operator helps in the resolution of doubts about the challenge brief requirements and public body needs. During the development of the technology, BCASA support consortia with inspection staff, security material and access to testing sites.
- D. Evaluation and selection: several stages of PDTI procedure includes proposals or technology evaluation and selection. Each phase of the technology development has its own evaluation procedure and criteria based upon the evaluation criteria settled in the Challenge Brief. In addition, BCASA is in charge of identification and preparation of representative testing sites for consortia evaluation.
- E. Communication and dissemination: consortia, ECHORD++ coordinators and BCASA have done many communication and dissemination actions during the project. Objectives are to stand out technology innovation in inspection robots, approaching robotics to end-users and highlight public body role in purchasing procedures that includes innovation

14.3 The Questionnaire: Inspection of the Sewer Network

The Questionnaire from ECHORD++ coordinators for the challenge's call was key to set out the public body expertise and an early challenge description.

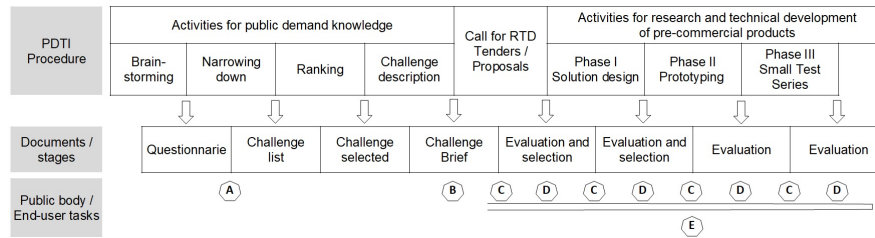


Fig. 14.2: End-user tasks during PDI procedure. Source: BCASA based on Puig-Pey et al

14.3.1 The Public Body Expertise

Barcelona Cicle de l'Aigua SA (BCASA) is a 100% public company created in 2014 by Barcelona City Council. The aim was to group together all the know-how related to urban water cycle existing in the city council. The mission of BCASA is the integral management of the urban water cycle in Barcelona, including water supply, sanitation, coastline management, alternative water resources management, fountains management and other areas of the water cycle. Specifically, BCASA manages the sewer network enhancing the transformation of the city drainage through hydraulic regulation and Real Time Control. These permits to minimize flooding; reduce and characterize Combined Sewer Overflows (CSO), especially in beaches but also in Besòs River and marina; increase coordination with WWTP during rain events; achieve a high level of automatic local control in the sewage management; and use water quality indicators in order to improve the bathing beach management.

Currently, Barcelona has full knowledge and access to data of its sewage net-work thanks to its IT systems:

- The GIS system collects static information about the network as an asset inventory. It includes exhaustive description of the network, description of each object and other underground data. It also includes information related to the location, structural features and its evolution, and operations carried out in the networks. It took over 12 years to digitalise the en-tire network from paper to the GIS and big efforts are made to maintain it accurate updated.
- The telecontrol system controls actuators and sensors like limnimeters, rain gauges or gates localized along the sewer network that permit real time control and advanced management of the network. All these sensors are controlled remotely from BCASA's control center that receives all the data signals, analyses and, in most cases, applies algorithms for automatically operate the network (Remote Automatic Control). Thus, the telecontrol system collects all the changing information and it is the basis for the daily management of the network as well as for obtaining average data for hydraulic modeling.
- The modeling system permits to take off a part of the network, like critical points, and run hydro-geological models in order to determine the current performance of the network and the hypothetical performance with an actuation over the network. Thus, manager can chose the more efficient way to improve the network. This part is basic for written up Sew-age Master Plans since it permits to prioritize actions on the network. These tools are strongly linked to each other and permit a better under-standing of the network and its performance in both dry and rainy time. Although all three are important for the whole sewer management, sewer inspection mostly relies on the GIS system.

14.3.2 Challenge Description

The sewer network of Barcelona is more than 1500 km long, from which approximately 50% is accessible, which means that the pipe is at least 1.5 m high and workers are allowed to enter into. One of the services that are critical for the performance of sanitation is the inspection of the sewer network. Former to the cleanness or the rehabilitation, inspection work has to be done in order to identify, localize and measure obstruction problems or structural defects. These visual inspections are done with different frequencies depending on the slope, historical information of critical points and other characteristics of the sewer. Workers walk all along the pipe and identify where it is necessary to clean or rehabilitate.

Because of sewer size and morphology, workers are forced to maintain forced positions during inspection and they face up to other risks like slippery sections, existence of frontal obstacles or biological risks from the eventually contact with waste water.

Furthermore, sewers are classified as confined spaces which require special measures for prevention. Since, no inspector must walk alone into sewers; each team normally has four inspectors: two of them go down into sewers and at least two more stay in surface near to open manholes. Thus, improvements through robotics could be done in order to reduce the time inspectors are into the sewer ex-posed to these risks.

The challenge is to develop a robotic tool that determines the quantity of sediments in the sewer by the detection of abnormal levels of water or obstructions in pipes. An additional service developed is the detection of abnormalities in the pipes structure (like cracks or subsidence) so the technology could help to decide which sections of the utility network have to be repair or replaced.

Additionally, other improvement areas could be automatization of information collection (localization, defects classification, etc.) or monitoring and sampling. This technology could be used as well to inspect abandoned mines and other underground structures for having the exact location and characteristics. In Barcelona case, this information can be introduced in the GIS and be useful for the Subsoil Police Department that is responsible for security in underground galleries and tunnels. Besides, this technology could be transferable to cities with similar sewers.

14.4 The Challenge Brief

The Challenge Brief was a step further in the challenge description and its impacts. It boosted the public body to describe in detail the current situation of the service, the current technology available, the functions and conditions for the new technology and finally how to measure the technology development. During this stage, Barcelona City Council, BCASA and ECHORD++ coordinators worked together in focusing the challenge brief in what the public body needs and not in what the robot had to do. This way ensured not to limit innovation and allowed the participant consortia to propose their own solutions to the challenge. Previous experience of the public body as operator of the service and its vast knowledge of the system was highly useful for writing up the Challenge Brief. The full document is available at ECHORD++ - PDTI web page [6] and it includes key aspects described next.

14.4.1 Current situation of the service

Classification of sewers according to their visitability.

As previously stated, the sewer network of Barcelona is 1532 km long, from which approximately 50% is visitable. This percentage is higher in Barcelona than in other similar cities where it is

normally less than 30%. This enabled us to test the technology in various sewer sizes and could facilitate the study of transferability of the technology to other cities or situations.

According to the characteristics of sewer sections, there are three possible classifications according to their height (H) and width (W) (see Figure 14.3).

- Visible sewers are sections that allow access for the inspector staff. This type includes sewers where H or $D \geq 150$ cm and $W \geq 60$ cm, except sewers without curb (in this case it is considered as semi visible sewer).
- Semi visible sewers are sections where H or $D \geq 100$ cm and $W \geq 50$ cm. In these cases, access is restricted and requires the application of additional measures, to be defined for each type of task.
- Non visible sewers do not allow secure access because of its dimension or morphology. Sections are classified as non visible when H or $D < 100$ cm or $W < 50$ cm.

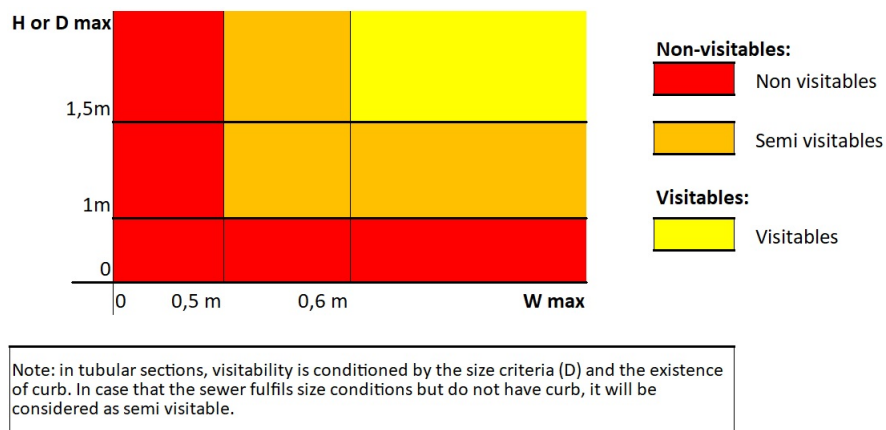


Fig. 14.3: Classification criteria for visibility of sewers. Source: BCASA

Sewer network data.

Sections that make up the Barcelona sewage network are widely varied. Data extracted in 2014, when Challenge Brief was presented to consortia, showed that there were up to 2.076 types of sections from which the most common were T111 and T130 (see Figure 14.4). Table 14.1 states the length of the sewer network, in lineal meters, according to their visibility. Since in the case of sewers with diameter below 0.8 m, inspection is solved with the existent technology, it was established that the future technology has to be focused in pipes with diameter over 0.8 m.

14.4.2 Functions and conditions for the new technology

Functions and conditions required for the new technology are those given by the inherent sewer characteristics and those related to specific end-user needs.

The conditions inside sewers that restrict the staff access in plenty of cases and that the robotic solutions will face are mainly the following:

- Different ranges of pipe sizes

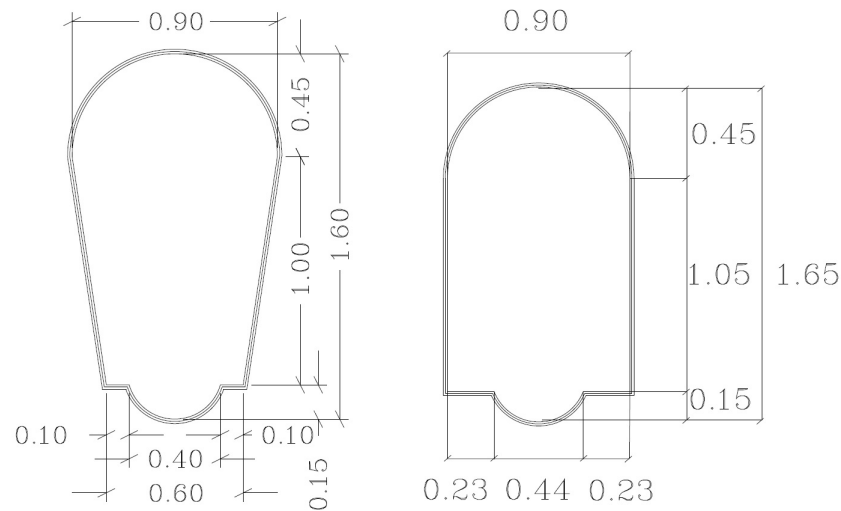


Fig. 14.4: Most common sewer sections in Barcelona: T111 and T130. Source: BCASA

TYPE OF SEWER	LENGTH (m)	PERCENTAGE
Non visitable sewers	541.000	35%
Semi visitable sewers	148.000	10%
Visitable sewers	843.000	55%
TOTAL	1.532.000	100%

Table 14.1: Length of existing sewers depending on its visitability. Source: BCASA

- Possible high concentration of, not explosive, but toxic gases as hydrogen sulphide or carbon monoxide
- Slippery areas
- Obstacles
- Atmosphere with 100 % humidity
- Water general presence
- No telecommunication coverage into sewers
- Although the standard manhole diameter in the city of Barcelona is 0.70 m, it is suggested to consider a diameter ≤ 0.60 m since it could be reduced by the manhole stairs and other singularities.

Related to specific end-user needs, general services required for well developing sewer inspection are the following:

- Remote operation that allows the robotic system to receive orders and to send images to the operator in real time
- The robotic system has to be able to navigate autonomously and avoid obstacles
- In-site recording digital images and videos

- 3D-scanning in order to compare inspection data with available data and determine section reduction and obstacles
- Robotic solution has to facilitate sewer elements location and mapping building

Based on these functions, the final objective is to obtain a robotic solution able to:

- Determine the sewer serviceability (water obstruction and sediment presence)
- Identify critical structural defects (sewer cracks, fractures, breaks or collapses)
- Monitor sewers with air and water sensors
- Sample water, air and sediment

14.4.3 Evaluation criteria

The evaluation of robotic solutions will be done according to three basic criteria:

1. Scientific and technological excellence
2. Quality and efficiency of the implementation and the management
3. Potential impact through the development, dissemination and use of the project. Economic impact.

BCASA mostly influenced in the description of Scientific and technological excellence criteria while the other two criteria were defined by ECHORD++ coordinators. Related to the Scientific and technological excellence criteria, the weight for each function required was established as shown in Table 14.2.

FUNCTIONS				WEIGHT	
Sewer serviceability inspection	Sewer performance (at least 1000 lineal meter/labour day)			10%	80%
	Images (Video)			40%	
	Geometric analysis (scanning)			20%	
	Monitoring	Air		9%	
		Water		1%	
Structural defect inspection				15%	
Sampling				5%	

Table 14.2: Criteria for evaluation of functions to be achieved by robotic solution

14.4.4 Expected Impact

Different impacts are expected to be achieved through robotic solutions from which the following impacts can be highlighted. In general, the main benefit of developing the technology will be to reduce the time that workers have to stay into the sewers especially into those with small section or presence of gases. Thus, there will be an important social impact for workers as its working conditions would be improved, and for citizens thanks to the optimization of a public service. Additionally, environmental impact is expected through enhancing sewer network performance by detection and location of obstructions or leaks thus preventing overflows and groundwater pollution.

Finally, economic impact could be achieved through reducing the cost of the inspection works about 30%, optimizing the approximately 1 million Euros per year required on staff expenses only, excluding equipment, machinery or prevention issues. Knowing that current performance of inspection works is about 1500 meters in 8 hours, the technology should enhance inspection works performance up to at least 1000 meters in 8 hours and reduce the cost below 0.50€/ lineal meter.

14.5 End user driven technology

End-user guidance along the whole project is being crucial for consortia to really understand public body needs and requirements. BCASA tasks in supporting technology developers and ECHORD++ coordinators are related to better know about field works and data that have to be obtained from inspections. Each phase of the technology development has its own evaluation procedure and criteria based upon the evaluation criteria settled in the Challenge Brief. BCASA support during selection, testing and evaluation includes:

- Resolution of doubts about the Challenge Brief requirements and public body needs
- Provide existing information of sewer network
- Identification of representative testing sites
- Facilitating inspection staff and security material for testing
- Supporting consortia and evaluators during tests and evaluation for accessing sewers
- Supporting ECHORD++ coordinators and external evaluators through evaluations and selection of consortia proposals

During the first part of the project, six consortia presented their proposal to the Call for RTD Tenders / Proposals. At this stage, BCASA elaborated a comparative matrix summarizing consortia solution for each functionality and characteristics required in the Challenge Brief (see Table 14.3). As established in PDTI procedure, with the help of the comparative matrix, evaluators selected three consortia that had passed to Phase I: ARSI, SIAR and Robodillos

After consortia selection, for the technology development phases, BCASA and ECHORD++ coordinators had decided specific test for each phase including field tests and indicators related to system performance. In all these stages, BCASA has determined one or several zones to be inspected and the consortia proposed how they would do the inspection in the most efficient way allowed by their robotic solution. BCASA has looked for locations that permits flexible tests for the consortia to decide the best way to face them.

In phase I, when the technology was less developed, tests were specifically designed for knowing the development level about mobility; communication and energy consumption (see Figure 14.5). These tests were made in bigger sewers so evaluators could see robots performance and required sewer adjustments so the robots could go through. After this evaluation, only two consortia could pass to next phase. ARSI and SIAR were the selected ones and this meant they get the funds for continuing developing the technology in Phase II and Phase III.

In phase II, test were focused in the global operative procedure with the robotic solutions (see Figure 14.6). The objective was to check to what extent the robotic solutions could reduce time in

Consortia information Acronym Project full name Consortium Type of robot Image	Communication and data processing Wireless technology Communication On-board data processing Off-line data processing Localization algorithms Navigation algorithms Mapping algorithms Structural inspection algorithms Sediment inspection algorithms Integration to GIS Data collected Outputs georeferenced Type of data reception Software features Other interested features
General specifications Movement Suitable for visitable sections Diameter of sewer Robot size, weight & other dimension characteristics Water/humidity protection (IP) Robot cost	
Operativity Teleoperated / Semi-autonomous / Full autonomous Energy Type of light Hours of autonomy How it works mobility and autonomy Speed Inspection cost (actual cost 0,75€/lineal meter)	Devices incorporated and relevant features Infrared camera Ultrasonic sensor Sonar sensor Electromagnetic sensor 3D representation Camera 3D (stereo camera) Laser sensor Lighting Images in 360° Lidar or Ladar VI-sensor (Visual-Inertial Sensor) 3D mapping
Functions Mapping Structural inspection Sediment inspection (hydraulic capacity reduction) Air inspection Water inspection Sampling (air, water or sediment)	
Specific devices and sensors Location and navigation devices Inspection devices Air quality sensors Water quality sensors	

Table 14.3: Characteristics of the robotic systems to be evaluated during the first selection

inspection works taking into account field works and data processing afterwards. Other assessed aspects were occupation of public space or the time the manholes were kept opened. In this case, communication with robot was made from outside of sewers and no adjustment in sewer was required.

Phase III is still ongoing and objectives are to check data obtained during inspection and its later processing for detecting obstructions and structural defects (see Figure 14.7). In addition, evaluation will assess replicability of the robotic systems since consortia has to prepare a second robotic platform and test it.



Fig. 14.5: Phase I tests at Pg. Sant Joan

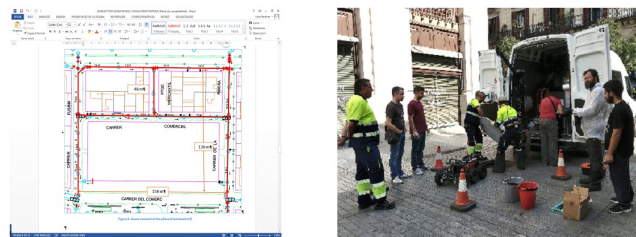


Fig. 14.6: Phase II tests at Mercat del Born with SIAR team

All along the project, consortia questions and concerns has made the public body to decide and prioritize some functions among others. This requires flexibility in both testing and evaluation, adjusting it to the project development, and being ambitious for boosting consortia to develop the robot as much as possible. From these decisions, during the last part of the project, functionalities required were classified in basic and assessable (see Table 14.4).

14.6 Conclusions and future actions

ECHORD++ PDTI project for urban challenges is having a big impact in approach robotics to services offered by BCASA and Barcelona City Council.

The project has helped to point out the expertise of BCASA about the service offered and its sewer network, allowing to answer with accuracy the questionnaire and to identify very specifically

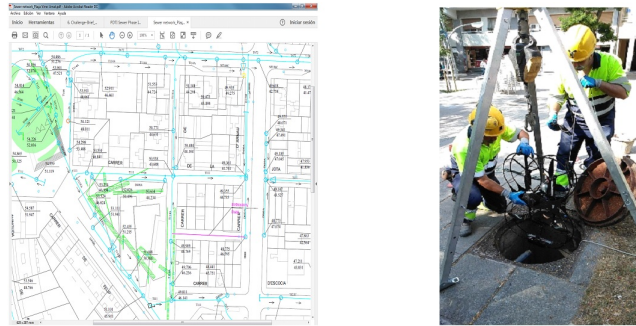


Fig. 14.7: Phase III tests at Virrei Amat square with ARSI team

FUNCTIONS			WEIGHT
Sewer service-ability inspection	Sewer performance (at least 1000 lineal meter/labour day)		Basic
	Images (Video)		Basic
	Geometric analysis (scanning)		Basic
	Monitoring	Air	Assessable
		Water	Assessable
Structural defect inspection			Assessable

Table 14.4: Criteria evolution during phase III

the needs to be covered by the technology. PDTI procedure has shown that functionalities required at the beginning of the project has to be wide in order to boost innovation. Then, testing has to be constant and in realistic conditions with the guidance of the public body in order to focus on the end-user needs. At the same time, testing and evaluation have to be flexible so the technology developers could propose their own ideas thus giving solutions to the end-user. This way it is possible to have not expected products halfway that could be useful for other type of services. Furthermore, public bodies usually ask for a full inspection service that could include different associated technologies.

Next actions are related to take advantage from the knowledge and products developed and continuing to spread teachings from this project about innovation through Barcelona City Council departments. Thus, robotics solutions are expected to be present in next tenders for the Barcelona sewer network management.

Finally, public bodies must transform to be flexible, open and capable of self-restructuration, so that city managers internalize their key role as public investors who are willing to create market conditions that enable innovation.

Acknowledgements ECHORD++ project has received funding from the European Union's Seventh Framework Programme for research, technological development and demonstration under grant agreement no 601116.

References

1. Vara Arribas, G., Van der Most, J.: Diagnosis en compra pública para la innovación. Evaluación comparativa con experiencias europeas. [Online] (2017) https://ajuntament.barcelona.cat/digital/sites/default/files/diagnosis-esp_v2.pdf
2. European Commission. The European Capital of Innovation (iCapital) Award. [Online] https://ec.europa.eu/info/research-and-innovation/funding/funding-opportunities/prizes/icapital_en
3. Barcelona City Council. Public procurement. Economy and Employment, Digital City and International Relations. [Online] <http://ajuntament.barcelona.cat/contractaciopublica/en/>
4. European Commission. Strategic public procurement - Brochure. [Online] <http://ec.europa.eu/DocsRoom/documents/25984>
5. Puig-Pey, A. et al.: Public entities driven robotic innovation in urban areas. *Robotics and Autonomous Systems* **92**, 162-172 (2017)
6. Barcelona City Council, Barcelona Cicle de l'aigua SA (BCASA). ECHORD++. PDTI. Urban Robotics. Sewer inspection. Challenge Brief.(2014) http://echord.eu/public/wp-content/uploads/2015/11/20141218_Challenge-Brief_Urban_Robotics.pdf